



University of Strathclyde
Renewable Energy Marine Structure Centre for Doctoral Training
Department of Naval Architecture Ocean and Marine Engineering

Geometric Shape Parameterization and Optimization of Floating Offshore Wind
Turbine Substructure within an MDAO Framework

Adebayo Ojo

A thesis submitted in partial fulfilment of the requirements for the degree of
Doctor of Philosophy

Supervisors: Prof. Maurizio Collu
Dr. Andrea Coraddu

Declaration of authenticity and author's rights

This thesis is the result of the author's original research. It has been composed by the author and has not been previously submitted for examination which has led to the award of a degree.

The copyright of this thesis belongs to the author under the terms of the United Kingdom Copyright Acts as qualified by University of Strathclyde Regulation 3.50. Due acknowledgement must always be made of the use of any material contained in, or derived from, this thesis.

Adebayo Ojo

May 2024

Statement on previously published work

In the course of this thesis, a number of papers have been published in scientific journals or still under review at the time of writing, as listed in section 1.7. The author of this thesis was and is in all these publications - even if the paper is co-authored - the main responsible person. The author's contributions to the publications, thus, comprise conceiving the works, administering the studies, realizing the works, performing literature studies, developing the methodologies, performing the researches, developing and applying the approaches, working with and extending the software, curating the data, verifying and validating the methods and results, analysing and investigating the data and results, post-processing and visualizing the results and findings, writing the papers and preparing the original drafts, interacting with the journals' editors and reviewers, as well as reviewing and editing the papers for the final publications.

Abstract

The urgent need to reduce greenhouse gases to attain net zero emission and reverse climate change has put the world at a turning point to explore cleaner form of energy generation. This has spiked an increase in the offshore wind forms of energy generation and, most recently, a focus on the Floating Offshore Wind Turbine (FOWT) sector. However, despite the advantages of FOWT installations amongst which are; less environmental impact and accessibility to deeper waters for richer wind resources needed for significant power generation, the technology is presently still economically less viable in comparison to the fixed bottom foundation counterpart. Several research studies, aimed at ensuring the economic feasibility of FOWT have been performed, such as floating foundation upscaling, surrogate designs, and multidisciplinary design analysis and optimization (MDAO) approach. This research is exploring the use of parametric curves to alter the design shapes within an MDAO framework to improve design, reduce analysis' computation time and ensure economic feasibility.

This thesis conducted a detailed literature review on shape parameterization techniques and MDAO framework for floating offshore substructures, highlighting research gaps related to their design. The focus of this thesis is to develop a conceptual platform for the design, analysis, and optimization of floating substructures for offshore wind turbine systems using shape parameterization techniques within an MDAO framework. This thesis utilized shape parameterization techniques like the Non-Uniform Rational B-Spline approximation curve characterized with local propagation shape control properties within Sesam GeniE and hydrodynamic analysis tools using the potential flow methodology (HydroD and Wave Analysis by Diffraction and Morisson theory - WADAM). Other shape parameterization techniques like the Cubic Spline, Cubic Hermite Spline and B-Spline approximation curve along with the Non-Uniform Rational B-Spline were assessed. The B-spline parameterization technique is the best performance curve using the Technique for Order of reference by Similarity to Ideal Solution (TOPSIS) to assess the curves given a set of criteria amongst which are computational time, curve continuity and propagation properties and minimizing the objective function. These tools are interfaced on a developed platform with glue codes using Python object-oriented programming language. The automated process within the interface platform includes generating panel model design geometry based on a set of design variables provided, modelling the ballast compartment, meshing the models in preparation for hydrodynamic assessment, evaluating mass distribution and buoyancy with the derivation of

the ballast mass distribution and conducting a hydrostatic assessment. The developed platform is further integrated with the gradient-free pattern search optimization algorithm with specified objective functions and constraints to select the most feasible design concept.

The developed model, framework, and approaches in this thesis - especially the concept of shape parameterization within a multidisciplinary design analysis and optimization framework are of potentially high value for both research and the floating offshore wind industrial sector. The achievements of this thesis are summarized herein.

1. This thesis introduces a simplified and innovative design approach by integrating parametric curves into a Multidisciplinary Design Analysis and Optimization (MDAO) framework. This integrated method allows for the exploration of an extensive design space, facilitating the selection of an optimal design within a significantly reduced computational time frame.
2. The thesis evaluates the performance of a set of parametric curves—Cubic Spline, Cubic Hermite Spline, B-Spline, and Non-Uniform Rational B-Spline (NURBS)—within the MDAO framework. The evaluation, based on a set of performance criteria employing the multicriteria decision matrix approach of TOPSIS, identifies B-Spline as the top performer, followed by the Cubic Spline, NURBS, and Cubic Hermite Spline.
3. The thesis demonstrates that optimizing the shape of a Spar platform using the NREL 5MW turbine in a 30MW configuration has the potential to reduce the levelized cost of energy by up to 8% compared to conventional designs. This finding underscores the economic viability and efficiency gains achievable through shape optimization approach.

This thesis provides valuable insights to diverse future applications, including enhanced design efficiency, reduced computational time for design and analysis, generation of unique design concepts for improved hydrodynamic performance, potential capital cost reduction, and lowered Levelized Cost of Energy (LCOE). Additionally, it paves the way for the advancement of advanced manufacturing techniques for unique shapes of floating foundations. These applications underscore the significance of the developed model framework, and approaches in advancing research, refining design practices, and fostering the development of economically viable and reliable support structures for floating offshore wind turbines.

Acknowledgement

I would like to thank Professor Feargal Brennan, Professor Maurizio Collu and Dr. Andrea Coraddu for taking a chance on me with the opportunity to pursue this Ph.D research. You provided me the opportunity to fulfil a childhood dream.

A big thanks to my first and second supervisors (Professor Collu and Dr. Coraddu) for the support, resources, and time invested to enable me take ownership of my research and navigate the obstacles and challenges associated with it.

I would like to thank my wife, Christine Hilditch and my children, Eilidh Ojo and Isla Ojo for their support and also persevering with me throughout the course of my research. We will catch up on lost time.

I would like to thank my father and siblings for their support and encouragement right from my formative years. I reflect how I was shaped by you all.

A big thanks to everyone involved with the Renewable Energy Marine Structures centre for doctoral training and the Naval Architecture Ocean and Marine Engineering department of the University of Strathclyde.

Finally, I dedicate this work to my late mother; Helen Abidemi Ojo. We had our last laugh together when I told you I was starting a Ph.D. Little did I know that would be my last conversation with you. Thanks for everything and continue to rest in peace.

Table of Contents

| | |
|---|------------|
| Declaration of authenticity and author’s rights | ii |
| Statement on previously published work | iii |
| Abstract | iv |
| Acknowledgement | vi |
| Table of Contents | vii |
| List of Figures | x |
| List of Tables | xii |
| List of abbreviations | xiv |
| Chapter 1 Introduction | 1 |
| 1.1 Overview | 1 |
| 1.2 Research Question | 5 |
| 1.3 Research Aim and Hypothesis..... | 5 |
| 1.4 Objectives | 6 |
| 1.5 Novel Contribution to Knowledge | 6 |
| 1.6 Thesis Structure | 7 |
| 1.7 Publications connected with this research..... | 9 |
| Chapter 2 Literature Review | 10 |
| 2.1 Background..... | 10 |
| 2.2 Floating Offshore Wind Turbine Substructure Overview | 12 |
| 2.3 Design of a FOWT Platform | 15 |
| 2.3.1 Preliminary/Concept Design..... | 16 |
| 2.3.2 Detailed Design..... | 17 |
| 2.4 Parameterization Techniques in Design | 18 |
| 2.4.1 Shape Parameterization Review | 19 |
| 2.4.2 Parameterization work in other sectors..... | 23 |
| 2.4.3 Parameterization work on FOWT support structures | 25 |
| 2.5 Dynamic Analysis Techniques | 27 |
| 2.5.1 Frequency Domain Approach..... | 27 |
| 2.5.2 Time Domain Approach | 29 |
| 2.5.3 Review of Analysis Domain for FOWT System Design..... | 30 |
| 2.6 Multidisciplinary Design Analysis and Optimization Approaches for Floating Offshore Wind Turbine System..... | 31 |
| 2.6.1 MDAO Overview..... | 31 |

| | | |
|---|--|------------|
| 2.6.2 | MDAO workflow | 34 |
| 2.6.3 | MDAO for FOWT Substructures..... | 39 |
| 2.7 | Research gaps and proposed future areas of research | 47 |
| 2.7.1 | Surrogacy and MDAO | 47 |
| 2.7.2 | Larger design space exploration | 49 |
| 2.7.3 | Upscaling of the platform design geometric variables | 51 |
| Chapter 3 Geometric Design Parameterization and Optimization of Spar Floating Offshore Wind Turbine Substructure | | 54 |
| 3.1 | Background..... | 54 |
| 3.2 | State-of-the-art in Design, Analysis, and Optimization | 55 |
| 3.2.1 | Design Analysis and Optimization Tools | 56 |
| 3.3 | Methodology..... | 58 |
| 3.3.1 | Design Variables..... | 58 |
| 3.3.2 | Framework Development Tools | 59 |
| 3.3.3 | Exploration Phase | 62 |
| 3.3.4 | Verification Phase..... | 65 |
| 3.4 | Substructure OC3 5MW Case Study..... | 66 |
| 3.4.1 | Overview..... | 66 |
| 3.4.2 | Frequency Domain – Potential Flow Theory OC3 spar..... | 68 |
| 3.4.3 | Time domain Coupling and Response Verification (Medium Fidelity Tools).... | 71 |
| 3.5 | Shape Design Parameterization, Analysis, and Optimization of Models | 74 |
| 3.5.1 | Geometric Shape Design and Variants generation. | 74 |
| 3.5.2 | Integration with Optimization algorithm | 74 |
| 3.5.3 | Definition of the Optimization Problem | 75 |
| 3.5.4 | Shape optimization process within MDAO framework..... | 78 |
| 3.6 | Global Response Assessment of Optimal Designs and Results..... | 81 |
| 3.6.1 | Global Limit state assessments of the design variants..... | 81 |
| 3.6.2 | Design load case | 82 |
| 3.6.3 | Environmental Parameters | 83 |
| 3.6.4 | Results and Discussion | 85 |
| Chapter 4 Parametric Curve Comparison for Modelling Floating Offshore Wind Turbine Substructures | | 100 |
| 4.1 | Overview | 100 |
| 4.1.1 | Shape Parameterization Technique..... | 101 |
| 4.1.2 | Design Analysis and Optimization. | 101 |
| 4.1.3 | Multi Criteria Decision Making Technique..... | 101 |
| 4.2 | Geometric Curves and Shape Parameterization | 102 |
| 4.2.1 | Explicit Representation..... | 103 |
| 4.2.2 | Implicit Representation..... | 103 |

| | | |
|---|---|------------|
| 4.2.3 | Parametric Representation from Free-form Curves | 103 |
| 4.3 | Methodology..... | 107 |
| 4.3.1 | Integrating Parametric Curves with the MDAO Framework..... | 107 |
| 4.3.2 | TOPSIS method | 108 |
| 4.4 | Optimized models, results, and discussions | 110 |
| 4.4.1 | Overview..... | 110 |
| 4.4.2 | Design, Analysis and Optimization | 110 |
| 4.4.3 | Results..... | 112 |
| Chapter 5 Preliminary Techno-Economic Study of Optimized Floating Offshore Wind Turbine Substructure | | 133 |
| 5.1 | Overview and Background..... | 133 |
| 5.2 | Economic Feasibility of FOWT Review | 136 |
| 5.2.1 | Overview..... | 136 |
| 5.2.2 | Financial Parameters..... | 139 |
| 5.3 | Methodology and LCOE | 140 |
| 5.3.1 | Overview..... | 140 |
| 5.3.2 | Hydrostatics for mass estimation..... | 142 |
| 5.3.3 | Floatability and maximum inclination angle requirements | 144 |
| 5.4 | Techno-economic analysis, results and discussion | 146 |
| 5.4.1 | Overview..... | 146 |
| 5.4.2 | Technical Assessment..... | 147 |
| 5.4.3 | Economic Feasibility study..... | 151 |
| Chapter 6 Conclusion and Recommendations | | 167 |
| 6.1 | Conclusion | 167 |
| 6.1.1 | Develop an automated MDAO framework with an integrated free-form curves parameterization technique | 168 |
| 6.1.2 | Develop an analytical methodology to investigate / rank the free-form curves within the MDAO framework..... | 170 |
| 6.1.3 | Positive contribution on the preliminary techno-economics of FOWT projects..... | 171 |
| 6.2 | Contribution to knowledge..... | 173 |
| 6.3 | Recommendations and Future Work..... | 177 |
| References | | 180 |

List of Figures

| | |
|--|----|
| Figure 1. Total global offshore wind pipeline by regulatory status (Musial et al., 2022)..... | 3 |
| Figure 2. Total global floating offshore wind energy pipeline (Musial et al., 2022)..... | 3 |
| Figure 3. Thesis structure – Flowchart..... | 7 |
| Figure 4. Floating Offshore Wind Turbine System, adapted with permission from (Jonkman and Matha, 2011)..... | 12 |
| Figure 5. Floater classification based on stability mechanism (Karimi et al., 2017): From left to right – TLP, Spar and Semi-submersible..... | 14 |
| Figure 6. Simplified diagram of an MDAO workflow comprising an analysis block of two modules and a driver | 34 |
| Figure 7. Two workflows with different system scope. Dashed arrows include components/disciplines 1 and 2 while straight arrows include 1, 2 and 3..... | 35 |
| Figure 8. Architecture / Framework with Optimization functionalities for FOWT..... | 37 |
| Figure 9. Surrogate / Meta Modelling as part of system optimization (left), Surrogate / Meta modelling techniques (right). (Frank Lemmer and Ricardo Faerron Guzman, 2016) | 48 |
| Figure 10. Deviation model from conventional semi-submersible design (Optimised model vs earlier generation models), adapted with permission from (Clauss and Birk, 1996). | 51 |
| Figure 11. Deviation from conventional spar design with automated shape generation using polynomial curves, adapted with permission from (Birk and Clauss, 2008). | 51 |
| Figure 12. Interface code for discipline integration..... | 61 |
| Figure 13. Flowchart of framework methodology – Exploration Phase – Hydrostatics..... | 62 |
| Figure 14. Flowchart of framework methodology – Selection and verification phase - Hydrodynamics | 62 |
| Figure 15. Variation of control points along the NURBS curve..... | 66 |
| Figure 16. OC3 spar Sketch..... | 67 |
| Figure 17. NURBS model of an OC3 FOWT System in Sesam GeniE..... | 67 |
| Figure 18. Added mass coefficients (B-spline model vs literature model)..... | 70 |
| Figure 19. Damping coefficients (B-spline model vs literature model)..... | 70 |
| Figure 20. Excitation loads and moment (B-spline model vs literature model) | 71 |
| Figure 21. Surge, Heave, and Pitch RAO (B-spline model vs literature model) | 71 |
| Figure 22. NURBS Platform Coupled Platform Response vs NREL 5MW OpenFAST Design Response | 72 |
| Figure 23. Selected models from pattern search optimization algorithm method | 80 |
| Figure 24. Wave Spectrum- 10.37m Hs and 14.7s Tp..... | 84 |
| Figure 25. Surge, Heave, Pitch and Nacelle displacement RAO for all three cases and the OC3 spar | 89 |
| Figure 26. Force per unit incident wave amplitude in the Heave DOF for all cases | 89 |
| Figure 27. FOWT system's Surge response spectrum for all three cases and OC3 spar..... | 91 |
| Figure 28. FOWT system's Heave response spectrum for all three cases and OC3 spar..... | 91 |
| Figure 29. FOWT system's Pitch response spectrum for all three cases and OC3 spar..... | 92 |
| Figure 30. FOWT system's Nacelle horizontal displacement response spectrum for all three cases and OC3 spar | 93 |
| Figure 31. Heave decay test for the three optimal variants..... | 95 |
| Figure 32. Pitch decay test for the three optimal variants..... | 95 |
| Figure 33. Surge decay test for the three optimal variants..... | 95 |

| | |
|---|-----|
| Figure 34. Platform optimal variants coupled translational and rotational response | 98 |
| Figure 35. Nacelle acceleration response spectrum from time domain simulation | 99 |
| Figure 36. Parametric curve and MDAO framework..... | 107 |
| Figure 37. TOPSIS process..... | 108 |
| Figure 38. Comparison of the parametric curves on OC3 spar model with the plots from the OC3 data points..... | 114 |
| Figure 39. OC3 shape variants from different spline model..... | 115 |
| Figure 40. Surge, heave, pitch and nacelle displacement RAO for all four parametric curves. | 117 |
| Figure 41. Comparison of the optimized shape parametric curves on model with the plots of the curves from the optimized data point along the length of the spar | 119 |
| Figure 42. Optimal shape variants from MDAO framework with different spline models | 120 |
| Figure 43. Optimal shape variants surge, heave, pitch and nacelle displacement RAO for all four parametric curves | 122 |
| Figure 44. Platform shape optimization and LCOE estimation of a FOWF | 142 |
| Figure 45. Sketch of forces and reference points of a representative spar FOWT..... | 145 |
| Figure 46. Optimal models from pattern search optimization algorithm and OC3 spar | 151 |
| Figure 47. Mass of platform types | 161 |
| Figure 48. 30MW Farm Total Platform Mass and Total Platforms Material Cost | 163 |
| Figure 49. 30MW Farm LCOE and Total Platforms Steel Cost | 163 |
| Figure 50. 60MW Farm Total Platform Mass and Total Platforms Material Cost | 164 |
| Figure 51. 60MW Farm LCOE and Total Platforms Steel Cost | 164 |

List of Tables

| | |
|--|-----|
| Table 1. Natural frequencies of floater types (Taboada, 2015)..... | 14 |
| Table 2: Analysis domain overview for optimization of FOWT system | 30 |
| Table 3: Examples of gains from application of MDAO in aerospace and automotive sectors(Agte et al., 2009) | 34 |
| Table 4: Open-source MDAO Tools..... | 38 |
| Table 5: Overview of applicable optimizers | 40 |
| Table 6: MDAO work on FOWT substructures..... | 46 |
| Table 7: Geometric parameters for OC3 spar (Jonkman, 2010) | 67 |
| Table 8: Floating platform structural properties (Jonkman, 2010) | 68 |
| Table 9: Tower and hub properties for OC3 floating system..... | 68 |
| Table 10: Structural properties of the turbine top sides | 68 |
| Table 11: OC3 Spar NURBS curve control points below sea water level..... | 70 |
| Table 12. Motion response statistics (OC3 model vs NURBS model) | 73 |
| Table 13:Definition of design variables..... | 76 |
| Table 14: Optimization Constraints | 78 |
| Table 15: Design data for selected models | 81 |
| Table 16: Seastate and environmental data Leimeister et al. (2020b) | 84 |
| Table 17. Platform mass and corresponding cost estimate | 86 |
| Table 18: Heave natural frequency estimate from mass added mass and stiffness..... | 88 |
| Table 19: Estimate of Heave displacement response magnitude at natural frequency | 88 |
| Table 20. Nacelle Acceleration RMS – Frequency Domain..... | 93 |
| Table 21. Natural Period of optimal variants from free-decay test..... | 95 |
| Table 22. Descriptive motion response statistics of optimal variants | 96 |
| Table 23. Nacelle acceleration statistics from time domain simulation..... | 98 |
| Table 24:Definition of design variables for all free-form curves assessed..... | 111 |
| Table 25. OC3 Spar-Buoy Cubic spline, Cubic Hermite spline, B-spline and NURBS. | 113 |
| Table 26. OC3 Nacelle acceleration RMS for the free-form curves..... | 117 |
| Table 27. Dimension of optimal shapes B-spline, CHS, NURBS and Cubic Spline..... | 121 |
| Table 28.OC3 Optimal variant mass for the free-form curves..... | 122 |
| Table 29. OC3 Optimal Nacelle acceleration RMS for the free-form curves..... | 122 |
| Table 30. Analysis system specification | 123 |
| Table 31. TOPSIS matrix data | 125 |
| Table 32. Scenarios for criteria weightage matrix | 125 |
| Table 33. Performance ranking from weighted normalized decision matrix - Scenario 1..... | 126 |
| Table 34. Performance ranking from weighted normalized decision matrix - Scenario 2..... | 127 |
| Table 35. Performance ranking from weighted normalized decision matrix - Scenario 3..... | 128 |
| Table 36. Performance ranking from weighted normalized decision matrix - Scenario 4..... | 129 |
| Table 37. Performance ranking from weighted normalized decision matrix - Scenario 5..... | 130 |
| Table 38. Performance ranking from weighted normalized decision matrix - Scenario 6..... | 131 |
| Table 39. Summary of curve ranking..... | 132 |
| Table 40. Design data for selected models and OC3 spar..... | 150 |
| Table 41. Platform mass and corresponding material cost estimate | 154 |

| | |
|--|-----|
| Table 42. Assumptions for hypothetical Hywind wind farm (30 MW – 6 Turbines)..... | 154 |
| Table 43. Total cost for hypothetical Hywind wind farm (30 MW – 6 Turbines) – OC3 Platform ... | 155 |
| Table 44. Total cost for hypothetical Hywind wind farm (30 MW – 6 Turbines) – 5 deg static pitch angle platform – Case A | 155 |
| Table 45. Total cost for hypothetical Hywind wind farm (30 MW – 6 Turbines) – 7 deg static pitch angle platform – Case B..... | 156 |
| Table 46. Total cost for hypothetical Hywind wind farm (30 MW – 6 Turbines) – 10 deg static pitch angle platform – Case C..... | 156 |
| Table 47. Total cost for scaled up Hywind wind farm (60 MW – 12 Turbines) – OC3 Platform | 156 |
| Table 48. Total cost for scaled up Hywind wind farm (60 MW – 12 Turbines)– 5degstatic pitch angle platform – Case A | 156 |
| Table 49. Total cost for scaled up Hywind wind farm (60 MW – 12 Turbines) – 7deg static pitch angle platform – Case B..... | 157 |
| Table 50. Total cost for scaled up Hywind wind farm (60 MW – 12 Turbines) – 10 deg static pitch angle platform – Case C..... | 157 |
| Table 51. Estimated total platform mass and material cost for 30 MW and 60 MW FOWF | 161 |
| Table 52. LCOE comparison for 30 MW OC3 base model and 5 deg, 7 deg and 10 deg Static Pitch angle constrained optimized models | 162 |
| Table 53. LCOE comparison for 30 MW and 60 MW FOWF with 10% discount rate..... | 162 |
| Table 54. Research value to stakeholders | 174 |

List of abbreviations

| | |
|----------|---|
| ABS | American Bureau of Shipping |
| AEP | Annual Energy Production |
| AHSE | Aero-Hydro-Servo-Elastic |
| BA | Bat Algorithm |
| B-Spline | Basis Spline |
| BV | Bureau Veritas |
| CAD | Computer Aided Design |
| CHS | Cubic Hermite Spline |
| CAPEX | Capital Expenditure |
| CCD | Central Composite Design |
| DNV | Det Norske Veritas |
| DLC | Design Load Case |
| DOE | Design of Experiment |
| DOF | Degrees of Freedom |
| EA | Evolutionary Algorithm |
| ELM | Extreme Learning Machines |
| FBSM | Feature Based Solid Modelling |
| FEM | Finite Element Mesh |
| FFD | Free-Form Deposition |
| FOWT | Floating Offshore Wind Turbine |
| GA | Genetic Algorithm |
| GB | Gradient Based |
| GF | Gradient Free |
| HAWT | Horizontal Axis Wind Turbine |
| HF | High Fidelity |
| IDF | Individual Discipline Feasible |
| IEC | International Electrotechnical Commission |
| JONSWAP | Joint North Sea Wave Project |
| K-BA | Kriging BAT Optimization Algorithm |
| LCOE | Levelized Cost Of Energy |
| LF | Low Fidelity |
| LHS | Latin Hypercube Sampling |
| MCDM | Multi Criteria Decision Making |
| MDAO | Multidisciplinary Design Analysis and Optimization |
| MDF | Multidisciplinary Feasible |
| MO | Multi-Objective |
| NURBS | Non-Uniform Rational B-Spline |
| OC3 | Offshore Code Comparison Collaboration |
| OWT | Offshore Wind Turbine |
| PSM | Pattern Search Model |
| PSO | Particle Swarm Optimization |
| RAO | Response Amplitude Operator |
| RMS | Root Mean Square |
| RNA | Rotor Nacelle Assembly |
| SAND | Simultaneous Analysis and Design |
| SOA | Soft Object Animation |
| SQP | Sequential Quadratic Programming |
| TLP | Tension-Leg Platform |
| TOPSIS | Technique for Order of Preference by Similarity to Ideal Solution |
| WADAM | Wave Analysis by Diffraction and Morison Theory |
| WAMIT | Wave Analysis at Massachusetts Institute of Technology |

Chapter 1 Introduction

1.1 Overview

Recent climate change occurrences, amongst which are flash flooding, wildfires, melting ice and seasonal drought across the globe, are clear indicators of the disruption the planet is experiencing as a result of excessive greenhouse gas emissions. The Glasgow Climate Pact from the annual Conference of the Parties summit - COP 26 edition highlights the urgency of taking action to mitigate the excessive greenhouse gas emissions with the use of renewable technologies GWEC (2022) amongst which are: offshore wind (floating and fixed bottom foundations), solar photovoltaic, green hydrogen, geothermal, nuclear and tidal.

Offshore wind turbines with fixed foundations such as gravity base, monopile, suction caisson, tripod, and jacket foundations are typically installed in water depths of less than 50m (Wu et al., 2019). The monopile is a common and cost-effective foundation type used in the North Sea, which uses its own weight to anchor to the seabed at water depths of 0-25m (Konstantinidis and Botsaris, 2016). A gravity-based foundation, typically made of reinforced concrete with ballast, is also commonly used for depths up to 25m. An alternative foundation type is the suction caisson, which uses suction force created by removing water from a caisson to facilitate easy installation. This type of foundation is suitable for water depths up to 25m. For depths between 20-50m, a tripod structure made of lightweight steel is often used, which provides good stability and stiffness. The frame is submerged in the water to provide support (Konstantinidis and Botsaris, 2016). Jacket structures, consisting of three or four-legged lattice structures made of tubular steel, are commonly used for water depths of about 20-50 meters, offering good stability and support for wind turbines from different original equipment manufacturers (Konstantinidis and Botsaris, 2016).

These foundation types are well-established and have been widely used in the offshore wind industry for many years. They offer a reliable and cost-effective solution for supporting offshore wind turbines in relatively shallow waters. However, the choice of foundation type depends on several factors, such as water depth, soil conditions, and cost-effectiveness. The water depth is a big limitation to the continuous development of fixed bottom offshore wind turbine. Shallow water depth in which fixed bottom foundation wind turbines are suited are mainly on the coastal region, which is used for other purposes apart from power generation amongst which are: agriculture, fishing, transport routes, docks, maritime construction base and in some countries, reclaimed land for buildings. These highlighted limitations and the

abundance of rich wind resources in deep waters make the concept of floating foundation a viable option to complement and eventually surpass the already established fixed bottom foundation wind turbines.

The concept of floating offshore wind turbines was proposed by Heronemus (1972) as far back as 1972. In as much as Heronemus' vision was dated back to 1972, it was in the mid-1990s that floating offshore wind turbine (FOWT) started to be considered, and after that several configurations of floating support platforms are being developed for Offshore Wind Turbines (OWTs) and performance of the concepts tested by numerical and experimental methods (Wang et al., 2010, Zheng and Lei, 2018). In spite of the history of floating offshore wind turbines dating back over 50 years since conception, the technology is currently still in the pre-commercial stage of development as highlighted in GWEC (2022), with commercial phase annual installation expected to surpass 1 GW from 2026. In contrast, the fixed bottom foundation/platform is the dominant technology in the OWT sector (Zheng and Lei, 2018). This is reiterated in the Offshore Wind Market Report Musial et al. (2022) where the total operating global offshore wind (Fixed bottom platform + Floating platform) is 50.623 GW as shown in Figure 1. The total present operating floating wind capacity out of the 50.623 GW is only 123 MW as shown in Figure 2 – which implies a five-thousandth of the total offshore wind turbine installation is made up of FOWT concept. This statistic is expected to improve as detailed in Musial et al. (2022) and shown in Figure 1. Figure 1 shows the recent year 2022 total offshore wind capacity (fixed and floating platform) under planning is 200,391 MW. The statistics in Musial et al. (2022), highlighted in Figure 2 shows that the total floating foundation offshore wind capacity under planning is 60,206 MW – representing one-third of the total planned capacity of offshore wind turbines. This ratio is expected to improve with bespoke design concept, improved manufacturing, and extensive development of the floating offshore wind technology.

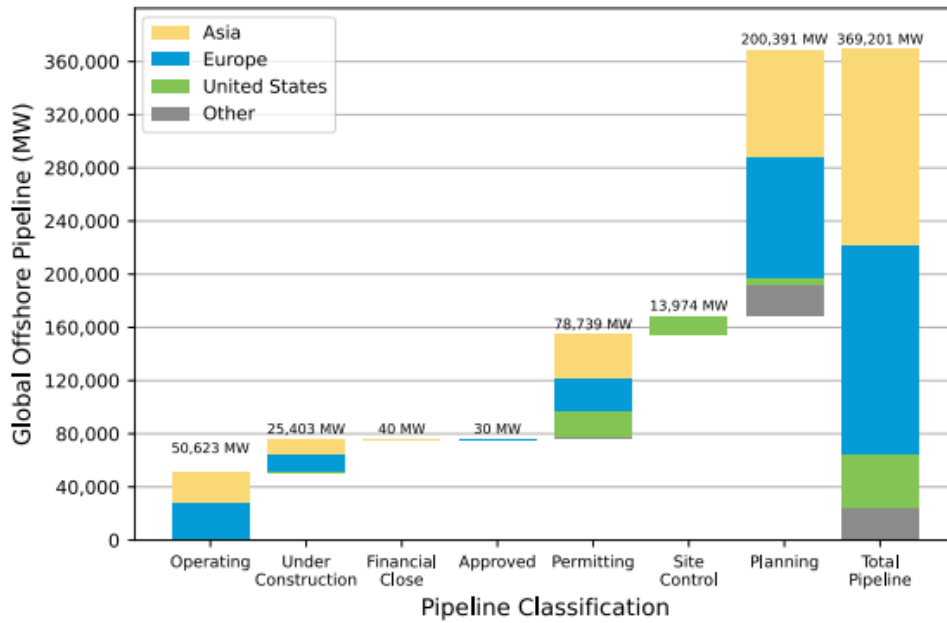


Figure 1. Total global offshore wind pipeline by regulatory status (Musial et al., 2022)

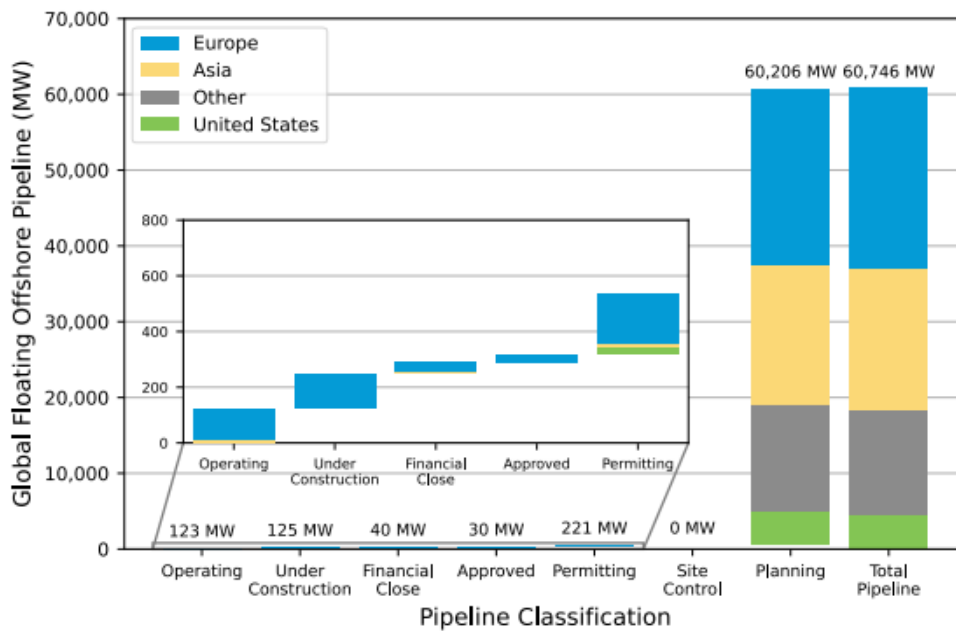


Figure 2. Total global floating offshore wind energy pipeline (Musial et al., 2022)

The adoption of floater concepts from the oil and gas industries has been a significant development for the offshore wind sector. The Spar, Semi-submersible, and TLP concepts have allowed for the economical generation of electricity from wind power in deeper offshore locations, providing a promising source of renewable energy. Some of the early FOWT platform concepts from the traditional oil and gas platforms are highlighted herein.

The FLOAT concept, a Spar concept floating wind turbine, was first presented in Tong (1998) with the objective of economically generating electricity from wind power in offshore locations with water depths of up to 100-300 meters. Similarly, the semi-submersible concept was adapted for floating wind turbines, with Henderson and Patel (1998) presenting analytical and numerical design tools to evaluate the performance of a semi-submersible floating wind turbine. Their focus was determining an optimum hull form for the floating system. They also developed analysis tools for the interaction of the motion in waves of the platform, with the turbine aerodynamic performance as well as the blade and hub loads.

The development of TLP floaters came after the spar and semi-submersible concept, with Withee (2004) performing a fully coupled time-domain simulation of the system responses for a 1.5 MW wind turbine mounted on a TLP floater with wind and wave forces. They showed the simulation results for surge free decay tests carried out to estimate the damping arising from the turbine rotor, and the wave and viscous damping arising from the buoy. Their findings showed that the two damping mechanisms arising from the turbine rotor and the buoy were comparable in magnitude.

Optimizing the substructure of a FOWT system is crucial in reducing capital expenditure (CAPEX), since it accounts for a significant percentage of the total cost. In comparison to fixed bottom wind turbines, FOWT systems can account for circa 29.5% of the capital expenditure (CAPEX), to a fixed bottom wind turbine accounting for 13.5% of the system's CAPEX (Ioannou et al., 2020). This highlights the need for more urgent optimization or geometric shape parameterization techniques to support in reducing the CAPEX cost of a FOWT platform.

Due to the complexity of the dynamic behaviour of FOWT systems, there is a need to balance the design and optimization of the substructures with computational cost (time) using Multi-Disciplinary Design, Analysis, and Optimization (MDAO) techniques. The optimization framework should make use of the appropriate model fidelity, including high fidelity, multi-fidelity / surrogates, and low fidelity models, to explore the design space efficiently. The selected model can then be verified with high-fidelity tools. This trade-off between optimization and computational cost is essential to ensure the optimal design of FOWT substructures. MDAO is a system engineering methodology that uses numerical optimization techniques to design and analyse multidisciplinary engineering systems like a FOWT system (Perez-Moreno et al., 2016). This tool is suitable for both present and future design and analysis requirements for conducting or executing the optimization of various multidisciplinary systems.

1.2 Research Question

As highlighted in Section 1.1, the offshore wind turbine sector is still in the pre-commercial stage with most of its design methodologies taken from the oil and gas sector. This is why the early to market floating platforms in the offshore wind sector are the ballast stabilized spar (Hywind Scotland) and the waterplane stabilized semisubmersible (Kincardine and Windfloat Atlantic wind farms).

The main question for this research is determining how a floating platform can be designed to minimize material used, meet hydrodynamic requirements and save design and analyses' computational time. This question is borne from the fact that the Hywind Scotland Spar floater – the world's first floating wind farm - is over-dimensioned for safety reasons, due to the low technology readiness level at the time (Leimeister et al., 2020b). Since the days of designing the Hywind Scotland wind farm, there has been substantial research to equip the industry with vital technical knowledge. A significant observation in the FOWT sector is that floating foundation designers are separate entities from the turbine manufacturers, i.e., foundation design and manufacturing companies like Ocergy and Stiesdal conduct their tasks separately from the turbines original equipment manufacturers leaving a gap between the foundation designers and the turbine OEM's. It is anticipated that shape parameterization within an MDAO framework can help bridge this gap if used by an independent entity from the foundation designers and the OEMs.

1.3 Research Aim and Hypothesis

The aim of this research is to develop a geometry shape optimization methodology within an MDAO framework to reduce the steel mass, and the design computational time for a bespoke geometric shaped FOWT platform coupled to a 5MW turbine.

The hypothesis of this research is that the developed framework is anticipated to reduce the mass of steel, which translates to economic reduction in the capital cost invested on floating platforms while also reducing the computational time. A critical factor that might increase the cost of the FOWT platform is the manufacturing cost that might be incurred for complex shaped structures. A continuous technological research and advancement in manufacturing with techniques like additive layer manufacturing (ALMs) is expected to nullify anticipated cost increase from manufacturing. In addition to the potential increase in cost from complex manufacturing, the complexity of the shapes might need redesigned when subjected to

structural assessment to estimate the fatigue life of the substructure. This research focused on the behaviour of the system with a detailed hydrodynamic response assessment as a criterion for selecting an optimal design. Other criteria like a detailed structural assessment, manufacturability and environmental impact were not considered. It is anticipated that considering a detailed structural assessment, there might be need to redesign the substructure with additional stiffness to meet the design life objective.

1.4 Objectives

The thesis aims to deliver the following objectives:

1. Conduct a review of multidisciplinary design analysis and optimization of floating offshore wind turbine substructure and an overview of parametrization techniques of the design using free-form curves.
2. Develop an automated MDAO framework integrating shape alteration free-form curves within the design loop to produce a bespoke platform shape.
3. Exploration and exploitation of optimal designs with bespoke shapes based on the objective functions and constraints specified in the frequency domain and verification of the constraints with a medium fidelity time domain tool.
4. Rank the free-form curves within the MDAO framework based on specified performance criteria using the Technique for Order of Preference by Similarity to Ideal Solution (TOPSIS) Multi-Criteria Decision Making (MCDM) technique.
5. Assess the impact the shape parameterization and MDAO framework have on the techno-economics of a floating wind farm with bespoke design concepts output from this research.

1.5 Novel Contribution to Knowledge

The main contribution to knowledge of this research is investigating the effectiveness of the parametric free-form curves integrated within a MDAO framework in reducing the mass of steel used in designing a floater.

Another contribution of this research is opening up a framework for the development of bespoke floater shapes other than the traditional shape from the oil and gas industry that meets fundamental design and analysis requirements of stability and allowable platforms' motion

response in operational sea states. This research also shows the potential reduction of the LCOE of a FOWF farm in comparison to the traditional spar buoy floating platform.

This research contributes to the knowledge of enhancing design systems through the application of shape parameterization techniques. These techniques can be used to modify the shape of an optimal design to augment the overall optimization of the system.

1.6 Thesis Structure

The thesis structure / flowchart is developed from the research aims and objectives highlighted in Section 1.4 and presented in Figure 3 with subsequent discussion in this section.

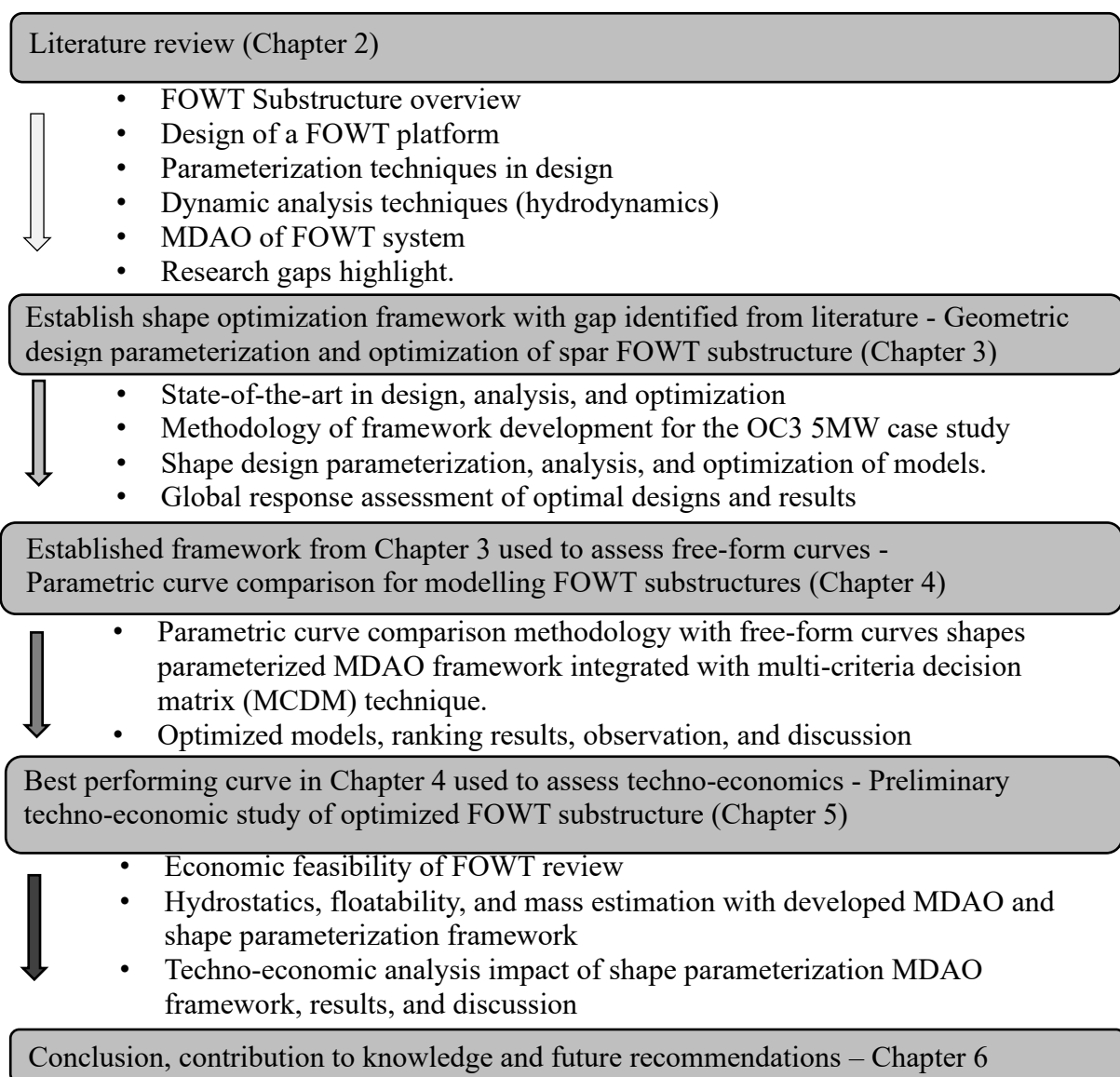


Figure 3. Thesis structure – Flowchart

This thesis is structured into Six Chapters. Chapter 1 examines the need for the FOWT concept and details the research questions and hypothesis of this thesis. In addition, Chapter 1 also highlights the research contribution and details the aim and objectives of this study to achieve the highlighted contribution.

Chapter 2 presents an in-depth literature review of MDAO approaches for floating substructures, detailing the design of the FOWT platform, the use of parameterization techniques in the design of a FOWT platform, and the dynamic analyses of offshore platform. Furthermore, Chapter 2 details the MDAO approaches for FOWT system highlighting the MDAO workflows, MDAO tools, and provides a comprehensive review of MDAO optimizers for FOWT substructures and MDAO work conducted for a FOWT system. Chapter 2 also identifies research gaps and proposed areas of research with the MDAO interfaced with a parametric free-form curve for bespoke floater designs.

Chapter 3 details the use of the NURBS curve for geometric alteration of the floater design within the MDAO framework, utilizing a gradient free pattern search optimization algorithm to explore and exploit the design space for the global optimum design. Chapter 3 shows the impact of the static pitch constraints and the geometric shape variation of the design on the mass of the optimal platform. Chapter 3 also utilizes the potential flow theory in the frequency domain, and the Cummins equation in the time domain to evaluate the hydrodynamic forces response on the FOWT system in severe sea states.

Chapter 4 investigates the performance and ranking of four parametric freeform curves integrated into the design phase of an MDAO framework utilizing gradient free optimization algorithm to explore the optimal design of a spar floater. This investigation made use of the TOPSIS MCDM technique to rank the performance of the free-form curves using criteria like estimated mass from MDAO framework, computation time, parametric continuity (slope and curvature), and nacelle acceleration assessment to determine the optimal alternative with the shortest distance to the positive ideal solution and hence, longest distance to the negative ideal solution.

Chapter 5 highlights the application of the geometric shape parameterization technique within the MDAO framework concept discussed in Chapter 3 and Chapter 4 on a hypothetical wind farm to assess the techno-economic feasibility of the farm with the bespoke shaped optimal floaters. The economic tool used in assessing the techno-economic feasibility of the farm is the Levelized Cost of Energy,

Chapter 6 provides a summary of this research work with elaboration on the contribution of the research to knowledge in industry and research while also detailing research conclusion and recommended future work.

1.7 Publications connected with this research

The articles (published and pending) developed during this research have been used to develop this thesis and are listed below:

1. Chapter 2 is developed on output from the journal article from Ojo, A., Collu, M., Coraddu, A., 2022a. Multidisciplinary design analysis and optimization of floating offshore wind turbine substructures: A review.
2. Chapter 3 is written with input from the pending journal article from Ojo, A., Collu, M., Coraddu, A. Geometric Design Parameterization and Optimization of Spar Floating Offshore Wind Turbine Substructure.
3. Chapter 4 is based on the journal article from Ojo, A., Collu, M., & Coraddu, A. (2023). Parametric curve comparison for modelling floating offshore wind turbine substructures.
4. Chapter 3 is supplemented with additional input from the article from Ojo, A., Collu, M., Coraddu, A., 2022b. Parametrisation Scheme for Multidisciplinary Design Analysis and Optimisation of a Floating Offshore Wind Turbine Substructure – OC3 5MW Case Study.
5. Chapter 5 is developed with output from the pending article from Ojo, A., Collu, M., Coraddu, A. Preliminary Techno-Economic Study of Optimized Floating Offshore Wind Turbine Substructure.

Chapter 2 Literature Review

2.1 Background

This chapter is primarily based on the publication by Ojo, A., Collu, M., Coraddu OJO, Multidisciplinary design analysis and optimization of floating offshore wind turbine substructures: A review Ojo et al. (2022a)

The study of a floating offshore wind turbine system is best conducted using a multidisciplinary approach that takes into consideration the aerodynamics, hydrodynamics, servo-dynamics, and elasto-dynamic aspects of the system. To produce an optimal design of a FOWT platform requires adequate consideration of the other components that make up the FOWT system. As highlighted in Chapter 1, it was in the mid-1990s that FOWT started becoming a widespread concept after which several configurations of floating support platforms are being developed for OWTs and performance of the concepts tested by numerical and experimental methods (Wang et al., 2010, Zheng and Lei, 2018).

Since the early days of OWT floater concepts borrowed from the oil and gas industry (Spar, Semi-submersible and TLP), extensive systems engineering analyses have been conducted in literature, and it was not until 2017 that the first commercial floating offshore wind farm went operational (WindEurope, 2019). However, with the world in urgent need to reduce the carbon emission footprint, to revert the existing trend of global warming and the need to reduce the levelized cost of electricity generated from wind, there have been increasing interest in the floating foundation/support for wind turbine system in recent years (Wang et al., 2010). Also, as offshore wind turbine installation frontiers gradually move into deeper waters with abundant and high-quality wind resources, the need for FOWT system has become imperative as the reliable fixed support/monopile foundation offshore wind turbines become very cost prohibitive in such environmental conditions (deep water > 60m) - Leimeister et al. (2018); Lefebvre and Collu (2012) and Spearman and Strivens (2020).

As highlighted in Chapter 1 and detailed in Ioannou et al. (2020), the substructure/platform for a FOWT system can account for circa 29.5% of the capital expenditure (CAPEX), while the corresponding substructure of a fixed bottom wind turbine accounts for 13.5% of CAPEX of the system (Ioannou et al., 2020); hence, the need for optimization or conducting a geometric shape parameterization technique with optimization on the substructure of the FOWT system to provide efficient means of reducing the costs is deemed more urgent than for offshore fixed bottom wind turbines. In addition, due to the complexity of the dynamic behaviour of a FOWT

system, there is need to balance the design and optimization of the substructures and the computational cost (time) with adequate optimization framework using the design, analysis, and optimization within a multidisciplinary framework technique (MDAO). Balancing the optimization process of the FOWT substructure with the computational cost is a very important trade-off, that should be considered in the MDAO framework of FOWT substructure. Ensuring the balance is to make use of the right model fidelity (high fidelity, multi-fidelity/ surrogates, and low fidelity models) to explore the design space. Any selected model can subsequently be verified with a high-fidelity tool.

A FOWT is an engineering system with a multidisciplinary set of complex subsystems, as indicated in Figure 4. These kinds of complex systems, in other industries, have successfully been optimized adopting a MDAO approach. As detailed in Chapter 1, MDAO is a system engineering approach with the capability designing, analysing and optimizing a multidisciplinary system.

MDAO is advantageous as it permits designers and engineers to incorporate all necessary disciplines simultaneously to explore the design and analysis space and select the optimal solution. This is a much superior approach to the sequential design and analyses process as it can exploit the integration and interface between disciplines. It is also a much quicker approach in comparison to when each discipline is treated as a standalone, and where the necessary links among disciplines are often implemented manually. However, simultaneous inclusion of multi-disciplines increases the complexity of the problem and poses some challenges. To execute an MDAO involves overcoming design and analysis challenges amongst which are design parameterization, computational time from modelling techniques, and exploration of design space (Sclavounos et al., 2008). Overcoming the challenges requires an optimization framework that uses the right model fidelity within the MDAO framework to solve the problem.

This review focuses on platform part of the FOWT substructure (platform, anchors and mooring system) as defined in the International Electrotechnical Commission's technical specification (IEC-61400-3-2, 2019)



Figure 4. Floating Offshore Wind Turbine System, adapted with permission from (Jonkman and Matha, 2011)

2.2 Floating Offshore Wind Turbine Substructure Overview

The three-floating substructure/platform configurations borrowed from the oil and gas industry as highlighted in Chapter 1 are the spar, semi-submersible, and tension leg platform (TLP). Floating substructures/platforms are classified based on the primary mechanism adopted to attain the static stability requirements (Borg and Collu, 2015, Taboada, 2015). The three main stabilizing mechanisms are the ballast stabilizing mechanism, waterplane or buoyancy stabilizing mechanism, and the mooring stabilizing mechanism, discussed in detail in (Borg and Collu, 2015, Taboada, 2015) while the advantages and disadvantages of each substructure configuration are detailed in Bashetty and Ozelik (2021) and highlighted below:

- **Ballast stabilized platforms**

A typical example of a ballast stabilized platform is the spar. This category of platform relies mainly on heavy ballast mass located at a deep draft, to ensure the platform's centre of mass is well below the centre of buoyancy, to produce a large restoring moment which counteracts rotational displacements. Some advantages of a ballast stabilized spar are simple design geometry, higher stability, and low wave induced motion on the structure, while amongst its disadvantages are higher fatigue loads in tower and its deep-water requirements for installation.

- Buoyancy stabilized platform

The semi-submersible platform is mostly classified as a buoyancy stabilized platform. This class of platform uses the waterplane area to ensure stability of the system. A large second moment of waterplane area is suitable to raise the metacentre of the platform above the centre of mass to ensure platform stability. Advantages of a buoyancy stabilized semi-submersible includes low draft requirements, low mooring costs, transportation ease to installation site and adequate suitability for deep-water utilization. Some of its disadvantages are its susceptibility to higher wave induced motions and the structural design are complex with several columns and braces.

- Mooring stabilized platform

TLP represents the mooring stabilized platforms. This category of FOWT platform uses taut vertical mooring lines to ensure the stability of the buoyant platform. These high tensioned lines can generate a restoring moment to counteract any inclination of the platform. Advantages of this class of substructures are the reduction in mass of steel required for construction and ease of assembly and commissioning onshore before transportation for installation offshore. Main disadvantage lies in the cost of the Taut mooring line which increases with respect to the water depth.

Research on the concept of non-operational stability requirement of FOWT was conducted by Collu et al. (2014). In this work, they proposed a set of guidelines to analyse the assembly and other temporary phases i.e. when turbine is assembled on the floating platform, the transport phase to the operational site and commissioning at operational site. The guideline was applied to the design of a floating support structure (semi-submersible) for the Novel Vertical Axis wind turbine NOVA (Collu et al., 2014), exploring their impact on the floating support structure design and evidencing an overall good performance. The application of the proposed rule to the selected test case showed that it is a sound starting point to assess the stability in the non- operational phase.

The three platform types under the stability requirement mechanism discussed are highlighted in Figure 5 a, b and c. representing the mooring line stiffness stabilized, the ballast stabilized and the buoyancy/waterplane stabilized platforms respectively (Karimi et al., 2017). The mathematical model of the inclining and restoring moment's physics is detailed in Borg and Collu (2015).

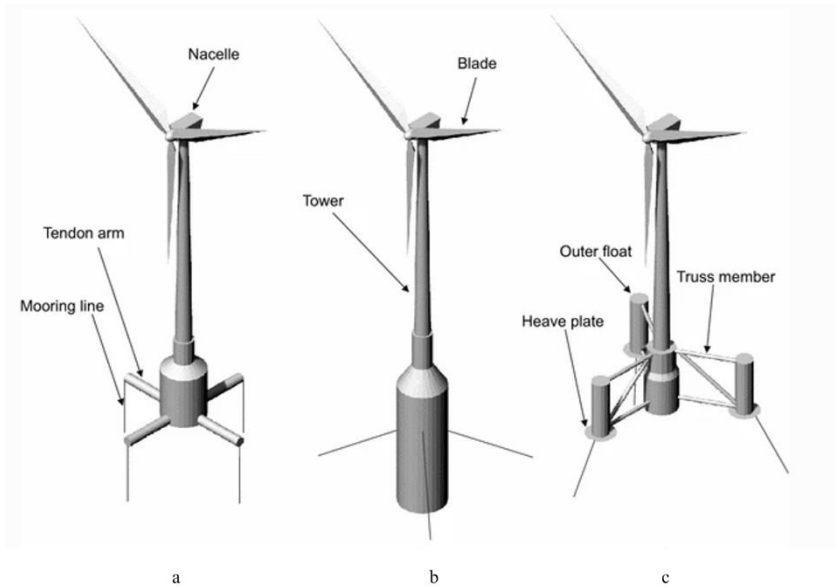


Figure 5. Floater classification based on stability mechanism (Karimi et al., 2017): From left to right – TLP, Spar and Semi-submersible

The dynamics of the floaters also vary because of the various mooring systems (tendons for TLP; catenary mooring for spar, semi-submersible, and barge) (Taboada, 2015). The natural frequencies for catenary-moored floaters are lower than the range of wave frequencies, while for the TLP, the natural frequencies for heave, roll, and pitch are higher than the first order wave load frequencies. Representative natural frequencies of the three platform types are highlighted in Table 1.

Table 1. Natural frequencies of floater types (Taboada, 2015)

| Degree of Freedom | Spar (Hz) | Semi-submersible (Hz) | TLP (Hz) |
|-------------------|-----------|-----------------------|----------|
| Surge | 0.02 | 0.02 | 0.04 |
| Sway | 0.02 | 0.02 | 0.04 |
| Heave | 0.07 | 0.07 | 0.44 |
| Roll | 0.05 | 0.05 | 0.43 |
| Pitch | 0.05 | 0.05 | 0.43 |
| Yaw | 0.02 | 0.02 | 0.04 |

Apart from the Spar, Semi-submersible, and the TLP platforms mentioned above, new and unique geometrically shaped platforms for the FOWT sector are being developed. Examples of these unique platform designs are the IDEOL “damping pool” barge platforms with the waterplane area stability mechanism, the TetraSpar floating concept, and the Hexafloat with

the ballast mass stability mechanism (Ghigo et al., 2020). The Floatgen IDEOL barge concept is an altered barge design that uses a moonpool, also referred to as damping pool system, for motion reduction (Leimeister et al., 2018). The Hexafloat is a floating concept developed by Saipem. It is a pendulum lightweight structure composed of a submersible floater made of tubular elements, a counterweight connected to the floater with tendons, simple mooring lines with drag anchors, and a lazy wave dynamic cable (Ribuot, 2019). The TetraSpar floating concept was developed by Stiesdal Offshore Technologies A/S. This concept aims to provide a low-cost FOWT platform that can be easily installed in any condition; hence, contributing to low cost of electricity in comparison to bottom-fixed OWT (Stiesdal, 2021). Depending on the site conditions, the TetraSpar can be configured as a semi-submersible, as a Spar (pendulum configuration), or as a TLP.

All these platform concepts – Spar, Semi-submersible, TLP, Floatgen IDEOL, Hexafloat are designed using optimization indicators / constraints. Common optimization objectives or problems in an optimization framework are minimizing the cost of the system and the LCOE, improving the performance of the system like the nacelle acceleration, system's dynamic response and fatigue. The objective functions / optimization problems are resolved by specifying constraints to the problem. These constraints are important for effective exploration by limiting the design space, improving computational time and optimization accuracy. Some of the constraints taken into consideration in the design and optimization of a FOWT substructure are; costs, static pitch angle, dynamic pitch angle and slackness in mooring lines as detailed in Hall et al. (2013).

2.3 Design of a FOWT Platform

The design procedure for a FOWT substructure follows the general engineering design process of preliminary / concept design followed by a detailed design of the selected concept (Friedemann Borisade et al., 2016). Some of the requirements for a successful support structure design are well detailed in DNV-OS-J101 (2013), DNVGL-ST-0119 (2018) and highlighted below:

- Ensure design stability in intact conditions.
- Ensure a suitable range of eigenfrequencies to avoid resonance with excitation forces from rotor, first-order and higher orders wave forces.
- Maximum offsets or displacements and limits on dynamic motions.

- Ensure safe operation of wind turbine during the design life of the turbine.
- Maintain acceptable safety for personnel and environment.
- Ensure adequate fatigue strength for 20 to 30 years operation of the system.

2.3.1 Preliminary/Concept Design

It is an iterative process that begins with concept selection or preliminary design. This is followed by a more detailed design and analysis of the loads and the system's response to ensure the structural strength is sufficient to withstand the load effects (DNVGL-ST-0119, 2018).

As discussed in Borg and Collu (2015), Kolja Müller and Simon Tiedemann (2017) and Lefebvre and Collu (2012), the preliminary design of a floating substructure is divided into two stages, which are the preliminary sizing of the support structure's concept, and the design for further development and refinement. The main requirements to fulfil when sizing is the hydrostatic stability requirements which are:

- Support structure must ensure floatability
- A maximum pitch/roll angle of 5 degrees for static equilibrium and a maximum dynamic angle that does not exceed +/- 15 degrees in order not to substantially compromise the performance of the FOWT (Borg and Collu, 2015). As mentioned in Borg and Collu (2015), this is only a guideline.
- Maximum floater offset or floater excursion in surge including static, first and second order loads is less than 50% of the water depth (Kolja Müller and Simon Tiedemann, 2017).

Other drivers to consider are the site conditions / metocean data designed for extreme driven ultimate limit state (ULS), turbine weight and inertias, and the thrust force on the turbine (Friedemann Borisade et al., 2016).

The preliminary sizing is based on two equations: the buoyancy force equation detailed in Lefebvre and Collu (2012) and the restoring moment equation detailed in Collu and Borg (2016). Both equations are also detailed in Chapter 5 of this Thesis (Equations (17) and (18)). The buoyancy force acting on the FOWT system is equivalent to the weight of the turbine and weight of the support structures (tower, platform, and mooring lines) while the restoring moment in roll/pitch is a summation of water plane stabilization parameters, ballast stabilization parameters and mooring stiffness discussed in Section 2.2.

An iterative method is used to solve the set of buoyancy force equation and restoring moment equation based on the substructure's geometry to select the concept for detailed design. The iterative method can also be in the form of optimizers to explore the design space based on design objectives like platform's motion response and platform's mass to select the optimal design concept.

2.3.2 Detailed Design

For a detailed design assessment, the preliminary design is refined to ensure the structural strength has been improved in intact conditions (Lefebvre and Collu, 2012). Due to the complexity of FOWT as an engineering system, its design must be governed by adequate industry's technical standards and guidelines. The most widely used design standards for FOWTs are Det Norske Veritas (DNV) (DNVGL Oslo, 2018, DNVGLAS, 2016, DNVGL-RP-0286, 2019, DNVGL-SE-0422, 2018, DNVGL-ST-0119, 2018, DNV-OS-J101, 2013), American Bureau for Shipping (ABS) (ABS, 2014, Updated July 2020.), Bureau Veritas (BV) (Veritas, 2010, Veritas, 2015, Updated 2019), Class NK (Kyokai., 2012) and the International Electrochemical Commission (IEC) (IEC-61400-1, 2014, IEC-61400-3-2, 2019, IEC-61400-3, 2009). The methodology used for most of the design standards highlighted is the "load and resistance factor design". The aim of this approach is to obtain design within the adequate safety level by considering safety factors to account for uncertainties in both structural load and structural resistance (Bachynski and Collu, 2019, DNV-OS-C105, 2008). In their work, Collu and Borg (2016) discussed the classifications criteria of the support structures based on existing codes and standards verification societies: BV (Veritas, 2010), ABS (ABS, 2015, Updated March 2018, 2020) and DNV (DNV-OS-J101, 2013).

BV (Veritas, 2010) adopts the classification criterion based on the floating platform's stability mechanisms i.e., ballast stabilized floating platforms (spar-buoy), buoyancy stabilized floating platforms (semi-submersibles and barges), and tensioned stabilized platform classes (TLP).

ABS (ABS, 2015, Updated March 2018, 2020) adopts the classification criterion based on the structural elements of the different floating substructure, without expressly defining the stabilizing mechanism.

For the DNV offshore standard, the criteria are based on whether a structure is restrained (displaced in the order of centimetres) or compliant (displaced in the order of meters or more).

An overview of the analysis approach for detailed design is provided in Jonkman and Matha (2011) and highlighted below:

1. Develop a model of each complete system with a comprehensive simulation tool capable of modelling the coupled dynamic response of the system from combined wind and wave loading. This form of modelling requires the application of comprehensive aero-hydro-servo-elastic simulation tools that incorporate integrated models of the wind inflow, aerodynamics, hydrodynamics (offshore systems), control (servo) dynamics and structural (elastic) dynamics in the time domain in a coupled nonlinear simulation environment. Some of the available commercial simulation and modelling tools for FOWT system are: DNV suites (Genie, HydroD, WADAM, SIMA), Ansys Aqwa, Nastran, Orcaflex. An important open source simulation and analysis tool is OpenFAST code, developed by (Jonkman, 2007). It enables medium-high fidelity model analysis and verification in the time domain.
2. Verify elements of each full system dynamics model from step 1 by checking its response predictions with responses predicted by a simpler model. When modelling a floating wind turbine, it is advantageous to check the sophisticated nonlinear time domain model against a much simpler linear frequency domain model. This kind of check can be made in terms of response amplitude operators (RAO) of system motions and loads for excitation by regular waves or in terms of probability distributions of system motions and loads for excitation by irregular waves.
3. Using each full system dynamics model from step 1, a comprehensive loads analysis is performed to identify the ultimate loads and fatigue loads expected over the lifetime of the system. Loads analysis involves running a series of design load cases (DLCs) covering essential design-driving situations, with variations in external conditions and the operational status of the system.
4. Improve each floating system design through design iteration of the above steps, ensuring that each of the system components is suitably sized through limit-state analyses.

2.4 Parameterization Techniques in Design

The main objective of parametric modelling is to prescribe the properties of a structure (Birk, 2006). This process reverses the flow of traditional structural modelling with interactive CAD systems. Parametric modelling approach starts with specification of the desired form parameters and properties. This is passed to the parametric modelling system for the evaluation of unspecified properties and return of evaluated data to the user with little or no user

interference (Birk, 2006). Some shape parameterization techniques from other industries and parameterization work in the offshore wind sector are highlighted below.

2.4.1 Shape Parameterization Review

Shape parameterization is an important concept in design. It facilitates the exploration of a conceptual design space and provides informed knowledge to make design decisions. Geometric shape parametric modelling cuts across all areas of design and has been widely researched in the aerospace, automotive, construction, architecture, manufacturing, and civil engineering sectors. Shape parameterization techniques review has been extensively conducted in the aerospace geometric design sector as detailed in the works of Samareh (1999), Samareh (2001) and Kulfan and Bussoletti (2006). For offshore hydrodynamic models, the application of shape parameterization techniques for design, analysis and optimization can be seen in works done by (Birk and Clauss (2002), Birk et al. (2004) and Birk and Clauss (2008)). Some of these techniques are from sectors like the aerospace and are highlighted in this section. Properties of a well conducted parameterization method as discussed in the works of Kulfan and Bussoletti (2006), Samareh (2001) and Zhu (2014) are:

1. Provide high flexibility to cover all the potential solutions in the design space.
2. Give as small number of design variable as possible.
3. Produce smoothness and reliability of geometric shapes.
4. Provide correct design parameters for geometric and physical understanding in design space exploration by the engineers.

An overview of some of the shape parameterization techniques are highlighted in sections 2.4.1.1 to 2.4.1.3.

2.4.1.1 Free Form Deformation (FFD)

FFD dates to the mid nineteen eighties. Algorithms for morphing images and deforming objects are quite common in the field of soft object animation (SOA) in computer graphics (Sederberg and Parry, 1986, Jamshid, 1999). SOA algorithm can serve as the basis for an efficient FFD shape parameterization technique. These algorithms (SOA) are powerful tools for modifying shapes as they use high-level shape deformation rather than manipulating lower geometric entities (Jamshid, 1999). The SOA algorithms treat the model as rubber that can be twisted, bent, tapered, compressed, or expanded, while retaining its topology (Samareh, 2001). The SOA algorithms relate the grid-point coordinates of an analysis model to a number of

design variables (Jamshid, 1999, Samareh, 2001). Coppédé et al. (2018) proposed a new approach for hull shape modification. Their proposal is based on a combination of the Subdivision Surface technique for hull surface modelling and FFD algorithm for shape variation. In their work, a transformation made of two FFDs on a fast ferry was analysed with respect to both local and global relevant geometric parameters. The results and the quality of the modified surfaces prove that the proposed combined SS-FFD approach can be applied for further specific design and variation studies like an automatic ship design by optimization process, where reduction of number of parameters is a key feature for faster convergence.

2.4.1.2 CAD-Based Approach

The use of commercial CAD systems for geometry modelling can potentially save development time for a multidisciplinary design optimization application; however, parameterizing an existing CAD model is still a challenging task as the models created can be deficient for automatic grid generation tools (Townsend et al., 1998). The use of feature-based solid modelling (FBSM) capable of creating dimension-driven objects in today's CAD system coupled with the geometry modelling allows designers to work in three-dimensional space while using topologically complete geometry that can be modified from the dimensions of the features from which it was created (Jamshid, 1999, Samareh, 2001).

Although the use of parametric modelling in design would make the FBSM tools ideal for optimization, existing FBSM tools are not capable of calculating sensitivity derivatives analytically (Samareh, 2001). Issues involved with the use of a CAD system for an MDO application are discussed in Townsend et al. (1998). Some of the issues identified are allowing for replacement of the CAD system when required and determining the analytical sensitivity derivatives required by a gradient-based optimizer.

Due to the large computer codes for commercial CAD systems, to differentiate the entire system with automatic differentiation tools may be very challenging, hence, the calculation of the analytical sensitivity derivatives of geometry with respect to the design variables could prove to be challenging within a commercial CAD environment (Townsend et al., 1998). For some limited cases, the analytical shape sensitivity derivatives can be calculated based on a CAD model (Jamshid, 1999, Samareh, 2001); however, this method will not work under all circumstances. One difficulty is that, for some perturbation of some dimensions, the topology of the CAD part may be changed. To control the dimension and topology effectively requires the use of polynomials and splines.

2.4.1.3 Polynomials and Spline Techniques

Polynomial and splines have been vastly used in engineering design, from the aerospace and automobile sectors to naval architecture and most CAD modelling are based on splines. The number of variables needed to generate a smooth shape can be greatly reduced by using a polynomial or spline representation (Samareh, 2001). Polynomials also have the capability of describing a curve in a compact form with a reduced set of design variables. It can be expressed in its standard power basis form shown in Equation (1).

$$\bar{R}_{(U)} = \sum_{i=0}^{n-1} \bar{C}_i u^i \quad (1)$$

Where \bar{C}_i is the coefficient vectors corresponding to three-dimensional coordinates in which their vector components can serve as design variables; \bar{R} is geometry sensitivity derivative with respect to \bar{C}_i and u^i . In this representation, the coefficient of vectors provides little geometric information about the shape of the curve. This polynomial representation in the power basis form is prone to round-off error when there is a large variation in the magnitude of coefficients (Straathof, 2012). It is difficult to predict how a change in the coefficient vector \bar{C}_i will influence the overall shape of the polynomial curve.

An improved representation of a polynomial curve is done through the Bezier representation highlighted in Equation (2).

$$\bar{R}_{(U)} = \sum_{i=1}^n \bar{P}_i B_{i,p}(u) \quad (2)$$

Where n is the number of control points, $B_{i,p}(u)$ is the degree p Bernstein polynomials, the coefficients \bar{P}_i are control points also utilized as design variables. The Bezier form is a much-improved representation of curves than the power basis (Farin, 1993b).

Although, the Bezier form and the power basis are mathematically equivalent, the computation of Bernstein polynomials which is a recursive algorithm (de Casteljaou algorithm) minimizes the round off error in the Bezier curve (Farin, 1993a, Samareh, 2001). In a Bezier curve, the control points approximate the curve as the convex hull of the Bezier control polygon contains the curve. The first and last control points in a Bezier curve are located at the beginning and the end of the curve respectively. The Bezier curve is a suitable representation for shape optimization and parameterization of simple curves.

Complex curves, however, requires a high degree Bezier form and as the degree of a Bezier curve increases, so does the roundoff error (Samareh, 2001). In addition, computing a high degree Bezier curve is computationally expensive and inefficient. As described in Samareh (2001), several low-degree Bezier segments can be used to represent a complex curve rather than using a high degree Bezier curve. The resulting composite curve is a spline more accurately referred to as B-spline. A multisegmented B-spline is described in Equation (3).

$$\bar{R}(u) = \sum_{i=1}^n \bar{\mathbf{P}}_i N_{i,p}(u) \quad (3)$$

Where $\bar{\mathbf{P}}_i$ are the B-spline control points, p is the degree, $N_{i,p}(u)$ is the i th B-spline basis function of degree p . In comparison to the Bezier representation, the low degree B-spline form can represent complex curves more efficiently and accurately. In Equation (2), the Bernstein polynomials $B_{i,p}$ is replaced by a set of B-spline basis functions $N_{i,p}$ and the Bernstein coefficient vector $\bar{\mathbf{P}}_i$ replaced by a B-spline control polygon $\bar{\mathbf{P}}_i$. A disadvantage of a regular B-spline representation is that it doesn't have the capability to represent implicit conic sections accurately. A different type of B-spline with the capability of rectifying this deficiency is Non Uniform Rational B-spline (NURBS) (Farin, 1990). NURBS can represent most parametric implicit curves without loss of accuracy (Farin, 1990, Samareh, 2001). A NURBS curve is defined as highlighted in Equation (4).

$$\bar{R}(u) = \frac{\sum_{i=1}^n \bar{\mathbf{P}}_i W_i N_{i,p}(u)}{\sum_{i=1}^n W_i N_{i,p}(u)} \quad (4)$$

Where $\bar{\mathbf{P}}_i$ are the control points, W_i are the weights and $N_{i,p}(u)$ is the i th B-spline basis function of degree p . non-uniformity allows some segments of a defined shape (between any two points) to be shortened or elongated relative to other segments in the overall shape. Rationality allows the ability to give more weight to some points in the shape than to other points in considering each positions relation to another object. A similarity between Basis, Bezier, regular B-spline and NURBS representation of curves is that the sensitivity derivatives with respect to the control points are fixed during optimization cycles. However, in a NURBS scenario, if the weights are selected as design variables, the sensitivity derivatives will be functions of the weight design variables (Samareh, 2001).

2.4.2 Parameterization work in other sectors

Various state-of-the-art parametric modelling techniques have been used in different sectors, ranging from the automobile, aerospace, maritime and oil and gas, to advance design and optimization process. Some of the aforementioned works are discussed in this section.

Harries and Nowacki (1999) contributed to the field of preliminary ship design by introducing a new approach to the geometric modelling of hull forms. The approach is based on form parameters, i.e., design relevant descriptors of the envisioned shapes. B-spline curves and surfaces are used to represent the hull's geometry. The modelling process is viewed as an optimization problem in which fairness measures are applied as quality criteria, form parameters are met as equality constraints and B-spline vertices are treated as free variables. By replacing the currently prevailing design methodology of purely interactive point manipulation, the new parametric method offers the capabilities for quick and accurate shape generation and variation while inherently producing excellent fairness, hence offering the essential requirements for the improvement of a ship's hydrodynamic performance.

Nam and Parsons (2000) designed the hull surface using the NURBS approach while considering the hull's major dimension and other parameters. Nam and Bang (2017) built an intermediate curve represented by NURBS to meet the specified geometric requirements in relation to the hull characteristic line.

Pérez et al. (2008) investigated the use of simple parametric design method for generation of simple hull lines in sailing ship hulls and round bilge hulls. The presented method starts with the generation of an offset-based representation, which meets certain hydrodynamic coefficients imposed by the designer. These coefficients are based on the sectional area curve and on the waterplane. This is done with the use of explicit curves and completed with an automatic surface modelling (lofting) from the NURBS parametric curves. The hull shape thus generated can be exported to naval architecture programs or can be used for CFD evaluation and be the initial case of an optimization process.

Katsoulis et al. (2019) presented a T-splines-based parametric modeller (TshipPM) for complex ship forms with the capability to provide smooth geometries at a low cost in comparison with parametric modellers (PM) employing the standard NURBS representation. The TshipPM affords the flexibility for representing challenging areas of the ship-hull geometry, such as bow, stern and the transition areas from mid-ship towards forward and afterward perpendiculars.

Moreno (2021) investigated and described the development of a regular hull meshing code

using cubic B-Spline curves. The discretization procedure starts with the definition of B-Spline curves over stations, bow and stern contours of the hull plan lines.

Zhou et al. (2022) achieved the parametric geometric deformation of the Series 60 ship by first analysing the hull geometric features and parameters, design the longitudinal feature curves and cross-section curves based on the NURBS technique, and establish the correlation between them. With this, they established a NURBS-based parametric modelling process for ship hull form, and the development of a parametric geometric model of a ship is completed with a Series 60 ship as an example. They generated the smooth hull surface by using the skinning technique and their study demonstrates that the NURBS-based parametric design method produces smoother surfaces.

Pérez et al. (2007) made use of the cubic B-spline curves to construct the body plan of bulbous bow subject to certain form parameters and the B-spline surfaces that fit these curves were constructed. The initial hull with bulbous bow generated from the method is optimized with CFD-based optimization method.

Yang (2016) applied the NURBS-based modification technique to the optimization of a series of Joint High-Speed Sealift with different bow configuration.

Kim and Yang (2013) applied the shifting method and the Radial Basis Function (RBF) method to move the NURBS control points of their hull model (Model 5279 hull) to achieve the global and local deformation of ship hull forms. This approach yielded an optimal hull with a bulbous bow and a stern end bulb.

Qi et al. (2018) developed a NURBS based hull surface modification method and integrated it with an in-house solver OPTShip-SJTU for the hydrodynamic optimization of ship hull forms. The developed method is applied to the hydrodynamic optimization of Series 60 model. The optimization results show the developed method is efficient and flexible for the deformation of hull surfaces and is suited for the optimization of real-life ship.

Jamshid (1999), Samareh (2001) conducted a literature review on form parameterization techniques for multidisciplinary optimization. The survey focuses on the suitability of available techniques for complex setups with suitability criteria based on ease of implementation, effectiveness, and efficiency. This survey highlights the design modelling concept of polynomial splines and free form deformation as effective tools for design modelling for numerical analysis.

2.4.3 Parameterization work on FOWT support structures

Most of the parameterization techniques used in designing FOWT platforms mainly alters the radii, draft, length, or breadth of the platform as discussed in Wayman (2006). This approach mainly serves to increase or reduce the whole platform or a section of the platform – more of holistic scaling or sectional scaling.

Wayman (2006) took early steps in the development of innovative cost-effective floating platforms to support 5MW wind turbines in water depth of 30m to 300m by developing an analysis tool in frequency domain for performing a coupled structural, aerodynamic, and hydrodynamic analysis on the floating wind turbine system. This work was progressed by Tracy (2007) in a study presenting a fully coupled dynamic analysis of floating wind turbines that enables a parametric design study of the floating wind turbine concepts and the mooring systems. They showed a Pareto optimal design that has a favourable combination of nacelle acceleration, mooring system tension, and displacement of the floating substructure supporting a 5 MW wind turbine. Their findings demonstrate that the Pareto optimal structures for a fully coupled dynamic analysis of the wind turbine, the floating substructure, and the mooring system, considering both wind and sea state environmental conditions, are typically either a shallow barge ballasted with concrete or a narrow deep drafted spar. The parameterization done in Tracy (2007) only holistically varies the draft and the diameter of the floating platform; hence, limiting the design space that can be explored.

Rahmdel et al. (2016) conducted a parametric study of spar-type floating offshore wind turbines by numerical investigations with the aim of conducting dynamic response analysis and developing design guidelines for spar FOWTs. They numerically obtained the dynamic responses of full-scale spar-type FOWT models with different values of three design variables (spar diameter, depth, and concrete ratio) in the time domain, and then experimentally validated their results by considering environmental conditions like wind, regular wave, and constant current loads, as well as the mooring line loads. Then, regression and perturbation analyses, which were also validated by the analysis of variance method, were performed to analyse the effects of the design variables and to propose design guidelines of spar-type FOWTs.

Another work on FOWT parameterization and optimization can be traced to Sclavounos et al. (2008). In this work, they presented a coupled dynamic analysis of floating wind turbines incorporating a parametric design study of floating wind turbine concepts and mooring system. They presented a Pareto optimal design that has a favourable combination of nacelle acceleration, mooring system tension, and displacement of the floating substructure supporting

a 5 MW wind turbine. Their results show that, for a fully coupled dynamic analysis conducted for the wind turbine, the floating substructure and the mooring system, considering both wind and sea state environmental conditions, the Pareto optimal structures are generally either a narrow deep drafted spar or a shallow barge ballasted with concrete. The varying parameters for this work are the holistic draft and diameter of the platform.

It can be observed from the examples provided that the parametric approach is mainly holistic varying of platform diameter and draft. To apply geometric shape parameterization technique, there is need to look at other offshore sectors like the oil and gas and maritime sectors. In their study, Zhang et al. (2008), noted that a successful hydrodynamic optimization of ship hull depends on the geometric variation of hull planer forms. The parametric design of hull forms involves; specifying form parameters, design of a set of longitudinal curves, parametric modelling of sections which forms the body parts and generating hull forms (Zhang et al., 2008). This curve parameterization technique has been successfully used in the design of ship hulls, and can be implemented in the design of FOWT platforms.

Ghigo et al. (2020) conducted platform optimization and cost analysis in a floating wind farm. The focus of their work is on the choice of floating platform that minimizes the global weight to reduce the material cost while ensuring buoyancy and static stability design requirement. Their study produced a new concept which is a variant of the Hexafloat platform concept with a notable change being the removal of all lateral brackets of the Hexafloat concept. This concept achieves the objective of the study which is to reduce the steel weight of the platform and lower investment cost in a wind farm project.

To further enrich the design space, there is need for effective control of the design variable not just from global / holistic shape control but local control of the shapes of the structure. To achieve this objective, Birk (2006) introduced the polynomial spline parametric modelling technique. This work was started over a decade earlier as hydrodynamic shape optimization of large offshore structures by the same authors (Clauss and Birk, 1996). Birk (2006) was able to present an optimization system / framework which integrates spline parametric modelling tools, numerical modelling tools – potential flow theory and controlled with optimization algorithm with specified objectives and constraints that enables the system to design offshore structure hulls with superior seakeeping qualities. This idea has been applied to a spar floating offshore wind turbine substructure by Ojo et al. (2022b). They used the B-Spline parameterization modelling technique to enhance the FEDORA multidisciplinary analysis (MDA) in-house framework, developed by researchers at Strathclyde University, which uses a

simpler parameterization scheme to discover unique configurations with reduced structural mass that leads to cost savings. The FEDORA MDA is integrated with the pattern search optimization algorithm tool in MATLAB for the optimal selection of designs describing rougher shapes. The B-spline library from Sesam GeniE is used to model each design representation, and a potential flow frequency domain analysis solver (HydroD/WADAM) is used for the hydrodynamic analysis. Validation of the selected designs within the design space is conducted with a benchmark NREL5MW spar hydrodynamic response results in literature with the hydrodynamic response of the frequency domain modelling approach using Sesam GeniE and HydroD/WADAM.

2.5 Dynamic Analysis Techniques

There are two primary methods for analysing the dynamics of a FOWT system: frequency domain analysis and time domain analysis. Both approaches are instrumental in assessing the dynamic response of the structure, especially in response to wind and wave forces that induce oscillatory motions in the FOWT system.

2.5.1 Frequency Domain Approach

The frequency domain approach has been extensively used in the oil and gas industry, as it enables the assessment of the system's wave response spectrum given the wave spectrum of the site and the response amplitude operator (RAO) of the given system (Journée and Massie, 2000, Patel, 2013). For a FOWT system in regular wave, the resultant system of equations of motion, in the frequency domain is highlighted in Coraddu et al. (2020) and Newman (2018).

The formulation for the radiation and diffraction boundary value problem and the resulting hydrodynamic added mass, damping matrices, and wave-excitation force transfer functions depends on frequency, water depth, as well as on the geometric shape of the support platform, its proximity to the free surface, and its forward speed. Additionally, the wave-excitation force depends on the heading direction of the incident waves (Jonkman, 2007). The frequency dependence of the hydrodynamic added mass and damping matrices is of a different nature to that of the wave-excitation force. In the frequency dependence of the hydrodynamic added mass and damping matrices, the matrices depend on the oscillation frequency of the particular mode of support platform motion. However, the frequency dependence of the wave-excitation force means that the force depends on the frequency of the incident wave. Both set of

frequencies (added mass and damping frequency and wave excitation frequency) are identical because the platform is assumed to oscillate at the same frequency as the incident wave.

By definition, the frequency-domain model assumes that the platform motions are at the same frequency as the incident waves and that the incident waves are regular. While this means that the system's transient response cannot be modelled, the assumption of linearity implies that the responses at different wave frequencies can be superimposed according to a wave spectrum to predict the system behaviour in irregular sea states (Hall et al., 2013). Extensive discussion of these hydrodynamic coefficients can be found in Anaya-Lara et al. (2018) and Journée and Massie (2000). The hydrodynamic coefficients (added mass, radiation damping, and first order wave excitation) can be approximated as the solution to the linear radiation-diffraction problem using the boundary element method. This is implemented in software like WAMIT, detailed in WAMIT-Inc (2020) and WADAM in DNVGL Høvik (2019).

The complex magnitude of the response transfer function between the amplitude of the wave and the amplitude of oscillation in the oscillatory degree of freedom is the RAO highlighted in Equation (5).

$$RAO_j = \left| \sum_{k=1}^6 \frac{X_k}{-\omega^2(M_{kj} + a_{kj}) + i\omega b_{kj} + c_{kj}} \right| \quad (5)$$

Where ω is the frequency of oscillation of the platform, M_{kj} is the total system mass matrix, a_{kj} is the hydrodynamic added mass coefficient, b_{kj} is the radiation damping coefficient without the consideration of viscous forces, and c_{kj} is the sum of the hydrostatic and mooring stiffness coefficients. X_k is the first order wave excitation load transfer function (Corradu et al., 2020, Newman, 2018).

The wave response spectrum should be minimized to minimize the displacements and accelerations of the FOWT system. It is important that the natural frequencies (periods) of the FOWT system should be outside the most energetic frequency (period) range of the wave spectrum (Collu and Borg, 2016). This depends on the location, but in general wave spectra are most energetic between the 5s and 25s period (1.25-0.25 rad/s), and therefore the structure should aim at having natural periods above 25s or below 5s in all the DOFs (Collu and Borg, 2016).

The frequency domain analysis approach is mostly used for preliminary design of FOWTs, as the RAO concept is strictly valid to estimate the regime response to waves and by definition

is a linear approach (Collu and Borg, 2016). To capture the transient behaviour of a FOWT due to non-linear loading from wind and irregular seastate, a more detailed approach is required as in the time domain approach.

2.5.2 Time Domain Approach

A time-domain approach adopts a time-domain coupled model of dynamics with the capability to consider nonlinear forces and estimate the transient regimes. With this approach, it is possible to estimate the loads acting on the structure and the displacements, velocities, accelerations, and time responses of the system in all DOFs (Journée and Massie, 2000, Collu and Borg, 2016). Adopting the use of statistical analysis, the maximum, minimum, mean, variance, standard deviation, and significant values of each of the displacements, velocities and acceleration can be determined to have a more realistic estimate of these values. However, it is more difficult to understand in depth how to modify the design in order to obtain a more suitable response to wind and wave forces (Collu and Borg, 2016).

A major contribution to time domain integrated dynamics design codes is discussed in Jonkman (2007). In his work, Jonkman developed a robust simulation tool for the coupled dynamic response of a horizontal axis wind turbine (HAWT) and performed integrated dynamic analysis on a HAWT mounted on a barge-type platform according to the IEC 61400-3 design standard. This tool is integrated into OpenFAST, which is one of the most widely used open-access FOWT design and simulation codes.

Just like in the frequency domain, Newton's second law yields the linear equation of motion in time domain (Journée and Massie, 2000). This is known as the Cummins equation and represented in Equation (6). Cummins equation does not consider the structural flexibility degrees of freedom; hence, it is the time domain equation of a rigid body.

$$X(t) = (M + A) \cdot \ddot{x}(t) + \int_0^{\infty} B(\tau) \cdot \dot{x}(t - \tau) \cdot d\tau + C \cdot x(t) \quad (6)$$

Where $\ddot{x}(t)$ is the translational or rotational acceleration at time (t), \dot{x} is the translational or rotational velocity at time (t), $x(t)$ is the translational or rotational displacement at time (t), M is the solid mass or mass moment of inertia, A is the hydrodynamic (or added) mass coefficient, $B(\tau)$ is the retardation functions, C is the spring coefficient from ship geometry and t, τ is time and time lag integration variable respectively. Details of how to determine coefficients A and B are discussed in Journée and Massie (2000).

2.5.3 Review of Analysis Domain for FOWT System Design

Table 2 shows a list of design analysis and optimization work done on FOWT system and the analysis domain adapted in each case. Most of the works shown in Table 2 adopt a frequency domain approach.

Table 2: Analysis domain overview for optimization of FOWT system

| Work | Analysis Domain | Reference |
|---|--|-------------------------------|
| Practical application of global optimization to the design of offshore structures | Frequency domain | Birk et al. (2004) |
| WINDOPT - An optimization tool for floating support structures for deep water wind turbines | Frequency domain | Fylling and Berthelsen (2011) |
| Evolving Offshore Wind: A genetic algorithm-based support structure optimization framework for floating wind turbines | Frequency domain | Hall et al. (2013) |
| A multi-objective design optimization for floating offshore wind turbine support structures | Frequency domain | Karimi et al. (2017) |
| Integrated design optimization of spar floating wind turbines | Frequency domain | Hegseth et al. (2020) |
| Platform Optimization and Cost Analysis in a Floating Offshore Wind Farm | Frequency domain | Ghigo et al. (2020) |
| Optimization of floating wind turbine support structures using frequency domain analysis and analytical gradients | Reduced order Time domain and Frequency domain | Dou et al. (2020) |
| Development of a framework for wind turbine design and optimization | Frequency domain | Leimeister et al. (2021) |

For optimization purposes that entails large design space exploration, time domain dynamics evaluation becomes computationally expensive and time consuming. The way around the computationally expensive time domain dynamics evaluation issue is to conduct the dynamic analysis in the frequency domain. Despite the frequency domain analysis advantage of being computationally less expensive, it has its own limitations amongst which are:

1. Frequency domain analysis is not suitable for non-linear dynamic systems. It only applies to linear systems such that the system's behaviour is linearly related to its displacement, velocity and acceleration (Journée and Massie, 2000).

2. Frequency domain analysis does not take into consideration the impulse response function – irradiated waves that keep exciting the body due to memory of past motion of the body even when the body has suddenly stopped (Journée and Massie, 2000). This memory effect is effectively covered in the time domain analyses using the Cummins equation (Journée and Massie, 2000).

These limitations are not deterrent to the use of frequency domain analysis technique to solve optimization problems in comparison to computationally expensive time domain techniques. As highlighted in Section 2.6.3, which reviews the multidisciplinary design analysis and optimization of a floating offshore wind turbine system, most of the analysis conducted for the research work reviewed are conducted using the frequency domain analysis technique. However, verification of the optimal design can be done with the more accurate non-linear time domain analysis technique, for a reduced design space.

2.6 Multidisciplinary Design Analysis and Optimization Approaches for Floating Offshore Wind Turbine System

2.6.1 MDAO Overview

MDAO is an engineering/research field that studies the use of numerical optimization techniques to design engineering systems that involves multiple disciplines, subsystems or components (Martins and Lambe, 2013). It is a systematic design and analysis process that deals with the interfacing between different components and disciplines within a system. This review looks at how MDAO is applied to the FOWT substructure system (platform and mooring/station keeping).

MDAO was initially developed in the aerospace industry as a result of strong influences between different disciplines (aerodynamics and structural dynamics) that affect the performance of the aircraft (Dykes et al., 2011). MDAO went to be further successfully applied in other industries amongst which are automotive, civil, and naval engineering (Perez-Moreno et al., 2016).

Gray et al. (2019) and Agte et al. (2009) highlighted the aerospace and the automotive sectors as the early adopters in the use of MDAO framework and its applications to the industry. Some of the MDAO application and gains from using MDAO within the aerospace and automotive sectors are highlighted in Table 3. A very detailed review of the application of MDAO in the

aerospace industry highlighting the problem, model structure, design variables, objective functions and constraints is presented in Gray et al. (2019).

The IEA (International Energy Agency) Wind Task 37 identified three important dimensions of an MDAO simulation set-up or workflow amongst which are: model fidelity, size and scope of simulation, and MDAO architecture (Bortolotti, 2019).

Earlier examples of applications of MDAO to wind energy systems are conducted by Crawford and Haines (2004); Bottasso et al. (2010) and He et al. (2011). Each of these optimization studies result shows a system-wide reduction in the cost of energy from 2% to 15%, based on the sub-system optimization (Dykes et al., 2011).

Crawford and Haines (2004) incorporated the National Renewable Energy Laboratory (NREL) aeroelastic design codes with a cost-scaling model based on linear, quadratic, and cubic function of the rotor diameter from the CAD geometry to influence the cost changes in the respective subsystems. The MDAO approach is the sequential optimization of the turbine using the NREL aeroelastic codes, CAD software interface, and the custom cost of energy algorithm.

The MDAO approach for Bottasso et al. (2010) is for the design of a wind turbine blade, focusing on the structural and aerodynamic trade-offs in blade design, taking into consideration the total aero-servo-elastic effects on the blade structure and the noise constraints. This study was conducted using a sequential MDAO approach that involves a comprehensive aero-hydro-servo-elastic analysis using non-linear finite-element-method-based multibody dynamics solver at a first level. The second level of the MDAO involves the use of a finite-element, cross-sectional model of the blade to perform a section-wise load calculations to determine the blade weight, which is essential in assessing the structural integrity of the blade design. The third level of the MDAO uses macro parameters to optimize the overall objective of the annual energy production (AEP) to weight ratio minimization. This optimization process finds the best combination of design parameters that would minimize the weight of the turbine while maximizing the annual energy production.

He et al. (2011) applied a multi-level MDAO approach to the system design utilizing two disciplines (maximizing annual energy production and minimizing blade root moment) under a system level analysis and optimization. Their work borrowed the NREL aeroelastic design codes and cost models and, in addition to the distinct multi-level approach, their work incorporated the use of the Kriging-based metamodels to replace higher fidelity models to save computation time required for the optimization process.

An extensive review of approaches in the design optimization of wind turbine support structures and the challenges associated with it is presented by Muskulus et al. (2014). In this work, the authors reviewed the different techniques of optimizing wind turbine structures amongst which are optimization of wind turbine structures using static analysis, optimization of wind turbine structures using frequency domain, and time domain dynamic analyses. Further to this, they reviewed Windopt - a well-known optimization tool used with the spar-type FOWTs. Windopt allows for the design of the spar buoy, mooring system, and the power cable, using sequential quadratic programming and a combination of commercial analysis tools. However, its limitation is that the wind turbine rotor is only represented as a state-dependent drag coefficient/force acting in a single node at the top of the tower. Also in their work, Muskulus et al. (2014) made recommendations to the field of structural optimization, and amongst their recommendations are the use of gradient-based and gradient-free optimization which are largely in use today. Other structural optimization recommendations made in Muskulus et al. (2014) are modelling with a hierarchy of fidelities, reduction of load cases and interfaces for efficient integrated design, and exploration of probabilistic design.

Dykes et al. (2011) researched MDAO works relevant to both wind turbines and wind farms. From this work, they laid the foundation for MDAO workflow WISDEM (Wind Plant Integrated System Design and Engineering Model). They observed that most research is conducted on singular components or disciplines and concluded there are large opportunities for MDAO research and development in the wind energy sector (offshore/onshore).

Ashuri et al. (2014) conducted research on design optimization, capable of simultaneous designs of wind turbine blade and tower subject to constraints on fatigue, stresses, deflections and frequencies with the Levelized Cost of Energy (LCOE) as the objective function. From their experiment, the results show an improvement in the quality of the design process with a realistic assessment of the LCOE and constraints, while preserving the coupling of the components and disciplines by using the power of numerical optimization. Since then, researchers like Hall et al. (2013), Karimi (2018) and Hegseth et al. (2020) have been able to demonstrate the effectiveness of using numerical optimization algorithms in MDAO for the design of FOWT substructures, and these research works are highlighted with more details in section 2.6.3.2.

Table 3: Examples of gains from application of MDAO in aerospace and automotive sectors(Agte et al., 2009)

| Industry/Sector | Component/Activity | Advantages/Gains from MDAO |
|-----------------|---|--|
| Aerospace | Nacelle Configuration | Noise reduction and 15% reduction in weight |
| Aerospace | Vertical fin major aircraft | Significant increase in effectiveness of the fin |
| Automotive | Optimized structural design for crash worthiness. | Significant reduction in time to achieve acceptable level of impact performance from 1.5 years to 1.5 days |
| Aerospace | Flight test program | Reduced from 2-3 years to less than 1 year. |

2.6.2 MDAO workflow

MDAO comprises of a workflow with a set of computational tools (analysis block) that represents different components and disciplines coupled together to simulate an entire system (Moreno, 2019). With this technique, drivers can be included to control how and when each tool can be executed. The functionality of the workflow is defined as a use case which describes any domain problem that can be solved by MDAO i.e., optimization of the objective function. A simplified diagram of an MDAO workflow is shown in Figure 6

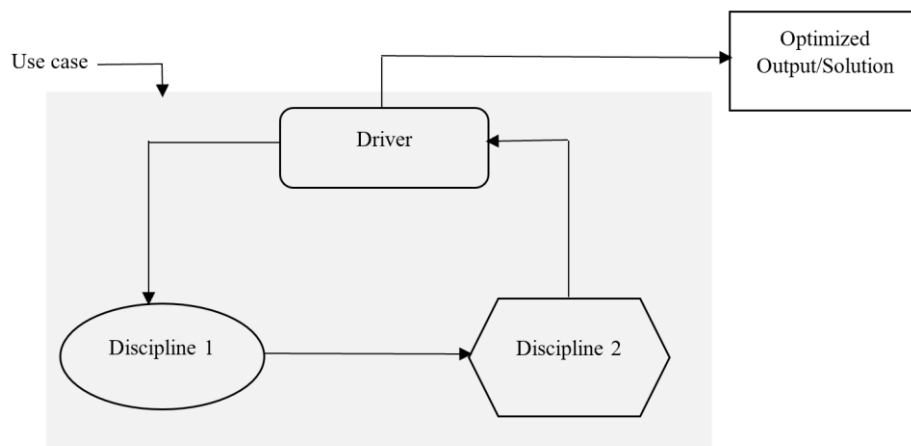


Figure 6. Simplified diagram of an MDAO workflow comprising an analysis block of two modules and a driver

The driver (numerical method governing the use case) integrating the modules in an MDAO workflow can have different uses amongst which are, performing uncertainty quantification (UQ), running design of experiments (DOE), or implementing optimization algorithms (Moreno, 2019). Optimization algorithms helps in finding the optimal system design that

maximizes system's performance by exploring the design space smartly. More on optimization algorithm is discussed in Section 2.6.3.

MDAO workflow consists of system scope, model fidelity, and architecture/framework. The system scope and model fidelity are highlighted in Section 2.6.2.1, and the MDAO architecture discussed in Section 2.6.2.2.

2.6.2.1 System Scope and Model Fidelity

The scope of the system is clearly defined before instantiating the MDAO workflow because, not all components or disciplines influence one another with the same intensity. Moreno highlighted two examples of use cases with different system scope in the field of wind energy (Moreno, 2019). The examples are the optimization of the layout of an offshore wind farm and the sensitivity analysis of LCOE with respect to foundation type. For the optimization of the layout of an offshore wind farm, the workflow will have to include the calculation of wake losses and cable lengths; however, for the latter, there is no need to re-analyse the performance or cost of the electrical connection system as the interaction between them are negligible. The scope of an MDAO example is shown in Figure 7.

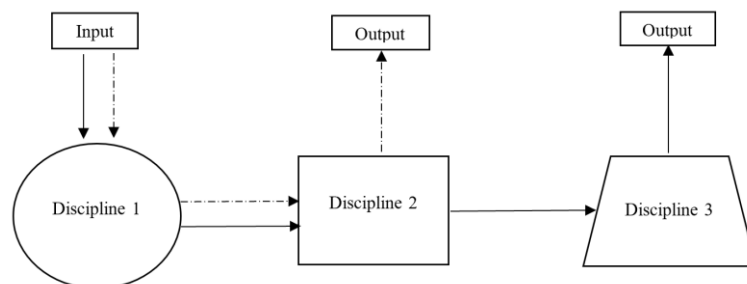


Figure 7. Two workflows with different system scope. Dashed arrows include components/disciplines 1 and 2 while straight arrows include 1, 2 and 3.

Model fidelity is very important in MDAO as it represents the degree to which a model or simulation reproduces the state and behaviour of a real-world object which helps to define the objective function within the optimization problem. Different model fidelities or levels of accuracy and sophistication of the integrated models are available for the different disciplines in a FOWT system. Examples are spreadsheet model, a simple beam model, or a full FEM model with a higher precision, or a computationally expensive CFD.

In System engineering, model fidelity ranges from low fidelity (LF) to the high-fidelity (HF) models while the middle model between the low and high-fidelity models can be classed as a

multi-fidelity surrogate model. Shi et al. (2020) demonstrated that to take advantage of HF and LF models, multi-fidelity surrogate models integrating information from both HF and LF models can be used and are increasingly gaining popularity.

Examples of multi-fidelity surrogate models are Kriging based, radial basis function (RBF) and support vector regression CO_SVR surrogate models (Shi et al., 2020). These surrogate models used with optimization algorithms provides competitive accuracy as HF models. An example of the multi-fidelity surrogate model where the Kriging based example has been employed is highlighted in (Karimi et al., 2017) and discussed in Section 2.6.3.2.

2.6.2.2 MDAO Architecture/Framework

MDAO architecture/framework defines how the different models are coupled and how the overall optimization problem is solved. Martins and Lambe (2013) highlights MDAO architecture as either monolithic or distributed. In a monolithic architecture approach, the MDAO problem is solved as a single optimization problem. A distributed approach solves the MDAO problem using a set of optimization problems or subproblems. MDAO architectures from the Monolithic approach are the simultaneous analysis and design (SAND), multidisciplinary feasible (MDF) and individual discipline feasible (IDF) architectures. The differences between these three architectures depends on the equality constraint group eliminated from the optimization problem. In the SAND approach, the consistency / equality constraint is eliminated from the optimization problem while for the IDF approach, the disciplinary analysis / inequality constraint is eliminated from the optimization problem. MDF approach is the most used of the monolithic approaches and both disciplinary analysis constraint and consistency constraint are eliminated from the optimization problem. For further reading, a comprehensive detail of other monolithic and distributed MDAO architectures is presented in Martins and Lambe (2013).

To develop MDAO architecture will require an automated framework. Example of an automated framework developed for wind turbine design optimization is highlighted in Leimeister et al. (2021). There are two parts to the framework which are automation and automation plus optimization. The first part of the framework (automated simulation) comprises of the modelling environment, simulation tool and the programming framework. The holistic framework integrates a driver/optimizer to the automated simulation framework (automation plus optimization). An example of a holistic architecture / framework with optimization functionalities that can be used with a FOWT system is highlighted in Figure 8.

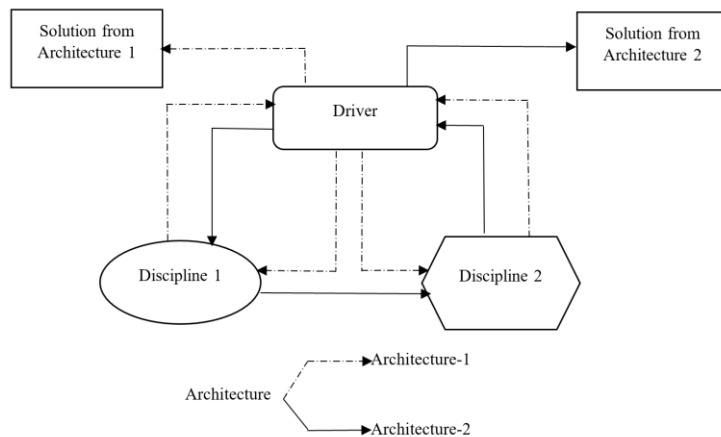


Figure 8. Architecture / Framework with Optimization functionalities for FOWT

2.6.2.3 MDAO Tools

MDAO architecture can be executed by developing detailed and effective scripts to execute design and optimize a problem of interest or use commercial MDAO packaged to provide solution to the problem of interest. The development of commercial MDAO frameworks dates back to the late 1990s with iSIGHT (Gray et al., 2019). Since the development of iSIGHT, several other commercial frameworks have been developed amongst which are: Phoenix Integration’s Model Center/CenterLink, Esteco’s model FRONTIER, TechnoSoft’s AML suite, Noesis Solutions’ Optimus, and Vanderplaats’ VisualDOC (Gray et al., 2019). Since the development of the highlighted frame works, MDAO framework has evolved. One of the recent evolutions of optimization framework is the open-source, freely available OpenMDAO (openmdao.org., 2016), with the capability of gradient-based and metaheuristic optimization algorithm, Pymdo and Dakota. These open-source MDAO tools are discussed in section 2.6.3.2.1 to 2.6.2.3.3 and summarized in Table 4.

2.6.2.3.1 OpenMDAO

Its origin dates to 2008 when researchers from NASA highlighted the need for a new MDO framework to deal with the challenges of aircraft design. It was developed by collaboration between researchers from MDO lab in Michigan university and NASA (Gray et al., 2019). OpenMDAO is an open-source multidisciplinary design, analysis, and optimization tool for the exploration and exploitation of coupled multidisciplinary system to determine the system’s global optimum design. OpenMDAO work done related to FOWT design and optimization is detailed in Hegseth et al. (2020). It also facilitates the solution of an MDO problem utilizing

distributed memory parallelism and high-performance computing resources with leverage on message passing interface (MPI) and Portable, Extensible Toolkit for Scientific Computation (PETSc) library.

2.6.2.3.2 PyMDO

PyMDO’s development dates back to the early 2000’s and it was the first object-oriented framework that focused on automating the implementation of different MDO architectures (Martins et al., 2009). In pyMDO, the general MDO problem is defined by the user and the framework would reformulate the problem in any architecture with no further user effort. Its ability to introduce parallel computing codes into the MDO framework is essential to realize the vision of a high-fidelity, integrated design environment.

2.6.2.3.3 DAKOTA

DAKOTA was developed in the mid-nineties at the Sandia National Laboratories. It is a Multilevel Parallel Object-Oriented Framework for Design Optimization, Uncertainty Quantification, Parameter Estimation, and Sensitivity Analysis. Dakota toolkit permits connection between analysis codes and iteration methods. This provides a robust, open-source interface to many different systems analyses methods that can be used alone or integral to more advanced optimization strategy. Dakota contains algorithms for optimization with gradient and non-gradient-based methods. An example of design, analysis and optimization study of ducted wind turbines using DAKOTA is detailed in Khamlaj and Rumpfkeil (2018).

Table 4: Open-source MDAO Tools

| Tool | Language | GB Algorithm | GF Algorithm | Reference |
|----------|----------------|-----------------------------------|-----------------------|---|
| OpenMDAO | Python | SNOPT, SLSQP, CONMIN | NSGA2, ALPSO | (Gray et al., 2019) |
| PyMDO | Python, C, C++ | SNOPT | | (Gray et al., 2019, Martins et al., 2009) |
| DAKOTA | C++ | SQP method, CONMIN, Newton method | EA, PS, Simplex, MOGA | (Khamlaj and Rumpfkeil, 2018) |

2.6.3 MDAO for FOWT Substructures

According to IEC-61400-3-2 (2019), FOWT substructure consists of the platform, the mooring, and the anchors, and a comprehensive assessment of the system involves the structural, hydrostatic and hydrodynamic disciplines. Multidisciplinary design and analysis (MDA) assessment from the model design to the analyses techniques that can be applied to a FOWT substructure is discussed within Section 2.6.3.2. Exploring a large design space requires the use of optimization algorithms to select the optimal design within the MDA framework giving rise to the much efficient MDAO approach.

2.6.3.1 Review of MDAO optimizers for FOWT substructures

The main objective of FOWT stakeholders is to minimize the cost of energy of wind turbines and increase its reliability to compete and surpass fossil-fuel sources of energy. Presently, as highlighted in Chapter 1, the floating platform accounts for about 29.5% of the total CAPEX of a FOWT system (Ioannou et al., 2020); hence, a clever way of designing a floating substructure to minimize the cost will contribute to the reduction of CAPEX for a FOWT system and subsequently, a reduction in the LCOE of the FOWT system. This innovative approach to design requires the need of optimization algorithms for selecting optimal solutions. The formulation of a general design optimization problem is defined in the context of minimizing/maximizing an objective function subject to constraints. This statement can be represented as expressed in Equation. (7).

$$\begin{aligned} & \min_{\mathbf{x} \in \mathbb{R}} J(\mathbf{x}) \\ & s. t. \begin{cases} \mathbf{x}_l \leq \mathbf{x} \leq \mathbf{x}_u \\ h_i(\mathbf{x}) = 0; i = 1 \text{ to } m \\ g_j(\mathbf{x}) \leq 0; j = 1 \text{ to } p \end{cases} \end{aligned} \quad (7)$$

Where \mathbf{x} is a k-dimensional vector of design variables with lower (\mathbf{x}_l) and upper (\mathbf{x}_u) bounds, $J(\mathbf{x})$ is a single objective function, m is the number of equality constraints and p is the number of inequality constraints.

For multidisciplinary optimization algorithms with many objectives, designers can identify the Pareto front / trade-off curve that reveals the weaknesses, anomalies, and rewards of a certain target like minimizing the LCOE or improving the performance metrics, such as the root mean square (RMS) of the nacelle acceleration (Chehouri et al., 2016). Optimization

algorithms are mainly categorized into two groups: Gradient Based (GB) and Gradient Free (GF) optimization algorithms.

GB methods are iterative methods that use gradient information of the objective function during iterations (Yang, 2019). They are efficient for finding local minima for high dimensional, non-linearly constrained convex problems.

GF, also called Metaheuristic optimization algorithms, are usually characterized by a superior search efficiency and robustness unlike GB that has the tendency of being stuck in local minima for optimization problem with a multimodal objective function (Hegseth et al., 2020). GF have been introduced to solve complex nonlinear optimization problems that GB optimization methods cannot deal with (Saad et al., 2017). Once the optimization problem has been defined, optimizers must be selected to solve the optimization task. A table of available optimizers is highlighted in Table 5. The optimizers are classed into Quasi-Newton method, Sequential Quadratic Programming (SQP), Evolutionary Algorithm (EA), Particle Swarm Optimization (PSO) and other types and grouped into the GB and GF optimization algorithms. Also highlighted in Table 5 are optimizers with the capability of handling Multi-Objective (MO) functions.

Table 5: Overview of applicable optimizers

| Class | Optimizer | GB | GF | MO | Reference |
|--------------|---|----|----|----|--|
| Quasi-Newton | Newton Conjugate Gradient (Newton-CG) | ✓ | | | Buckley (1978) |
| | Powell | ✓ | | | Xian et al. (2006) |
| | Truncated Newton (TNC) | ✓ | | | (Izzo, 2015, Leimeister et al., 2021) |
| | Broyden-Fletcher-Goldfarb-Shanno (BFGS) | ✓ | | | (Izzo, 2015, Leimeister et al., 2021) |
| | Limited-memory BFGS with Box constraints (L-BFGS-B) | ✓ | | | (Izzo, 2015, Leimeister et al., 2021) |
| SQP | Feasible SQP (FSQP) | ✓ | | | (Izzo, 2015, Leimeister et al., 2021, openmdao.org., 2016) |
| | Preconditioned SQP (PSQP) | ✓ | | | (Izzo, 2015, Leimeister et al., 2021, openmdao.org., 2016) |

| | | | | | |
|---|--|---|---|---|---|
| | Sequential Least Squares Quadratic Programming (SLSQP) | ✓ | | | (Izzo, 2015, Leimeister et al., 2021) |
| EA | Genetic Algorithm (GA) | | ✓ | ✓ | (Izzo, 2015, Siarry, 2016) |
| | Non-dominated Sorting GA II (NSGAI) | | ✓ | ✓ | (Hadka, 2015, Leimeister et al., 2021, openmdao.org., 2016, Izzo, 2015) |
| | Non-dominated Sorting GA III (NSGAIII) | | ✓ | ✓ | (Hadka, 2015, Leimeister et al., 2021, openmdao.org., 2016, Izzo, 2015) |
| | Steady-state Epsilon-MO EA (EpsMOEA) | | ✓ | ✓ | (Hadka, 2015, Leimeister et al., 2021, openmdao.org., 2016) |
| | MO EA based on Decomposition (MOEAD) | | ✓ | ✓ | (Hadka, 2015, Leimeister et al., 2021, openmdao.org., 2016) |
| | Generalized Differential Evolution 3 (GDE3) | | ✓ | ✓ | (Hadka, 2015, Leimeister et al., 2021, openmdao.org., 2016) |
| | Strength Pareto EA 2 (SPEA2) | | ✓ | ✓ | (Hadka, 2015, Leimeister et al., 2021, openmdao.org., 2016) |
| | Indicator-Based EA (IBEA) | | ✓ | ✓ | (Hadka, 2015, Leimeister et al., 2021, openmdao.org., 2016) |
| | Parallel Eas (PEAS) | | ✓ | ✓ | (Hadka, 2015, Leimeister et al., 2021, openmdao.org., 2016) |
| | Pareto Envelope-based Selection Algorithm (PESA2) | | ✓ | ✓ | (Hadka, 2015, Leimeister et al., 2021, openmdao.org., 2016) |
| Covariance Matrix Adaptation Evolution Strategy (CMAES) | | ✓ | ✓ | (Hadka, 2015, Leimeister et al., 2021, openmdao.org., 2016, Izzo, 2015, Siarry, 2016) | |
| PSO | Augmented Lagrangian PSO (ALPSO) | | ✓ | | (Izzo, 2015, Leimeister et al., 2021) |

| | | | | | |
|--------|---|---|---|---|---|
| | Our multi-objective PSO (OMOPSO) | | ✓ | ✓ | (Hadka, 2015, openmdao.org., 2016) |
| | Speed-constrained multi-objective PSO (SMPSO) | | ✓ | ✓ | (Hadka, 2015, openmdao.org., 2016) |
| Others | Non-linear Optimization Mesh Adaptive Direct (NOMAD) | | ✓ | ✓ | Le Digabel (2011) |
| | Sparse Nonlinear OPTimizer (SNOPT) | ✓ | | | (Izzo, 2015, Leimeister et al., 2021) |
| | CONstrained function Minimization (CONMIN) | ✓ | | | (Leimeister et al., 2021, Izzo, 2015) |
| | Interior Point OPTimizer (IPOPT) | ✓ | | | (Izzo, 2015, Leimeister et al., 2021) |
| | Nelder-Mead | | ✓ | | (Izzo, 2015, Leimeister et al., 2021) |
| | Constrained Optimization BY Linear Approximation (COBYLA) | | ✓ | | (Izzo, 2015, Leimeister et al., 2021) |
| | Simulated Annealing (SA) | | ✓ | | (Izzo, 2015, Janga Reddy and Kumar, 2020, Siarry, 2016) |

2.6.3.2 Review of MDAO work for FOWT system

Modelling FOWT systems involves complex integration/coupling of multidisciplinary systems together. The coupling of the FOWT system can be done using the monolithic or distributed architecture described in section 2.6.2.2, with the monolithic architecture the most commonly used in the field of FOWT. The MDF architecture which is one of the monolithic approaches and most dominant approach for coupling FOWT system is well defined in Ashuri et al. (2014) .

As illustrated in Figure 8 of section 2.6.2.2 and highlighted in Leimeister et al. (2021), with the MDF architecture, the multidisciplinary analysis model simulation with the design variables are passed to an optimizer. Figure 8 can also be illustrated with the use of the extended design structure matrix (XDSM) standard detailed in Martins and Lambe (2013). The hydrodynamic, mooring, aerodynamic, and structural design variables are passed to the multidisciplinary framework for analysis simulation from which the objective functions are computed. Then, the

computed objectives and specified constraints are passed back to be assessed by the optimizer and the iterative approach continues until the convergence is reached.

MDAO tools like OpenMDAO allows data transfer / coupling design variables between disciplines using variations of system iterative solvers like Gauss-Seidel, Jacobi, and Newton's method to achieve solution's convergence. The convergence of the solution is dependent on the nature of the optimization problem specified in the objective function. If the objective function is a convex function, the solution will converge to a global minimum or maximum. A nonconvex function will have multiple locally optimal solutions.

2.6.3.2.1 MDAO and Design Parameterization Offshore Substructures

MDAO and parameterization of a system go hand in hand as the parametric scheme describes the design space of the system for exploration. Some examples of parametric studies conducted on floaters are reviewed here. A precursor to the parametrization of floating offshore wind turbine substructure is the parametric design model of oil and gas substructures, optimized to reduce the downtime through improved seakeeping by Birk et al. (2004). In this work, they automated the hull design stage by introducing parametric shape generation, numeric hydrodynamics analysis assessment tools, and non-linear programming algorithms for process control. Their investigation compares the performance of three different optimization algorithms (SQP, GA and SA) within a shape optimization framework and found that the GF optimizers (SA and GA) require more computation time and do not always produce better results than the classical deterministic SQP method. However, both sets of algorithms show significant improvement of seakeeping qualities. A parametric optimization of a semi-submersible platform with heave plates was conducted by Aubault et al. (2007). Their work was conducted on Minifloat, a novel concept of semi-submersible platform developed to enable hydrocarbon production from marginal fields in deep and ultra-deep water. In their work, they developed a simplified hydrodynamic model to capture the parametric sensitivity of the platform responses to primary design parameters as the hydrodynamic responses of the platform are driven by its mass properties and geometric parameters, including that of the heave plates. Also, the use of GA to optimise the responses of the platform was discussed in this work, and an optimized design solution was found for the simple Minifloat platform with no substructure accessories. Results with static constraints show a linear relationship between the payload and the platform displacement. However, the need of a sizeable draft is determined by hydrodynamic considerations, the GA optimization process for the Minifloat resulted in a shallow operating draft. For FOWT, Bachynski conducted a parametric work related to TLP as

part of her thesis in Bachynski (2014). Here, hydrodynamic wave loading of first, second and third order is considered with the combination of the controller and controller faults in extreme sea states.

2.6.3.2.2 MDAO of FOWT Substructures

A couple of MDAO studies in the offshore wind turbine industry are detailed in this section. In the work of Fylling and Berthelsen (2011), a GB optimization approach (SLSQP) for a spar floater, including the mooring lines and the power cables, was presented. The objective function modelled the cost of the system, and the design variables represented the geometric properties of the spar and mooring system. The constraints considered are the nacelle acceleration, tower inclination, and maximum tensions in mooring lines. The results indicate that response can be optimized by modifying the cylindrical shape of the spar.

In Hall et al. (2013), the authors conducted a study on the hull shape and mooring line optimization of FOWT across different substructure categories using a GA and a frequency domain model derived from FAST software, with a linear representation of the hydrodynamic viscous damping and no representation of the wind turbine control. The GA is applied for single and multi-objective optimization, and the results indicate an un-conventional design that shows the necessity for cost function refinement.

Karimi et al. (2017) improved the work of Hall et al. (2013) by using a new optimization algorithm and a linearized dynamic model, which improved the optimal solutions. Karimi et al. (2017) incorporated a fully coupled frequency domain dynamic model and a design parameterization scheme to evaluate the system motions and forces in turbulent winds and irregular wave scenarios. They also selected the Kriging-Bat optimization algorithm (a surrogate-based evolutionary algorithm) to represent the design exploration and exploitation of optimal designs across three stability classes of platform (MIT/NREL TLP, OC3-Hywind Spar, and OC4-DeepCwind semi-submersible platform). This optimization aimed to explore the cost implications of platform stability, expressed through the nacelle acceleration objective function, across the three FOWT platform stability classes. An improved correlation between cost and substructure design was obtained in this study in comparison to the work of Hall et al. (2013).

Hegseth et al. (2020) developed a linearized aero-hydro-servo-elastic model to optimize the platform, tower, mooring, and blade-pitch controller of a 10MW spar floating wind turbine. In this work, optimal design solutions are found using GB optimization algorithm, considering fatigue and extreme response constraints, taken into account as objective function – a weighted

combination of system cost and power quality. The geometric shape of the platform below the waterline is an hourglass shape that maximizes the distance between the center of buoyancy and center of gravity, to increase the restoring moment and natural frequency in pitch. The large bottom diameter of the platform increases the added mass in heave, which helps to place the natural frequency outside the wave frequency to avoid resonance. The optimization results show that local minima occur in both the soft-stiff and stiff-stiff range of the first tower bending mode. It is shown in this study that achieving a feasible solution that complies with the fatigue constraints within the optimization framework necessitates the adoption of a stiff-stiff tower design for the coupled FOWT system.

The work of Ghigo et al. (2020) is based on the use of an in-house hydrostatic tool used to estimate the main hydrostatic parameters of five different floating substructures. Some of the hydrostatic parameters estimated by the in-house tools are the metacentric height and hydrostatic stiffness in heave, roll, and pitch. Furthermore, by application of a thrust force at the center of the rotor, the maximum inclination angle in pitch can be estimated. Ghigo et al. (2020) verified the validity of results from their in-house tools by comparing with results obtained from Ansys Aqwa. The inhouse tool was further enhanced introducing a GA-based optimization framework order to identify the best concept in terms of reducing the LCOE while satisfying all design requirements and the constraints imposed by the standards. This work yielded a new floating platform concept, a derivative of the Hexafloat with all lateral brackets removed from the Hexafloat in order to reduce weight and cost of the new substructure.

The authors of Dou et al. (2020) developed an optimization framework for floating wind turbine support structure (spar-buoy floater), including the mooring system. The framework builds on frequency domain modelling, and the analysis capabilities are extended to provide analytical design sensitivities for the design requirements. This capability allows quick optimization using SQP optimization algorithm (Dou et al., 2020).

Recently, Leimeister et al. (2021) developed a holistic and highly flexible framework for automated simulation and optimization of wind turbine systems, including all components within the system and their fully coupled aero-hydro-servo-elastic behaviour. The framework consists of a modelling environment using the MoWiT software, the simulation engine (Dymola) and a gradient free multi-objective (GF MO) genetic optimization algorithm. This holistic framework provides suitable applications in the areas of design optimization of floating wind turbine support structures, optimization of wind turbine performance (power output) and

loading (thrust force), tuning of wind turbine controller for load reduction and other optimization tasks within a wind farm.

A recent investigation of estimating a platform’s hydrodynamic response by surrogacy approach is conducted by Corradu et al. (2020). Their work demonstrates the feasibility and performance of a surrogate model to determine the hydrodynamic response of an axis-symmetric spar-buoy type of platform. To conduct their analyses, Corradu et al. (2020) used a family of meta-model choice listed in Figure 9 (ANN) and the sub family of the ANN meta-model choice used is the Extreme Learning Machines (ELMs), developed with dataset of simulations from state-of-the art potential flow based computational code. The authors found that based on the result of a state-of-the- art potential flow code on a limited set of geometries, the ELM based surrogate model developed to approximate the RAO of the axis-symmetric spar-buoy type of FOWT can predict the RAO of any FOWT geometry to an average Mean Absolute Percentage Error (MAPE) OF 2% across all DOFs. This demonstrates the feasibility of replacing computationally expensive and accurate time domain solvers with fast and reasonably accurate surrogate model. The categorization of MDAO work done from literature on FOWT platform is presented in Table 6.

Table 6: MDAO work on FOWT substructures

| Architecture | Type | Algorithm | Platform | Reference |
|--------------|----------------|-----------------------|--------------------------------|--------------------------------|
| MDF | Gradient Based | SNOPT using SQP | Spar | Hegseth et al. (2020) |
| MDF | | SQP | Spar | Dou et al. (2020) |
| MDF | | SQP | Spar | Fyilling and Berthelsen (2011) |
| MDF | Gradient Free | GA | Spar; Semi-submersible; TLP | Hall et al. (2013) |
| MDF | | Bat (BA) | Spar; Semi-submersible; TLP | Karimi et al. (2017) |
| MDF | | GA | Spar | Leimeister et al. (2021) |
| MDF | | GA | New concept | Ghigo et al. (2020) |

2.7 Research gaps and proposed future areas of research

As highlighted in the background section of this review, the floating offshore wind turbine sector is still at an infancy stage, with most of the design and optimization methodologies transferred from the oil & gas sector (fixed and floating structure). The reliance on these prompts the need to identify gaps needed for development within the FOWT sector, as the design requirements for an oil and gas structure is different from a FOWT structure. From the review conducted on MDAO and shape parameterization, several gaps in the FOWT sector craving for more research are detailed in the following subsections.

2.7.1 Surrogacy and MDAO

A surrogate is a mathematical approximation method used to predict the behaviour of a system using a set of sampling points, generally acquired from numerical simulations (Saad et al., 2019). Surrogate models/metamodels are models that mimic or clone the behaviour of the engineering system or the asset under investigation as closely as possible while being computationally less expensive to evaluate in comparison to the simulation model. The concept of surrogacy in any multidisciplinary system is fundamental. The surrogate model provides a more realistic representative model of the system than a low fidelity model, while also avoiding the high computational expense associated with high fidelity models, as discussed in Section 2.6.2.1. Different surrogate/meta modelling techniques of choice for multidisciplinary design analysis and optimization study are presented in Figure 9. Detailed review of these surrogate modelling techniques are provided in Younis and Dong (2010) and Jin (2011) .

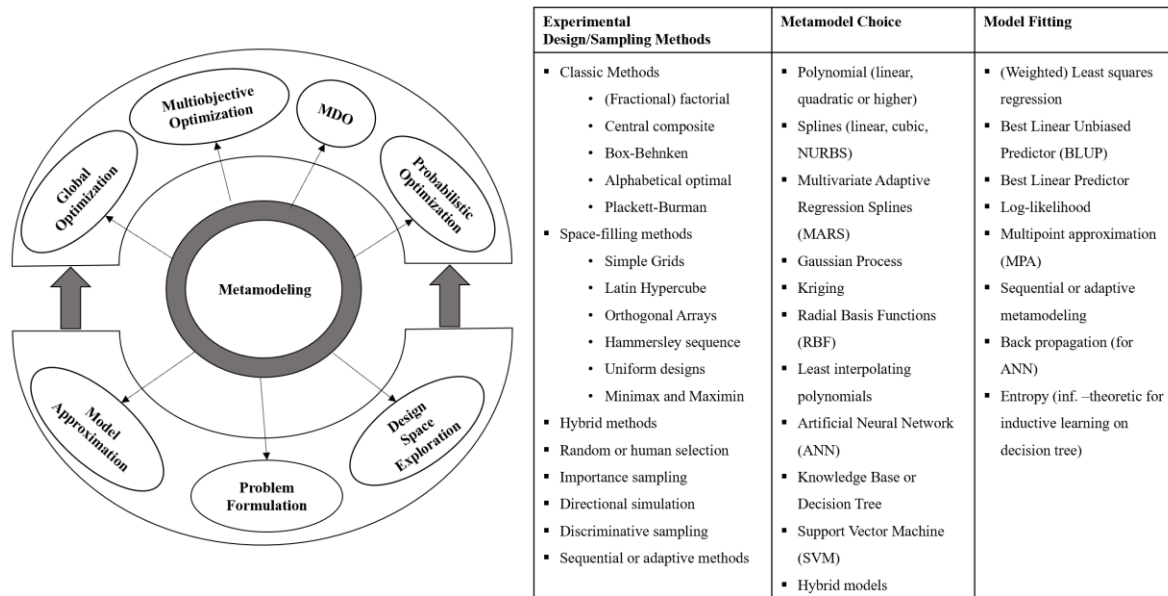


Figure 9. Surrogate / Meta Modelling as part of system optimization (left), Surrogate / Meta modelling techniques (right). (Frank Lemmer and Ricardo Faerron Guzman, 2016)

Optimization technique within an MDAO framework can have a combination of metamodel choices and optimization algorithms for effective system optimization. In the research conducted by Karimi (2018) on multidisciplinary design optimization of floating offshore wind turbine support structures for levelized cost of energy, the Kriging BAT (K-BA) optimisation algorithm was used to increase the efficiency of the BA algorithm to find the global optimal solutions. Just like the K-BA, these surrogate modelling techniques highlighted in Figure 9 can be combined with optimization algorithms for FOWT substructure optimization.

As highlighted in the works of Karimi (2018) and Saad et al. (2019), surrogacy (in this case Kriging-Surrogate model) helps to increase the efficiency of the BA algorithm to find global optimal solutions. Results of the work done by Saad et al. (2019) shows that in terms of search capability, efficiency and robustness, the new K-BA could demonstrate superior capability and suitability to other well-known global optimization (GO) algorithms. This is an area of research to be explored as it has the potential to make feasibility studies of projects to be conducted faster. Figure 9 also mentions the design of experiments (DOE), a technique for the optimal placing of test points within the design space to estimate the actual system model using one of the surrogate techniques (Saad et al., 2019). Some of the widely used DOE techniques shown in Figure 9 are Fractional Factorial, Central Composite Design (CCD), Box-Behnken, and Latin Hypercube Sampling (LHS).

2.7.2 Larger design space exploration

Design space exploration provides the ability to explore design alternatives prior to implementation (Kang et al., 2011). Design space exploration is important to perform optimization, eliminate inferior designs, and select a set of final design candidates for further study or validation. Large design space exploration and exploitation can be tailored to optimize the FOWT support structures.

In the works of Karimi et al. (2017) and Hall et al. (2013), the design space explored for optimization purposes spans across three stability classes of platforms with the main parameterization variables of diameter and draft. This design space can be made more expansive by including the mooring line design variables and constraints to increase the design space. A more expansive design space exploration and exploitation has the capability of providing more information with regards to the understanding and optimization of FOWT systems. At the moment, design space exploration of FOWT substructural system is mainly confined to the stability of the FOWT substructure. In simpler cases, the design space may be characterized as single body substructure (Spar) or multi-body substructure (Semi-submersible, TLP).

Instead of focusing on the diameter and draft variables for characterizing the design space as highlighted in Hall et al. (2013), (Karimi et al., 2017), perturbation of the geometry can expand the design space and enhances the selection of optimal and richer designs. Expanding a design space is achievable by increasing the variables in the parameterization scheme. Increasing the number of combinations of substructural parameters, or the use of robust parametric schemes to describe the design space, increases the chances of identifying an optimally designed system. The search for the optimal system is conducted using an optimization search algorithm and in cases where the search is exhaustive, surrogate-based optimization algorithms as discussed in section 2.7.1 - Surrogacy and MDAO can be used to identify the optimal design.

Another way of creating a large design space is to deviate from the traditional design in terms of geometric shapes and size as highlighted in Section 2.7.2.1.

2.7.2.1 Deviation from the traditional geometric shapes of FOWT substructure

The floating substructure configurations adopted by the FOWT industry have been based on the stability classes highlighted in section 2.2. In this infancy stage of FOWT systems, there is a need for deviation from the traditional shapes of floating substructure/ platforms for design

and optimization purposes. From this review, a research gap in platform's geometric shapes design for optimization purpose is identified with a need to develop a novel design framework that allows the exploration and analysis of unconventional floating support structural geometries optimized for FOWT requirements i.e., minimal requirements of effective hydrodynamic stability in deep waters coupled with the provision of a low levelized cost of energy (LCOE) from the FOWT system.

A design and optimization framework developed in the work of Leimeister et al. (2021) shows that the OC3 floating spar-buoy wind turbine system is heavily over-dimensioned as unnecessarily high safety factors are applied which inherently makes the design more costly (but should be noticed that this OC3 spar design has been developed more as a concept for numerical verification and comparison than a reference of an optimised spar). Leimeister et al. (2021) designed a FOWT system which is safely operating but close to the operational limits while constraining the outer floater dimensions to less than what obtains in the OC3 floater design; hence, a potential cost reduction.

As highlighted in section 2.4, design curve parameterization technique used for the design of ship hulls in Birk et al. (2004), Zhang et al. (2008) and Birk and Clauss (2008) can methodically be applied to the design of FOWT system to optimize floater design and generate design with optimal shapes satisfying the design requirements. A good representation of the different optimal shape is shown in Figure 10 and Figure 11. Figure 10 shows early shape design of semi-submersible and a new optimized semi-submersible shape in comparison to older generations of semi-submersibles – GVA 4000 (1983) and Transdetter (1987) while Figure 11 shows different design shape configuration for spar platform. This process of parameterization of the polynomial curves to automatically generate shapes for platform is discussed in the work of Birk et al. (2004) and Clauss and Birk (1996) although this is for platforms used in the oil and gas sector. This concept of shape generation and subsequent optimization can be used to increase the design space and design, analyse, and select optimal platforms for a floating wind turbine.

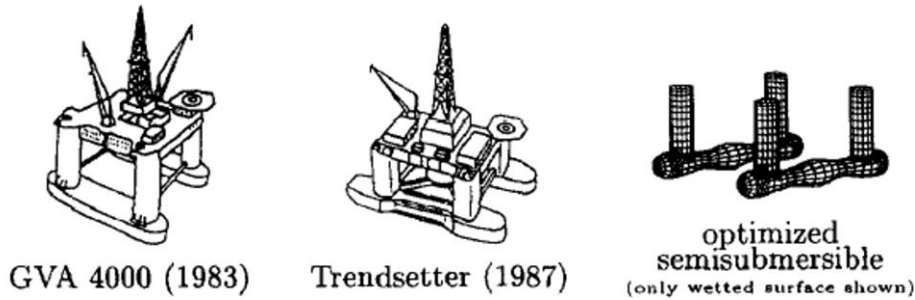


Figure 10. Deviation model from conventional semi-submersible design (Optimised model vs earlier generation models), adapted with permission from (Clauss and Birk, 1996).

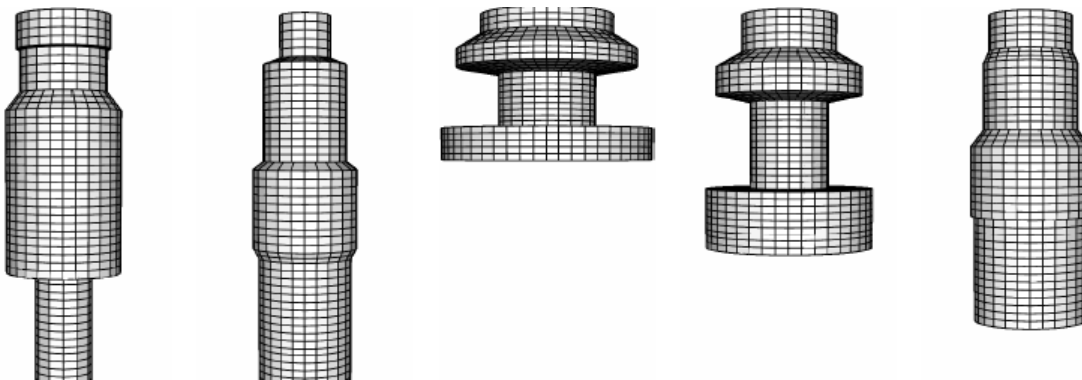


Figure 11. Deviation from conventional spar design with automated shape generation using polynomial curves, adapted with permission from (Birk and Clauss, 2008).

2.7.3 Upscaling of the platform design geometric variables

The concept of upscaling is a common tool employed in engineering design. An increase in turbine size contributes to the reduction in the levelized cost of energy. However, the substructure (Fixed bottom or floating) on which the turbine and tower is mounted must get larger. Instead of redesigning the support structure, the concept of upscaling the baseline substructure to the target substructure can be employed.

As detailed in the Light Rotor project (Bak et al., 2012), there has been a continuous upscaling of wind turbines since the early 70's. The Light Rotor project showed the design of a rotor and a wind turbine for a 10 MW wind turbine from a 5 MW wind turbine. The main objective is the use of a systems' approach to change the design of the blades to increase the stiffness and overall performance of the rotor taking into account aero-servo-elastic dynamics consideration. This kind of upscaling can be challenging because the mass of the turbine increases with the

cube of the rotor radius with linear upscaling. It's concluded that upscaling laws tend to overestimate the mass of the nacelle and drivetrain. Thus, the mass of the nacelle and drivetrain was reduced relative to the 5 MW wind turbine.

Few studies have been done on upscaling a FOWT system with a focus on the platform and some of the work done in upscaling FOWT system are highlighted in this section.

FOWT substructures, being a complex multidisciplinary structure can be optimized with regards to key performance metrics such as costs, structural integrity, reliability, nacelle acceleration subject to various constraints. Another means of optimizing a FOWT substructure is by upscaling the optimal shape parameterized floaters to highly rated and larger turbines. Just like a baseline design, the main criteria for upscaling a geometrically parameterized and optimized substructure for a FOWT system are stability, eigen frequencies, dynamic behaviour and response in accordance to recommended design requirements guidelines.

An example of linear or rational upscaling process of a FOWT substructure is discussed in the work of Leimeister et al. (2016b) in which they upscaled a 5 MW OC4 semi-submersible (baseline model) to 7.5 MW semi-submersible (target model). Upscaling of the semi-submersible FOWT substructure was based on the simple upscaling procedure in which the geometrical scaling factor is determined by the power rating of the wind turbines. The scaling factor of the platform is the square root of the ratio between the targeted power rating and the baseline power rating. They observed that the upscaled FOWT system had excess pitch stability and higher natural period than the baseline design. Building on this methodology, Ferri et al. (2020) proposed an optimization procedure that is able to reduce the peak response amplitude operator (RAO) in pitch up to 50% with respect to a traditional scaling factor based on the square root of the ratio of turbine power ratings.

Another example of rational upscaling is reported in Kikuchi and Ishihara (2019) in which the authors upscaled a 2 MW floating wind turbine used in the Fukushima FORWARD project to 5 MW and 10 MW by scaling the floater column radius with the cubic root of the mass ratio between turbines, and then scaling the column distance to preserve the static balance in pitch between overturning moment and pitch restoring moment. They found the overturning moment to scale roughly proportional to the power rating between turbines, or with the square of the turbine scale factor rather than the cubed scaling that would be expected in linear upscaling. Furthermore, Kikuchi and Ishihara (2019) estimated that capital costs per kW can be reduced by up to 57% when upscaling a 2 MW FOWT to 10 MW.

Further example of FOWT upscaling is detailed in Leimeister et al. (2016a). In this work,

7.5 MW and 10 MW semi-submersibles were developed based on the 5 MW OC4 semi-submersible platform. This work is based on an assumption made for scaling the overturning moment and this involves scaling the pitch restoring stiffness proportionally between the base design and the target design to preserve the maximum target pitch angle. Wu and Kim (2021) took this further by upscaling a 5 MW OC4 semi-submersible to a 15 MW semi-submersible. They developed two different scaling approaches: one that scales column radius and distance together with the same scale factor (referred to as Distance and Radius Scaling), and one that only scales the distance between columns (referred to as Distance Scaling). They found that scaling column radius was found to increase the metal mass and ballast mass of the platform, slowing the elevation of the center of gravity, and raising the heave natural period. Also, scaling column distance only was found to slightly reduce the heave natural period, which may pose issues related to resonant effects during storm conditions with long wave periods.

A comprehensive upscaling study was recently conducted by Papi and Bianchini (2022). The goal of their study is to define a set of metrics easily replicable by researchers that could enable a sufficiently fair comparison of turbines having different sizes. The two turbines compared in their study are the NREL 5 MW DeepCWind semi-submersible and the UMaine IEA 15 MW semi-submersible. The actual scale factors for the components within the FOWT system was presented in their study and the platform scale factor is lower than the values obtained using rational upscaling. With the use of a medium-fidelity tool OpenFAST, both sets of FOWT systems were analysed. Papi and Bianchini (2022) showed from their study that although platform RAOs peak frequencies decrease, tower loads are influenced by wave loading to a greater extent in the larger FOWT system. This is due to the increase in weight of the RNA, despite the fact that due to technological advancements RNA weight has increased far less than what would be expected from looking at turbines of a decade ago (Papi and Bianchini, 2022). Tower weight also contributes to increasing gravitational loading, especially in the IEA 15 MW, where the towers design required stiffening to support the additional loads.

For this review, the novelty of upscaling can be used on the geometrical shape parameterized and optimized floater scaled up to larger sizes based on the power rating of the new FOWT system. This approach is anticipated to reduce the cost of material expended on the system and also save a lot of computational time required for MDAO of a bigger turbine.

The novelty of the gaps highlighted in this review can further be enhanced by coupling the substructure / platform variants developed from each gap with the nouvelle multi-rotor turbines to reduce the footprint of materials used and enhance efficiency of the FOWT system.

Chapter 3 Geometric Design Parameterization and Optimization of Spar Floating Offshore Wind Turbine Substructure

3.1 Background

This chapter is based on an in-review publication pending final decision by Ojo, A., Collu, M., Coraddu, A. Geometric Design Parameterization and Optimization of Spar Floating Offshore Wind Turbine Substructure.

Geometric shape alteration is a useful tool for designing, analysing, and optimizing bespoke shape engineering designs like the FOWT platform designs. By exploring innovative geometric shapes, designers and engineers can potentially find new solutions that offer improved performance, reduced costs, and better reliability. A bespoke shape design that is fit for purpose and convincingly meet the engineering design requirements of a floating foundation can offer significant benefits over a traditional rectangular or cylindrical design. This is because a bespoke shape design can offer better dynamic response to external loads, reduced weight, improved stability, and reduced drag, all of which can improve the overall efficiency and performance of the offshore wind turbine system. Furthermore, the reduction in the weight of the floating platform contributes to the reduction in the capital cost of the platform and cumulative reduction of weight of several platforms can result in substantial reduction of capital cost when a FOWT project is scaled up.

The use of advanced computational tools, simulation techniques, and effective methodology to implement the framework can help to optimize the performance of bespoke shape designs and minimize computational cost (time), allowing designers to explore a wide range of design options and identify the most promising solutions. Details of the design and simulation tools used within the developed framework is highlighted further in this Chapter. Overall, geometric shape innovation can play an important role in advancing the design and performance of bespoke shape floating offshore wind turbine platforms, helping to drive the growth and development of the offshore wind industry by facilitating the design and production of platform types with capability to access richer wind resources in deeper waters (water depth greater than 60m). To speed up the increase in use of floating technology, there is need to reduce the floating foundation cost in comparison to the fixed foundation. Also, apart from the capital cost reduction, the computational cost of the design and analysis in time is also essential. This leads to the need of bespoke geometric designs with adequate parameterization technique integrated

within a multidisciplinary design analysis and optimization (MDAO) framework, as detailed in the gaps highlighted in Chapter 2.

The platform considered in this work is of the spar type. Although the spar concept is one of the most mature and also convenient for mass production and certification as a result of its simple geometry, it is still being advanced with innovative designs to unlock its potential, amongst which are: improved system's motion performance, simplified handling (construction, assembly, transportation and installation), and reduction in cost (Leimeister et al., 2018).

As highlighted in Chapter 2, geometric alterations of parametric free-form curves within an optimization framework have been implemented in the maritime, automotive, aerospace, and oil and gas sectors. This Chapter aims to implement the concept of geometric shape optimization within a MDAO framework to generate bespoke platform designs.

Early studies that have applied an optimization framework to enhance the hydrodynamic response of a floating offshore structure for the oil and gas industry are detailed in Clauss and Birk (1996), Birk (2006) and this knowledge is being adopted in the FOWT sector. Although FOWT system is still in the pre-commercial stage, there is now a lot of interest in the technology allowing a flurry of optimization studies to be conducted in advancing the design of the system. Optimization studies that detail the cost reduction and enhancing the hydrodynamic response of FOWT systems are highlighted in Karimi et al. (2017), Karimi (2018), Karimi et al. (2019), Fylling and Berthelsen (2011), Hall et al. (2013), Sandner et al. (2014). The examples of innovative work highlighted here are all based on a cylindrical spar design, with the design parameters subject to change limited to the diameter of the cylindrical spar and the draught. A change in this approach is highlighted in Ojo et al. (2022b), where the authors have used the FEDORA framework developed within the University of Strathclyde with commercial software from the DNV Manager suite (SESAM Genie and HydroD/WADAM) to parameterize and optimize the geometry of a 5MW OC3 spar.

3.2 State-of-the-art in Design, Analysis, and Optimization

Details of state-of-the-art review on optimization and analysis methodology to develop a robust MDAO framework that compliments the parameterization techniques discussed in this section are presented in Chapter 2. Integrating these design parameterization techniques with the optimization algorithm for exploration and exploitation yields an effective MDAO framework, as highlighted in Section 3.3 of this Chapter. While the properties of the different disciplines are considered within this MDAO framework – aerodynamics, structural, servo and

hydrodynamics, the optimal design is selected based on the hydrodynamic response of the system. This is because hydrodynamic response in the optimization of a FOWT system is essential for ensuring stability, maximizing energy production, reducing costs, and ensuring safety and regulatory compliance. Hydrodynamic forces have a profound impact on the overall performance and viability of FOWTs, and their detailed analysis and optimization as detailed in this Chapter are fundamental to the development of the FOWT sector.

Although the impact of structural response in the optimization of a FOWT system is not considered in this thesis, it is crucial for ensuring structural integrity, maximizing performance, enhancing cost-effectiveness, and complying with regulatory and environmental standards. Optimizing the structural response ensures that FOWTs operate safely and efficiently in the challenging offshore environment to reduce greenhouse emission and minimise costs and risks.

3.2.1 Design Analysis and Optimization Tools

Geometric shape optimization is an important component of engineering design. In the offshore industry, an efficient platform shape design process relies on several crucial components, including a structural geometry modeler, a capable mesh creator, advanced AHSE (Aero-Hydro-Servo-Elastic) solvers, and a cutting-edge optimizer. This section delves into some of the cutting-edge work carried out in the realm of floating offshore wind design and optimization.

3.2.1.1 Parametric Modelling Technique

As highlighted in Chapter 2, an extensive review of the state-of-the-art geometric parametric modelling of a system has been provided in Samareh (2001). For the purpose of this framework, the parametric modelling technique of use is the polynomial spline (NURBS option). NURBS are polynomial curves with the capability and flexibility to design a wide range of shapes ranging from points to straight lines and conic sections. NURBS are particularly useful for 3-D modelling as they make it simple for designers to manipulate control vertices / ISO curves as well as control the curvature and smoothness of contours. Both control points and weights define NURBS and it also requires little data for its definition. NURBS surfaces have many good properties, including visual fairness and perfect smoothness compared to design surfaces represented by discrete meshes. Unlike other parametric curves like B-Spline and Bezier curves, NURBS can represent most parametric implicit curves without loss of accuracy (Farin,

1990, Samareh, 2001). A representation of a NURBS curve is highlighted in Equation (4) of Chapter 2.

For the purpose of this study, the NURBS curve was utilized from the commercial software DNV SESAM Genie. Sesam Genie has a NURBS library with control point shape alteration feature for panel modelling, and FEM generation capability for frequency domain assessment.

3.2.1.2 Discipline Solvers and Optimizers

The solvers used for the multi-disciplinary analyses are either in the frequency or time domain. The choice between frequency domain and time domain solvers for multi-disciplinary assessment depends on a host of factors amongst which are and not limited to; computational time, desired accuracy, nature of the problem (linear/harmonic response or non-linear/transient response) and requirements of the analysis.

3.2.1.2.1 Frequency Domain

The frequency domain approach has been extensively used in the oil and gas industry. It enables the assessment of the system's response spectrum given the wave spectrum of the site and the response amplitude operator (RAO) of the given system (Journée and Massie, 2000, Patel, 2013). The resultant system of equations of motion in regular wave that governs the frequency domain approach is highlighted in Newman (2018). In depth details of the frequency domain approach and its application on offshore platforms for FOWT system are presented in Newman (2018) and reviewed in Chapter 2. The boundary element approach is used to approximate the hydrodynamic coefficients (added mass, radiation damping) and first order wave excitation forces, as a solution to the linear radiation-diffraction problem. This is implemented in commercial software like WAMIT and HydroD/WADAM – used in this study.

3.2.1.2.2 Time Domain Approach

The time domain approach adopts a time-domain coupled dynamics model with the ability to consider nonlinear forces and transient regimes. In order to get a more accurate assessment of these values, statistical analysis can be used to find the maximum, minimum, mean, variance, standard deviation, and significant values of each of the displacements, velocities, and acceleration. The time domain approach's comprehensive details are presented in Journée and Massie (2000) and reviewed in Chapter 2.

3.2.1.2.3 Optimizers

The nature of an optimization problem is greatly influenced by its objective or fitness function, which describes the quality or cost of a solution. Different characteristics of this function, such as whether it's concave, convex, linear, or non-linear, play crucial roles in determining how easy or difficult the problem might be to solve, and which optimization techniques are most appropriate. The formulation of a general design optimization problem is defined in the context of minimizing or in some cases maximizing an objective function subject to the design constraints. This statement can be represented for a single objective function problem as expressed in Equation (7) in Chapter 2 utilizing the gradient free pattern search method (PSM). The k-dimensional vector of design variables with lower and upper bounds, a single objective function, and the number of equality constraints and inequality constraints are carefully defined in Equation (7) in Chapter 2. This section further details bespoke methodology, which includes the use of GF optimizers to optimize a FOWT substructure while also taking the geometric shape into consideration with local perturbation of the control points to alter the shape of the geometric segment.

3.3 Methodology

Within an MDAO framework, the optimal geometric design perturbation using a parameterization technique aims to modify the shape of a FOWT substructure. Evaluating the new dynamic response characteristics of this altered shape necessitates an iterative process. However, this can be computationally intensive, leading to significant time and cost expenses.

As highlighted in Chapter 1, this research aims to develop An MDAO framework with a focus on altering the geometric shape of the floater within a FOWT system. This leads to the definition of an efficient shape parameterization approach for FOWT substructures, and the exploration of the design space with an optimization algorithm.

3.3.1 Design Variables

The selected design variables are mainly the set of diameters along the control points of the NURBS freeform curve. A typical spar design is characterized by a steel or concrete cylinder with a small water plane area and ballasted with water and/or solid ballast to keep the centre of gravity below the centre of buoyancy (Ghigo et al., 2020). Unlike the traditional spar platform, this variant of spar had varying diameters along specified control points located on the draft of the spar. The diameters at the control points along the length of the spar will affect the restoring

moment and hence the stability of the spar. Therefore, selecting the appropriate diameters for the design is carefully assessed to meet the stability requirement within the MDAO framework, which is a prerequisite met at the hydrostatic leg in Figure 13 before the hydrodynamic assessment.

Selecting the appropriate values for the design variables requires careful consideration of the seastates taken into account, the turbine and tower, and the desired static and dynamic response. A comprehensive MDAO framework integrated with NURBS shape parameterization technique is capable of generating an optimal spar-buoy floater design that is stable, cost-effective, and performs well in various environmental conditions.

3.3.2 Framework Development Tools

The MDAO framework depicted in Figure 13 and Figure 14 employs interface glue codes for discipline integration as shown in Figure 12 design, analysis, and optimization of multiple disciplines within the framework, aiming to efficiently resolve the optimization problem. The optimization problem in this study is the reduction in steel material required for the platform's design. The multidisciplinary design and analysis (MDA) is highlighted in Figure 13 and Figure 14 with the structural discipline design and shape parameterization technique and the platform's hydrostatic analysis assessed in Figure 13. The hydrodynamic analysis assessment is conducted in frequency domain to predict the system's response with the panel method, widely used in solving potential flow problems in Figure 14.

The selection of the optimal design is based on the meta-heuristic pattern search optimization algorithm (Torczon and Trosset, 1998). The tools used are Python suite, MATLAB for optimization and DNV suites - Sesam Genie with NURBS library with control point shape alteration feature for panel modelling, and FEM generation of the bespoke shaped spar design variants and HydroD/WADAM to investigate system's responses in the frequency domain.

3.3.2.1 DNV Suite

Three main DNV tools used within the MDAO framework are Sesam GeniE, HydroD and WADAM highlighted herein:

3.3.2.1.1 Sesam GeniE

Sesam GeniE is a tool for high level geometry modelling of beams, flat plates and stiffened shells (DNV, 2021). It is also used for load modelling amongst which includes equipment,

explicit loads, wind loads and generation of compartments in floating structures. This study has made use of the free-form parametric curves in Sesam GeniE to effect a change in the shape of the platform for optimization purposes within the framework.

3.3.2.1.2 DNV HydroD

The HydroD suite is used for hydrostatic assessment for stability and equilibrium of the floating structure (DNV, 2021). It provides analysis workflows for execution of WADAM as multiple floating equilibrium positions can be computed depending on mass and compartment filling fraction, estimated using the glue or interface code detailed in Section 3.3.2.3.

3.3.2.1.3 WADAM (Wave Analysis by Diffraction and Morison Theory)

WADAM is a general hydrodynamic analysis program for estimating wave-structure interaction for fixed and floating structures of arbitrary shape (DNV, 2021). WADAM performs hydrodynamic analysis in frequency domain using airy waves and it is based on the potential theory (radiation / diffraction) methodology for large volume structures (DNVGL Høvik, 2019, DNV, 2021).

3.3.2.2 OpenFAST

OpenFAST is a multi-physics, multi-fidelity tool for simulating the coupled dynamic response of wind turbines (OpenFAST, 2023). OpenFAST is an open-source framework that couples aero-hydro-servo-elastic engineering models for wind turbines – onshore and offshore in time domain. It is used to verify the frequency domain limit state results are still acceptable in the non-linear time domain assessment conducted this study.

3.3.2.3 Glue/Interface Code

This study developed a glue code to integrate the disciplines and operations within the framework as highlighted in Figure 12. The main programming languages used in the glue code are Python and MATLAB. The glue code facilitates the dynamic transfer of the random design variable within the specified bounds of the optimization algorithm to the NURBS control points within the panel modelling tool Sesam GeniE. This panel modelling process is the platform for a successful exploration of the design space for further characterization with design objective and constraints that leads to the selection of optimal designs. In addition to passing design variables from optimization algorithm to the control points along the NURBS curve for panel shape modelling, other tasks within the glue code are highlighted herein:

- Estimate the ballast filling fraction

- Pass design variables for Compartment shape from the optimization algorithm
- Assess optimization constraints in the hydrostatic leg
- Assess optimization objective function
- Sets framework to run automatically.

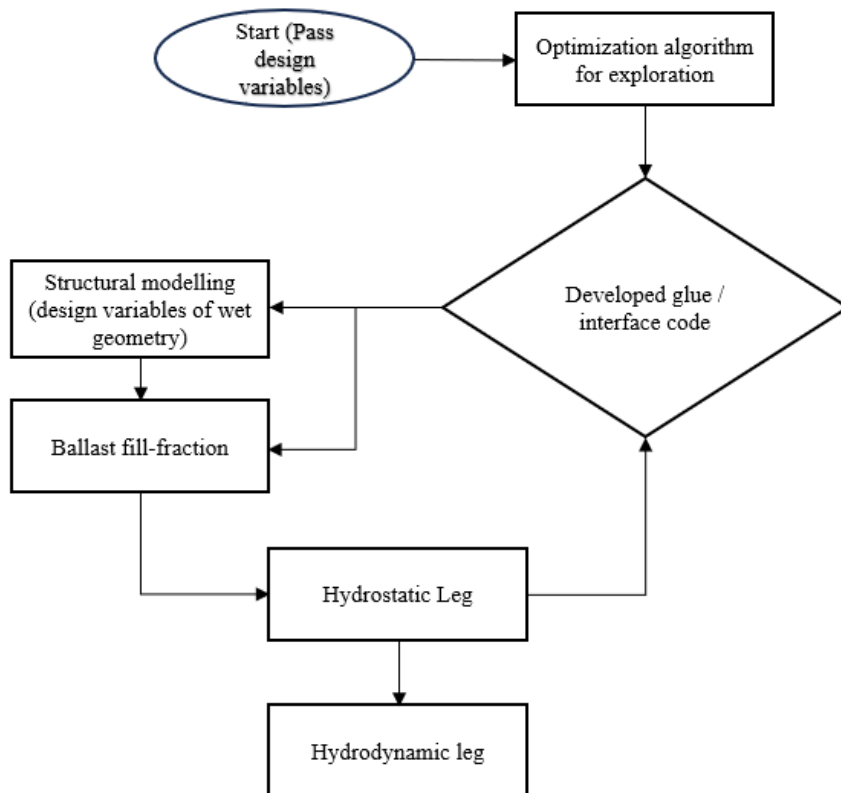


Figure 12. Interface code for discipline integration

The methodology proposed in this study is split into two phases to optimize the computational time. The phases are the **exploration** and **exploitation** phase and the constraint verification phase as shown in Figure 13 and Figure 14 respectively.

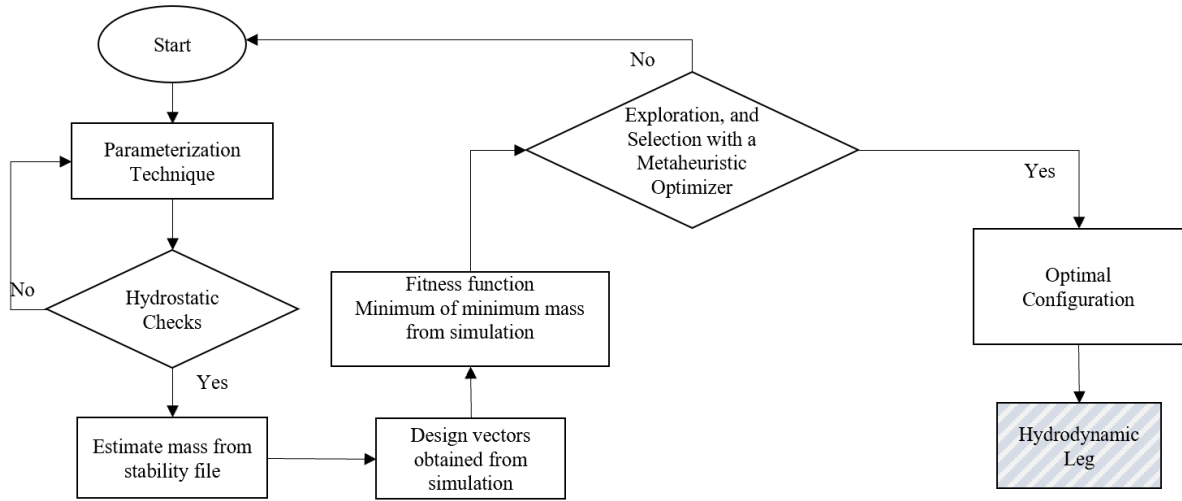


Figure 13. Flowchart of framework methodology – Exploration Phase – Hydrostatics

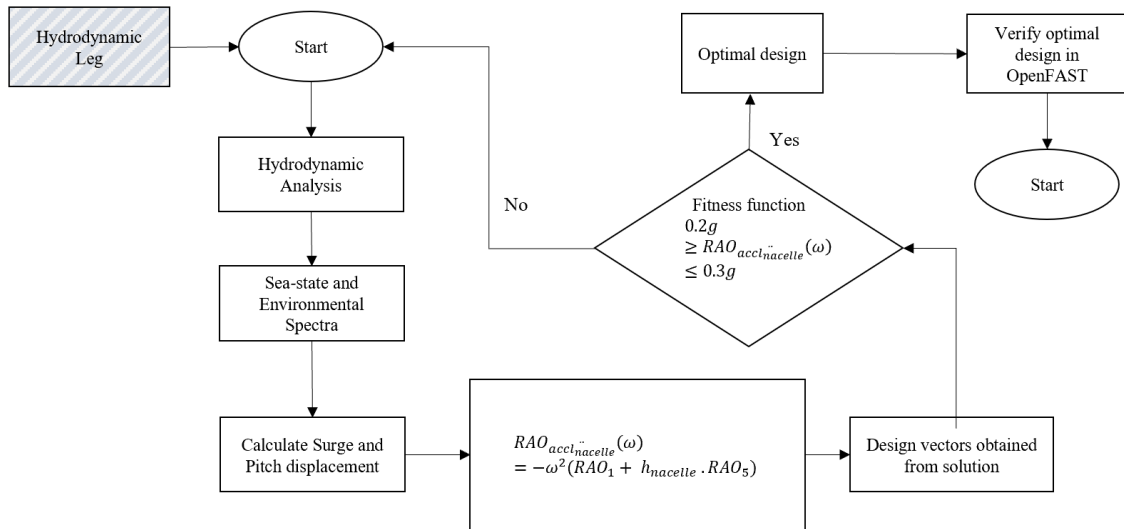


Figure 14. Flowchart of framework methodology – Selection and verification phase - Hydrodynamics

3.3.3 Exploration Phase

The first phase is the exploration stage, which is focused on the hydrostatic analyses to select the designs that satisfy the stability requirements, and also assess the objective function of the design with minimal mass. The optimization problem is defined in the exploratory phase as detailed in Section 3.5.3. For this work, the optimization problem is a non-convex, non-linear objective with a set of non-linear constraints as defined in Equation (7). In the exploration stage, a multidisciplinary design analysis and optimization scheme using curve

parameterization to alter the shape of the platform design is conducted. The parametric curve for the design is the cubic polynomial ordered NURBS curve from the commercial software DNV SESAM Genie. The design vector is composed of the control points defining the radii along the length of the spar, as shown in Figure 17 of Section 3.4.1 and Table 11 of Section 3.4.2. The parameterized NURBS curve is autonomously converted to a panel model and finite element mesh (FEM) files to prepare the designed structure for hydrostatic and hydrodynamic analyses. Three FEM files are generated from the cubic polynomial NURBS curve for hydrostatic and hydrodynamic assessment – panel model, compartment model and the total mass model.

3.3.3.1 Panel Model

This is the model defining the wet geometry of the platform below the sea water level. A couple of assumptions made in the panel model are highlighted in Journée and Massie (2000) amongst which includes inertia loads is the dominant loads, fluid is incompressible, irrotational and inviscid. To ensure a standard panel model, a CAD model providing a detailed geometric representation of the platform within the fluid domain is conducted with Sesam Genie. This includes information about its shape, size mass and dimension. The next step is to apply a mesh density size to the platform and a triangular mesh with 0.7m size was applied to the CAD model. A load case is created, and a dummy hydrostatic pressure is applied to the platform's draft below the MSL to create the wet geometry required for the velocity potential formulation and FEM generation. The generation of a finite element mesh to discretize the fluid domain. This involves dividing the continuous geometry from the CAD model into a finite number of smaller interconnected nodes and elements. This finite element mesh generated provides the numerical representation of the substructure beneath the MSL used in the hydrostatic phase.

3.3.3.2 Compartment Model

This is carefully designed considering that the compartment's shape has to change as the panel shape or outer shell changes, since different design vectors are passed through the iteration process. The authors developed a code which was integrated with the JavaScript code in Sesam Genie to align the compartment shape with the shape of the outer shell of the platform, and also calculate the equivalent ballast mass or compartment content filling fraction to stabilize the platform in the hydrostatic analysis phase.

The filling fraction is estimated from the hydrostatic result file. This is done adjusting the total mass of the system to the equivalent displaced mass of the platform. The ratio required to work the filling fraction for the ballast mass within the compartment model is highlighted in Equation (8).

$$Fill\ Fraction = \frac{Pfm_{dispmass} - Pfm_{mass}}{System_{totalmass} - Pfm_{mass}} \quad (8)$$

where $Pfm_{dispmass}$ is the mass of the displaced volume of seawater by the platform;

Pfm_{mass} is the steel mass or corresponding material mass of the platform;

$System_{totalmass}$ is the total mass of the platform, mooring, tower and rotor nacelle assembly.

3.3.3.3 Total Mass

The total mass model of the system, which includes the platform panel, the compartment, the tower, and the rotor nacelle assembly, are modelled to account for the system's total mass, which is used for estimating the restoring moment of the FOWT system. This is also essential for estimating the structural mass moment of inertia in all degrees of motion for the FOWT system. To accurately model the total mass; the nacelle's mass and center of gravity, the tower mass and its center of gravity and the substructure mass and center of gravity are accounted for in a unique name set or model subset. A finite element mesh is generated for this named set to capture the geometric and physical properties and serve as a numerical representation of the structure in the hydrostatic phase.

The analysis part of the MDAO framework assesses the hydrostatics and hydrodynamics characteristics of the system, using the potential theory approach, and it is discussed in detail and verified for the reference OC3 FOWT system, modelled with the NURBS curve in Section 3.4.2, with the results of the hydrodynamic coefficient added mass, damping, force excitation and the values of the response amplitude operators showing a good agreement with the published data.

Coupling the optimization algorithm with the design and analysis stages completes the autonomous MDAO framework. The MDAO framework is automated with a set of MATLAB and Python codes to ensure that the whole MDAO cycle, from the definition of the design vector to the hydrostatic and hydrodynamic analyses, to the evaluation of the objective function and

the definition of the next design vector, is fully automatic, i.e., no manual input is required. The iterative process continues until the design space has been substantially explored and exploited. The variation of the control points because of the autonomous input of the design vectors by the pattern search method (PSM) along the length of the NURBS curve is schematically illustrated in Figure 15. The straight lines used in Figure 15 can be described as a parametric curve of zero continuity, hence, the sharp edges at the radii of the control points changes. The NURBS curve used in this study has a C^2 (slope and curvature) continuity, which ensures continuous smoothness of the NURBS curve at the control points along the spar. Details of the integrated parametric design within the MDAO framework, to select feasible design that satisfies the stability requirements are discussed in Sections 3.5.1 to 3.5.4.

3.3.4 Verification Phase

The second stage is the verification phase. This stage is focused on the hydrodynamics of the selected designs from the exploration phase, analysed with low-fidelity frequency domain hydrodynamic analysis tools - Sesam HydroD (WADAM/WAMIT) - and verification of the results with a medium-fidelity hydrodynamic tool - OpenFAST due to its capability of accounting for non-linearities from mooring systems and aerodynamic systems of the FOWT system. The process required for this verification stage is detailed in the flowchart in Figure 14. This verification phase is more of a confirmation that the constraints within the MDAO framework are still within the allowable values from the design codes and standards in a time domain assessment when non-linear forces are considered.

A standalone case study for an OC3 platform with a normal sea-state is analyzed hydrodynamically to assess the response of the system and verify the assessed responses with a medium fidelity time domain tool, as detailed in Section 3.4.3. Similarly, a detailed hydrodynamic analysis with a severe sea state using DLC1.6 design load case from IEC-61400-3-2 (2019) with the selected optimized shape variants from the design space is detailed in Section 3.6 with results highlighted in Section 3.6.4.1. The verification of the design with medium fidelity time domain analytical tool is presented in Section 3.6.4.2.

An alternative approach would be to combine phase 1 and 2 (i.e., Figure 13 and Figure 14) into a single framework, such that the hydrodynamic analysis is performed in conjunction with the structural and hydrostatic analyses. However, this kind of framework is too computationally expensive since there may be the possibility that non-feasible designs, i.e., designs that do not

satisfy the static stability requirement at the hydrostatic check, which can be verified without a hydrodynamic analysis, are needlessly further analyzed in the hydrodynamic phase, leading to an unnecessary waste of computational time. Hence, the separation of the MDAO framework into two phases for optimization of the computation time. Therefore, the split ensures that only shapes that can be feasibly modelled and provide possible solutions to the optimization problem from the first phase are hydrodynamically assessed in the second phase with high/medium-fidelity tools to assess the response of the system before selection.

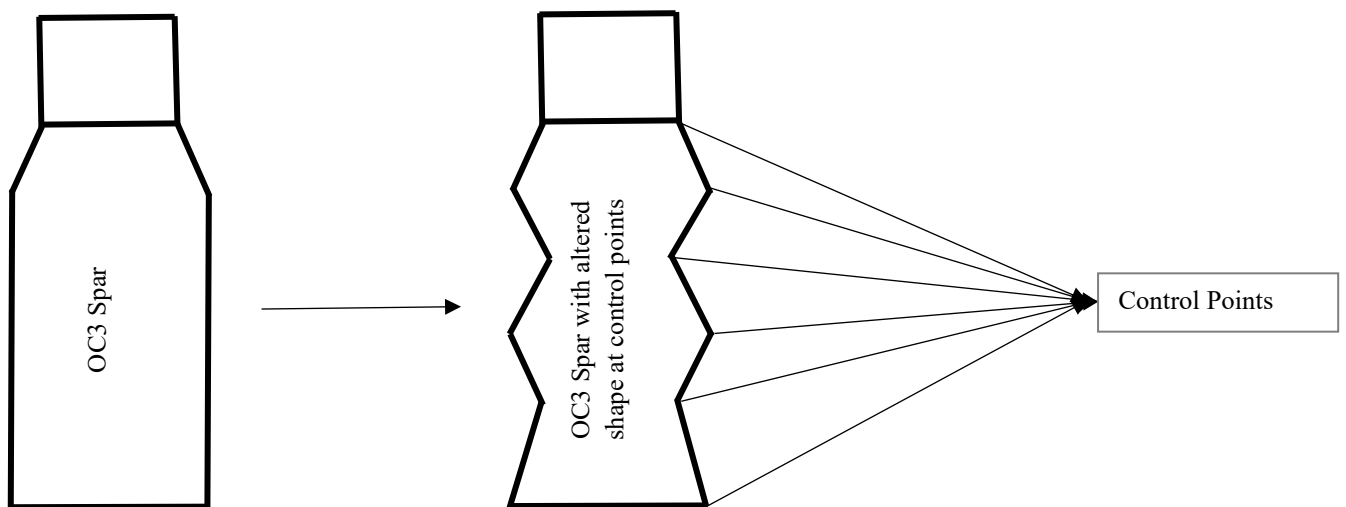


Figure 15. Variation of control points along the NURBS curve

3.4 Substructure OC3 5MW Case Study

3.4.1 Overview

The OC3 phase IV spar floater is an axis-symmetric ballast stabilized platform coupled to a horizontal axis wind turbine (HAWT). It is moored with three catenary mooring lines with equally spaced fairlead positions at a depth of 70m below SWL, and a radius of 5.2m from platform centreline. The anchors are located at a water depth of 320m and at a radius of 853.87m from platform centreline. It is a derivative of the Hywind spar (Siemens, 2009) and it is modified to support the NREL 5MW reference wind turbine (Jonkman et al., 2009). Comparison of the structural parameter values shows that the dimensions, apart from the improved and reduced draft of the real systems, lie between the dimensions of the Hywind

Demo for a 2.3MW wind turbine and the Hywind Scotland floater supporting a 6.0 MW wind turbine (Leimeister et al., 2020a).

A representative sketch of the OC3 spar FOWT system is highlighted in Figure 16 with the floater model shown in Figure 17. The geometric parameters for the spar are presented in Table 7. The structural parameters like the mass of the spar including ballast, center of mass, moments of inertia, and additional linear damping in surge, sway, and yaw are detailed in Jonkman (2010), and highlighted in Table 8. The NREL 5MW reference turbine is mounted on the OC3 Spar to complete the FOWT system. A detailed description of the platform geometric properties, platform structural properties, tower and hub properties, and structural properties of the wind turbine topsides are presented in detail in Jonkman (2010), and highlighted in Table 8 to Table 10 respectively.

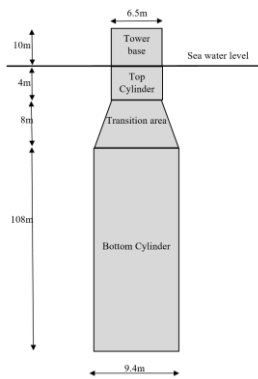


Figure 16. OC3 spar Sketch

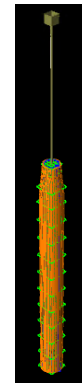


Figure 17. NURBS model of an OC3 FOWT System in Sesam GeniE

Table 7: Geometric parameters for OC3 spar (Jonkman, 2010)

| Parameters | Dimensions (m) |
|---|----------------|
| Top cylinder diameter | 6.5 |
| Height of top cylinder | 4 |
| Diameter at top of transition area | 6.5 |
| Diameter at base of transition area | 9.4 |
| Height of transition area | 8 |
| Bottom cylinder diameter | 9.4 |
| Bottom cylinder height | 108 |
| Base of bottom cylinder to base of tower base (Draft) | 120 |

Table 8: Floating platform structural properties (Jonkman, 2010)

| Parameters | Values per Literature |
|---|-----------------------|
| Platform mass (including ballast) - (kg) | 7,466,330 |
| Center of mass below Sea water level (SWL) – (m) | 89.9155 |
| Platform roll inertia- about center of mass – kgm ² | 4,229,230,000 |
| Platform pitch inertia- about center of mass – kgm ² | 4,229,230,000 |
| Platform yaw inertia- about central axis – kgm ² | 164,230,000 |

Table 9: Tower and hub properties for OC3 floating system

| Parameters | Values per Literature |
|--|-----------------------|
| Tower top diameter – (m) | 3.87 |
| Tower top wall thickness – (m) | 0.019 |
| Tower base diameter – (m) | 6.5 |
| Tower base wall thickness – (m) | 0.027 |
| Hub height – (m) | 90 |
| Elevation of tower top – (m) | 87.6 |
| Elevation of tower base – (m) | 10 |
| Material density – kg/m ³ | 8500 |
| Proportional gain at minimum blade-pitch setting – s | 0.006275604 |
| Integral gain at minimum blade-pitch setting | 0.0008965149 |

Table 10: Structural properties of the turbine top sides

| Parameter | Value per Literature |
|--|----------------------|
| RNA mass – kg | 350000 |
| Tower mass – kg | 249700 |
| Center of tower mass (above SWL, along central axis) - m | 43.4 |

3.4.2 Frequency Domain – Potential Flow Theory OC3 spar

The modelling process of a FOWT system or FOWT substructure can be done with a host of state-of-the-art design tools based on different simulation codes with varying capabilities for handling AHSE calculations as detailed in (Cordle and Jonkman, 2011). Some of the tools highlighted in Cordle and Jonkman (2011) are OpenFAST/FAST, ADAMS (Automatic Dynamic Analysis of Mechanical Systems), Bladed and SIMO/RIFLEX (Simulation of Marine

Operations). Most of these design tools are time domain analysis tools; hence, more computationally expensive.

For the purpose of this work, the tools used for the design and analysis of the OC3 spar is the Sesam suite (GeniE and WADAM). GeniE is a tool for concept or high-level modelling of beams, stiffened plates, shells and curved edges. GeniE has an extensive library of guiding geometry tools that helps create beams, plates and curved surfaces. Some of these tools are circular / elliptic arcs, cubic splines, B-splines, polycurves and NURBS. The NURBS curve from GeniE is used to model the spar substructure with 14 control points (13 below sea water level and 1 above) representing the radii along the draft of the platform. Each green grid in Figure 17 represents the control point in which the NURBS curve passes, and information/details about these control points is shown in Table 11. The thickness of the platform is calculated from the mass of steel derived from the product of the estimated mass based on geometry of the displaced volume and a ratio of 0.13 (Bachynski and Collu, 2019). Based on the steel mass to mass of displaced volume ratio, the iterative process estimates the thickness value that corresponds to the target value of the system's total mass to be equivalent to the mass from the buoyancy force. After several iterations, a wall thickness value of 0.04m along the length of the spar correspond to the buoyancy mass / total mass of the system.

The tower and the rotor nacelle assembly (RNA) are modelled in GeniE as a dummy beam, with the center of mass assigned to the dummy beam corresponding to the calculated center of mass of the tower and the RNA. The dummy beam with the assigned center of mass is connected to the OC3 spar and meshed in GeniE. Three FEM files are required from the modelling stage. The first is the FEM file for the panel model for potential flow theory, i.e., the wetted surface. This allows the capture of the three potentials from first order wave excitation which are the potential due to incident wave, the diffraction potential due to the presence of a fixed platform and the radiation potential caused by the first order oscillatory motion of the body (platform) in the fluid. The second FEM mesh required is for the compartment model, and the third FEM file represents the total structure i.e., the platform and the dummy load representing the tower and the rotor nacelle assembly.

The FEM files taken to the WADAM solver for hydrodynamic analysis to investigate the system's response. WADAM uses the first and second order 3D potential theory for the wave load calculations in which the incident wave is an Airy wave and the analysis is performed in the frequency domain. Using the NURBS parametric technique to model the OC3 spar with data from Table 11 in Sesam GeniE and conducting hydrodynamic analysis using the potential

flow theory discussed in Section 3.2 with the WADAM option in the Sesam HydroD tool, a host of results compared with literature results from Jonkman (2010) are highlighted in this section. The compared results highlighted are the added mass coefficients, radiation damping coefficients, force and moment excitation and the response amplitude operators in Figure 18 to Figure 21.

The results reported from Figure 18 to Figure 21 verifies the fidelity of using the potential flow approach and conducting simulation in computationally less expensive low-fidelity frequency domain tool with the alignment of the simulation model results with results from the literature.

Table 11: OC3 Spar NURBS curve control points below sea water level

| OC3 Radii along vertical axis representing B-spline | Height (m) | 0 | 4 | 12 | 30 | 40 | 50 | 60 | 70 | 80 | 90 | 100 | 110 | 120 |
|---|------------|---|------|------|-----|-----|-----|-----|-----|-----|-----|-----|-----|-----|
| | Radius (m) | | 3.25 | 3.25 | 4.7 | 4.7 | 4.7 | 4.7 | 4.7 | 4.7 | 4.7 | 4.7 | 4.7 | 4.7 |

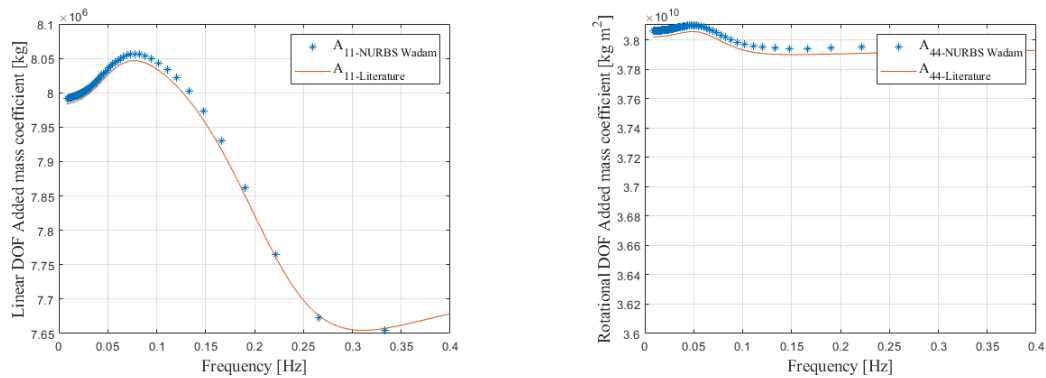


Figure 18. Added mass coefficients (B-spline model vs literature model)

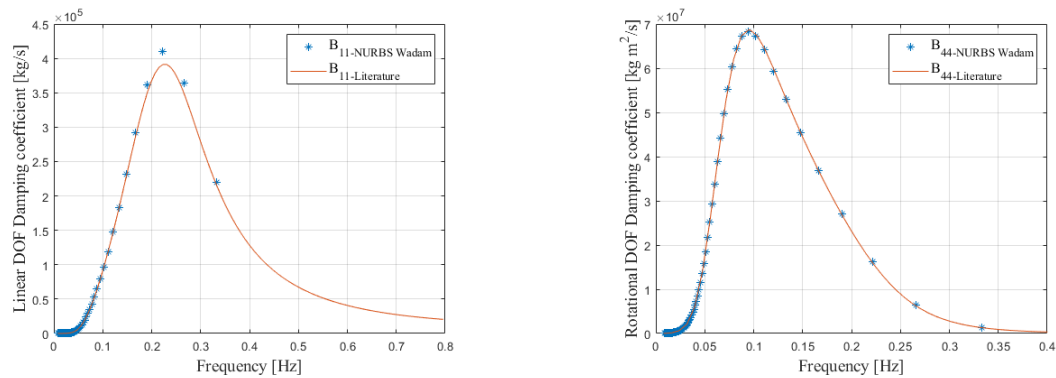


Figure 19. Damping coefficients (B-spline model vs literature model)

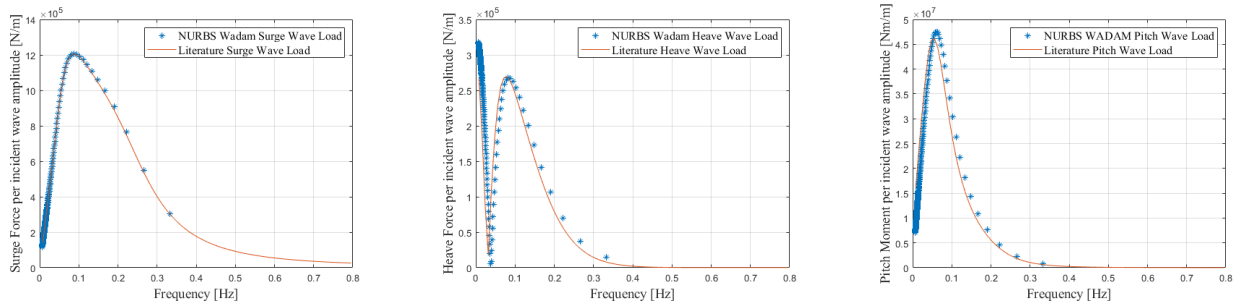


Figure 20. Excitation loads and moment (B-spline model vs literature model)

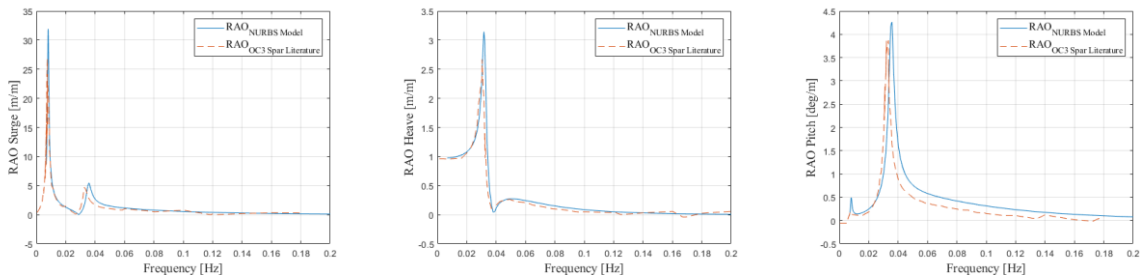


Figure 21. Surge, Heave, and Pitch RAO (B-spline model vs literature model)

3.4.3 Time domain Coupling and Response Verification (Medium Fidelity Tools)

A time domain analytical assessment is conducted with OpenFAST – a medium fidelity tool with the capability of using the Cummins equation time domain analysis approach highlighted in Section 2.5.2 of Chapter 2 for modelling the substructure of a rigid body, taking into consideration the non-linear forces acting on the system. The potential flow model from WADAM produces added mass, radiation damping, and first order wave forces in the frequency domain. The frequency-dependence added mass and damping for radiation force and the wave load transfer functions are included in the Cummins equation.

In assessing the time domain with OpenFAST, the substructure files (added mass and radiation damping file, first order wave excitation force/moment file, and the hydrostatic file) from the frequency domain analysis, discussed in Section 3.4.2, are used by OpenFAST. A time domain simulation for a sample design load case was performed, taking into account a normal environmental sea state with a significant wave height of 6m, and a peak period of 10s, and a rated wind speed of 11.4m/s. Figure 22

The plots in Figure 22 shows a close match in the motion response across all degrees of

freedom. Table 12 further highlights the mean percentage error statistics for the motion response in each degree of freedom from the plots in Figure 22, comparing the reference 5MW NREL OC3 model from OpenFAST with the equivalent NURBS platform model coupled to the reference 5MW NREL turbine. The results indicate minimal mean percentage error, with the largest deviation observed in the heave degree of freedom at 7.5%. Despite this, the difference remains minimal, showcasing consistency between the OpenFAST and NURBS model results.

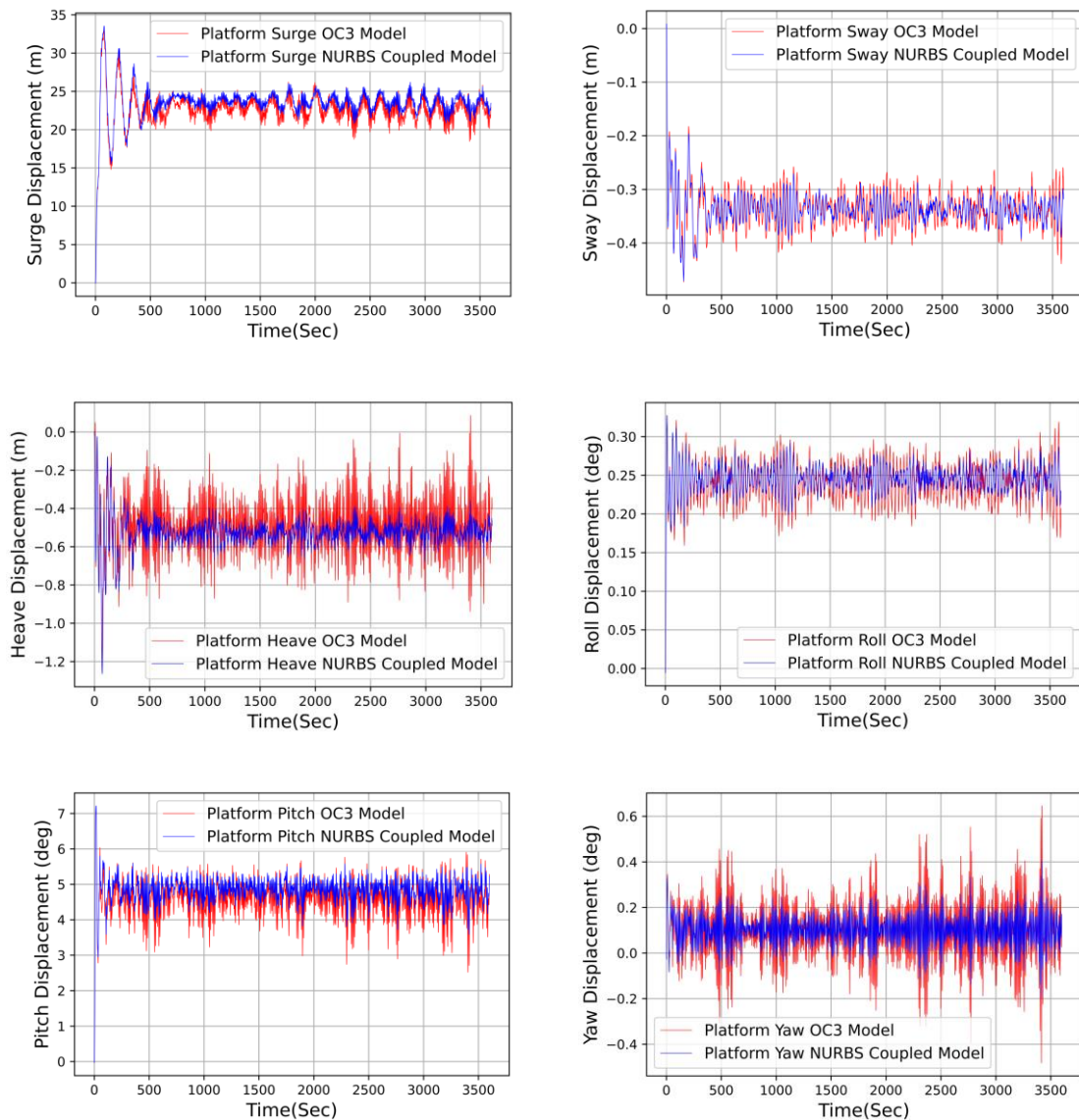


Figure 22. NURBS Platform Coupled Platform Response vs NREL 5MW OpenFAST Design Response

Table 12. Motion response statistics (OC3 model vs NURBS model)

| Degree of Freedom | Maximum OC3 | Maximum NURBS Coupled | Maximum Percentage Error | Mean OC3 | Mean NURBS Coupled | Mean Percentage Error | Minimum OC3 | Minimum NURBS Coupled | Minimum Percentage Error |
|-------------------|-------------------|-----------------------|--------------------------|-------------------|--------------------|-----------------------|--------------------|-----------------------|--------------------------|
| Surge | 26.22m | 26.02m | 0.77% | 22.73m | 23.51m | 3.32% | 18.47m | 20.79m | 11.16% |
| Sway | -0.25m | -0.27m | 7.41% | -0.34m | -0.33m | 3.03% | -0.44m | -0.39m | 12.82% |
| Heave | 0.09m | -0.35m | 125.71% | -0.49m | -0.53m | 7.55% | -0.94m | -0.68m | 38.24% |
| Roll | 0.32 ⁰ | 0.29 ⁰ | 10.34% | 0.24 ⁰ | 0.25 ⁰ | 4.00% | 0.17 ⁰ | 0.20 ⁰ | 15.00% |
| Pitch | 5.91 ⁰ | 5.58 ⁰ | 5.91% | 4.60 ⁰ | 4.85 ⁰ | 5.15% | 2.52 ⁰ | 3.59 ⁰ | 29.81% |
| Yaw | 0.65 ⁰ | 0.40 ⁰ | 62.50% | 0.10 ⁰ | 0.10 ⁰ | 0.00% | -0.48 ⁰ | -0.20 ⁰ | 140.00% |

3.5 Shape Design Parameterization, Analysis, and Optimization of Models

This section details the use of polynomial curves and their integration with a state-of-the-art optimizer to effectively explore the design space and select optimal design variants, with varying shapes satisfying the stability design requirements for offshore floaters. The optimal variants selected will be subject to further analysis to verify their suitability.

3.5.1 Geometric Shape Design and Variants generation.

The NURBS curve is used to model the spar platform with 14 control points and 13 segments as highlighted in Table 15. The NURBS curve is a generalization of B-Spline; hence, it has important geometric properties of B-Spline (Samareh, 2001), amongst which are:

- The order or degree chosen for the curve is independent of the control points.
- Unlike a Bezier curve, NURBS/B-Spline have the local propagation property which enables effective control of the local shape around the control points of interest.
- NURBS/B-Splines are invariant under Affine transformation. This ensures the curve doesn't change under transformations like translation, rotation, scaling, and shearing
- It has a convex hull property and a partition of unity property

The local propagation property of the NURBS curve is essential for the geometric shape variation and optimization that will be extracted from the axis-symmetric spar floater. The varying parameter along the fixed length of the spar is the radii at all the specified control points. The variation of the radii along the spar's length is automated and follows an iterative process where the set of radii from the specified objective function is written into the modelling file in Genie before a hydrostatic analysis is conducted in HydroD.

3.5.2 Integration with Optimization algorithm

The optimizer utilized in this geometric shape parameterized modelling framework is the meta-heuristic pattern search optimization algorithm method (PSM). PSM is one of the most frequently used methods designed to solve the gradient free optimization problems.

The use of an optimization algorithm like Pattern Search is advantageous because it has global convergence capability as its primary property, which prevents stagnation in local minimum because it presents an exhaustive search throughout the search (Palacio-Morales et

al., 2021). For this work, a multi-start method is encoded within the pattern search algorithm. The multi-start enhanced Pattern Search algorithm strategically samples the solution space of the optimization problem. This technique alternates between two phases for a predetermined number of global iterations. The first stage develops a solution, while the second stage aims to enhance the result. The algorithm's final output is the best overall solution, which is the best of the local minima within the global design space. On completion of the sampling process, the global optimum is selected from the list of local minima as the solution that mostly satisfies the objective function. To produce an efficient method for producing high-quality solutions, the interaction between the two phases balances search diversification with search improvement. The nature of the optimization problem is described in Equation (7) of Chapter 2, in which the solution is to minimize the objective function (mass of the substructure).

3.5.3 Definition of the Optimization Problem

This work uses the local propagation properties of the NURBS curve with a PSM optimization algorithm to solve a defined optimization problem. The optimization problem in Equation (7) has a non-linear and non-convex objective with a series of non-linear constraints. To resolve this optimization problem, different methodologies can be exploited as detailed in Kochenderfer and Wheeler (2019). A series of no free-lunch theorems Wolpert and Macready (1997) ensure that there is no way to choose a priori the best optimization algorithms for a particular problem and the only option is to empirically test multiple approaches to verify the most feasible approach. Nonetheless, PSM has been used in this work (Findler et al., 1987, MathWorks, 2021), supported by findings in other disciplines amongst which is its capability to navigate large, multimodal search spaces with ease, finding optimal solutions where others might struggle as detailed in Torczon and Trosset (1998), Saenz-Aguirre et al. (2022).

Moreover, based on floating foundation optimization conducted in Frank Lemmer and Ricardo Faerron Guzman (2016) considering simple algorithm (GA, Particle swarm algorithm and PSM approaches), it was recommended to use pattern search as the optimization solver to be integrated into the dynamic simulations.

Since the starting point influences the convergence of all the PSM algorithm, a multi-start strategy is employed for this study (Laguna and Martí, 2003). The starting points for the optimization process have used 50 random points uniformly distributed in the domain induced by the non-linear constraints of the optimization problem in Equation (7). The optimization methods have been implemented using the Matlab 2017 environment.

In this work, the optimization problem is defined to minimize the objective function as detailed in Equation (7). This optimization problem shows the objective function – \mathbf{J} to be minimized is dependent on the design variables x and the inequality constraints – g . The parameters that make up the optimization problem to generate a novel shaped optimized platform are detailed in the Sections 3.5.3.1 to 3.5.3.3.

3.5.3.1 Design Variables

The design variable for modelling the spar is a set of 14 control points along the NURBS curve and a draft value of 120 meters for each static pitch design considered. The control points are in steps of 10 meters apart from the base of the tower to the base of the platform. Mathematical expression and description of the variables is presented in Table 13.

Table 13: Definition of design variables

| Platform design variables | Description | Compartment design variables | Description |
|---------------------------|--------------------------|------------------------------|--------------------------|
| x_1 | Radius at tower base | - | - |
| x_2 | Radius at MSL | x'_1 | Radius at MSL |
| x_3 | Radius at 4m below MSL | x'_2 | Radius at 4m below MSL |
| x_4 | Radius at 12m below MSL | x'_3 | Radius at 12m below MSL |
| x_5 | Radius at 30m below MSL | x'_4 | Radius at 30m below MSL |
| x_6 | Radius at 40m below MSL | x'_5 | Radius at 40m below MSL |
| x_7 | Radius at 50m below MSL | x'_6 | Radius at 50m below MSL |
| x_8 | Radius at 60m below MSL | x'_7 | Radius at 60m below MSL |
| x_9 | Radius at 70m below MSL | x'_8 | Radius at 70m below MSL |
| x_{10} | Radius at 80m below MSL | x'_9 | Radius at 80m below MSL |
| x_{11} | Radius at 90m below MSL | x'_{10} | Radius at 90m below MSL |
| x_{12} | Radius at 100m below MSL | x'_{11} | Radius at 100m below MSL |
| x_{13} | Radius at 110m below MSL | x'_{12} | Radius at 110m below MSL |
| x_{14} | Radius at 120m below MSL | x'_{13} | Radius at 120m below MSL |

An example of the optimal design variables for design use cases assessed is shown in Table 15. The design variables are set within bounds – Lower and upper bounds. The lower bound is the minimum value that can be passed into the control points to vary the substructure’s shape locally and the upper bound is the maximum value to be passed into the control points. The lower and upper bound values set for the shape optimization assessment in this chapter is 1m and 7 m respectively.

3.5.3.2 Objective function and constraints

The objective function, to be minimised, is the structural mass of the geometrically modified spar, and the output is dependent on the hydrostatics assessment of the design models. The structural mass has the capability of directly influencing the material cost, labour cost (manufacturing), transportation cost and cost of installation (increase or decrease in the size of lifting equipment). General expression for minimizing objective function is highlighted in Equation (7). The mathematical expression for calculating the mass of the optimal substructure design which is the main objective in this work is shown in Equation (9).

$$\begin{aligned} mass &= \rho_{steel} * Vol_{Substructure} \\ Vol_{Substructure} &= \int_{-draft}^{10} A_x(x) dx \end{aligned} \quad (9)$$

Where ρ_{steel} is the density of steel, $Vol_{Substructure}$ is the volume of the substructure, A_x is the sectional area and (x) is the sectional height along the length of the substructure. For the optimization framework utilized in this study, a multi start approach is employed to eliminate local minima issues; hence, the minimum of the minima is selected as the optimal design variable in the explored design space.

3.5.3.3 Optimization Constraints

With a focus on shape parameterization within the optimization framework in this study and in order to simplify amount of design variables, the draft length is kept constant and constrained to a value of 120 m and the set of design variables radii that are passed into the control points are randomly varied in every iteration.

The main constraint driving the platform's shape alteration and optimization within the framework is the static pitch angle constraint derived from the restoring and inclining equation of the FOWT system with a thrust force of 785KN at the nacelle to estimate the inclining moment. Derivation of the static pitch angle is detailed in Section 5.3.3 of Chapter 5 The static pitch angle derived should not exceed the maximum operational static pitch angle of inclination set for the FOWT system. This non-linear constraint is key in estimating the optimized platform's masses and three use cases of 5 deg, 7 deg and 10 deg static pitch angles are considered. Other constraints developed along with the static pitch angle constraint are the

floatability constraint, imposed as having a ballast mass greater than zero, and the nacelle acceleration constraint. Summary of these constraints are presented in Table 14.

Table 14: Optimization Constraints

| Inequality Constraint | Formal expression | Description |
|--------------------------|---|---|
| g_{SP_05} | $g_{SP_05} \leq 5^\circ$ | Maximum static pitch less than or equal to 5 deg |
| g_{SP_07} | $5^\circ \leq g_{SP_07} \leq 7^\circ$ | Maximum static pitch greater than 5deg and less than of equal to 7 deg |
| g_{SP_10} | $7^\circ \leq g_{SP_10} \leq 10^\circ$ | Maximum static pitch greater than 7deg and less than of equal to 10 deg |
| $g_{ballast}$ | $g_{ballast} \in \mathbb{R}$ | Calculated ballast a positive real number |
| $nacelle_{acceleration}$ | $nacelle_{acceleration} \leq 2.943$ | Nacelle acceleration less than 30% of gravitational acceleration. |

3.5.4 Shape optimization process within MDAO framework

As highlighted in the optimization constraint section, the driving constraint is the maximum operational static pitch angle of inclination. The maximum pitch angle of inclination (static) is varied, defining three cases: 5 deg, 7 deg, and 10 deg, in the context of the hydrostatic analysis phase highlighted in Figure 13. Based on the defined constraints and objective function, the MDAO framework is executed following the steps highlighted below:

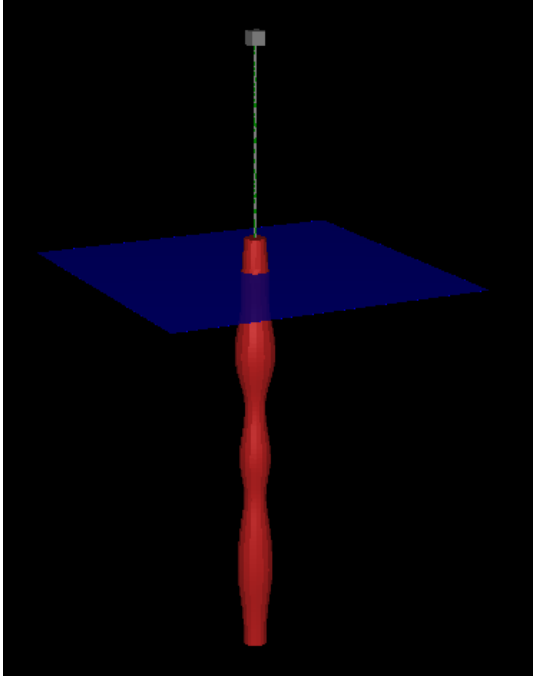
1. A sampling size “n” is defined within the multi-start code embedded in the PSM. “n” is an integer and for the purpose of this framework, set as 50.
2. Upper and lower bounds for the design vector variables are set within the PSM (to write the design variables into the NURBS curve within DNV Sesam Genie’ Java Script (JS) file). The upper bound and lower bound diameter values of 7m and 1m respectively are specified within the PSM.
3. Three finite element mesh (FEM) models are generated from running Sesam Genie. The first FEM is the Panel FEM model for potential flow analysis in HydroD. The second FEM is the compartment FEM model for ballasting the spar for structure stability. The third FEM model represents the entire structure i.e., the substructure (platform) and the superstructure (tower and rotor nacelle assembly) represented with a point mass.
4. The three FEM files are hydrostatically assessed in HydroD for each iteration.

5. The results are benchmarked against the static pitch angle constraint, and a pool of feasible results are created from the samples.
6. The results are compared with the single objective of minimizing the mass of the structure and the most feasible / optimal design is selected for each of the static pitch angle constraints of 5 deg, 7 deg and 10 deg respectively.
7. The selected / most feasible design is hydrodynamically assessed in frequency domain and in a medium-fidelity time domain tool (OpenFAST). The FOWT system's response including the nacelle acceleration are assessed against the acceptable limit defined in standards (Leimeister et al., 2020b, Rasekhi Nejad et al., 2017).

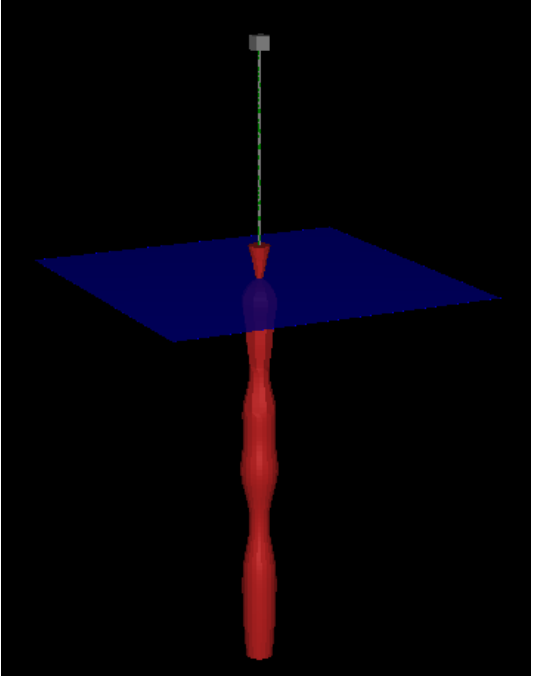
3.5.4.1 Selection of optimal design variants

This MDAO framework loops through thousands of iterations and a set of feasible designs that mostly satisfies the constraints are selected. The control points and radii at each control point along the vertical axis of the three optimal parametric designs and their geometries are highlighted in Figure 23 and Table 15 cases A, B, and C, respectively for maximum pitch angles of 5 deg, 7 deg and 10 deg respectively. All the cases are coupled with the NREL 5MW wind turbine rotor nacelle assembly.

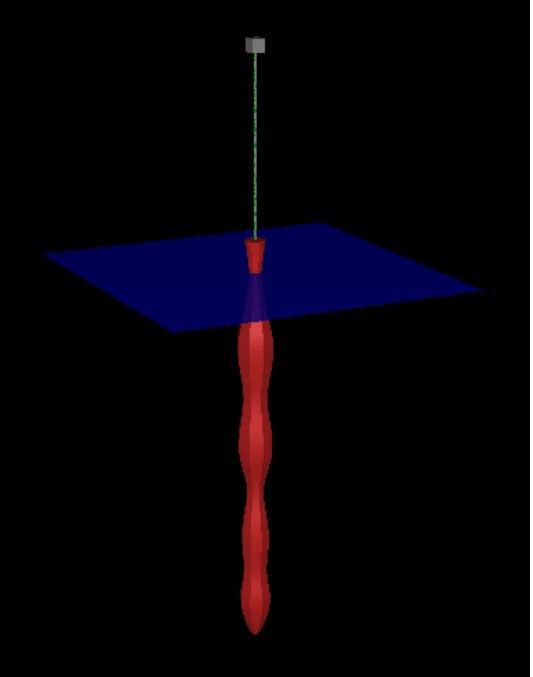
This study is a proof of concept that uses free-form curve (NURBS) within an MDAO framework specifying a set of constraints and a single objective function of minimizing mass to reduce the quantity/mass of material (Steel) required for manufacturing with the potential of reducing the capital cost of the FOWT platform. However, achieving this objective of capital cost minimization from reducing material for manufacturing the platform can be jeopardized by the additional costs incurred from manufacturing complex shapes. This limitation is highlighted in Chapter 6 which also includes potential recommended solution.



Case A



Case B



Case C

Figure 23. Selected models from pattern search optimization algorithm method

Table 15: Design data for selected models

| | | | | | | | | | | | | | | | |
|--------|------------|------|------|------|------|------|------|------|------|------|------|------|-------|-------|-------|
| Case A | Height (m) | 0.0 | 4.0 | 12.0 | 20.0 | 30.0 | 40.0 | 50.0 | 60.0 | 70.0 | 80.0 | 90.0 | 100.0 | 110.0 | 120.0 |
| | Radii (m) | 4.11 | 4.36 | 3.85 | 6.13 | 6.67 | 2.46 | 3.73 | 5.68 | 2.65 | 4.51 | 5.56 | 5.72 | 3.58 | 3.56 |
| Case B | Height (m) | 0.0 | 4.0 | 12.0 | 20.0 | 30.0 | 40.0 | 50.0 | 60.0 | 70.0 | 80.0 | 90.0 | 100.0 | 110.0 | 120.0 |
| | Radii (m) | 1.00 | 6.74 | 4.12 | 4.36 | 1.93 | 5.95 | 4.01 | 6.69 | 3.01 | 2.72 | 5.31 | 5.20 | 4.91 | 4.01 |
| Case C | Height (m) | 0.0 | 4.0 | 12.0 | 20.0 | 30.0 | 40.0 | 50.0 | 60.0 | 70.0 | 80.0 | 90.0 | 100.0 | 110.0 | 120.0 |
| | Radii (m) | 1.91 | 2.34 | 3.00 | 6.29 | 5.70 | 3.25 | 5.49 | 6.14 | 1.64 | 4.30 | 4.91 | 2.85 | 6.78 | 1.25 |

3.6 Global Response Assessment of Optimal Designs and Results

3.6.1 Global Limit state assessments of the design variants

The global limit states assessment considered for this study are the pitch angle, nacelle acceleration, and translational motion under severe sea state as stipulated in IEC-61400-3-2 (2019). The global response assessment of the optimal design cases highlighted will be conducted using the conservative design load case – DLC 1.6 detailed in International Electrotechnical Commission standard (IEC) - IEC61400-3-1 (2019) and IEC-61400-3-2 (2019) highlighted in Section 3.6.2. FOWT Pitch Angle

The system's pitch angle is an essential design and optimization constraints used in exploiting and selecting the optimal design from a large design space. As highlighted in Section 3.5.4.1, the pitch angle constraints specified in the design and optimization framework are 5 deg, 7 deg and 10 deg respectively. A conventional value of 10^0 is used based on Kolios et al. (2015) and Leimeister et al. (2020b). For the purpose of this study, global response assessment is conducted for the 5 deg and 7 deg pitch angles of the FOWT system in addition to the 10 deg pitch angle.

3.6.1.1 Nacelle Acceleration

The nacelle consists of sensitive components amongst which are the gearbox, generator, and bearings, essential for electricity production. As highlighted in Rasekhi Nejad et al. (2017), a common operational limit for the maximum allowable nacelle acceleration is below 30% of

the gravitational acceleration (g), which translates to a maximum value 2.943 m/s^2 . For conservative design, the lower bound of 1.962 m/s^2 is set as the maximum allowable nacelle acceleration for this study.

3.6.1.2 Translational Motions

As a result of the wind and wave loading on the FOWT system, the system will drift during operation. However, the drift varies between different FOWT system configurations based on the station keeping system adopted i.e., the translation motions in a TLP FOWT system are highly restricted due to the tendons employed for station keeping as highlighted in Bachynski and Moan (2012). For other FOWT design configurations like the spar, there are no publicly available limits for the translational motion as the allowable motion of the power cable is the critical criteria for restricting the translational motion of the FOWT system (Leimeister et al., 2020b). The total translational displacement (combined surge, sway, and heave motion) has two parts that must be distinguished in analysing translational motion: the static, or average, displacement, which is primarily caused by the aerodynamic thrust acting on the wind turbine rotor, and the dynamic displacement, which represents the oscillatory motion caused by turbulent wind loading and oscillating wave loads. In Leimeister et al. (2020b), the dynamic displacement is constrained to a max value of 20% of the water depth, while in Kolja Müller and Simon Tiedemann (2017) the maximum floater offset or floater excursion in surge, including the static and the dynamic component, the last one resulting from both first and second order loads, is less than 50% of the water depth. This work will consider translational motion value of 15% water depth for more conservative results i.e., 15% of the water depth (48 m of translational displacement) is a much-constrained allowable design requirement than 50% water depth (160 m of translational displacement).

3.6.2 Design load case

The global response assessment of the optimal design cases highlighted will be conducted using the conservative DLC 1.6 highlighted in International Electrotechnical Commission standard (IEC) - IEC61400-3-1 (2019) and IEC-61400-3-2 (2019). DLC 1.6 is a very conservative load case matrix with the following characteristics:

- The DLC 1.6 uses normal current and turbulent wind models while taking into account a severe irregular sea state. The wind turbine is generating power in a normal production mode.

- This DLC 1.6 highlights critical conditions for a wind turbine in an area where waves are dominant. The severe irregular sea state is associated with significant fluctuations in the wave elevation time series, which causes excitation of the FOWT system in oscillatory motion.
- DLC 1.6 is expected to yield critical values for the nacelle acceleration and the dynamic translational motion if the FOWT system is wave sensitive.

The DLC1.6a is selected for this study in order to carefully assess the response of the system's motions in all six degrees of freedom and also the nacelle acceleration in an extreme sea state for conservative design and analysis of the system.

3.6.3 Environmental Parameters

The wind and wave environmental parameters considered for this study are highlighted in this section.

3.6.3.1 Wind

The 5MW spar FOWT system is operated at the rated wind speed of 11.4m/s. The rated wind speed is used in this research for conservative purposes, as the system is expected to experience the largest response at the rated wind speed. This ensures the most demanding response of the system is captured. For the purpose of time domain assessment, a Kaimal wind spectrum is utilized to generate the turbulence wind inflow in this work and like Jonkman (2007) the turbulence intensity category B with a power law shear exponent of 0.14 is used for normal turbulence model. Six seeds are paired between the rated wind speed and the extreme seastate highlighted in section 3.6.3.2. This means a turbsim output file (.bts) generated for each seed is paired with the corresponding extreme wave seed for a detailed time domain analysis. Detailed impact of turbulence intensity and wind shear on the FOWT substructure are discussed in Li et al. (2019). They concluded the wind shear has a limited effect on the global responses of the floating wind turbine whereas its influence on each individual blade is considerable. However, in a wind field with high turbulence intensity, Li et al. (2019) concluded the platform motions become more violent and the structural loads are increased substantially.

3.6.3.2 Wave

For DLC1.6, the severe sea state is used to conduct the global response assessment. For the purpose of this work, the wave spectrum of interest is the irregular JONSWAP wave spectrum.

The sea state for the site is as used in Leimeister et al. (2020b) and taken for an assumed water depth of 320m. The JONSWAP wave spectrum expression is detailed in DNVGL Oslo (2018) highlighting the required spectral parameters for estimating the wave spectrum for a defined sea-state. Figure 24 shows the calculated wave power spectrum from the detailed JONSWAP expression in DNVGL Oslo (2018) over a time period of 5 to 200 seconds in steps of a second. A step of 1 second is used as HydroD/WADAM cannot accommodate more than 200 vectorial frequencies. The peak frequency of the power spectrum is shown at circa 0.068 Hz, which corresponds to the peak period of 14.7 seconds. The peak power for the calculated wave spectrum is about 305 m²/Hz.

Table 16: Seastate and environmental data Leimeister et al. (2020b)

| Wind and Wave Parameters | | |
|--------------------------|-------|---|
| H _s (m) | 10.37 | Significant wave height of the spectrum |
| T _p (sec) | 14.70 | Peak period of the wave spectrum |
| Peak / Gamma factor | 3.30 | Non-dimensional peak shape parameter |
| σ ₁ | 0.07 | Spectral width parameter for angular frequency ≤ peak angular frequency |
| σ ₂ | 0.09 | Spectral width parameter for angular frequency > peak angular frequency |
| U _{ref} (m/s) | 11.4 | Rated wind speed |
| V _{ref} (m/s) | 50 | 10 min. mean ref wind speed (50 years return period) at hub height |
| Wind shear exponent | 0.14 | Extreme wind shear exponent |

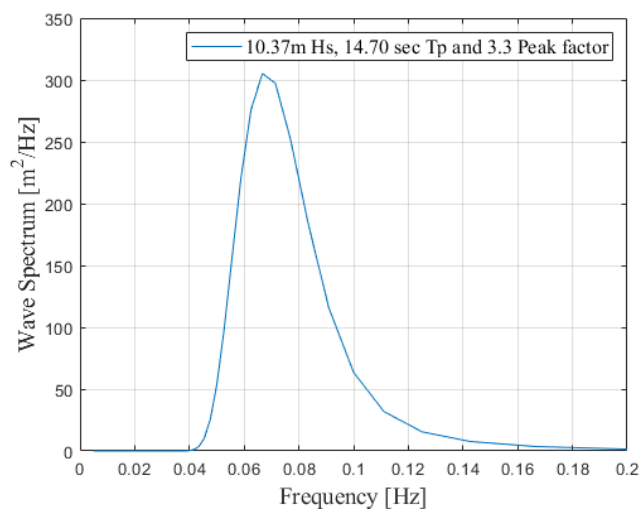


Figure 24. Wave Spectrum- 10.37m Hs and 14.7s Tp

3.6.4 Results and Discussion

The results and discussion are organised in frequency domain and time domain analytical approach.

3.6.4.1 Frequency Domain Global Dynamic Response Analysis

This section highlights the system's response based on the environmental conditions used to model the JONSWAP wave spectrum. The frequency domain panel model utilized in the MDAO framework in Section 3.5 for selecting the optimal design based on stability analysis is used in conducting the potential-flow based hydrodynamic analysis. This approach provides a high-level estimate of the system's responses in different degrees of freedom. The system's responses are determined for all the three cases (A, B and C or 5 deg, 7 deg and 10 deg static pitch angles respectively) and plotted in comparison to the OC3 NREL 5MW FOWT system. Figure 25 shows the RAOs in surge, heave, pitch and horizontal nacelle displacement motion for the three design cases (corresponding to the 5 deg, 7 deg and 10 deg static pitch angles) and the OC3 spar. It is shown in Figure 25 that the peak response frequencies in surge, heave, pitch and nacelle displacement motions are around the low frequency region. With first order wave loads usually occurring between 0.04Hz and 0.2Hz, the peak responses highlighted in Figure 25 are below lower threshold of the first order wave, outside the excitation frequency range of the first order wave load. Furthermore, the nacelle's horizontal displacement Response Amplitude Operator (RAO) is determined by summing the surge RAO and the product of the pitch RAO and the hub height of the FOWT system. As illustrated in Figure 25, the increase in the magnitude of the peak nacelle horizontal displacement RAO, compared to the surge and pitch RAO, is as a result of summation of response in the surge and pitch DOF.

An important feature in the result from the platform mass of the optimal cases (A, B and C) based on static pitch angle constraints 5 deg, 7 deg and 10 deg and the OC3 model with the NURBS curve is that the OC3 model has the largest mass. However, it is shown from the other results that as the static pitch angle constraints increases from 5 deg to 7 deg and 10 deg, the mass of the optimal/ feasible design selected from the optimization framework is reduced, as seen in Table 17. Estimated cost of the platform is highlighted in Table 17, using the cost of steel per tonne of 537GBP from Ioannou et al. (2020).

Table 17. Platform mass and corresponding cost estimate

| Platform Type | Steel mass (Tonnes) | Cost- Steel (GBP) |
|---------------|---------------------|-------------------|
| OC3 | 1763.53 | 947.02E+03 |
| Case A | 1750.03 | 939.77E+03 |
| Case B | 1708.43 | 917.43E+03 |
| Case C | 1641.17 | 881.31E+03 |

For this optimization framework, in which the objective function is to minimize the mass of the steel structure used in designing the platform of the FOWT system, an effective way to minimise the objective function is to increase the pitch angle constraints. For conservatism, the maximum static pitch angle constraint under rated wind speed for this study is set at 10 deg. Figure 25 shows that of all the three optimal variants selected, case A design variant has the largest peak motion response in surge, heave, pitch and the nacelle horizontal displacement with values of about 30m/m, 4.9m/m, 7deg/m and 40m/m respectively.

The dynamic responses of the system in the 6DOFs, for each of the cases assessed, are different from the dynamic responses of the reference system, due to a number of factors that affect the natural frequency and the damping. These factors include:

- the platform’s mass distribution (COG and mass matrix),
- the frequency dependent (hydrodynamic) added mass matrix,
- the stiffness (hydrostatic and mooring) matrices,
- and frequency dependent hydrodynamic (potential) damping.

All these factors are dependent on the wet geometry of the floating substructure, and in turn determine the RAOs of the platform – and, in particular, the largest effects can be observed in the heave DOF, as highlighted in Figure 25. To develop a fundamental understanding of how the aforementioned factors change the RAOs, a simplified decoupled, 1-DOF analysis, based on prime principles, is provided.

Given the mass (M), the heave added mass at the infinite frequency (A_{33}), the hydrostatic ($C_{hyd,33}$) and mooring ($C_{moor,33}$) stiffness in the heave DOF, as derived through the numerical analyses conducted (Table 18), the 1-DOF, uncoupled heave (undamped) natural frequency can be derived with Equation (10).

$$F_{n,33(\text{undampened})} = \sqrt{\frac{C_{\text{hyd},33} + C_{\text{moor},33}}{M + A_{33}}} \quad (10)$$

From the results in Table 18, the 5 deg configuration (CaseA) presents a higher heave natural frequency in comparison with the benchmark (OC3 model) configuration. Taking Equation (10) into consideration, coupled with the scenario of a constant heave mooring stiffness across both configurations and a slight change in the total mass, the higher natural frequency in Case A in comparison to the baseline model can be explained as highlighted below.

Although, the added mass for Case A is circa 45% larger than the added mass for the baseline model, the circa 58% higher hydrostatic stiffness more than compensate for the added mass increase; hence, pushing the heave displacement response of Case A at its natural frequency to circa 29% higher than the Benchmark OC3 model's heave displacement response at its natural frequency. However, for Case B and Case C, while the added masses are circa 156% and 62% respectively greater than the corresponding added mass for the benchmark model, the hydrostatic stiffnesses of Case B and Case C are respectively 88% and 64% lower than the corresponding hydrostatic stiffness of the benchmark OC3 model. This occurrence reduces the heave natural frequency of Case B and Case C with regards to the benchmark model's heave natural frequency by 58% and 33% respectively.

Furthermore, an estimate of the magnitude for the peak heave responses at the natural frequencies of all the cases is conducted with the heave wave load at the natural frequencies shown in Figure 26 and highlighted in Table 18. This assessment is conducted with Equation (5) in Chapter 2 utilizing the mass of the structure, Mooring and hydrostatic stiffness in heave and the frequency dependent heave added mass and damping highlighted in Table 18. The calculated result presented in Table 19 shows a good agreement with the corresponding simulated results shown in Table 19. Although the calculated and simulated results show good agreement, there are still slight differences between the two results. This difference is due to the simplified 1 DOF uncoupled approach i.e., using the parameters - mass, added mass, radiation damping and stiffness in only one degree of freedom. However, for the simulated results, there are contributions from coupled motions in other degrees of freedom. Furthermore, additional linear damping from Jonkman (2010) is added on top of the hydrodynamic load in the three translational DOF and the yaw rotational DOF in order to match the free-decay responses as detailed in Jonkman (2010).

Table 18: Heave natural frequency estimate from mass added mass and stiffness

| | OC3 Benchmark | Case A | Case B | Case C |
|--|------------------|----------|----------|----------|
| Mass (Kg) | 8.16E+06 | 8.13E+06 | 7.67E+06 | 7.34E+06 |
| Heave Added mass | 2.26E+02 | 3.27E+02 | 5.80E+02 | 3.67E+02 |
| Heave Hydrostatic Stiffness (N/m) | 3.43E+05 | 5.43E+05 | 4.21E+04 | 1.25E+05 |
| Heave Mooring Stiffness (N/m) | 1.19E+04 | 1.19E+04 | 1.19E+04 | 1.19E+04 |
| Damping at Natural Frequency (NS/m) | 1.32E-01 | 6.91E-01 | 2.98E-03 | 5.44E-01 |
| Heave Wave Load (N/m) | 82891 | 166743 | 15077 | 29881 |
| Heave Frequency (Hz) | 0.0322 | 0.0400 | 0.0122 | 0.0180 |

Table 19: Estimate of Heave displacement response magnitude at natural frequency

| | OC3 Benchmark | 5DEG | 7DEG | 10DEG |
|------------------------------------|---------------|------|------|-------|
| Simulated Heave Response (m/m) | 3.17 | 4.70 | 1.21 | 1.01 |
| Calculated Heave response (m/m) | 3.31 | 4.03 | 1.68 | 0.70 |

In addition to the number of factors affecting the dynamic response of the system discussed, the additional damping due to ballast in the 6 DOF and additional stiffness from the mooring configuration should be optimal for each platform variant. The coupled surge motion for the optimal variants at very low frequencies in the Pitch DOF RAO plot shown in Figure 25 is large in comparison to the coupled surge motion also at low frequency for the NREL OC3 base model. This is because the additional damping from ballast in the 6 DOF and additional stiffness from the mooring configuration used for the NREL OC3 base model is not optimal for the other variants.

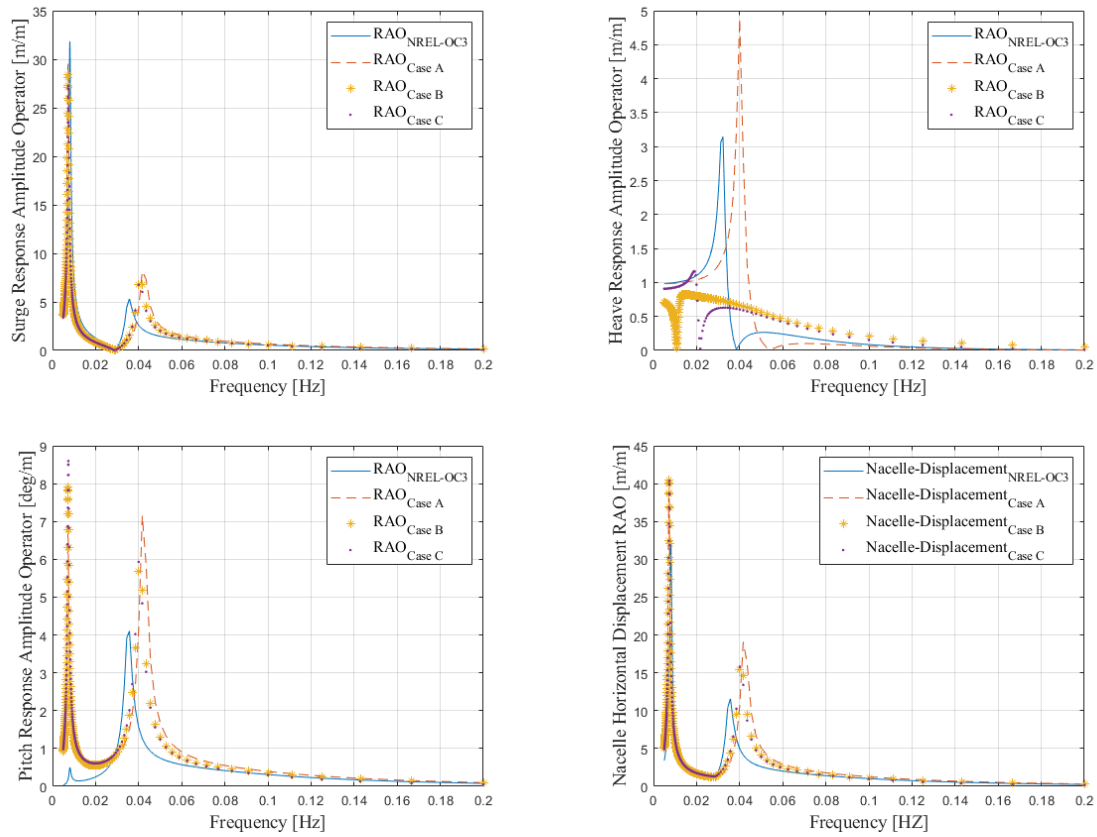


Figure 25. Surge, Heave, Pitch and Nacelle displacement RAO for all three cases and the OC3 spar

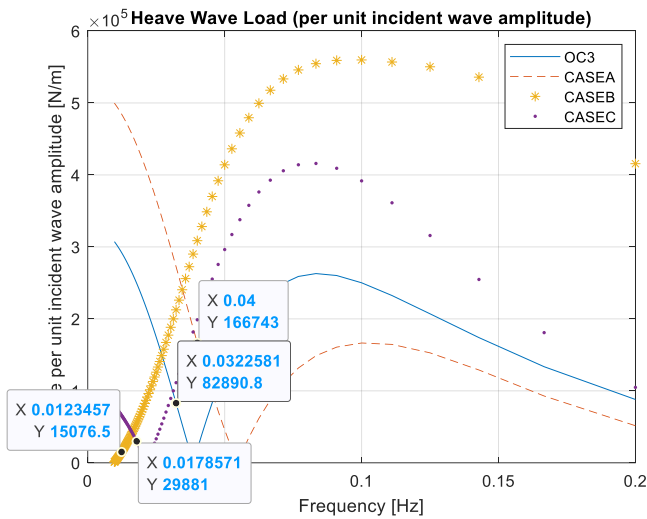


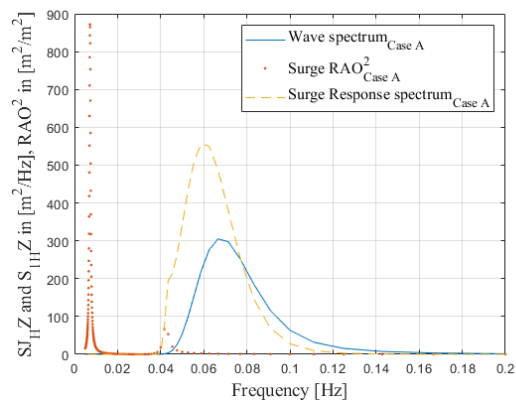
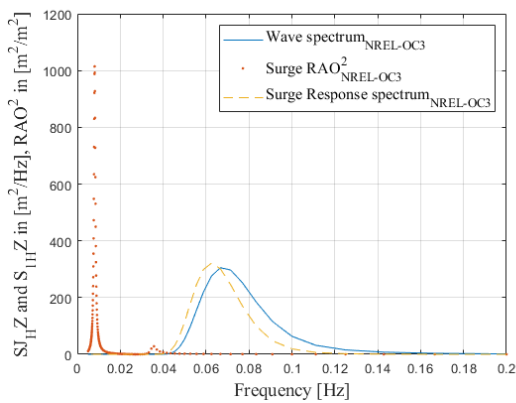
Figure 26. Force per unit incident wave amplitude in the Heave DOF for all cases

Figure 27 to Figure 30 shows the system's response spectrum in surge, heave, pitch, and nacelle horizontal displacement with the corresponding dynamic response (RAOs) and the wave spectrum for all the three optimal design variants and the OC3 spar FOWT system.

Considering the specific sea state from Table 16 and the dynamic response in all DOFs for all the cases (A-C and OC3 spar) in Figure 27 to Figure 30, the range of frequencies over which the surge, heave, pitch and nacelle response amplitude operators are significant does not substantially mirror or overlap the range of frequencies with which there is a substantial wave energy. The RAOs (surge, heave, pitch, and nacelle) are well decoupled from the wave spectrum analysed; hence, it ensures that the area below the system’s response spectrum which is proportional to the energy in the waves absorbed by the platform in these degrees of freedom is relatively small. This is a characteristic of a well-designed platform.

The estimated nacelle accelerations RMS values for the OC3 model and the 3 variants are shown in Table 20 and they are all below the 1.962 m/s^2 or 20% of acceleration due to gravity value recommended as the benchmark for nacelle acceleration used in this study as highlighted in section 3.6.1.1.

An observation from the frequency domain study is that for cases A, B and C, their dynamic response is higher than the OC3 design’s dynamic response. However, the variant cases A, B and C responses still satisfy the allowable design constraints from standards used in assessing the optimal designs. This shows the OC3 design is much more conservative than the optimal variant cases A, B and C. This conclusion is only valid for this work as only one design load case for extreme seastate is being considered (DLC 1.6). This observation might not be valid if other design load cases and other constraints like the structural integrity constraints are imposed; hence, this can be explored in future work.



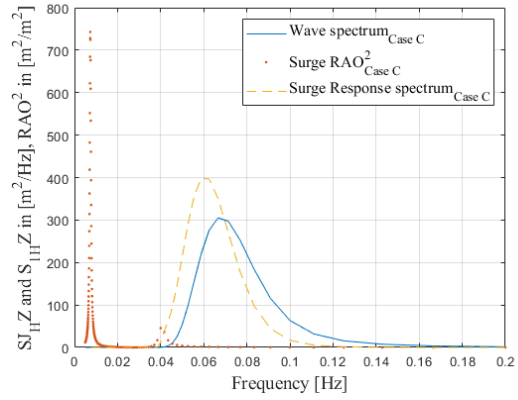
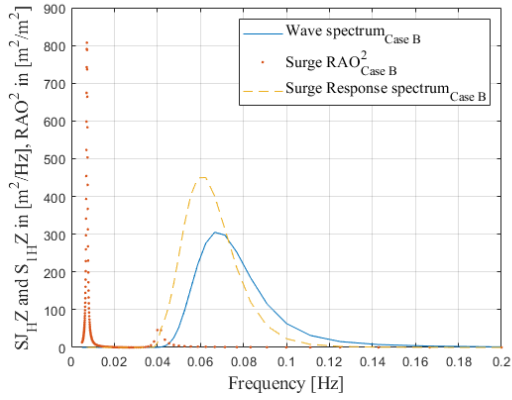


Figure 27. FOWT system's Surge response spectrum for all three cases and OC3 spar

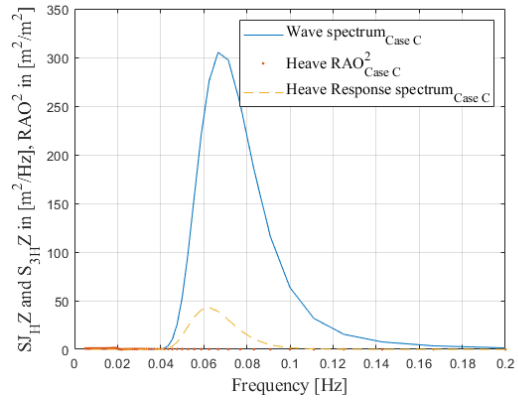
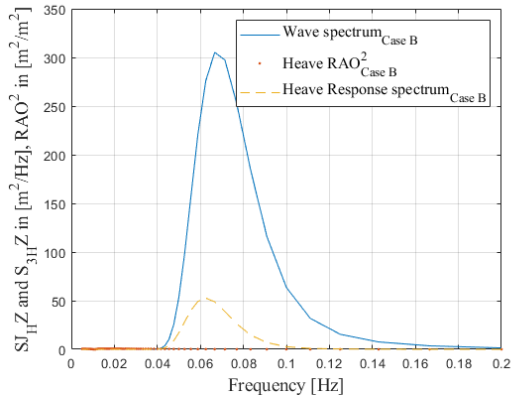
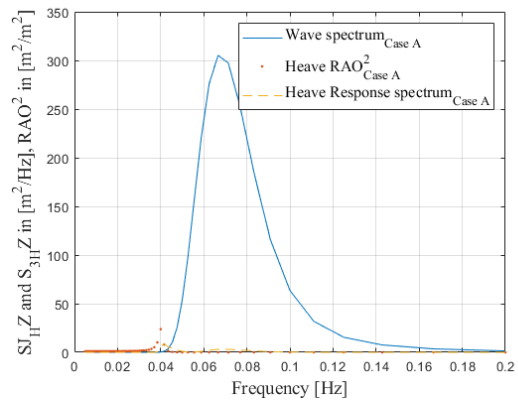
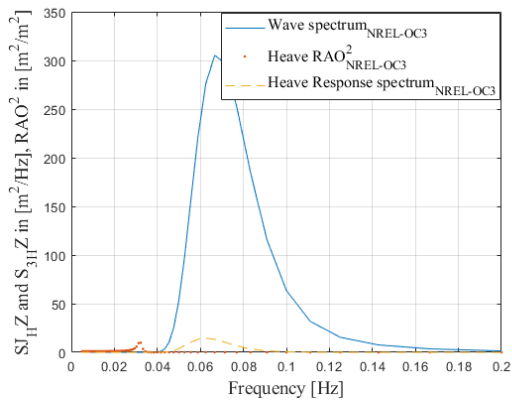


Figure 28. FOWT system's Heave response spectrum for all three cases and OC3 spar

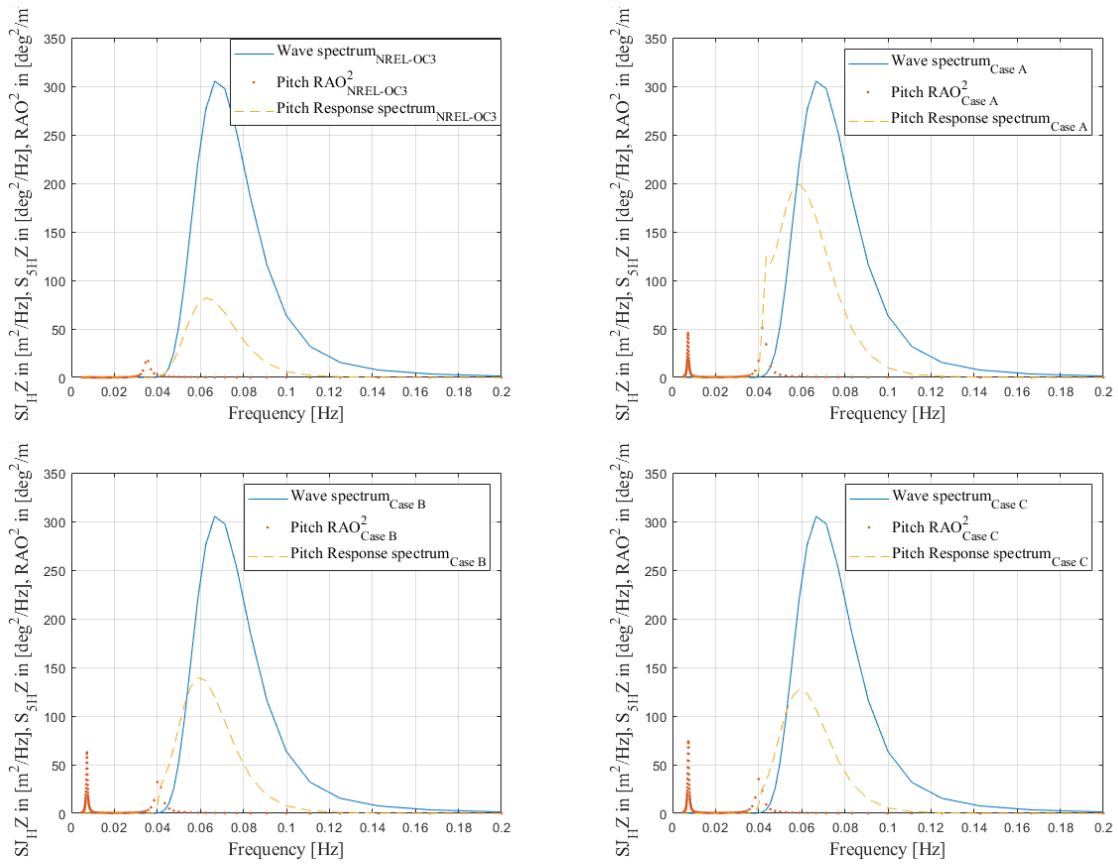
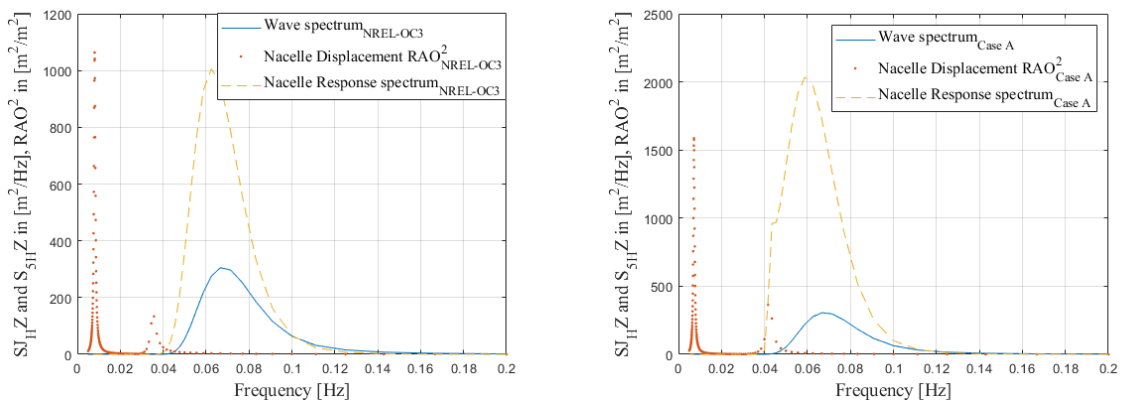


Figure 29. FOWT system's Pitch response spectrum for all three cases and OC3 spar



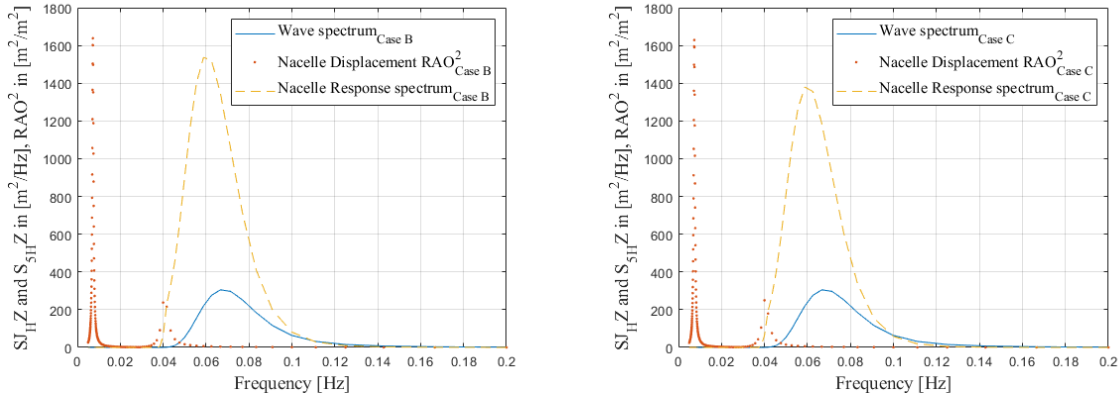


Figure 30. FOWT system's Nacelle horizontal displacement response spectrum for all three cases and OC3 spar

Table 20. Nacelle Acceleration RMS – Frequency Domain

| | OC3 spar | Case A | Case B | Case C |
|---------------|----------|--------|--------|--------|
| Zeroth Moment | 0.0060 | 0.0117 | 0.0089 | 0.0075 |
| Nacelle RMS | 0.0777 | 0.1083 | 0.0942 | 0.0868 |

3.6.4.2 Time Domain Analysis

Analysis of the coupled FOWT system in time domain allows the assessment of the system's response to wind and wave loads including non-linear forces, which cannot be represented in the frequency domain approach. In this study, the frequency domain analytical approach described in Section 2.5.1 of Chapter 2 is verified against the results obtained with OpenFAST. OpenFAST is an open-source wind turbine simulation tool capable of a detailed time domain coupled AHSE analysis of an onshore / offshore wind turbine system (OpenFAST, 2023). To represent the optimal geometric shaped platform selected in Section 3.5 with OpenFAST, the hydrodyn and elastodyn source code has not been changed. However, the hydrodyn and elastodyn input files are updated to account for the hydrodynamic and structural changes in the optimal design variant cases A, B and C. As highlighted in Jonkman (2007), the hydrodyn module accounts for the following:

- Linear hydrostatic restoring stiffness of the floating system.
- Added mass and damping contributions from linear wave radiation accounting for the free-surface memory effects.
- Incident wave excitation from linear diffraction in any sea-state (regular or irregular);
- Nonlinear viscous drag from incident wave kinematics, sea currents and platform motion.

For the coupling process, the linear hydrostatic restoring stiffness is obtained from the WAMIT

output files in the frequency domain analysis conducted in Section 3.5. The added mass and damping contributions and the incident wave excitation from linear diffraction are extracted from the HydroD output on completion of the frequency domain analysis in WADAM. Finally, the displaced volume of water when the platform is in its initial equilibrium position, obtained from the stability analysis in frequency domain, is set in the hydrodyn module to represent the optimal design variant assessed. The elastodyn module's file is updated with the optimal platform's mass, the center of mass' distance to the mean sea level, the calculated platform's rotational inertia in the roll, pitch and yaw DOFs. The updated elastodyn and hydrodyn modules are simulated with the aerodyn and servodyn module for a holistic multidisciplinary simulation of all the different disciplines within a FOWT system.

The two analyses conducted for the coupled FOWT system from the optimal geometric platform selected in section 3.5.4.1 are:

- Free decay test
- FOWT system's dynamic response analysis

3.6.4.2.1 Free Decay Analysis

The free decay analyses are conducted prior to the system's dynamic analyses to obtain the natural periods of the system. This analysis is conducted by coupling the AHSE component of the FOWT system in OpenFAST and then switching off the aerodynamic flag and the wave mode flag to ensure no aerodynamic load and wave load respectively. The platform is displaced from an assigned initial position in the degree of freedom of interest to determine the natural period. For the purpose of this work, the Surge, Heave and Pitch DOF are estimated for the system's natural period. The corresponding initial displacement of the platform and estimated natural periods for each DOF considered for the three optimal platforms are shown in Table 21. In addition, the decay responses in the specified DOFs (heave pitch and surge) for the three optimal variants are shown in Figure 31 to Figure 33. The natural period in the heave DOF presented for the three optimal cases in Figure 31 shows how the platform waterplane area geometry affects the system's natural period. The 7 deg static pitch angle case has the lowest heave stiffness at the mean sea level (MSL) as a result of the significantly small diameter of the control point at the water level. This leads to significant heave motion and natural period in this case in comparison to the other two cases (5 deg and 10 deg static angle variants) with larger diameter of the control points at the MSL.

Table 21. Natural Period of optimal variants from free-decay test

| Optimal Case | Static Pitch Angle (Degrees) | Degree of Freedom | Initial Displacement | Natural Period (sec) |
|--------------|------------------------------|-------------------|----------------------|----------------------|
| Case A | 5 | Surge | 15 m | 121 |
| Case A | 5 | Heave | 10 m | 25 |
| Case A | 5 | Pitch | 5 deg | 28 |
| Case B | 7 | Surge | 15 m | 116 |
| Case B | 7 | Heave | 10 m | 87 |
| Case B | 7 | Pitch | 5 deg | 32 |
| Case C | 10 | Surge | 15 m | 110 |
| Case C | 10 | Heave | 10 m | 48 |
| Case C | 10 | Pitch | 5 deg | 40 |

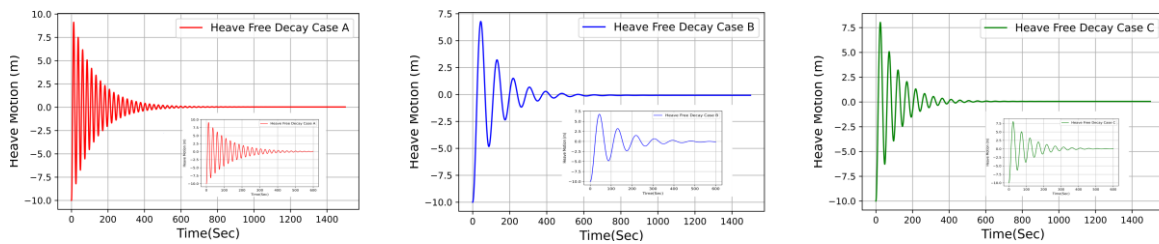


Figure 31. Heave decay test for the three optimal variants

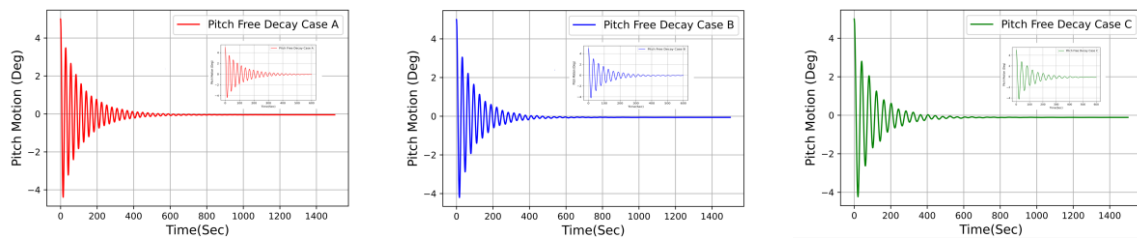


Figure 32. Pitch decay test for the three optimal variants

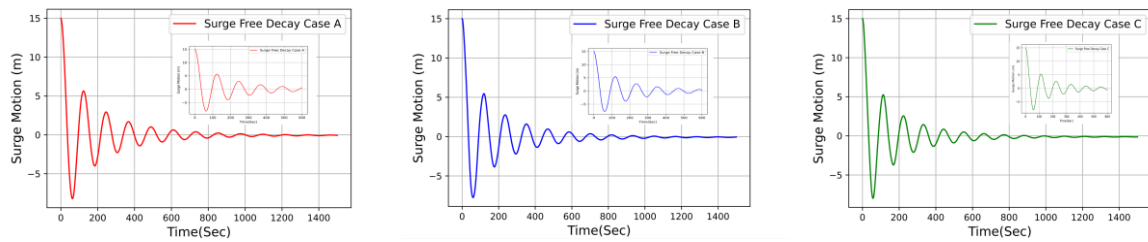


Figure 33. Surge decay test for the three optimal variants

3.6.4.2.2 FOWT System Dynamic Response Analysis -Optimal Variants

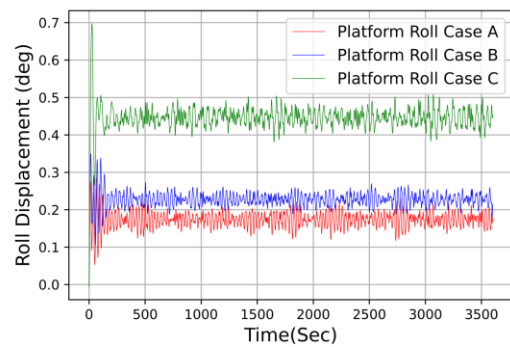
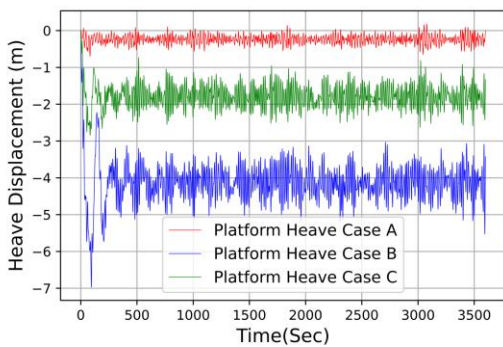
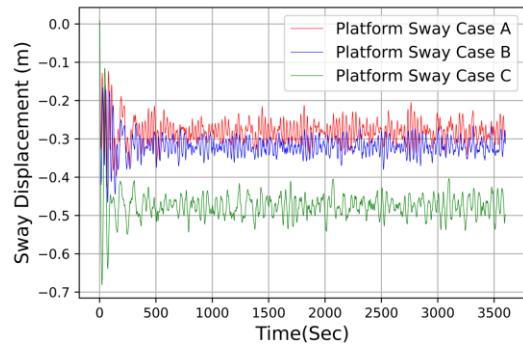
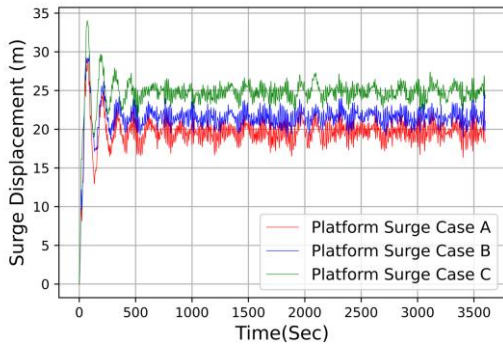
The dynamic analysis for this study is conducted according to the DLC1.6 load case from IEC-61400-3-2 (2019) considering severe sea state of 50 years return period. The corresponding sea state utilized is highlighted in Table 16 with a significant wave height of 10.37m, peak period of 14.7 seconds at a rated wind speed of 12m/s. The wind and wave loads are set to be colinear on the FOWT system along the surge DOF of the platform for conservative analysis. This simulation has been conducted for severe sea state requirements as highlighted in IEC-61400-3-2 (2019) and Jonkman (2007) with a six 1-hour simulations at each sea state and the simulations are differentiated by the wave seeds. The average of the simulations from the 6 wave seeds are plotted to determine the system’s response as highlighted in Figure 34. As highlighted in the global dynamic analysis in the frequency domain section 3.6.4.1, Figure 27 to Figure 30, the system’s RAO in all DOFs considered are well decoupled from the associated wave spectrum indicating a good design.

The platform motions in the 6 DOFs presented in Figure 34 are estimated considering a simulated time of 3600 seconds. The platform motion in time domain showing the maximum, mean, minimum motion and standard deviation for the selected optimal cases in all DOFs is highlighted in Table 22 excluding the initial transient period of around 500 seconds of the simulation time. Figure 34 shows the platform response in the surge degree of freedom for the three optimal cases with Case C (10 deg static pitch angle) showing the largest average displacement in surge of 24.79m. The average displacement of 24.79m shows the surge motion is still less than 15% of the water depth of 320 metres which is the allowable translational motion benchmark set for this study. The most notable maximum mean heave displacement of all the three optimal cases is highlighted in Case B (-4.13m). This is due to the geometric shape of the platform at the waterplane area. A small diameter at the water plane area results in a reduction in the magnitude of the heave stiffness and an increase in the platform’s heave motion and its natural period as highlighted in the heave free decay test in Figure 31. For the pitch displacement, Case C (10 deg static pitch angle constraint) has the largest pitch displacement as it also has the largest static pitch angle constraint used for the optimization process in Section 3.5.4.1. This shows the platform’s optimal shape from the optimization constraint is a huge contributory factor to the pitching displacement of the FOWT system.

Table 22. Descriptive motion response statistics of optimal variants

| Optimal Cases | Static Pitch Angle | Degree of Freedom | Maximum | Mean | Minimum | Standard Deviation |
|---------------|--------------------|-------------------|---------|------|---------|--------------------|
|---------------|--------------------|-------------------|---------|------|---------|--------------------|

| | (Degrees) | | | | | |
|--------|-----------|-------|----------|-------------------|-----------|------|
| Case A | 5 | Surge | 22.77m | 19.62m | 16.36m | 1.05 |
| Case A | 5 | Sway | -0.20m | -0.28m | -0.35m | 0.02 |
| Case A | 5 | Heave | 0.18m | -0.24m | -0.65m | 0.11 |
| Case A | 5 | Roll | 0.23 deg | 0.17 ⁰ | 0.12 deg | 0.02 |
| Case A | 5 | Pitch | 4.29 deg | 3.07 ⁰ | 1.41 deg | 0.42 |
| Case A | 5 | Yaw | 0.55 deg | 0.09 ⁰ | -0.34 deg | 0.10 |
| Case B | 7 | Surge | 24.94m | 21.55m | 18.89m | 0.87 |
| Case B | 7 | Sway | -0.27m | -0.32m | -0.38m | 0.02 |
| Case B | 7 | Heave | -3.02m | -4.13m | -5.53m | 0.37 |
| Case B | 7 | Roll | 0.27 deg | 0.23 ⁰ | 0.18 deg | 0.01 |
| Case B | 7 | Pitch | 5.39 deg | 4.14 ⁰ | 2.89 deg | 0.34 |
| Case B | 7 | Yaw | 0.42 deg | 0.12 ⁰ | -0.19 deg | 0.08 |
| Case C | 10 | Surge | 27.40m | 24.79m | 21.53m | 0.85 |
| Case C | 10 | Sway | -0.40m | -0.47m | -0.54m | 0.02 |
| Case C | 10 | Heave | -0.73m | -1.79m | -2.63m | 0.28 |
| Case C | 10 | Roll | 0.51 deg | 0.45 ⁰ | 0.38 deg | 0.02 |
| Case C | 10 | Pitch | 9.25 deg | 8.12 ⁰ | 6.91 deg | 0.37 |
| Case C | 10 | Yaw | 0.48 deg | 0.16 ⁰ | -0.23 deg | 0.11 |



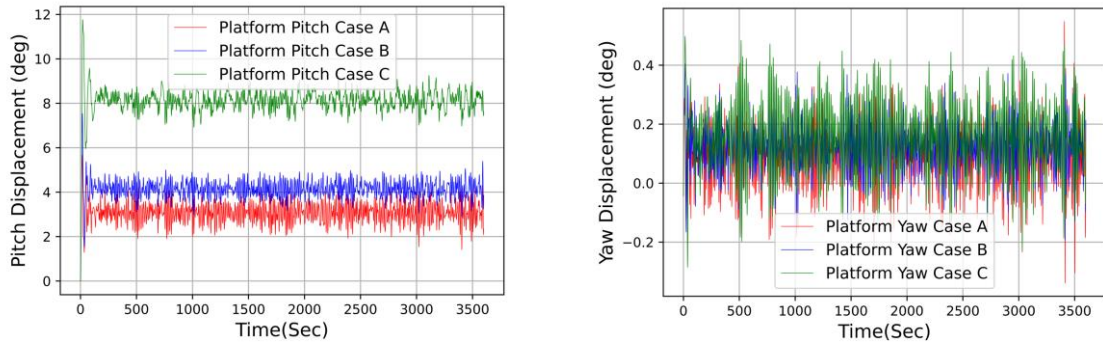


Figure 34. Platform optimal variants coupled translational and rotational response

3.6.4.2.3 Nacelle acceleration

A key global performance metric used in assessing the selected designs is the nacelle acceleration RMS value. The allowable limit for the nacelle acceleration of a FOWT system is below 30% of the gravitational acceleration (g) (Leimeister et al., 2020b, Rasekhi Nejad et al., 2017). This is equivalent to less than 2.943 m/s^2 . The statistics of the RMS value of the nacelle acceleration is determined from the time signal of the nacelle acceleration in the three translational DOF is highlighted in Table 23 and Figure 35.

Table 23. Nacelle acceleration statistics from time domain simulation

| | Case A (m/s^2) | Case B (m/s^2) | Case C (m/s^2) |
|-----------------------------|---------------------------|---------------------------|---------------------------|
| Nacelle Acceleration RMS | 0.310 | 0.260 | 0.202 |

From Table 23, Case A optimal variant has the largest nacelle acceleration RMS value of 0.31 m/s^2 . This largest nacelle acceleration RMS value of 0.31 m/s^2 of the three optimal variants is less than the lowest allowable nacelle acceleration value of 1.962 m/s^2 (20% of g) highlighting the operational capability of the of the selected optimal design variants in severe sea states. As expected, the RNA fore-aft accelerations derived with the non-linear, time-domain approach are higher than their counterparts derived with the frequency domain approach.

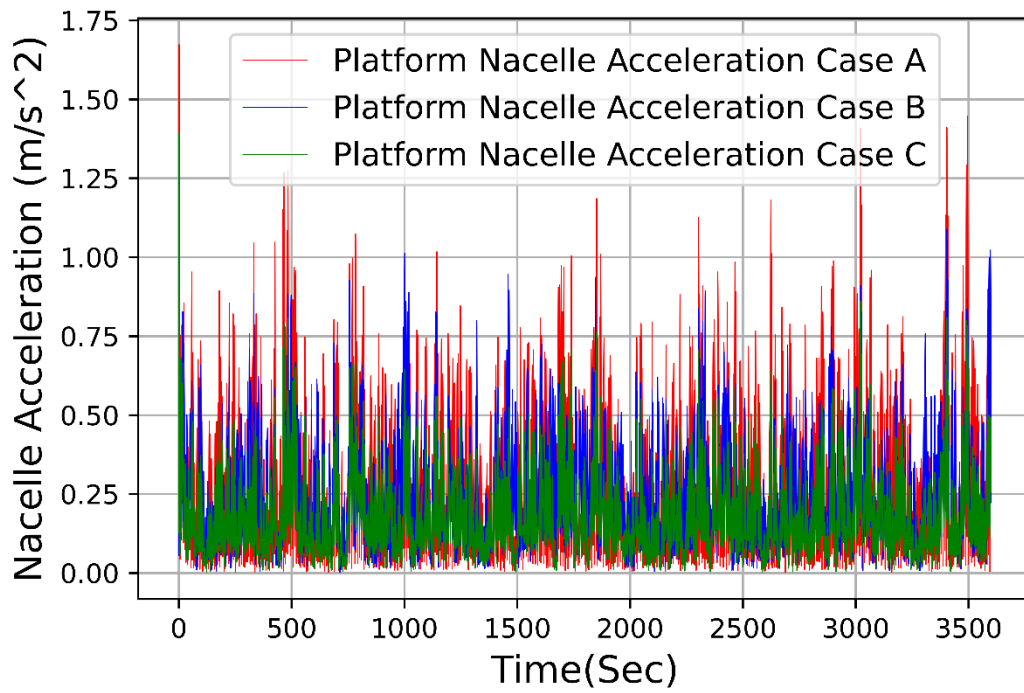


Figure 35. Nacelle acceleration response spectrum from time domain simulation

Chapter 4 Parametric Curve Comparison for Modelling Floating Offshore Wind Turbine Substructures

4.1 Overview

This chapter is developed from the publication by Ojo, A., Collu, M., & Coraddu, A. (2023). Parametric curve comparison for modelling floating offshore wind turbine substructures and Ojo, A., Collu, M., Coraddu, A., 2022b. Parametrisation Scheme for Multidisciplinary Design Analysis and Optimisation of a Floating Offshore Wind Turbine Substructure – OC3 5MW Case Study.

This Chapter investigates and presents a systemic analysis of free-form parametric curves for optimization applications. The chapter further explores and compares the use of several parametric free-form curves in the design, analysis, and optimization framework for spar FOWT systems, utilizing the multi-criteria decision-making technique, TOPSIS.

The innovative shapes generated for the optimal designs due to the local control property of the free-form curves distinguishes the parametric curve approach from others, like CAD model, where the global dimension of the design is altered, i.e., the entire length or diameter of the platform, rather than local segmentation changes in diameter at the control points. The TOPSIS technique uses weighted criteria (computational time, platform mass, local control properties of free-form curve, parametric continuity, and nacelle acceleration estimates). This can potentially give different perspective to designers to save cost and time and deliver innovative platform concepts as the FOWT sector gradually moves into the commercial phase of development. The parametric curves compared are the cubic spline, cubic Hermite spline (CHS), B-spline, and the Non-Uniform Rational B-spline.

The development of new floater concepts aimed at improving performance and reducing the overall cost of FOWT system involves the exploration of state-of-the-art techniques including:

1. Shape Parameterization Technique: This technique focuses on the parameterization of the floater's shape, allowing for flexible and optimized design adjustments.
2. Design, Analysis and Optimization Technique: as detailed in Chapter 3, this approach involves a comprehensive process that involves designing the floater, conducting detailed analysis, and optimizing the model to achieve improved performance and cost-effectiveness (time or money).

Additionally, the selection of the most suitable free-form curve for the shape parameterization is guided by Multi Criteria Decision Making (MCDM) techniques, which are further detailed in section 4.3.2."

These techniques have the potential to play a pivotal role in advancing the capabilities and efficiency of FOWT systems.

4.1.1 Shape Parameterization Technique

As detailed in Chapter 2, the concept of parameterization is used in many engineering and design disciplines, including the floating offshore wind platform design sector. The shape parameterization technique in this context involves defining the shape of the platform of a FOWT system using a set of parameters, which can be adjusted to optimize the design of different performance metrics. The shape parameterization techniques explored in this study are free-form curves detailed in section 4.2.3, with some of the free-form curve techniques reviewed in section 2.4.1. These free-form curves will allow for a large number of design variations to be explored quickly and efficiently.

4.1.2 Design Analysis and Optimization.

A review of design, analysis, and optimization techniques have been conducted in Chapter 2 with the methodological process / framework of utilizing the design analysis and optimization tools detailed in Chapter 3. However, for the investigation conducted in this Chapter, geometric design is modelled with different free-form curves for effective shape alteration of the design and efficient generation of finite element meshes required for analysing the design, and the analysis is conducted with the potential flow methodology in the frequency domain. The optimization framework utilized is the derivative free Pattern search optimization algorithm, as highlighted in Chapter 3.

4.1.3 Multi Criteria Decision Making Technique

MCDM techniques are useful tools for decision makers faced with selecting options in situations where there are multiple, often conflicting, criteria to consider (Caylor and Hanratty, 2020). These techniques allow decision makers to evaluate the options based on multiple criteria simultaneously, which can lead to more informed and effective decision making. A survey of seven MCDM methods amongst which are Weighted Sum Model (WSM), Analytical

Hierarchy Process (AHP), Technique for Order of Preference by Similarity to Ideal Solution (TOPSIS), Preference Ranking Organization METHod for Enrichment of Evaluations (PROMETHEE), VlseKriterijumska Optimizacija I Kompromisno Resenje (VIKOR), elimination et choix traduisant la realit  (ELECTRE) and Reference Ideal Method (RIM) is conducted in Caylor and Hanratty (2020). Their survey concluded selecting a suitable method can be challenging. As highlighted in Roszkowska (2011), some of the attributes of TOPSIS MCDM technique are: simplicity, rationality, comprehensibility, good computational efficiency, and the ability to measure the relative performance of each alternative in a simple mathematical form. These attributes make it suitable for engineering design, like FOWT support structures. Based on the highlighted attributes of TOPSIS, the comparison of the free-form curves within the design and optimization framework in this study is conducted with the TOPSIS technique. The use of TOPSIS in the offshore wind and floating offshore wind sector are detailed in Kolios et al. (2016), Lozano-Minguez et al. (2011), Leimeister et al. (2018), Leimeister and Kolios (2018).

The selection of the best free-form curve for the shape parameterization technique is an important step in the design process. This is where MCDM Techniques come in. MCDM techniques are used to evaluate and rank the different design options based on a set of predefined criteria, such as performance, cost, and safety. This allows the designer to select the best design option that meets the project requirements.

This investigation is a methodological approach to assess the best parametric curves suitable for modelling the substructure of a FOWT system. It must be said that the best performance curve highlighted in this study is based on the performance criteria used in assessing the curves. Performance of the curves can also depend on the MCDM approach utilized properties and curve weightage sensitivities which are not assessed in this study.

4.2 Geometric Curves and Shape Parameterization

A brief review of shape parameterization in design is discussed in Chapter 2. This Section provides a detailed review of free-form curves and their properties. For any parameterization technique to influence design shape, an understanding of the geometry of the design concept is essential to the effectiveness of selecting an optimal altered and bespoke shape from the design space explored within the optimization framework. This process requires knowledge of the parametric curves to alter the geometric shape of the design concept. Geometric curves and surfaces can be described in a variety of ways. The explicit, implicit, and parametric description

are the three primary types. Each of them has distinct formulations for analyzing continuities, derivatives, and geometric characteristics of the curve or surface, and each has advantages and disadvantages for certain applications.

An overview of the three representations is summarized herein.

4.2.1 Explicit Representation

The explicit representation of a curve is the simplest and most constrained curve representation technique. In this technique, one coordinate is a function of the other one, i.e., $y = f(x)$ for a curve, and for surfaces, the z coordinate is a function of x and y ; $z = f(x, y)$ (Goldman, 2003).

As highlighted in Forrest (1991), an advantage of the explicit representation is the simplicity of evaluating the derivatives and obtain geometric properties like slope and curvature. It is also easy to determine if a given point is on the curve and to determine the intersection of two curves.

A significant disadvantage is that using an explicit representation to draw a curve like a circle will require the specification of several conditions. Furthermore, this representation is axis-dependent, i.e., a quadratic interpolant through three points is different for every different coordinate system. For this reason, the explicit representation is rarely used for modeling in computer aided design.

4.2.2 Implicit Representation

A curve with implicit representation is depicted by equations of the form $f(x, y) = 0$ or in the case of surfaces, $f(x, y, z) = 0$ as reported in (Goldman, 2003). The implicit representation can be used to describe important geometric properties like the radius in a circle. It is easy to determine whether a point is on the curve or not, much like the explicit representation. However, finding the point where two curves cross is difficult. Although the range of potential curves is greater than in the case of explicit representation, it is still limited. The difficulty in finding the correct analytical function in modelling free-form curves and surfaces makes the implicit and explicit representation not practical.

4.2.3 Parametric Representation from Free-form Curves

The parametric description is the most suitable representation for a free-form geometry. The

x, y, and z coordinates are explicit functions of an independent parameter (or two independent parameters for surfaces). This representation offers the widest range of potential geometries and is very flexible to adopt for design purposes, as it has the capability to define space curves rather than defining curves on planes like the implicit and explicit representation. The independent parameter, often represented as t , i.e., $x = x(t)$, $y = y(t)$, $z = z(t)$ is specified in the range $a \leq t \leq b$ and usually normalized to $[0,1]$ (Goldman, 2003). A limitation of the parametric representation is the difficulty to determine whether a point lies on the curve and, also, find the intersection of two curves.

This work evaluates four parametric representations of curves for modelling a spar FOWT platform. The four curves are the Cubic spline, CHS, which is a variation of the cubic spline, B-Spline, and NURBS.

4.2.3.1 Cubic Spline

A cubic spline is a piecewise cubic function that interpolates a set of data points and guarantees smoothness at the interpolated points (McClarren, 2018). It is a piecewise interpolation model that fits a cubic polynomial to each piece in a piecewise function. It is used to avoid Runge's phenomenon, which is an oscillatory issue at the edges of an interval when using polynomial interpolation, with polynomials of high degree over a set of equally spaced interpolation points (Farin, 1990). For a cubic spline, every point where two polynomials meet results in the equality of the first and second derivatives to ensure a smooth fitting line.

A detailed mathematical construction of a cubic spline curve for interpolation and geometry design is presented in Biran (2019).

Some properties of the piecewise cubic spline are highlighted herein:

- The piecewise cubic polynomial function interpolates all data points on the geometric curve and guarantees smoothness at the data points.
- The piecewise cubic polynomial function is continuous. It has both slope continuity and curvature continuity.
- When the data points are close together and have extreme differences in value, Cubic spline interpolation doesn't work either. This is because cubic spline uses slope calculations (change over distance) to figure out the shape of the curve along the design model.

4.2.3.2 Cubic Hermite Curve

The CHS is a curve in which each piece is a third-degree polynomial specified in the Hermite

form which is by its values and first derivatives at the end points of the associated parametric domain interval. It is conceptually the simplest of the parametric slope continuity C^1 interpolants, although not the most practical one, as reported by Farin (1990).

CHS is commonly used to construct interpolation curves in engineering modelling and designs for providing solutions to practical engineering problems (Farin, 1990, Li and Liu, 2022).

Some of the properties of CHS are highlighted below:

- CHS are readily available and simple to use for engineering models.
- It has local propagation property which allows the designer to locally control the shape of the curve at the control points.
- As a result of its slope / C^1 continuity, it cannot accurately represent some common engineering curves like elliptical arc, circular arc, quadratic parabolic arc, astroid arc and cubic parabolic arc.

4.2.3.3 B-Spline

A basis spline, often known as a B-spline, is a piecewise polynomial function with unique characteristics that specify the degree/order of the polynomial (Farin, 1990). B-spline curve is capable of determining a unique polynomial representation of a set of data which might be for structural points in 3D space or a set of data on a graph.

A B-spline curve is a linear combination of control points \bar{P}_i and B-spline basis function $N_{i,k}$ as highlighted in Equation (3) of section 2.4.1 where the control points, degree/order of the spline and the B-spline basis function are highlighted.

B-spline curve has good attributes that make it favorable among engineers for design purposes. Some of the attributes / properties are:

- The curve has local propagation properties which makes it possible to locally alter the shape of the design rather than altering the entire shape as it is with curves like the Bezier curve.
- B-spline curve is invariant under affine transformation.
- B-spline curve has partition of unity properties.
- The number of segments in a B-spline curve is derived from the degree and the number of control points in the curve, i.e., number of segments is $n-k+2$ where n is the number of control points and k is the degree/order of the curve.

- The continuity of B-spline curve can go beyond the C^2 / curvature continuity to ensure a higher level of smoothness of the curve. A B-spline curve is $C^{(k-2)}$ continuous.
- A given control point influences 1 or 2 or K curve segments. This ensures B-spline localized shape control property.

4.2.3.4 Non-Uniform Rational B-Spline

NURBS is at the forefront of several CAD systems in the academic and commercial modelling sector for geometric designs as it has the capability to describe analytic and freeform shapes (Dimas and Briassoulis, 1999). A regular B-spline representation is effective for describing freeform shapes, but it does not have the capability to represent implicit conic sections accurately. NURBS is a different type of B-spline with the capability of rectifying this deficiency (NURBS) (Farin, 1990). NURBS can represent most parametric implicit curves without loss of accuracy (Farin, 1990, Samareh, 2001). A NURBS curve is defined as highlighted in Equation (4) of section 2.4.1 where the control points, degree/order of the spline, the B-spline basis function and the weights of the spline are highlighted. Another similarity between B-spline and NURBS representation of curves is that the sensitivity derivatives with respect to the control points are fixed during optimization cycles. However, there can be a slight difference in a NURBS scenario if the weights selected as design variables, the sensitivity derivatives will be functions of the weight design variables (Samareh, 2001).

Some properties /attributes of NURBS curves are detailed in Dimas and Briassoulis (1999) and highlighted herein:

- Evaluation of NURBS curve is straightforward, fast, and computationally stable;
- They offer a common mathematical representation for free-form surfaces and commonly used analytical shapes such as natural quadrics, extruded surfaces, and surfaces of revolution.
- They are affine (rotation, scaling, translation) invariant as well as invariant under shear transformations.
- It is easy to change the shape of design from NURBS curve through the manipulation of control points, weights and knots.
- NURBS curves are more general than Bezier and B-Spline curves and tensor product surfaces.
- Bad choice of weights can lead to bad curve/surface parameterization.

- Point member classification is a difficult problem for parametric surfaces. Therefore, it is particularly difficult to include NURBS as nodes in a constructive solid geometry system.

4.3 Methodology

The process adopted in selecting the optimum parametric curve for modeling a FOWT substructure in this study is split into two phases:

1. Integrate the parametric curves in the MDAO framework developed by Ojo et al. (2022b), using the DNV suite software (Sesam Genie, HydroD Stability and HydroD WADAM) and a derivative free pattern search optimization algorithm;
2. Adopt TOPSIS MCDM process, to rank the parametric curves techniques against established marking criteria.

4.3.1 Integrating Parametric Curves with the MDAO Framework.

As discussed in Chapter 2, and demonstrated in Chapter 3, the MDAO framework involves an integration of all the multi-disciplines within the FOWT system coupled together, analyzed and benchmarked against the objective function and a set of design and analysis constraints to select the optimal model.

It involves defining a parameterization scheme with a robust design space configuration, using the varieties of free-form curves discussed in Section 4.2.3. The next step is to analyze design models within the design space using frequency domain analysis tools, such as DNV Sesam suite (Genie and HydroD/WADAM). The penultimate step is to explore the design space to select the optimal design by integrating the analysis with the recommended optimizer (derivative free Pattern Search optimization algorithm). Finally, a multi-criteria decision-making process assessment is conducted on the different parametric curves to rank them in order of modelling durability. The methodological process described is highlighted in Figure 36.

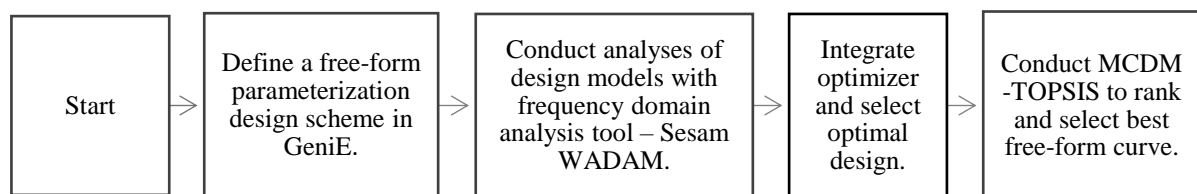


Figure 36. Parametric curve and MDAO framework

4.3.2 TOPSIS method

The TOPSIS method was pioneered by Hwang and Yoon (1981). The method was developed based on the concept that the optimal alternative should have the shortest distance from the positive ideal solution and the longest distance from the negative ideal solution (Hwang and Yoon, 1981, Lozano-Minguez et al., 2011, Kolios et al., 2016). This method is used in this work for benchmarking the parametric curve/spline modelling techniques for FOWT substructure. The TOPSIS flowchart is presented in Figure 37 and a summary overview of the processes involved are highlighted herein.

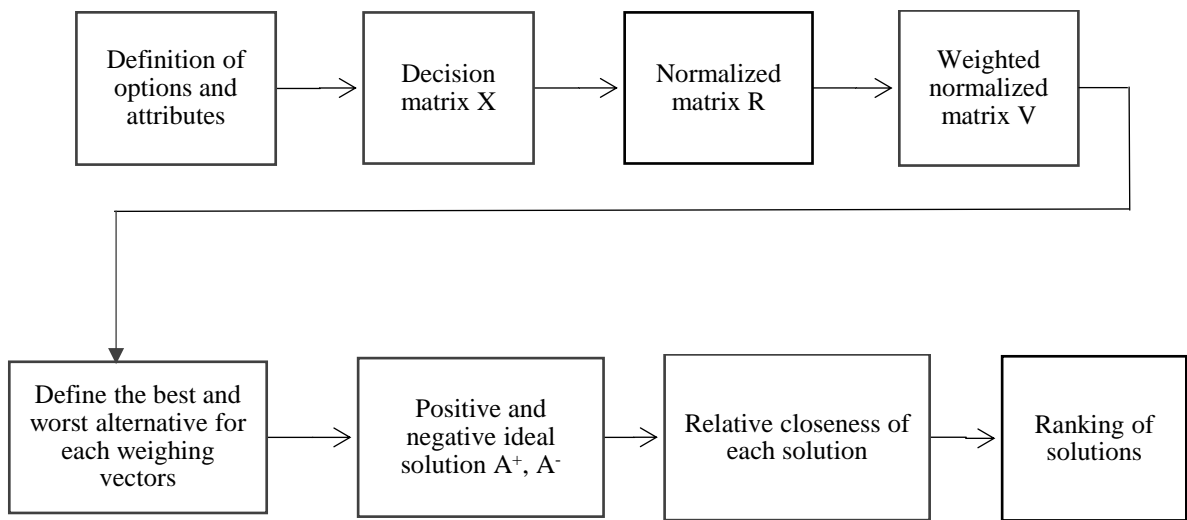


Figure 37. TOPSIS process

The TOPSIS process reported in Figure 37 is detailed below.

1. Define criteria, options, and attributes used in the selection of the optimal process.
2. Obtain a decision matrix using selected input data of design options and criteria $x_{i,j}$, where $i = 1, \dots, m$ represents the design options and $j = 1, \dots, n$ represents the design criteria.
3. The decision matrix is normalized along each column. This is done by dividing each cell within the matrix by the summation of the square of all cells within the matrix column of interest. The decision matrix is derived as highlighted in Equation (11).

$$r_{i,j} = \frac{x_{i,j}}{\sqrt{\sum_{j=1}^m x_{i,j}^2}} \quad (11)$$

4. The relative weighting factor is applied to the normalized matrix considering the characterization of the variables as positive or negative as highlighted in Equation (12).

$$v_{i,j} = w_j r_{i,j} \quad (12)$$

5. Define the best and worst alternative for each of the weighing vectors within the weightage normalized decision matrix.
6. The ideal maximum and minimum values for each column are calculated with the set of equations shown in Equation. (13).

$$x_{i,j}^+ = \max_{1 \leq j \leq n} (x_{i,j}) \text{ and } x_{i,j}^- = \min_{1 \leq j \leq n} (x_{i,j}) \quad (13)$$

The relative distances from the positive and negative ideal solutions can be estimated using the n-dimensional equivalent of Pythagoras' theorem as described with the expressions shown in Equation. (14).

$$D_i^+ = \sqrt{\sum_{j=1}^m (a_{ij}^+ - a_{ij})^2} \quad (14)$$

And

$$D_i^- = \sqrt{\sum_{j=1}^m (a_{ij}^- - a_{ij})^2}$$

7. The closeness rating for ranking the results based on their overall performance is estimated with the expression in Equation. (15)

$$C_i = \frac{D_i^-}{D_i^- + D_i^+} \quad (15)$$

The best design option or solution selected is the one that is both far from the negative ideal solution and close to the positive ideal solution, deriving the highest score.

The TOPSIS process as applied to this research is a systematic approach that helps the designer in identifying the order of performance of the different modelling curves based on unique sets of criteria detailed in section 4.4.3.4.

4.4 Optimized models, results, and discussions

4.4.1 Overview

This section details the design and analysis technique and optimization process conducted to explore the design space. The baseline substructure is the OC3 5MW substructure. This work is based on the MDAO framework developed in Chapter 3, integrated with the shape parameterization free-form curves discussed in Section 4.2.3, with a reduced number of control points to improve the computational time.

The OC3 spar is made of two cylinders connected by a truncated cone at the sea water level. The geometric and structural parameters that make up the OC3 spar-buoy are highlighted in Section 3.4.1.

For the environmental parameters, an extreme sea state (DLC1.6) is used to conduct the global response assessment as detailed in Table 16 of Section 3.6.3.

4.4.2 Design, Analysis and Optimization

4.4.2.1 Design and Analysis

In this study, the OC3 5MW Spar platform's external wet geometry, center of gravity, and moments of inertia are modelled with the DNV Sesam Genie software package, and a potential flow-based hydrodynamic analysis is conducted with DNV Sesam HydroD. Sesam GeniE has an extensive library of explicit, implicit, and parametric free-form curves that helps create beams, plates, and curved surfaces. Some of these tools are circular / elliptic arcs, cubic splines, CHS, B-splines, polycurves, and NURBS. HydroD tools are utilized for the computation of hydrostatics and stability, wave loads, and motion response for the FOWT substructure (DNV, 2021).

The hydrodynamic forces are composed of radiation forces (frequency dependent added mass and damping matrices) and wave excitation forces (including diffraction forces and Froude–Krylov forces). The substructure design is assessed hydrodynamically with the potential flow methodology highlighted in Chapter 2.

4.4.2.2 Definition of Optimization Problem

The optimization problem assessed in this Section is as defined in Section 3.5.3. However, the optimization is conducted in this section on each free-form curve assessed as part of the MCDM process to determine the best performing curve. In addition, unlike the number of design variable used in Table 15 of Section 3.5.4.1 less number of design variables are used to model the platform as highlighted in Table 24 in order to improve computation time of the optimization process.

Table 24: Definition of design variables for all free-form curves assessed

| Platform design variables | Description | Compartment design variables | Description |
|---------------------------|--------------------------|------------------------------|--------------------------|
| x_1 | Radius at tower base | - | - |
| x_2 | Radius at MSL | x'_1 | Radius at MSL |
| x_3 | Radius at 4m below MSL | x'_2 | Radius at 4m below MSL |
| x_4 | Radius at 12m below MSL | x'_3 | Radius at 12m below MSL |
| x_5 | Radius at 60m below MSL | x'_4 | Radius at 60m below MSL |
| x_6 | Radius at 120m below MSL | x'_5 | Radius at 120m below MSL |

The meta-heuristic PSM utilized in Chapter 3 is the optimizer used to integrate the different free-form curves (cubic spline, CHS, B-spline, and NURBS) into the shape parameterization and optimization framework.

PSM is chosen for this study due to its global convergence property. This characteristic helps prevent stagnation in local minima by ensuring an exhaustive search throughout both the exploration and exploitation processes (Palacio-Morales et al., 2021).

The single objective for the optimization problem is to minimize the mass of steel material used for the spar-buoy platform. This translates to minimizing the cost of steel used for the spar-buoy platform. The constraints considered for all the parametric free-form curves considered in this work are highlighted below:

1. The maximum static pitch angle of inclination of the system does not exceed 5 degrees.
2. A positive ballast mass to ensure floatability.

3. Nacelle acceleration less than 30 % of gravitational acceleration.

The formulation of the optimization problem is described as shown in Equation. (7) in section 2.6.3.1.

4.4.3 Results

The results from this study are split into three sections highlighted below.

1. Parametric curves modelling of the OC3 platform with few control points (6 control points and 5 segments): estimate mass and system's response from models of parametric curves using the OC3 dimension (Jonkman, 2010).
2. Shape variation and optimization with MDAO framework: estimate the system's response using the developed MDAO framework for all the parametric curves discussed in this article. All optimized curves yielded different shapes according to the specified constraints and objective function.
3. Ranking parametric curves: employ the TOPSIS methodology to rank the best design.

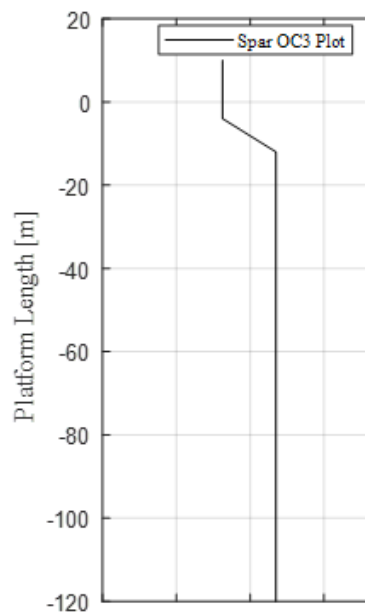
4.4.3.1 Parametric curves modelling and analysis with OC3 reduced order dimension

The first results section presents an evaluation of the system's response, specifically the nacelle acceleration, alongside the estimated mass of steel used in the design. This is in relation to the free-form parametric modeling curves applied to the dimensions of the OC3 platform.

The present analysis assesses the estimated mass of steel and nacelle acceleration response from other parametric modelling curves (cubic spline, CHS, B-spline, and NURBS), using the sea-state presented in Table 16 of Section 3.6.3.2. The design model's data for the parametric curves considered is presented in Table 25. The number of control points is reduced to 5, as highlighted in Table 25, to reduce the dimensionality of the design space investigated by the MDAO framework. A comparison of the parametric curves on the OC3 design model with a plot of the design data points in Table 25 is presented in Figure 38. It is shown in Figure 38 that all the parametric curves on the model are smooth curves with higher continuity compared to the OC3 data plots from Table 25. The system model for the hydrostatic and hydrodynamic analyses is shown in Figure 39.

Table 25. OC3 Spar-Buoy Cubic spline, Cubic Hermite spline, B-spline and NURBS.

| | | | | | | |
|--------------------------------|------|------|------|-----|-----|------|
| Height (m) / Control Points | 10 | 0 | -4 | -12 | -60 | -120 |
| Radius (m) | 3.25 | 3.25 | 3.25 | 4.7 | 4.7 | 4.7 |



OC3 radii straight line plot

Cubic spline curve on OC3 model (blue)

CHS curve on OC3 model (blue)

B-Spline curve on OC3 model (blue)

NURBS curve on OC3 model (blue)

Figure 38. Comparison of the parametric curves on OC3 spar model with the plots from the OC3 data points

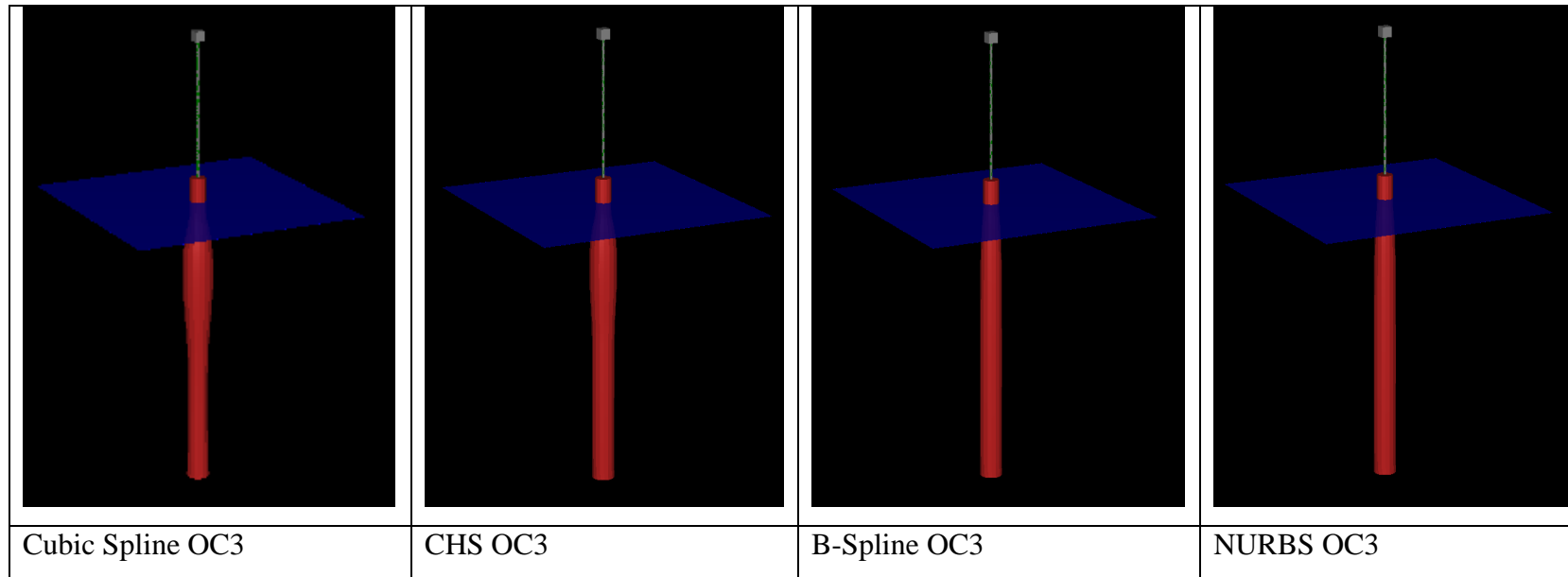


Figure 39. OC3 shape variants from different spline model

4.4.3.2 Wave Spectrum and Response Amplitude Operator Results for Free-form curve OC3 Models

The wave energy spectrum for the site is derived from the data provided in Table 16, and it is represented in Figure 24 in section 3.6.3.2, with a peak period of 14.7 seconds and a Significant wave height of 10.37m.

The surge, heave, and pitch response amplitude operators for all the free-form models developed from the dimensions in Table 25 are represented in Figure 40.

It is shown in Figure 40 that for the parametric free-form curves and all the degrees of freedoms (surge, heave, pitch) assessed, including the nacelle displacement, the peak responses of the NURBS model and the B-spline model appear to be below the range of first order wave excitation force frequencies (i.e. the region between $\sim 0.04\text{Hz}$ to $\sim 0.2\text{Hz}$) for the surge and pitch degrees of freedom, while the cubic spline model and the CHS model are just within this frequency range for the same degrees of freedom. This shows that the models designed with the cubic spline and CHS may have a larger dynamic response than the configurations obtained with the NURBS and the B-spline approaches. However, the heave response peak is outside the first order wave excitation region for all the approaches.

The same observation is made with the nacelle displacement response. The geometries obtained with the NURBS, and the B-spline approaches show the peak response of the nacelle displacement to be outside the first order wave excitation region, while the peak response of the geometries from the cubic spline and the CHS are just within this region, again increasing the likelihood of a larger dynamic response to waves.

The nacelle acceleration of the parametric free-form curves assessed with the OC3 spar-buoy dimension are highlighted in Table 26. The CS free-form curve has the largest nacelle acceleration of 0.184m/s^2 , which is still within the allowable nacelle acceleration of 20%-30% of the acceleration due to gravity (Leimeister et al., 2020b).

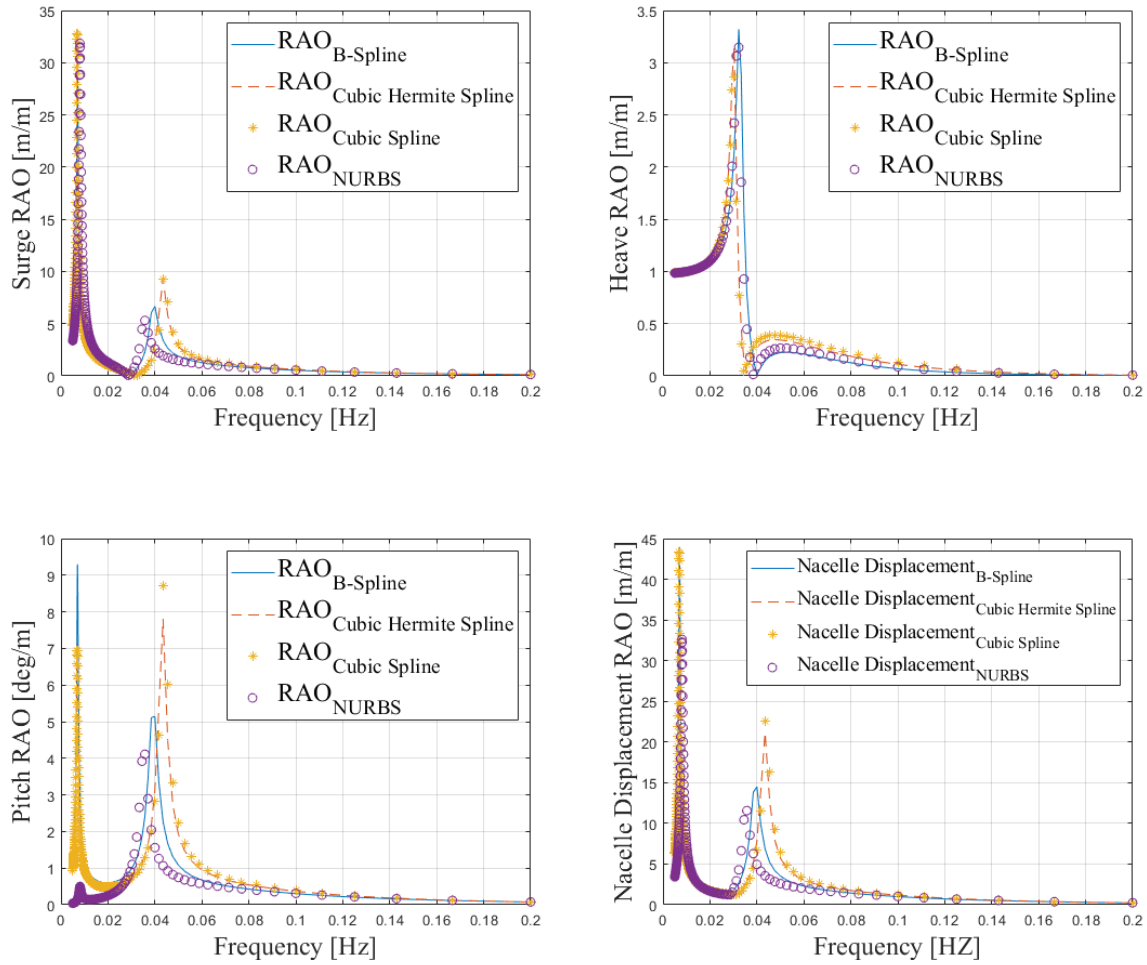


Figure 40. Surge, heave, pitch and nacelle displacement RAO for all four parametric curves.

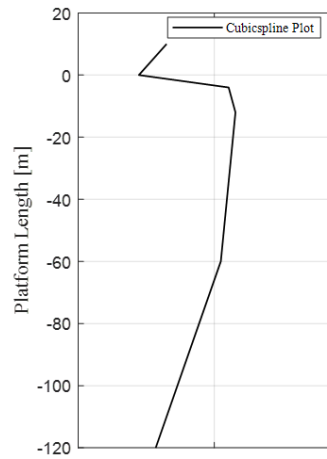
Table 26. OC3 Nacelle acceleration RMS for the free-form curves

| | | CS | CHS | B-Spline | NURBS |
|-----------------------------|---------------------|--------|--------|----------|--------|
| Nacelle | Acceleration | 0.1184 | 0.1110 | 0.0842 | 0.0780 |
| RMS(m/s²) | | | | | |

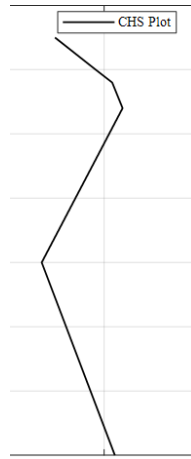
4.4.3.3 Shape Variation and Optimization with MDAO Framework

The shape variation and optimization process results in the selection of optimal design from the parametric curve and MDAO framework. The objective of the MDAO framework is to minimize the mass of steel used for design which invariably reduces the capital cost of the spar-buoy platform. Also, the result satisfies the static pitch angle constraint of 5 deg set for all the four free-form parametric curves assessed. Other constraints set are to ensure a positive ballast,

which is a way to impose floatability, and maintain allowable nacelle acceleration. The results of the optimal shape variants, when the objective and constraints are applied to the MDAO framework as discussed in this section. The optimized dimension or data on the varying control points along the curve are highlighted in Table 27. The difference between the optimized shape parametric curves on the wet geometry model of the spar and with the plots of the curves from the optimized data point along the length of the spar is shown in Figure 41 and the hydrodynamic model shown in Figure 42.



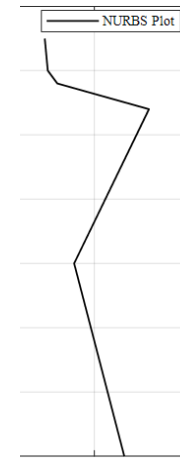
Optimized cubic spline data plot



Optimized CHS data plot



Optimized B-spline data plot



Optimized NURBS data plot



Optimized Cubic Spline curve on model (blue)



Optimized CHS curve on model (blue)

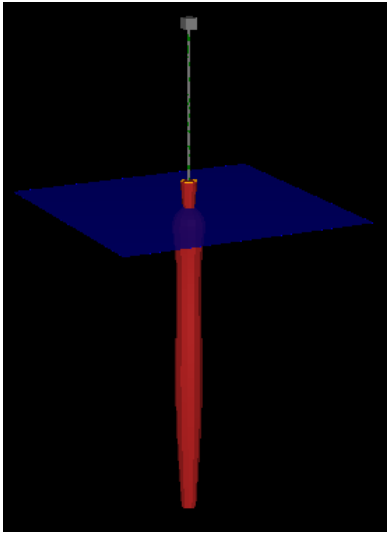


Optimized B-Spline curve on model (blue)

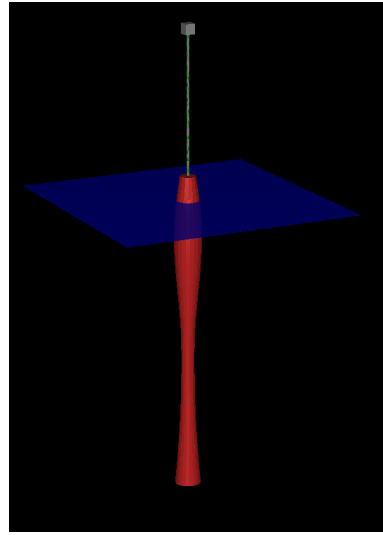


Optimized NURBS curve on model (blue)

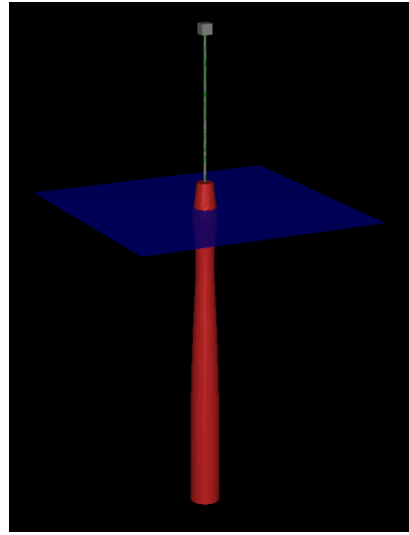
Figure 41. Comparison of the optimized shape parametric curves on model with the plots of the curves from the optimized data point along the length of the spar



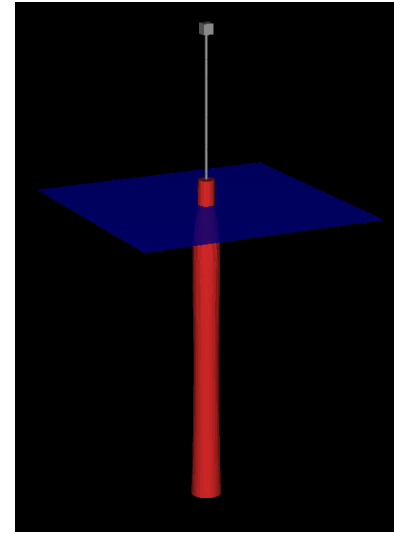
Reduced MDAO Optimized
Cubic Spline



Reduced MDAO Optimized
CHS



Reduced MDAO Optimized B-
Spline



Reduced MDAO Optimized
NURBS

Figure 42. Optimal shape variants from MDAO framework with different spline models

Table 27. Dimension of optimal shapes B-spline, CHS, NURBS and Cubic Spline

| | | | | | | | |
|--------------|-----------------------------|--------|--------|--------|--------|--------|--------|
| B-spline | Height (m) / Control Points | 10 | 0 | -4 | -12 | -60 | -120 |
| | Radius (m) | 3.2500 | 4.4265 | 6.3936 | 1.0000 | 6.3405 | 5.7031 |
| CHS | Height (m) / Control Points | 10 | 0 | -4 | -12 | -60 | -120 |
| | Radius (m) | 3.2500 | 4.6989 | 5.2885 | 5.6596 | 2.7773 | 5.3838 |
| NURBS | Height (m) / Control Points | 10 | 0 | -4 | -12 | -60 | -120 |
| | Radius (m) | 3.2500 | 3.3567 | 3.6938 | 6.9297 | 4.2880 | 6.0581 |
| Cubic Spline | Height (m) / Control Points | 10 | 0 | -4 | -12 | -60 | -120 |
| | Radius (m) | 3.2500 | 2.2297 | 5.5297 | 5.7791 | 5.2409 | 2.8487 |

The response results for the optimal shape variants are presented in Figure 43. The peak response for the surge and the pitch degrees of freedom, as well as the peak of the nacelle displacement RAO, are well outside the first order wave excitation range for all the design parameterization techniques considered. However, for the heave degree of freedom, the peak of the response for the CHS is within the first order wave excitation range, which may lead to a larger dynamic response of this platform to typical sea states, while the same does not happen for the other parameterization curves, whose peaks are outside this region.

The other results assessed for the optimal variants selected from each free-form curve are the mass estimate from the hydrostatic analysis highlighted in Table 28, and the nacelle acceleration computed with the nacelle acceleration root mean square values highlighted in Table 29. The results show that, from a mass minimization point of view, the CHS provided the best configuration. However, for the nacelle acceleration assessment, it is the B-spline curve that yielded the minimum nacelle acceleration value. The nacelle acceleration results are within the allowable limit of 20% to 30% of acceleration due to gravity, as mentioned in Rasekhi Nejad et al. (2017); hence, selecting the curve to use requires a trade-off of what criteria is most important to the designer/analyst. To address this trade-off, the TOPSIS ranking procedure is employed to include other criteria assessed in the analysis to rank the curves in their order of importance. This ranking assessment is presented in detail in section 4.4.3.4.

Table 28.OC3 Optimal variant mass for the free-form curves

| Parametric Curve | B-Spline | CHS | NURBS | Cubic Spline |
|------------------|-----------|-----------|-----------|--------------|
| Mass (kg) | 1 893 231 | 1 640 495 | 1 950 902 | 1 792 532 |

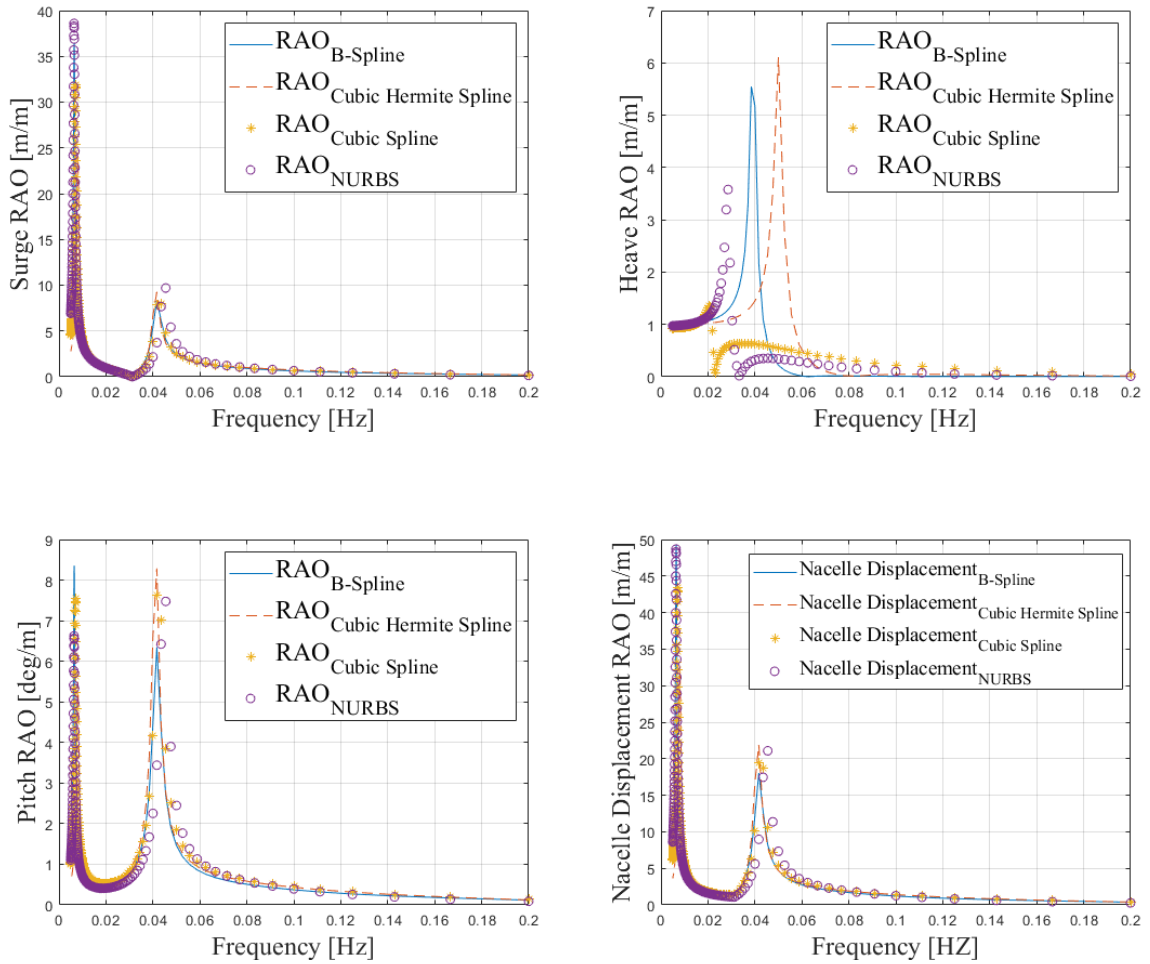


Figure 43. Optimal shape variants surge, heave, pitch and nacelle displacement RAO for all four parametric curves

Table 29. OC3 Optimal Nacelle acceleration RMS for the free-form curves

| | CS | CHS | B-Spline | NURBS |
|-----------------------------|--------|--------|----------|--------|
| Nacelle Acceleration | | | | |
| RMS(m/s²) | 0.1162 | 0.1105 | 0.1017 | 0.1262 |

4.4.3.4 MCDM Assessment - Ranking Free-Form Curves

This section highlights the results from the process of using the TOPSIS method to select the parametric free-form curve that is most suitable for modelling the spar platform. The criteria considered are:

- parametric continuity of curves,
- computational time (for the optimization MDAO framework to successfully end),
- estimated mass of platform,
- shape control capability of the curve,
- nacelle acceleration response.

The hydrostatic and hydrodynamic analyses to select the optimal design were conducted on a computer system with the system properties highlighted in Table 30. The properties show the system used in running the computationally intensive hydrostatic and hydrodynamic analyses is a standard.

Table 30. Analysis system specification

| | |
|----------------------------|--|
| System processor | Intel(R) Core(TM) i7-7700 CPU @ 3.60GHz |
| Operating System | Microsoft Windows 10 |
| Random Access Memory (RAM) | 8.00 GB |
| Storage | 460 GB |
| System type | 64-bit operating system, x64-based processor |

The TOPSIS matrix is provided in Table 31. The values within the matrix in Table 31 are obtained from the analysis conducted, while the criteria values of shape control and parametric continuity are based on the beneficial advantages on the design curve – score of 2 represents high design advantage and score of 1 represents little or no advantage on the curve. For this study, six random scenarios corresponding to different weightages, as highlighted in Table 32, are considered to estimate the performance values and subsequent ranking of the free-form curves. The matrix obtained when the weightage has been multiplied by the normalized performance value is the weightage normalized decision matrix. This is highlighted in Table 33 to Table 38 for the different scenarios considered. The ideal best and ideal worst values for each criterion is determined taking into consideration if the criteria are classed as beneficial criteria or non-beneficial criteria. The rule is that for beneficial criteria, the highest value is selected, and the least value is selected for non-beneficial criteria. The ideal best and ideal worst values are located on the last two rows of the scenarios considered in Table 33 to Table

38. The Euclidian distance from the ideal best solution and the ideal worst solution is estimated for all the weightage scenarios assessed and the performance score is derived with the Euclidian distance from the ideal best and ideal worst solutions. The performance ranking of the parametric curves used for design, analysis, and optimization of the OC3 substructure is based on the estimated performance score assessed for all the weighted scenarios considered as highlighted in Table 33 to Table 38.

Scenario 1 in Table 33 shows a baseline weightage of 1 across the five criteria applied on the normalized decision matrix to estimate the ranking of all the curves. It is shown in Table 33 that the optimized geometric shape of the spar platform modelled with the uniform knot vector B-spline curve is closely followed by the optimized geometric shape modelled with the cubic spline curve, then the NURBS optimized geometric shape, and lastly cubic Hermite spline optimized geometry model.

The performance ranking from Table 34 follows the same trend as results from Table 33, with different and unequal weightages.

For all the weighted scenarios assessed, the B-spline free-form curve is the best performing as it is the only curve that outperformed all the other free-form curves. Following the B-spline curve closely is the cubic spline free-form curve as it is the next best performing curve in all of the 6 random weighted scenarios assessed. In summary, all the assessed free-form curves - B-spline, NURBS, CHS and cubic spline can alter the geometric shape design of a spar FOWT, meeting the design objective and constraints. However, assessing the design process with the criteria highlighted in Table 31 shows the B-spline free-form curve is the most efficient parametric curve for the design and optimization of spar platform used for FOWT system.

The summary of the free-form curve ranking of each scenario is presented in Table 39. The best two performing curves in Table 39 are the B-spline and the cubic spline curves. This result correlates perfectly well with the response results obtained in section 4.4.3.1 (Parametric curves modelling and analysis with OC3 reduced order dimension) and section 4.4.3.3 (Shape variation and optimization within MDAO framework).

Table 31. TOPSIS matrix data

| | Computational Time (Sec) | Estimated mass (kg) | Shape control | Parametric Continuity | Nacelle RMS (m/s²) |
|-------------------------------|---------------------------------|----------------------------|----------------------|------------------------------|--------------------------------------|
| Optimized B-Spline | 115417 | 1893231 | 2 | 2 | 0.1017 |
| Optimized CHS | 125083 | 1640495 | 1 | 1 | 0.1105 |
| Optimized NURBS | 162544 | 1950902 | 2 | 2 | 0.1262 |
| Optimized Cubic Spline | 132355 | 1792532 | 2 | 2 | 0.1162 |
| $\sum_{j=1}^n x_j^2$ | 237550 | 18204272 | 3.6055513 | 3.6055513 | 0.2279957 |

Table 32. Scenarios for criteria weightage matrix

| Weightages | | | | | |
|-------------------|---------------------------|-----------------------|----------------------|------------------------------|--------------------|
| | Computational Time | Estimated mass | Shape control | Parametric Continuity | Nacelle RMS |
| Scenario 1 | 1 | 1 | 1 | 1 | 1 |
| Scenario 2 | 1 | 2 | 0.5 | 1 | 2 |
| Scenario 3 | 1 | 0.5 | 2 | 2 | 1 |
| Scenario 4 | 2 | 1 | 0.5 | 0.5 | 1 |
| Scenario 5 | 2 | 2 | 1 | 1 | 0.5 |
| Scenario 6 | 1 | 2 | 1 | 1 | 2 |

Table 33. Performance ranking from weighted normalized decision matrix - Scenario 1

| | Computation Time | Estimated mass | Shape control | Parametric Continuity | Nacelle RMS | Euclidian distance from ideal best solution | Euclidian distance from ideal worst solution | Sum of Euclidian distances | Performance score | Ranking |
|-------------------------------|-------------------------|-----------------------|----------------------|------------------------------|--------------------|--|---|-----------------------------------|--------------------------|----------------|
| Optimized B-Spline | 0.4275 | 0.5192 | 0.5547 | 0.5547 | 0.4461 | 0.0693 | 0.4428 | 0.5122 | 0.8647 | 1 |
| Optimized CHS | 0.4633 | 0.4499 | 0.2774 | 0.2774 | 0.4847 | 0.3957 | 0.1767 | 0.5725 | 0.3087 | 4 |
| Optimized NURBS | 0.6020 | 0.5351 | 0.5547 | 0.5547 | 0.5535 | 0.2219 | 0.3922 | 0.6142 | 0.6386 | 3 |
| Optimized Cubic Spline | 0.4902 | 0.4916 | 0.5547 | 0.5547 | 0.5097 | 0.0986 | 0.4125 | 0.5111 | 0.8071 | 2 |
| Weight | 1.0000 | 1.0000 | 1.0000 | 1.0000 | 1.0000 | | | | | |
| Ideal best solution | 0.4275 | 0.4499 | 0.5547 | 0.5547 | 0.4461 | | | | | |
| Ideal worst solution | 0.6020 | 0.5351 | 0.2774 | 0.2774 | 0.5535 | | | | | |

Table 34. Performance ranking from weighted normalized decision matrix - Scenario 2

| | Computation Time | Estimated mass | Shape control | Parametric Continuity | Nacelle RMS | Euclidian distance from ideal best solution | Euclidian distance from ideal worst solution | Sum of Euclidian distances | Performance score | Ranking |
|-------------------------------|-------------------------|-----------------------|----------------------|------------------------------|--------------------|--|---|-----------------------------------|--------------------------|----------------|
| Optimized B-Spline | 0.4275 | 1.0385 | 0.2774 | 0.5547 | 0.8921 | 0.1386 | 0.3792 | 0.5178 | 0.7323 | 1 |
| Optimized CHS | 0.4633 | 0.8998 | 0.1387 | 0.2774 | 0.9693 | 0.3216 | 0.2253 | 0.5468 | 0.4119 | 4 |
| Optimized NURBS | 0.6020 | 1.0701 | 0.2774 | 0.5547 | 1.1070 | 0.3250 | 0.3223 | 0.6473 | 0.4979 | 3 |
| Optimized Cubic Spline | 0.4902 | 0.9832 | 0.2774 | 0.5547 | 1.0193 | 0.1645 | 0.3409 | 0.5054 | 0.6745 | 2 |
| Weight | 1.0000 | 2.0000 | 0.5000 | 1.0000 | 2.0000 | | | | | |
| Ideal best solution | 0.4275 | 0.8998 | 0.2774 | 0.5547 | 0.8921 | | | | | |
| Ideal worst solution | 0.6020 | 1.0701 | 0.1387 | 0.2774 | 1.0193 | | | | | |

Table 35. Performance ranking from weighted normalized decision matrix - Scenario 3

| | Computation Time | Estimated mass | Shape control | Parametric Continuity | Nacelle RMS | Euclidian distance from ideal best solution | Euclidian distance from ideal worst solution | Sum of Euclidian distances | Performance score | Ranking |
|-------------------------------|-------------------------|-----------------------|----------------------|------------------------------|--------------------|--|---|-----------------------------------|--------------------------|----------------|
| Optimized B-Spline | 0.4275 | 0.2596 | 1.1094 | 1.1094 | 0.4461 | 0.0347 | 0.8062 | 0.8409 | 0.9588 | 1 |
| Optimized CHS | 0.4633 | 0.2250 | 0.5547 | 0.5547 | 0.4847 | 0.7862 | 0.1473 | 0.9335 | 0.1578 | 4 |
| Optimized NURBS | 0.6020 | 0.2675 | 1.1094 | 1.1094 | 0.5535 | 0.2093 | 0.7857 | 0.9950 | 0.7896 | 3 |
| Optimized Cubic Spline | 0.4902 | 0.2458 | 1.1094 | 1.1094 | 0.5097 | 0.0917 | 0.7927 | 0.8844 | 0.8963 | 2 |
| Weight | 1.0000 | 0.5000 | 2.0000 | 2.0000 | 1.0000 | | | | | |
| Ideal best solution | 0.4275 | 0.2250 | 1.1094 | 1.1094 | 0.4461 | | | | | |
| Ideal worst solution | 0.6020 | 0.2675 | 0.5547 | 0.5547 | 0.5097 | | | | | |

Table 36. Performance ranking from weighted normalized decision matrix - Scenario 4

| | Computation Time | Estimated mass | Shape control | Parametric Continuity | Nacelle RMS | Euclidian distance from ideal best solution | Euclidian distance from ideal worst solution | Sum of Euclidian distances | Performance score | Ranking |
|-------------------------------|-------------------------|-----------------------|----------------------|------------------------------|--------------------|--|---|-----------------------------------|--------------------------|----------------|
| Optimized B-Spline | 0.8549 | 0.5192 | 0.2774 | 0.2774 | 0.4461 | 0.0693 | 0.4149 | 0.4842 | 0.8568 | 1 |
| Optimized CHS | 0.9265 | 0.4499 | 0.1387 | 0.1387 | 0.4847 | 0.2123 | 0.2983 | 0.5106 | 0.5842 | 3 |
| Optimized NURBS | 1.2040 | 0.5351 | 0.2774 | 0.2774 | 0.5535 | 0.3750 | 0.1961 | 0.5712 | 0.3434 | 4 |
| Optimized Cubic Spline | 0.9804 | 0.4916 | 0.2774 | 0.2774 | 0.5097 | 0.1467 | 0.3038 | 0.4505 | 0.6743 | 2 |
| Weight | 2.0000 | 1.0000 | 0.5000 | 0.5000 | 1.0000 | | | | | |
| Ideal best solution | 0.8549 | 0.4499 | 0.2774 | 0.2774 | 0.4461 | | | | | |
| Ideal worst solution | 1.2040 | 0.5351 | 0.1387 | 0.1387 | 0.5535 | | | | | |

Table 37. Performance ranking from weighted normalized decision matrix - Scenario 5

| | Computation Time | Estimated mass | Shape control | Parametric Continuity | Nacelle RMS | Euclidian distance from ideal best solution | Euclidian distance from ideal worst solution | Sum of Euclidian distances | Performance score | Ranking |
|-------------------------------|-------------------------|-----------------------|----------------------|------------------------------|--------------------|--|---|-----------------------------------|--------------------------|----------------|
| Optimized B-Spline | 0.8549 | 1.0385 | 0.5547 | 0.5547 | 0.2230 | 0.1386 | 0.5288 | 0.6674 | 0.7923 | 1 |
| Optimized CHS | 0.9265 | 0.8998 | 0.2774 | 0.2774 | 0.2423 | 0.3992 | 0.3274 | 0.7265 | 0.4506 | 4 |
| Optimized NURBS | 1.2040 | 1.0701 | 0.5547 | 0.5547 | 0.2768 | 0.3921 | 0.3922 | 0.7843 | 0.5001 | 3 |
| Optimized Cubic Spline | 0.9804 | 0.9832 | 0.5547 | 0.5547 | 0.2548 | 0.1540 | 0.4603 | 0.6143 | 0.7493 | 2 |
| Weight | 2.0000 | 2.0000 | 1.0000 | 1.0000 | 0.5000 | | | | | |
| Ideal best solution | 0.8549 | 0.8998 | 0.5547 | 0.5547 | 0.2230 | | | | | |
| Ideal worst solution | 1.2040 | 1.0701 | 0.2774 | 0.2774 | 0.2768 | | | | | |

Table 38. Performance ranking from weighted normalized decision matrix - Scenario 6

| | Computation Time | Estimated mass | Shape control | Parametric Continuity | Nacelle RMS | Euclidian distance from ideal best solution | Euclidian distance from ideal worst solution | Sum of Euclidian distances | Performance score | Ranking |
|-------------------------------|-------------------------|-----------------------|----------------------|------------------------------|--------------------|--|---|-----------------------------------|--------------------------|----------------|
| Optimized B-Spline | 0.4275 | 1.0385 | 0.5547 | 0.5547 | 0.8921 | 0.1386 | 0.4489 | 0.5875 | 0.7640 | 1 |
| Optimized CHS | 0.4633 | 0.8998 | 0.2774 | 0.2774 | 0.9693 | 0.4014 | 0.2253 | 0.6266 | 0.3595 | 4 |
| Optimized NURBS | 0.6020 | 1.0701 | 0.5547 | 0.5547 | 1.1070 | 0.3250 | 0.4019 | 0.7269 | 0.5529 | 3 |
| Optimized Cubic Spline | 0.4902 | 0.9832 | 0.5547 | 0.5547 | 1.0193 | 0.1645 | 0.4170 | 0.5815 | 0.7171 | 2 |
| Weight | 1.0000 | 2.0000 | 1.0000 | 1.0000 | 2.0000 | | | | | |
| Ideal best solution | 0.4275 | 0.8998 | 0.5547 | 0.5547 | 0.8921 | | | | | |
| Ideal worst solution | 0.6020 | 1.0701 | 0.2774 | 0.2774 | 1.0193 | | | | | |

Table 39. Summary of curve ranking

| Ranking based on weighted scenarios | | | | |
|--|-----------------------|-----------------------|-----------------------|-----------------------|
| | 1st | 2nd | 3rd | 4th |
| Scenario 1 | B-spline | Cubic Spline | NURBS | CHS |
| Scenario 2 | B-spline | Cubic Spline | NURBS | CHS |
| Scenario 3 | B-spline | Cubic Spline | NURBS | CHS |
| Scenario 4 | B-spline | Cubic Spline | CHS | NURBS |
| Scenario 5 | B-spline | Cubic Spline | NURBS | CHS |
| Scenario 6 | B-spline | Cubic Spline | NURBS | CHS |

This ranking shows the B-Spline curve as the best performing curve based on the assessment criteria used in the TOPSIS MCDM technique utilized in the study.

Chapter 5 Preliminary Techno-Economic Study of Optimized Floating Offshore Wind Turbine Substructure

5.1 Overview and Background

This chapter is based on an in-review publication pending final decision by Ojo, A., Collu, M., Coraddu, A. Preliminary Techno-Economic Study of Optimized Floating Offshore Wind Turbine Substructure

With more than three-quarters of the world's offshore wind resource potential available in waters deeper than 60m along the coastline of many countries, the potential for fixed bottom offshore wind systems becomes limited (GWEC, 2022). This highlights the need for Floating Offshore Wind Turbine (FOWT) technology to see a true global growth of the clean technology (FOWT) to contribute to reducing greenhouse emissions.

MegaWatts' (MW) scale floating technologies have only been tested in the last ten years through demonstration and pilot projects in both Europe and Asia. With the completion of the demonstration projects, deployment of floating offshore wind turbine systems is yet to enter the commercial or industrial phase as development has just entered the pre-commercial stage with a shift in emphasis moving towards a larger first-of-a-generation schemes (GWEC, 2022). By 2026, FOWT system deployment is anticipated to move into the commercial phase with yearly installations surpassing 1 GW – a milestone achieved by fixed offshore wind in 2010 (DNV-GL, 2020).

The most efficient offshore foundations are floating offshore wind platforms because of their advantages. First and foremost, they enable the exploration and exploitation of huge sections of ocean that are deeper than 60 metres. Secondly, they make it easier to set up turbines, even in mid-depth circumstances (30–50 m),

and they might eventually present a less expensive option than solid foundations. FOWT technology provides the capability to move further offshore to exploit better wind resources while limiting visual impact from land and away from competing with other sea users (Kaldellis et al., 2016). Additionally, due to less invasive construction methods on the seabed than fixed-bottom designs, floating foundations typically provide environmental advantages over the fixed-bottom foundation turbines.

The world's forecast growth of floating offshore wind keeps evolving incrementally. It was 17MW in 2020 and is expected to reach 6.5GW by 2030 (GWEC, 2022). This forecast will be subjected to fluctuations dictated by the economic and fiscal capabilities of stakeholders across industry and government policies across the world.

As highlighted in Chapter 2, three main floating platform concepts (spar, semisubmersible, and tension leg platform) from the oil and gas industry are the early adapters (early to market floaters) in the FOWT sector. The stabilization mechanisms of the three platforms highlighted are: ballast, waterplane / buoyancy, and mooring stabilization. Furthermore, Leimeister et al. (2018) highlighted several floating solutions that have currently been developed that are anticipated to be appropriate and considerably financially viable in depths more than 60 m. These new floating solutions still adapt the stability mechanisms used in the early adapter platforms from the oil and gas sector. Further details of the stability mechanism of the early adapted floaters and their benefits and challenges are detailed in Chapter 2.

Different geographic conditions and sea-states will be suited to different FOWT platforms. The choice of the platform used for a FOWT system will also depend on elements like stability mechanism of choice (ballast, waterplane, or mooring stabilization), political necessity, localization potential, local infrastructure, and

various turbine designs. As a result, the market will likely adjust to changing situations rather than rationalize around a single sort of floating platform (GWEC, 2022). It is expected to see innovation in design, construction, operation, and maintenance as the industry evolves to facilitate the build and operation of larger FOWT projects. Continuous innovation in design is expected to yield new technologies and products capable of supporting better mooring and anchor solutions, deep water substations and dynamic cabling, management of FOWT system's response to environmental conditions and sea-states and the design, analysis, and manufacturing of bespoke floating platforms.

The average CAPEX of a floating platform is higher than that of a fixed bottom platform. As highlighted in Chapter 1, the floating substructure of a reference wind power plant accounts for approximately 29.5% of the CAPEX for the project in contrast to 13.5% for a fixed-bottom reference project. These average values can be significantly higher or lower depending on the platform type employed and will significantly impact the profitability of the project.

Bringing the cost of floaters/platforms used in the FOWT system down to the level of fixed bottom foundations needs an extensive developmental process and ideas exploration. Some of the processes and ideas that can be explored in driving down the cost of FOWT systems are:

1. Geometric shape parametric design, analysis, and optimization of the FOWT platform (Clauss and Birk, 1996, Birk and Clauss, 2002, Birk, 2006, Ojo et al., 2022a);
2. Upscaling design platform to fit with larger and bigger turbines (Leimeister et al., 2016b, Kikuchi and Ishihara, 2019, Papi and Bianchini, 2022);
3. Multidisciplinary design analysis and optimization of all components within the FOWT system (Turbine, tower, platforms, mooring lines and anchors) (Leimeister et al., 2020a, Karimi et al., 2017, Karimi, 2018);

4. Provision of government subsidies to floating wind projects in the precommercial stage to add economic value until the FOWT technology becomes cost competitive with the fixed-bottom OWTs (Markus Lerch, 2019).

The main aim of this study is to investigate the economic implication of use of bespoke geometric shape parameterization, design, analysis, and optimization framework of spar platforms on a 30 MW floating wind farm and the cumulative effect of this bespoke approach and economies of scale on a 60 MW floating wind farm. This investigation will be conducted using some of the financial parameters highlighted in section 5.2.2 in conjunction with the methodology discussed in section 5.3. The techno-economic study highlighting the impact on costing is detailed in section 5.4.

5.2 Economic Feasibility of FOWT Review

5.2.1 Overview

At the turn of the millennium, the total installed costs for offshore wind farms were evaluated from those of existing shallow water and extrapolated to deeper waters for deep water offshore farms. The extrapolation resulted in increased costs of foundations, grid connection, and installation. The new farms designed increased the average cost of offshore wind installations from 2.3 €/kW in the year 2000 to a peak of 5.0 €/kW between 2011 and 2014. However, from 2015, the total costs of FOWFs started decreasing and in 2018, the decrease was down to 4.0 €/kW (Maienza et al., 2022, IRENA, 2019b, IRENA, 2019a)

The predicted cost for FOWFs is also expected to decrease further, according to a recent study, primarily due to technological advancements. These allow capacity

factors to rise while lowering overall installation and maintenance costs (Maienza et al., 2022). The rise in FOWT technology's competitiveness can be efficiently improved by increasing the designers' experience, which reduces project development costs, time, and risks. Additionally, it can also be achieved by adopting the processes and ideas explored in driving down the cost of FOWT discussed in Section 5.1.

The future development of floating wind technology will benefit from accurate financial analyses sustaining the economic and technical value of FOWTs. Some of the techno-economic studies on FOWTs are detailed herein.

Ghigo et al. (2020) conducted a study on platform optimization and cost analysis in a floating offshore wind farm. This study focuses on choosing a floating platform that minimizes the global weight, to reduce the material cost, but ensuring buoyancy and static stability. Subsequently, the optimized platform is used to define a wind farm located near the island of Pantelleria off the Italian coast in order to meet the island's electricity needs. A sensitivity analysis to estimate the LCOE for different sites is presented by analyzing the parameters that influence it most, i.e., capacity factor, weighted average capital cost (WACC), and number of wind turbines. The study concluded that the decrease of many CAPEX cost items and the evolution of the offshore wind market will make this technology even more competitive in a few years.

Ioannou et al. (2020) conducted a preliminary parametric techno-economic study of offshore wind platform concepts. This study investigates through a parametric study the total mass and cost of three floater concepts: spar, barge, and semi-submersible, particularly focusing on the material and manufacturing costs. A survey from floating offshore wind industry professionals was conducted to determine the manufacturing complexity factors' values, which were used to calculate the manufacturing cost. The main conclusion of this work is that, given

the specified conditions, steel-based semi-sub structures proved to be the most expensive configuration, followed by spar as spar prices fall with higher draught values due to the increase in ballast mass. The barge solution is the least expensive option of the three configurations. Also, the study highlighted that the risks and benefits of different configurations should also be considered, as they could lead to savings throughout the asset's service life.

Castro-Santos et al. (2016) presented an approach for evaluating the lifecycle costs of combined or hybrid floating offshore renewable energy systems like a FOWT. Their methodology expressly takes into account the life cycle stages, amongst which are concept generation and definition, design and development, manufacturing, installation, exploration, exploitation, and decommissioning. It is a tool for strategic planning and decision-making, allowing for a better understanding of technical advancements and factors that could either expedite or slow down the growth of the FOWT sector. Their findings from two sites show that the exploitation, manufacturing, and installation costs are the most important life-cycle costs on the LCOE, but the importance of the three costs could be site dependent.

A detailed mapping study of the LCOE for floating offshore wind in the European Atlantic was conducted by Martinez and Iglesias (2022), where they highlighted that understanding the spatial variation of the LCOE of offshore wind is fundamental for identifying potential areas for the development of the FOWT technology. The study presented a large-scale mapping of the LCOE of floating offshore wind over the European Atlantic, with a focus on floating semi-submersible platforms. The energy production is estimated accurately at every site using hindcast wind data combined with the power curve of an exemplar wind turbine. From their study, the lowest LCOE values of approximately 95 €/MWh correspond to the areas where the wind resource is most abundant: off Great Britain

and Ireland, in the North Sea, and off the north-west of Spain, while higher LCOE values of approximately 125 €/MWh are observed off Portugal and Norway, and much higher LCOE values greater than 160 €/MWh is observed in the Gulf of Biscay and south of the Iberian Peninsula. The study defines a methodology for the economic feasibility analysis of a floating offshore wind farm composed of tensioned leg platforms, which are part of the EU ARCWIND research project. In this context, the phases and subphases of its life-cycle process are considered to deal with aspects such as bathymetry, characteristics of the platforms, distance from the farm to shore, distance from the farm to port and offshore wind speed. All the costs and other external parameters such as capital cost, electric tariff, interest rate, percentage of financing and corporate tax have been analysed to calculate the internal rate of return, net present value, discounted pay-back period and levelized cost of energy of the farm. The work studies a farm composed of TLP offshore wind platforms designed by CENTEC and located at Ribadeo in Spain, indicating that the platform is economically feasible for the selected location.

5.2.2 Financial Parameters

The financial parameters are important instruments used in assessing the suitability and profitability of businesses in general - energy businesses inclusive. Financial parameters like the Net Present Value, Internal Rate of Returns, Discounted Pay-Back Period and the LCOE are proven methods for estimating the economic indicators of offshore renewable energies (floating offshore wind, floating wave energy and floating hybrid offshore, including wind and waves) in different locations and extensively discussed in Castro-Santos et al. (2016), Filgueira-Vizoso et al. (2022a), Filgueira-Vizoso et al. (2022b). These metrics play a pivotal role in evaluating the project's profitability and its appeal to stakeholders. However, this Section focuses on using the LCOE to estimate the economic

feasibility of the hypothetical site considered.

5.2.2.1 LCOE

The LCOE is theoretically the price at which the electricity produced would have to be sold to reach the break-even point. It is therefore a fundamental parameter in analysing the economic viability of an energy project and serves as a standardised approach to compare costs of different energy sources (Martinez and Iglesias, 2022) – renewables and fossil fuel based. The LCOE can be defined as the ratio of the costs of an energy project to the electricity production over its lifetime, which is usually expressed as highlighted in Equation. (16).

$$LCOE = \frac{\sum_{t=1}^n (CAPEX_t + OPEX_t)(1+r)^{-t}}{\sum_{t=1}^n (AEP_t)(1+r)^{-t}} \quad (16)$$

where the costs are subdivided into CAPEX, i.e., the costs spent prior to the operation of the project, and OPEX, i.e., the costs of the electricity production and maintenance of the energy farm. AEP represents the annual energy production of the project, which constitutes the main source of income. The variable “t” represents the project's lifetime in years and r denotes the discount rate.

5.3 Methodology and LCOE

5.3.1 Overview

The majority of wind turbines are rated according to their power output (Ramachandran et al., 2013), and each rated turbine has a unique rotor nacelle assembly design. To effect quick optimization changes on the FOWT system for economic feasibility purposes is best done on the substructures - platform,

mooring, and anchor designs. As highlighted in Section 5.1, the cost of a FOWT platform is substantially more than the fixed-bottom design configuration. It has been shown, in Birk and Clauss (2002) and Ojo et al. (2022b), that the mass of steel used in the design of ship hull and FOWT platforms can be reduced using shape parameterization techniques like B-spline within an optimization framework. This reduction in the mass of steel material used in manufacturing the hull/platform substantially reduces the cost of the substructure. For mooring optimization, Munir et al. (2021) showed that FOWTs with shared mooring systems can be one of the most cost-effective solutions for reducing mooring costs, and mooring footprint on the seabed which invariably minimized the disruption or total loss of the Ocean biodiversity.

The methodological approach selected in this work is to estimate the LCOE of 30MW and 60 MW wind farms, using an optimized platform distinguished by applying static pitch angle constraints in the optimization process. The optimal platforms based on the constraints are utilized in hypothetical wind farms to compare the economic feasibility using the LCOE financial parameter.

The process adopted is similar to the approach used in Ojo et al. (2022b), with an additional task of preliminary LCOE estimation added to the framework. The proposed methodology for the exploration, exploitation, and preliminary LCOE estimation of a FOWT farm is to first define a parameterization scheme with a robust design space configuration using the free-form curves parameterization technique – B-spline. This is followed by assessing the design models within the design space with frequency domain analysis tools - Sesam suite by DNV (Genie and HydroD/WADAM). The next stage is integrating the analysis with the optimizer for optimal design selection for the 5 deg, 7 deg, and 10 deg static pitch angles. The last stage involves estimating the LCOE for a 30 MW and 60 MW FOWFs, respectively – 6 platforms for each optimal design are selected with each

static pitch angle constraint for the 30 MW FOWF and 12 platforms selected for each static pitch angle constraint for the 60 MW FOWF. For this preliminary assessment, the hydrostatic analysis is sufficient to estimate the mass of the optimal platform. The described methodological process is shown in Figure 44 The schematic configuration of the FOWF estimated is shown in Figure 45.

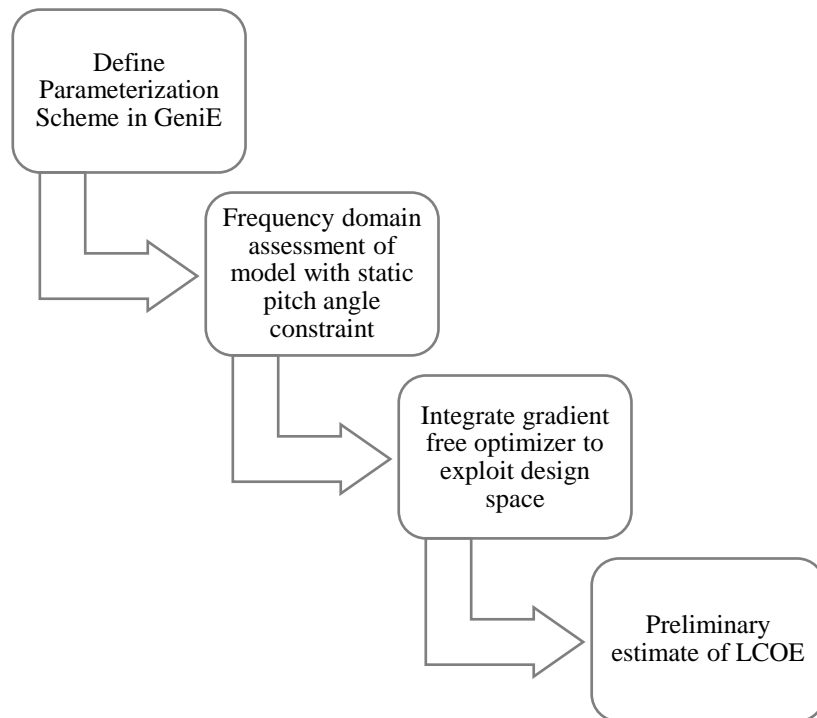


Figure 44. Platform shape optimization and LCOE estimation of a FOWF

5.3.2 Hydrostatics for mass estimation

The design and optimization of any type of floating offshore wind system must satisfy the stability requirement. This needs a detailed hydrostatic assessment to ensure the floater provides enough buoyancy to support the turbine, tower, and

mooring lines while restraining the heave, roll, and pitch motions within allowable limits. The hydrostatic equations in pitch for the available stability mechanisms based on ballast, waterplane area, and mooring systems are represented with the buoyancy equations and the restoring equation highlighted in Equation (17) and (18), respectively.

$$M_{Total} = \rho_w V \quad (17)$$

$$(\rho_w g I_y + F_b z_{CB} - F_w z_{CG} + C_{55,moor})\theta = F_T (z_{hub} - z_{MLA}) \quad (18)$$

where M_{Total} is the total mass of the FOWT system which consists of the substructure components (platform, mooring lines, ballast, and anchors) and the superstructure components (tower and turbine), ρ_w is the water density and V is the volume of the displaced fluid, g is the acceleration due to gravity, I_y is the second moment of area of the initial waterplane area (within the approximation of small angle of inclination, the waterplane area remains constant) with regards to the X axis, F_b is the buoyancy force, z_{CB} is the center of buoyancy (the point at which the resultant buoyancy forces on the body act), F_w is the system's weight force, z_{CG} is the system's center of gravity (the point at which the total system weight acts), $C_{55,moor}$ is the contribution of the mooring stiffness to the pitch stiffness, θ is the pitch inclination angle, F_T is the thrust force from the wind speed, z_{hub} is the hub height and z_{MLA} is the center of mooring line assembly.

The expressions on the left-hand side of Equation. (18) highlights the stability mechanisms within the FOWT system. The first expressions highlight the water plane stability mechanism, the second and third expression represents the ballast stability mechanism, while the fourth expression represents the mooring stability mechanism (Collu and Borg, 2016). A schematic highlighting all the forces and reference points mentioned for a representative spar FOWT system is shown in Figure 45.

5.3.3 Floatability and maximum inclination angle requirements

The floatability requirement is satisfied with Equation (17), which highlights the equality of the platform's buoyancy force and the substructure's total mass. Regarding the maximum angle of inclination, it is equivalent to imposing a minimum pitch stiffness derived from Equation (18) and highlighted in Equation (19) (Ioannou et al., 2020).

$$\frac{F_T(z_{hub} - z_{MLA})}{(\rho_w g I_y + F_b z_{CB} - F_w z_{CG} + C_{55,moor})} \leq \theta_{max}$$

(19)

Where $\rho_w g I_y + F_b z_{CB} - F_w z_{CG} + C_{55,moor}$ is the minimum total stiffness resulting in maximum angle of inclination.

The expression in Equation (19) is very important in the early stages of design as a constraint for exploring the design space based on the allowable static pitch angle required for the FOWT system before conducting detailed design analysis.

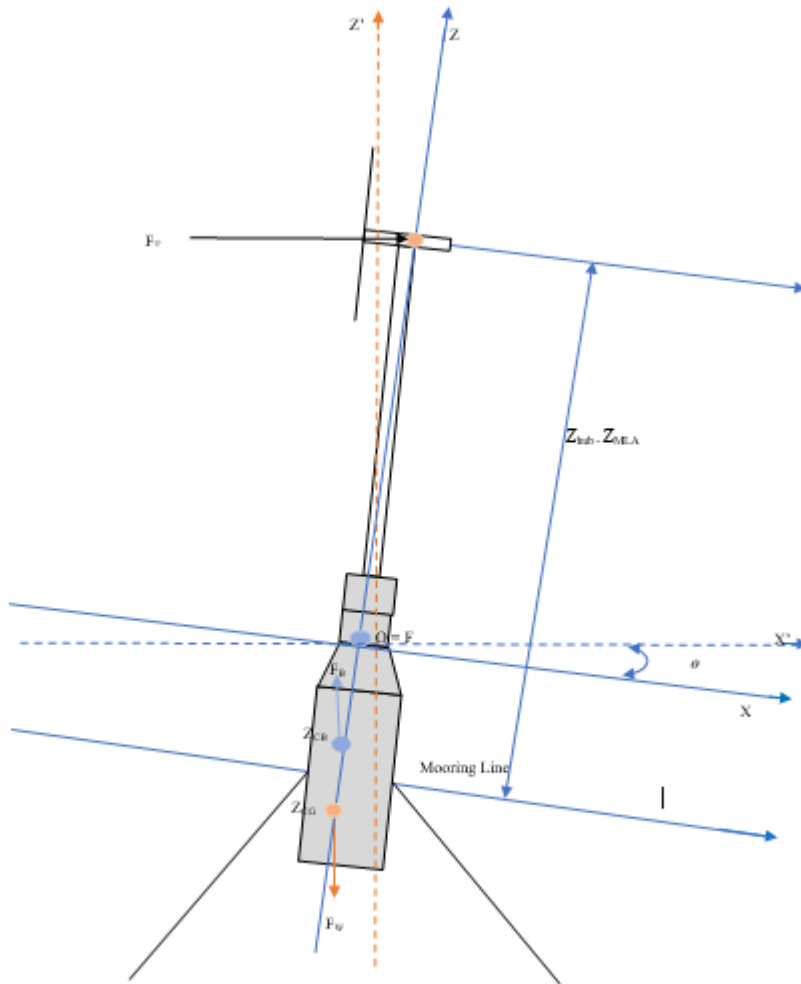


Figure 45. Sketch of forces and reference points of a representative spar FOWT.

5.4 Techno-economic analysis, results and discussion

5.4.1 Overview

As highlighted in section 5.2, the LCOE is an essential financial parameter for assessing any energy generating project – wind farms inclusive as it is the ratio of the costs of an energy project to the electricity production over its lifetime. A host of factors can reduce the LCOE amongst which are listed below and detailed in Markus Lerch (2019).

- CAPEX reduction due to optimization
- Cost reduction potential through industrialization
- Cost reduction due to economies of scale
- Cost reduction due to discount rate.

Exploring the four factors listed above will ensure the commercial viability of the FOWT concept and bring the LCOE cost for FOWT concepts down to what obtains in the fixed bottom offshore wind turbines. For this research, the preliminary techno-economic assessment is based on the CAPEX reduction due to optimization of the geometric shape design of the platform. The CAPEX cost this study influences significantly, is the cost of the platform which makes up about 30% of the total CAPEX cost of a floating wind project (Shields et al., 2021). The shape of the platform is geometrically optimized with the objective of reducing the mass of steel used which will potentially reduce the cost of steel. The technicality involved in the shape optimization is highlighted in Section 5.4.2 and the effect of mass reduction of steel for platform development is highlighted in Section 5.4.3.

5.4.2 Technical Assessment

A high-level numerical simulation from a reference FOWT model (NREL OC3 spar platform) is assessed within a multidisciplinary design analysis and optimization framework to explore, exploit, and select optimal design variants from the design space. The optimal design variants are then assessed with a preliminary economic feasibility study using a representative wind farm with material and cost assumptions from the literature.

5.4.2.1 Reference Design

The reference design for this study is the OC3 spar platform supporting a conventional three-bladed, upwind variable-speed 5MW baseline horizontal axis wind turbine. The geometric and structural properties of the OC3 spar platform are reported in Section 3.4.1.

5.4.2.2 Technical Selection of optimal variants within an MDAO framework

This study assesses a high-level hydrostatic study of a spar substructure discipline in a FOWT system. The design is conducted using the B-Spline shape parameterization technique to enable the exploration of a rich design space for optimal variant selection. B-spline is utilized due to its capability to alter the shape of the design locally when the control point values are changed as highlighted in Section 4.2.3.3. This gives the designer an effective control of the shape with the capability of exploring a richer design space.

As previously explored in chapters 3 and 4, the optimization problem addressed in the initial techno-economic study is characterized as a non-convex, non-linear, single objective, as defined in Equation 7. The main objective is to minimize platform costs, which directly translates to a reduction in the required steel material. The main driving constraint of this optimization problem is the utilization

of static pitch angles, further complemented by the scaling up of the FOWFs capacity.

A metaheuristic pattern search optimization algorithm is used to select the optimal design satisfying the specified objective function and constraints provided within the optimization framework. The specified objective function in this study is minimizing the mass of the platform. This objective is estimated by conducting a hydrostatic analysis using DNV suite – GeniE and WADAM stability software. The process involved in the technical selection within the MDAO framework are detailed herein.

5.4.2.3 B-Spline design of Spar.

B-spline parameterization technique is selected for this study due to its many suitable properties amongst which are: it has local propagation property for effective control of the shape of a design - highlighted in Section 5.4.2.2, its capability to explore large and rich design space, its invariance property under affine transformation and its quick simulation turnaround time as detailed in Section 4.2.3.3 and highlighted in Samareh (2001).

Samareh (2001) showed that several low-degree Bezier segments can represent a complex curve rather than a high degree Bezier curve. The resulting composite curve from this low degree representation is a spline more accurately referred to as B-spline as detailed in Equation (3) of Section 2.4.1.3. B-spline form can represent complex curves more efficiently and accurately than other curve representation like the Bezier, cubic Hermite spline, cubic spline and polycurves.

This multi-segmented curve, as detailed in Equation (3) of Section 2.4.1.3, is used in modelling the curve defining surface of the spar platform used for the hydrostatic analysis of the FOWT system's substructure. Modelling was conducted with the B-spline tool in DNV Sesam GeniE software.

5.4.2.4 Hydrostatics and Optimization.

The high-level hydrostatic and optimization assessments in this study are conducted synchronously to obtain the optimal design. The hydrostatic assessment is based on the stability Equations. (17) and (18), highlighted in section 5.3.2, in which the buoyancy force of the spar from the volume of liquid it displaces is equivalent to the total mass of the system while also considering the contribution of the stability mechanisms. Equation. (18) is also evolved into Equation. (19) which is an assessment of the maximum static pitch angle of the system. This is an important parameter utilized as a constraint in the optimization assessment of the optimal design variant.

The optimization algorithm used in this study is the pattern search method. Pattern search is a relatively inexpensive but effective optimization technique (Findler et al., 1987). It is based on the heuristic of repeating the best search direction in exploratory moves as long as the response function improves. It also has the capability to adequately disperse an appropriate number of starting points – multi-start ability to overcome noise and the danger of getting trapped in local optima.

The optimization problem for this study is represented with the Equation. (7) as described in Section 2.6.3.1 where the k-dimensional vector of design variables with lower and upper bounds, the single objective function, the number of equality constraints and inequality constraints are highlighted. The main objective of this optimization study is to minimize the mass of steel and, invariantly, the cost of the steel material used for the spar platform. The two main constraints considered for all the parametric free-form curves considered in this study are highlighted below:

1. Three maximum static pitch angles of inclination of the system set at 5 deg, 7 deg, and 10 deg, respectively.
2. A positive ballast mass to ensure floatability requirement.

The control points on the B-spline curve in Sesam GeniE are interfaced with the optimization algorithm with python codes to ensure that design variables within the specified boundary conditions in the optimizer are passed into Sesam Genie’s Java Script (back-end files) without human intervention. Also, this ensures the static pitch angle constraint highlighted in Equation. (19) is coded into the optimization framework to integrate the hydrostatic analysis and the optimization algorithm for feasible optimal design selection.

The optimal design variables obtained for the 12 segmented spar with 13 control points and a modelled OC3 spar with its dimension from literature are highlighted in Table 40 . The optimal variants in Table 40 based on the static pitch constraints of 5 deg, 7 deg, and 10 deg are named case A, case B and case C respectively. The model visuals from Sesam GeniE are presented in Figure 46.

Table 40. Design data for selected models and OC3 spar

| | | | | | | | | | | | | | | |
|------------|--------|------|------|------|------|------|------|------|------|------|------|------|------|------|
| OC3 (m) | Height | 0 | 4 | 12 | 30 | 40 | 50 | 60 | 70 | 80 | 90 | 100 | 110 | 120 |
| | Radius | 3.25 | 3.25 | 4.7 | 4.7 | 4.7 | 4.7 | 4.7 | 4.7 | 4.7 | 4.7 | 4.7 | 4.7 | 4.7 |
| Case A (m) | Height | 0 | 10 | 20 | 30 | 40 | 50 | 60 | 70 | 80 | 90 | 100 | 110 | 120 |
| | Radius | 6.91 | 6.86 | 7.22 | 6.04 | 5.00 | 0.55 | 0.50 | 0.50 | 0.50 | 0.50 | 0.53 | 3.38 | 3.92 |
| Case B (m) | Height | 0 | 10 | 20 | 30 | 40 | 50 | 60 | 70 | 80 | 90 | 100 | 110 | 120 |
| | Radius | 4.13 | 4.92 | 4.69 | 4.42 | 4.18 | 3.95 | 3.48 | 0.72 | 0.50 | 0.50 | 0.50 | 4.05 | 4.18 |
| Case C (m) | Height | 0 | 10 | 20 | 30 | 40 | 50 | 60 | 70 | 80 | 90 | 100 | 110 | 120 |
| | Radius | 3.72 | 4.13 | 4.01 | 3.89 | 3.77 | 3.65 | 3.54 | 2.64 | 0.50 | 0.50 | 0.50 | 3.65 | 3.71 |

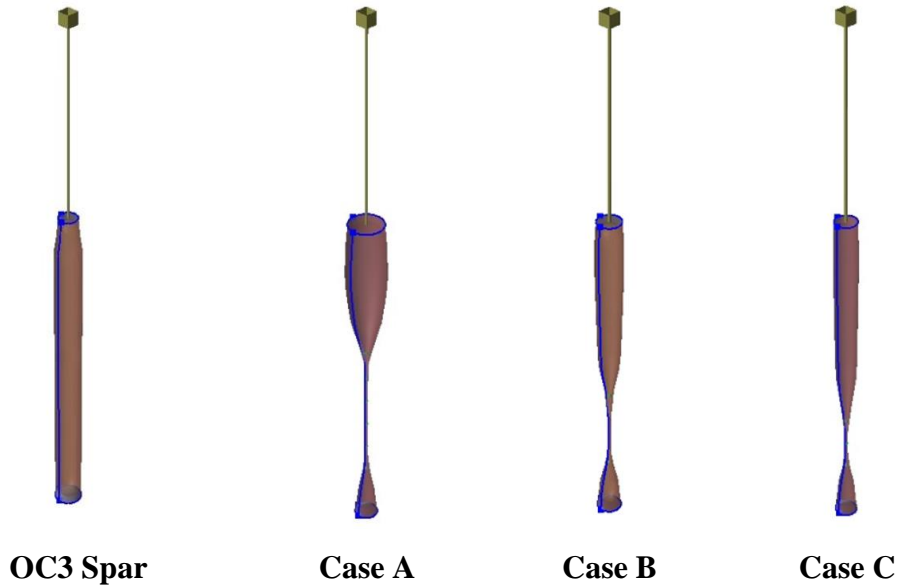


Figure 46. Optimal models from pattern search optimization algorithm and OC3 spar

5.4.3 Economic Feasibility study

Some of the financial parameters used in assessing various projects in literature are highlighted in section 5.2.2. However, for the purpose of this study, the financial parameter chosen to assess the economic feasibility of the farms considered in this work is the LCOE.

The wind farm site used to assess the LCOE for this study is the Hywind wind park, with a hypothetical water depth of 320m. It is essential to utilize measured data for the project site's annual energy production (AEP) estimation. For this work, the AEP estimate of the Hywind site is taken from Saenz-Aguirre et al. (2022) where they have used the conventional Weibull distribution based calculation for the estimated energy generation at the site during a studied climate period between 1991 and 2020. Their calculations are summarized as a fitting of the shape parameter and scale parameter related to the Weibull distribution to match the 30-year wind speed data, and a latter implementation of the power curve of the FOWT

on the fitted histogram to estimate its energy production. Based on the work done in Saenz-Aguirre et al. (2022), the AEP value for the study is 139.8 GWh. Based on the AEP value of 23.3 GWh for a FOWT, the capacity factor worked out from a name-plate wind farm of 30 MW is 52.97%. The capacity factor of 52.97% estimated from this study is much more conservative than the AEP capacity factor of 65% recorded for the HyWind Scotland floating wind farm site in Aldersey-Williams et al. (2020); hence, results in this study are expected to be conservative.

5.4.3.1 CAPEX, OPEX, and DECEX Estimation

Due to the large number of cost components and frequent difficulty and complexity of the FOWT system, the Capital Expenditure (CAPEX) for a Floating offshore wind farm (FOWF) is challenging to quantify. According to the Carbon Trust (James, 2015), the main cost items are related to turbines, towers, platforms, moorings, anchors and the balance of the system, amongst which are the cost of installation of the components that makes up the holistic system, cost of the electrical grid and connections to shore.

As highlighted in Maienza et al. (2020), CAPEX contributions are mostly determined analytically and /or as a function of the wind farm's installed power. The costs for components and installations are considered separately, in part because the former is moderately dependent on the site of installation while the latter heavily depends on the site of installation. The CAPEX is the largest cost and it includes all investment costs to be faced before the commercial operation date (Maienza et al., 2022). The contributions to OPEX are also calculated analytically and /or as a function of the installed power of the wind farm while contributions to DECEX (decommissioning and clearance) are calculated as a percentage of the installation procedures cost (Maienza et al., 2020).

For this work, the CAPEX costs are going to be taken from literature and in cases where they are not available, assumptions are made. The percentage split of a spar FOWF's CAPEX, OPEX and DECEX for this study is 77%, 19% and 4% respectively as specified for a spar FOWF in Maienza et al. (2020).

The masses of the spar platform and corresponding estimated costs based on the platforms masses is shown in Table 41. The mass of the optimal design variant tends to reduce as the static pitch angle is increased as highlighted in Table 41 where the static pitch angle 5 deg – Case A, 7 deg – Case B and 10 deg – Case C yielded reduced platform masses respectively. The reduction in the platform's mass based on the design and optimization constraints leads to a reduction in total cost of the wind farm as subsequently discussed in this section.

The estimation of the costs and assumptions made based on references from literature are presented in Table 42 while the total cost estimate for the hypothetical 30MW Hywind site based on the variation in cost of the platform due to the static pitch angles are presented in Table 43 to Table 46. Similarly, a sensitivity study is conducted for a larger FOWF site – 60 MW farm to assess the total cost estimate for the OC3 platform and the optimal design variants based on the selected constraints and data presented in Table 47 to Table 50.

A clear trend of results from Table 43 to Table 46 shows that the Hywind farm with the OC3 platform has the largest total cost and this is partly due to the observation made in Leimeister et al. (2020b) that the OC3 spar floater is highly over-dimensioned for safety reason; hence, more material cost for the platform, which impacts the total cost of the wind farm as highlighted in Table 43. The total cost estimates of the wind farms in Table 44 to Table 46 shows the static pitch angle constraint used within the design and optimization framework highlighted in section 5.4.2 has the capability of reducing or increasing the mass of the optimal design variant. The increase or decrease in the mass of the optimal platform's

design variant is proportional to an increase or decrease in the cost of steel material for the platform and a cumulative effect of the cost increase or decrease is seen in a sample windfarm as highlighted in Table 43 to Table 46. The same observation is made on a larger FOWF i.e., the larger the static pitch angle, the smaller the mass of the platform and hence, the total cost of material which significantly contributes to the total cost of the farm. The impact of the static pitch angle design constraint on the LCOE of the farm is discussed in section 5.4.3.2.

Table 41. Platform mass and corresponding material cost estimate

| Platform Type | Mass (Tonnes) | Cost- Steel (GBP) |
|---------------|---------------|-------------------|
| OC3 | 1069.86 | 1.50E+06 |
| Case A | 811.29 | 1.14E+06 |
| Case B | 781.84 | 1.09E+06 |
| Case C | 736.55 | 1.03E+06 |

Table 42. Assumptions for hypothetical Hywind wind farm (30 MW – 6 Turbines)

| CAPEX Components | Assumption | Unit | Reference |
|----------------------|-----------------|------------------|--|
| Turbine | 1.3 | [million GBP/MW] | (Ghigo et al., 2020) |
| Platform | Material cost.f | [million GBP] | (Maienza et al., 2020, Ghigo et al., 2020) |
| Anchors | 80000/ Anchor | [GBP] | (James, 2015) |
| Moorings | 500 | [GBP/m] | (Myhr et al., 2014) |
| Export marine cables | 400 | [GBP/m] | (Ghigo et al., 2020) |
| Array marine cables | 600 | [GBP/m] | (Ghigo et al., 2020, Maienza et al., 2020) |
| Installation | 1.5 | [m GBP/MW] | (James, 2015) |

| | | | |
|--------------------------------|--------------------------|---------------|-----------------------------------|
| Offshore electrical substation | 3312000 | [million GBP] | Scaled from Maienza et al. (2020) |
| Onshore electrical substation | 1653600 | [million GBP] | Scaled from Maienza et al. (2020) |
| | | | |
| OPEX | | | |
| Operating Expenditure | 19% of Total Expenditure | | (Maienza et al., 2020) |
| | | | |
| DECEX | | | |
| Decommissioning and clearing | 4% of Total Expenditure | | (Maienza et al., 2020) |

Table 43. Total cost for hypothetical Hywind wind farm (30 MW – 6 Turbines) – OC3 Platform

| | |
|----------------------|-------------|
| CAPEX Estimate (GBP) | 171063720 |
| OPEX Estimate (GBP) | 42210528.31 |
| DECEX Estimate (GBP) | 8886427.013 |
| Total Cost (GBP) | 222160675.3 |

Table 44. Total cost for hypothetical Hywind wind farm (30 MW – 6 Turbines) – 5 deg static pitch angle platform – Case A

| | |
|----------------------|-------------|
| CAPEX Estimate (GBP) | 160203780 |
| OPEX Estimate (GBP) | 39530802.86 |
| DECEX Estimate (GBP) | 8322274.286 |
| Total Cost (GBP) | 208056857.1 |

Table 45. Total cost for hypothetical Hywind wind farm (30 MW – 6 Turbines) – 7 deg static pitch angle platform – Case B

| | |
|----------------------|-------------|
| CAPEX Estimate (GBP) | 158966880 |
| OPEX Estimate (GBP) | 39225593.77 |
| DECEX Estimate (GBP) | 8258019.74 |
| Total Cost (GBP) | 206450493.5 |

Table 46. Total cost for hypothetical Hywind wind farm (30 MW – 6 Turbines) – 10 deg static pitch angle platform – Case C

| | |
|----------------------|-------------|
| CAPEX Estimate (GBP) | 157,084,700 |
| OPEX Estimate (GBP) | 38,756,225 |
| DECEX Estimate (GBP) | 8,159,205 |
| Total Cost (GBP) | 203,980,130 |

Table 47. Total cost for scaled up Hywind wind farm (60 MW – 12 Turbines) – OC3 Platform

| | |
|----------------------|---------------|
| CAPEX Estimate (GBP) | 320,827,440 |
| OPEX Estimate (GBP) | 79,165,212.47 |
| DECEX Estimate (GBP) | 16,666,360.52 |
| Total Cost (GBP) | 416,659,013 |

Table 48. Total cost for scaled up Hywind wind farm (60 MW – 12 Turbines)– 5degstatic pitch angle platform – Case A

| | |
|----------------------|---------------|
| CAPEX Estimate (GBP) | 305,407,560 |
| OPEX Estimate (GBP) | 75,360,307.01 |
| DECEX Estimate (GBP) | 15,865,327.79 |
| Total Cost (GBP) | 396,633,194.8 |

Table 49. Total cost for scaled up Hywind wind farm (60 MW – 12 Turbines) – 7deg static pitch angle platform – Case B

| | |
|----------------------|---------------|
| CAPEX Estimate (GBP) | 302,933,760 |
| OPEX Estimate (GBP) | 74,749,888.83 |
| DECEX Estimate (GBP) | 15,736,818.7 |
| Total Cost (GBP) | 393,420,467.5 |

Table 50. Total cost for scaled up Hywind wind farm (60 MW – 12 Turbines) – 10 deg static pitch angle platform – Case C

| | |
|----------------------|---------------|
| CAPEX Estimate (GBP) | 299,129,400 |
| OPEX Estimate (GBP) | 73,811,150.65 |
| DECEX Estimate (GBP) | 15,539,189.61 |
| Total Cost (GBP) | 388,479,740.3 |

5.4.3.2 LCOE Estimation

The LCOE calculation is the ratio of the net present value of total cost to the net present value of electricity generation. It is a method used to obtain the cost of one unit energy produced and is typically applied to compare the cost competitiveness of different power generation technologies and concepts (Markus Lerch, 2019). LCOE's results are based on the discounted values of CAPEX, OPEX and DECEX before being distributed relative to the energy generation (Myhr et al., 2014). LCOE returns the constant real energy price required to generate the return equal to the discount rate used over the project's full life (Aldersey-Williams and Rubert, 2019).

The discount rate is a critical criterion in estimating the LCOE as the higher the discount rate, the larger the range of LCOE in the future and the lower the discount rate, the lower the LCOE in the future (Aldersey-Williams and Rubert, 2019). The

discount rate typically presents values in the range of 8 % - 12 % for offshore wind investments (Martinez and Iglesias, 2022). For conservative purpose, this study is adopting a discount rate of 10% and the lifetime of the project is set to be 20 years. Furthermore, for this study, the CAPEX values are distributed as per the values in Table 43 to Table 46 for the 30 MW demonstration wind farm for the four varying optimal platform designs considered and in Table 47 to Table 50 for the 60 MW demonstration project considered for the different optimal platform designs considered. The OPEX costs are assumed to be evenly distributed over the 20 years of operation. The DECEX cost is assumed to be a one-off distribution process after the operation phase.

The mass of the designed platform tends to vary based on the design constraint specified as shown in Figure 47 and highlighted in Table 41 where the mass of the optimal platform variants reduces as the static pitch angle constraint is increased. The cumulative effect of the reduction in mass due to the design constraint on the total cost of the farm is discussed in Section 5.4.3.1. However, the cumulative effect of the reduction in mass due to design constraint on the platform cost for 30 MW farm and 60 MW farm are highlighted in Table 51 and shown in Figure 48 and Figure 50 respectively. Table 51 shows that for both the 30 MW and 60 MW FOWFs, the total mass of the platforms used in both sides reduces as the static pitch angles are increased from 5 deg to 7 deg and 10 deg respectively for both farms. This reduction in the mass of material – Steel used in manufacturing the designed platforms also culminates in the reduction in the cost of the materials used in manufacturing the platforms as detailed in Table 51 for both FOWFs. This occurrence (reduction in total mass of platform due to increase in static pitch angle) is also shown in Figure 48 and Figure 50 for the 30 MW and 60 MW FOWFs respectively.

The LCOE for the 30 MW site and the 60 MW site is developed based on the site's total costs for each optimal design highlighted in Section 5.4.3.1 and Section 5.4.3.2 respectively. This study investigates the LCOE result from two fronts highlighted below:

1. The impact of the design constraint on the estimated LCOE of the FOWF.
2. The effect of scaling up a FOWF on the LCOE of the project.

The impact of the design constraint – mainly the static pitch angle on the LCOE is demonstrated on a 30 MW FOWF as highlighted in Table 52 and shown in Figure 49. In assessing this impact, the OC3 model is the base model while the percentage difference on the 5 deg, 7 deg and 10 deg static pitch angle constraint optimized design variants are measured relative to the OC3 base model. Table 52 shows that the LCOE of the optimized variants relative to the OC3 base model is reduced by 6.34%, 7.07% and 8.18% for the 5 deg, 7 deg and 10 deg static pitch angle constraint optimized design variants respectively. These percentage differences of the optimized floaters with respect to the standard 5MW OC3 model shows how significant the reduction in masses / material of the platforms can play in reducing the LCOE of a small wind farm.

The study on the effect of scaling up the 30 MW FOWF is conducted by doubling its capacity to 60 MW. The LCOE result for the 30 MW and 60 MW FOWF are highlighted in Table 53 and also shown in Figure 49 and Figure 51 respectively. The LCOE for the 60 MW OC3 platform FOWF is 6.23 % lower than the LCOE of the 30 MW OC3 platform FOWF. Similarly, the 5 deg, 7 deg and 10 deg static pitch angle constraint design variants of the 60 MW FOWF is 4.68 %, 4.72 % and 4.78 % lower in LCOE value than the corresponding optimal design variants for the 30 MW FOWF.

This significant reduction in LCOE values between the 60 MW FOWF and the 30 MW FOWF is a cumulative effect of the mass optimization of the platform as

detailed in section 5.4.2 and the concept of scaling up the floating wind size (economies of scale). Equation (20) shows the CAPEX parameter in the LCOE expression in Equation (16) of Section 5.2.2.1. This equation shows that for the FOWF assessed, the constant parameter change is the cost of the platform resulting from the optimization of the platform's shape driven by the static pitch angle constraints. This platform variation drives the changes in LCOE of the FOWF. However, in doubling the size of the FOWF, the platform variants will contribute significantly to the reduction of the LCOE. This and other factors like suppliers' discount for large scale supplies of components and systems will further reduce the LCOE of the FOWF.

$$\begin{aligned} & \sum \text{CAPEX} && (20) \\ & = \sum \begin{array}{l} \text{Platforms, Turbine, Moorings, Anchors, Marine cables,} \\ \text{Offshore, electrical substations,} \\ \text{Onshore electrical substations and Installation} \end{array} \end{aligned}$$

The concept of increasing the farm size is detailed in Myhr et al. (2014) where they showed that by increasing the number of turbines from 100 to 200 would lower the LCOE by approximately 10 % and that by increasing the turbines to 600 results in an LCOE reduction of up to 15 %. The reduction in the LCOE value for the optimal design variants between the 60 MW and 30 MW FOWFs considered in this study is less than 5 %. The 5 % reduction in LCOE value is not as significant as the 10 % to 15 % reduction in LCOE values recorded in Myhr et al. (2014). However, comparing the number of turbines - 200 it took Myhr et al. (2014) to attain 10 % reduction in LCOE value with the 12 turbines used to attain about 5 % reduction in LCOE value in this study, the approach adopted using platform mass optimization in combination with scaling up the floating wind farm is a much more

effective approach to reducing the value of the LCOE in comparison to just scaling up the farm size or conducting platform mass optimization alone.

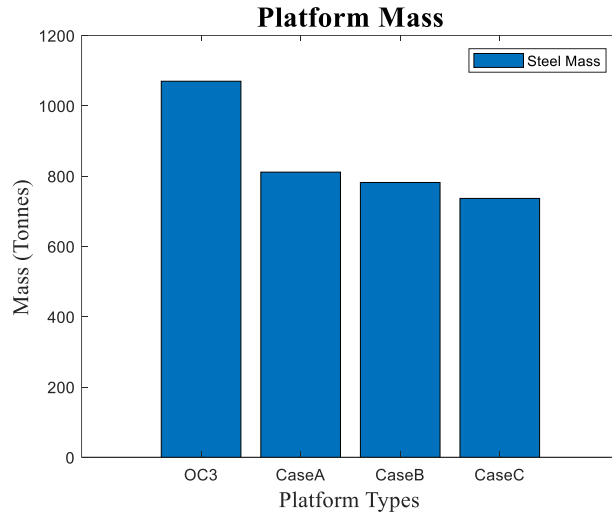


Figure 47. Mass of platform types

Table 51. Estimated total platform mass and material cost for 30 MW and 60 MW FOWF

| Design Variants | 30 MW FOWF Platform mass (Tonnes) | 60 MW FOWF Platform mass (Tonnes) | 30 MW FOWF Platform cost (£) | 60 MW FOWF Platform cost (£) |
|-----------------------------------|---|---|---------------------------------------|---------------------------------------|
| OC3 Design | 6419.16 | 12838.32 | 8.99E+06 | 1.80E+07 |
| Case A- 5 deg Static Pitch angle | 4867.74 | 9735.48 | 6.81E+06 | 1.36E+07 |
| Case B- 7 deg Static Pitch angle | 4691.04 | 9382.08 | 6.57E+06 | 1.31E+07 |
| Case C- 10 deg Static Pitch angle | 4419.3 | 8838.6 | 6.19E+06 | 1.24E+07 |

Table 52. LCOE comparison for 30 MW OC3 base model and 5 deg, 7 deg and 10 deg Static Pitch angle constrained optimized models

| Design Variants | LCOE – 30 MW FOWF (£/MWh) | Design Variants | LCOE – 30 MW FOWF (£/MWh) | Percentage Difference (%) |
|-----------------|---------------------------|--------------------------------|---------------------------|---------------------------|
| OC3 Design | 197 | Case A- 5° Static Pitch angle | 185 | 6.34 |
| OC3 Design | 197 | Case B- 7° Static Pitch angle | 183 | 7.07 |
| OC3 Design | 197 | Case C- 10° Static Pitch angle | 181 | 8.18 |

Table 53. LCOE comparison for 30 MW and 60 MW FOWF with 10% discount rate

| Design Variants | LCOE – 30 MW FOWF (£/MWh) | LCOE – 60 MW FOWF (£/MWh) | Percentage Difference (%) |
|-----------------------------------|---------------------------|---------------------------|---------------------------|
| OC3 Design | 197 | 185 | 6.23 |
| Case A- 5 deg Static Pitch angle | 185 | 176 | 4.68 |
| Case B- 7 deg Static Pitch angle | 183 | 175 | 4.72 |
| Case C- 10 deg Static Pitch angle | 181 | 173 | 4.78 |

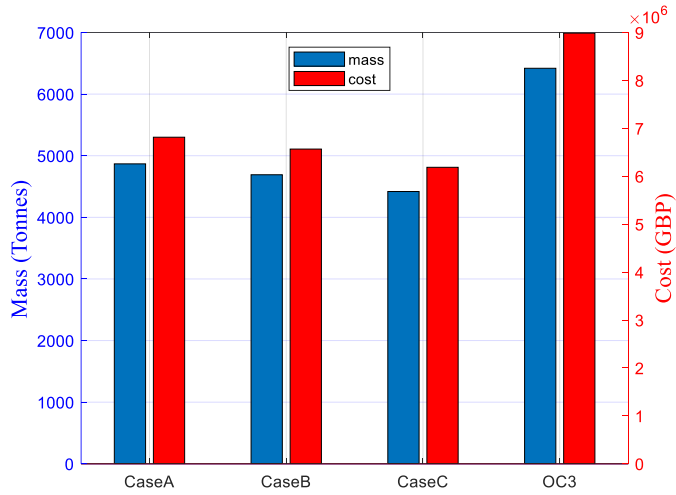


Figure 48. 30MW Farm Total Platform Mass and Total Platforms Material Cost

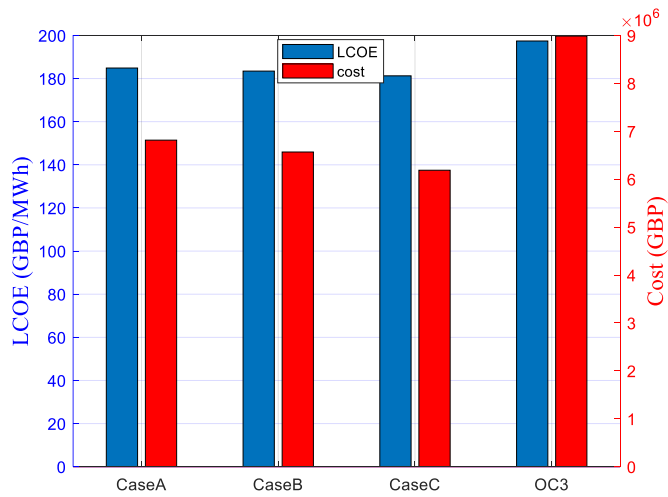


Figure 49. 30MW Farm LCOE and Total Platforms Steel Cost

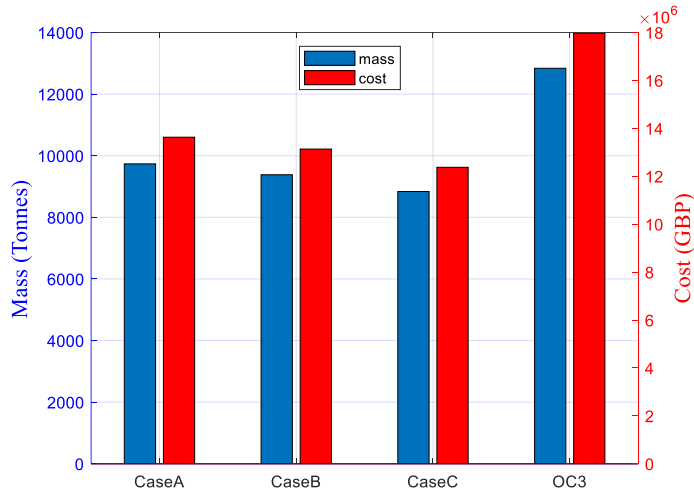


Figure 50. 60MW Farm Total Platform Mass and Total Platforms Material Cost

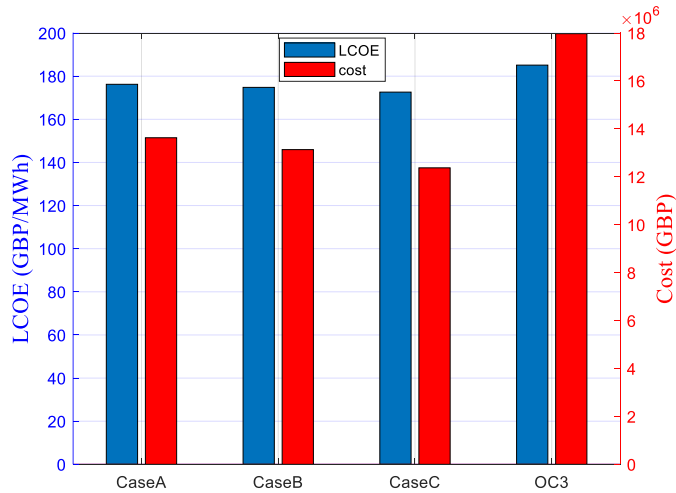


Figure 51. 60MW Farm LCOE and Total Platforms Steel Cost

The ratio of the net present value of total cost to the net present value of electricity generation which translates to the LCOE is the financial parameter used in assessing the different scenarios considered in this study (30 MW FOWFs and 60 MW FOWFs for OC3 NREL platforms, 5 degrees, 7 degrees and 10 degrees

static pitch constrained platforms). The LCOE values for the 30 MW FOWFs based on the OC3 platform model and static pitch constraints platform models of 5 deg, 7 deg and 10 deg are 197 £/MWh, 185 £/MWh, 183 £/MWh and 181 £/MWh respectively. On scaling up the farm size to 60 MW, the estimated LCOE values for the 60 MW FOWFs based on the OC3 platform model and static pitch constraints platform models of 5 deg, 7 deg and 10 deg are 185 £/MWh, 176 £/MWh, 175 £/MWh and 173 £/MWh respectively - which is 6.23 %, 4.68 %, 4.72 % and 4.78 % lower than the corresponding optimal design variants for the 30 MW FOWF. This is due to a combination of design shape parameterization and optimization framework utilized in this study and economy of scaling up the FOWFs.

In addition to the need for determining the structural integrity of FOWT structures as highlighted in Section 3.2, a detailed structural analysis of the FOWT system is essential for determining the LCOE estimate of the system at a farm level. While detailed structural assessment hasn't been considered in this thesis, it is essential for techno-economic assurance for the design life of the structures. This is because fatigue life is a fundamental factor in estimating the design life of an offshore structure. It influences the material selection, structural design, maintenance strategies, safety, reliability and cost efficiency of the FOWT system.

Adequate understanding and prediction of how the structural response of the system over time can ensure if the design life is met or exceeded, while also maintaining safety, reliability and cost-effectiveness throughout the structure's operational period is critical prior to making an LCOE estimate.

Design life of a FOWT is critical factor that impacts the CAPEX and OPEX, as well as overall operational efficiency and reliability of the system. A careful optimization of the fatigue life from detailed structural assessment can result in favourable LCOE by increasing the operational life of the system, making FOWT

concepts more economically viable. This is a balancing act between initial cost and long-term benefits requiring detailed analysis of not just the hydrodynamic discipline but the structural discipline within the MDAO framework.

Chapter 6 Conclusion and Recommendations

6.1 Conclusion

FOWT technology is presently not as competitive as its fixed bottom counterpart, due to the substantial cost (computational time and capital cost) involved in its design, analysis, and manufacturing, either individually or as a wind farm. This is partly due to the FOWT technology still being in the precommercial stage. The main purpose of this research is to develop a methodology leveraging available design tools, theories, and optimizers to produce bespoke design, analysis, optimization, and selection of feasible floating foundations that satisfies design requirements, improves system's response, and reduces floater's weight and required design computational time. This can potentially advance and expedite the development of FOWT technology as weight and cost, as well as development time reduction are key to the expected commercialization. Commercializing the FOWT technology will require making it as competitive as its fixed bottom wind turbine counterpart. The proposed method of addressing commercializing FOWT technology in this research is adapting the use of shape parameterization technique within an MDAO framework.

This research contributes to knowledge by developing a novel framework that provides value to potential stakeholders as highlighted and discussed, having achieved the following:

1. Developed an automated MDAO framework, integrating the free-form curves within the design loop, to produce a bespoke platform shape. This framework has a robust capability to explore and exploit large and rich design spaces, for optimal designs, with bespoke shapes, based on the

objective functions and constraints specified in frequency domain, and verifying the constraints with a medium fidelity time domain tool.

2. Developed an analytical methodology to investigate / rank the free-form curves within the MDAO framework based on specified performance criteria using the Technique for Order of Preference by Similarity to Ideal Solution (TOPSIS) Multi-Criteria Decision Matrix (MCDM) technique. Although MCDM's are based on weightage of performance criteria and analyst's opinion, it is a robust technique for performance ranking in engineering design.
3. Assess developed framework via a preliminary techno-economic study by applying the framework to the design of a wind farm and assess the impact of reduction in mass of floater steel to the economics of the wind farm.

The conclusions of this thesis are summarized below and detailed in Subsection 6.1.1 to 6.1.3.

6.1.1 Develop an automated MDAO framework with an integrated free-form curves parameterization technique

This research highlights the use of parametric curves to alter the geometric shapes of a FOWT substructure, while simultaneously optimizing the FOWT system. The automatic numerical MDAO framework developed for this study employs the use of parametric free-form curves, structural, hydrostatics and hydrodynamic modelling and analysis tools in frequency domain (DNV suites), together with a meta-heuristics optimizer to estimate the system's fitness for purpose. The use of free-form curves for modelling the spar platform of the FOWT system allows the geometric shape alteration as a result of the local propagation property along the control points on the parametric free-form curve. This capability

is the core novelty of the present methodology as it differs from previous work in this area, where a simpler approach of changing only the global diameter and height of the cylindrical sections representing the platform was used – the present methodology therefore allows the exploration of richer design space for optimal selection. An important constraint utilized in the optimizers is the static pitch constraints for hydrostatic equilibrium. Static pitch angles of 5 deg, 7 deg, and 10 deg are considered and for each pitch angle case as the MDAO framework cycles through an average of 2500 iterations to select the optimal design.

Verification of each of the optimal design is conducted with medium-fidelity OpenFAST time domain AHSE tool. The platform's frequency dependent added mass and damping data, the excitation force data and calculation of the heave, pitch, and roll hydrostatic stiffnesses are coupled in OpenFAST. In addition to this, the platform's pitch, roll, and yaw inertia are calculated for the optimal variants, and coupled with the platform mass and centre of mass in the structural section of the AHSE OpenFAST tool and a dynamic analysis in a severe seastate is conducted while the FOWT system is operating at the rated wind speed. The response and performance of the system's design variants at the rated wind speed are all acceptable and within allowable limits from the design standards.

A key finding of this study shows that the mass of steel required for the design and manufacturing of a FOWT platform reduces as the static pitch angle increases from 5 deg to 7 deg, and 10 deg respectively. This reduction in mass inherently translates to lower capital cost on materials for manufacturing and build. In addition to reducing the mass of steel used in the design, bespoke geometric shapes of the platforms with acceptable hydrodynamic motion responses in severe seastates are generated. An important advantage of this MDAO framework with geometric alteration capability is that it can be applied to any design concept, optimally

varying its shape, improving some of the key global response performance while aiming at reducing the structural weight, ultimately leading to a lower capital cost.

6.1.2 Develop an analytical methodology to investigate / rank the free-form curves within the MDAO framework

This research developed an analytical process for ranking the performance of parametric free-form curves within an MDAO framework, using the spar platform of an NREL 5MW floating offshore wind turbine as a case study. The parametric free-form curves investigated are the cubic spline, the CHS, the B-spline and the NURBS curve. These curves were used to model and optimize a spar platform for floating wind turbines, based on the NREL OC3 spar platform's dimension. The hydrodynamics assessment is conducted with the potential flow theory approach in the frequency domain to estimate the response amplitude operator of the system. Each parametric curve was integrated within an MDAO framework, using a combination of the Sesam DNV package software and in-house programming and data analysis codes, to interface the different disciplines.

The objective function within the MDAO framework is to minimize the mass of steel used in the design. The constraints are to ensure the maximum pitch angle of inclination of the system does not exceed 5 degrees and ensure a positive ballast for stability and floatability of the system. The results from the MDAO framework satisfying the objective function and constraints are assessed with TOPSIS MCDM technique to determine the best performing curve using different marking criteria such as the computational time, designed mass of the platform, nacelle acceleration and properties of free-form curve (shape control capability and parametric continuity of the curve). Different scenarios are considered by varying the weightage of each marking criteria of the TOPSIS analysis conducted as the

ranking depends on the weightages. However, a defined trend with all the scenarios assessed is that the best parametric curve approach is the B-spline curve while the worst one is the CHS. The second and third performance curve kept changing between the NURBS and the cubic spline, depending on the scenario. This result correlates with the observation from the response results derived within the MDAO framework, with the model from B-spline and NURBS producing results with peak response frequencies in the surge, heave, and pitch degrees of freedom occurring outside the first order wave excitation frequency range (0.04Hz – 0.5Hz), while the optimized configurations from CHS and cubic spline have peak response frequencies in the surge and pitch degree of freedom slightly within the first order excitation range. This study shows the use of the TOPSIS technique to prove B-spline and NURBS can serve as effective parameterization curves to use for modelling within an MDAO framework.

6.1.3 Positive contribution on the preliminary techno-economics of FOWT projects

This research investigates the economic implication of use of bespoke geometric shape parameterization, design, analysis, and optimization framework of spar platforms on a 30 MW floating wind farm and the cumulative effect of this bespoke approach and economies of scale on a 60 MW floating wind farm. The bespoke technical assessment was conducted using the free-form shape parameterization technique within an MDAO framework to design, analyze and optimize the concept. The main design constraint within the optimizer to facilitate the shape alteration within the MDAO framework is the static pitch angle. Similar to approach discussed in Section 6.1.1, this study also considered the static pitch angles of 5 degrees, 7 degrees, and 10 degrees, respectively, and the OC3 NREL

model. As highlighted in literature, the OC3 model is over-dimensioned for safety reasons; hence, it has the largest mass of all the optimal models considered. It is followed by the 5 deg static pitch angled optimal model then the 7 deg and 10 deg static pitch angled optimal model respectively, just as highlighted in section 6.1.1. This shows that relaxing the constraint on the max static pitch angle results in the reduction of the mass of the optimal platform model variants. The mass reduction of the platform as a result of the constraints used in the design contributes to a reduction in material cost – a vital component of the total CAPEX cost for a FOWF.

The ratio of the net present value of total cost to the net present value of electricity generation which translates to the LCOE is the financial parameter used in assessing the different scenarios considered in this study (30 MW FOWFs and 60 MW FOWFs for OC3 NREL platforms, 5 deg, 7 deg, and 10 deg static pitch constrained platforms). The LCOE values for the 30 MW FOWFs based on the OC3 platform model and static pitch constraints platform models of 5 degrees, 7 degrees and 10 degrees are 197 £/MWh, 185 £/MWh, 183 £/MWh and 181 £/MWh respectively. On scaling up the farm size to 60 MW, the estimated LCOE values for the 60 MW FOWFs based on the OC3 platform model and static pitch constraints platform models of 5 deg, 7 deg, and 10 deg are 185 £/MWh, 176 £/MWh, 175 £/MWh and 173 £/MWh respectively - which is 6.23 %, 4.68 %, 4.72 % and 4.78 % lower than the corresponding optimal design variants for the 30 MW FOWF. This is due to a combination of design shape parameterization and optimization framework utilized in this study and economy of scaling up the FOWFs.

This research shows that in addition to other means of ensuring FOWT technology is as economically and technically viable as the fixed-bottom counterpart (platform upscaling, government subsidy, holistic system MDAO),

geometric shape design and optimization of FOWT platform is an effective method that can be explored in reducing the cost of floating wind farms.

6.2 Contribution to knowledge

This research contributes to knowledge in novel and scientifically sound ways with potential significant values for stakeholders in the floating offshore wind sector. Furthermore, the value of this research to stakeholders can be significantly useful and applicable in the real world. In the course of this research, two peer reviewed scientific journals have been successfully published and a further two are awaiting publication pending peer review completion. Furthermore, one peer-reviewed scientific conference paper has also been successfully published during this research. Also, two presentation talks were given at conferences. The research value to stakeholders is highlighted in Table 54

Table 54. Research value to stakeholders

| Section | Novelty | Value to stakeholders | Chapter |
|---|--|---|----------|
| <p>Detailed review of MDAO in the FOWT sector and shape parameterization techniques</p> | <p>The detailed literature review of MDAO and shape parameterization concepts led to identification of novel concepts that can be potentially explored in developing the floating offshore wind from its present state of infancy to maturity. Some of the gaps highlighted are:</p> <ul style="list-style-type: none"> • Larger design space exploration combining free-form design and parameterization curves with MDAO framework to deviate from the traditional geometric shapes of a FOWT substructure to a feasible design shape that is fit for purpose while meeting all | <p>The novel gaps highlighted in the literature study of this thesis can provide valuable insights for both researchers and industrial experts involved in the development of FOWT substructures. Improved understanding of these techniques will allow researchers and industrial experts to develop more accurate and efficient design and analysis tools for floating offshore wind systems. Research enables better prediction of the response of the system in real-time, allowing for more informed decision-making throughout the design and operation of the system. This can facilitate the development of new design concepts that meet the objectives and requirements of a floating offshore wind system.</p> | <p>2</p> |

| | | | |
|---|--|---|---|
| | the specified design requirements. | | |
| Automated MDAO framework with freeform parameterization curve | <p>This is a gap from the literature study that this thesis has addressed in detail. The novelties are highlighted herein.</p> <ul style="list-style-type: none"> • Develop a state-of-the-art framework for simultaneously conducting shape parameterization of free-form curves and the design, analysis and optimization of a FOWT substructure. | This method can be used to generate bespoke concepts with improved hydrodynamic response and computational time. This methodology is valuable to the stakeholders as it has the potential to filter out optimal design within a large design space that meet the objectives and constraints | 3 |
| Framework to rank effectiveness of free-form curves | Explore the concept of using a multi-criteria decision matrix technique (TOPSIS) to assess the effectiveness of free-form curve within the design analysis and optimization context of a | This systemic approach of ranking the best performance free-form curve for modelling the substructure of a FOWT provides the base for a solid MDAO/free-form parameterization to explore large design space with the best performing curve. | 4 |

| | | | |
|--|--|--|---|
| within MDAO framework | FOWT substructure. This helps to highlight the best performing free-form curves based on a set of criteria within the MCDM framework. | | |
| Shape parameterization and optimization on techno-economics of FOWT projects | This explores the application of bespoke FOWT substructure design generated from the shape parameterization and optimization framework to assess the LCOE of a FOWT wind farm utilizing the farm's AEP and capacity utilization. | The value of the techno-economic work shows a big potential in utilizing the shape parameterization and optimization framework in reducing the LCOE of FOWT wind farm projects potentially to the level of fixed bottom wind farm project. | 5 |

6.3 Recommendations and Future Work

This framework can potentially be extended to different platform types utilizing different stability mechanisms, like the semi-submersible (waterplane-stabilised) and the TLP (mooring-stabilised) configurations. This will enhance the design of the platform types, as the various stability mechanisms contributing to the platform's stability requirements will be optimized in the design process.

Upscaling concept can be integrated with the geometric shape parameterization technique within an MDAO framework to further optimize the design process. This can be done by upscaling an optimal bespoke shaped floater to be coupled with larger and bigger turbines, rather than designing a floater for a big turbine from scratch. Although research studies have been conducted on platform upscaling in other offshore sectors and the FOWT sector, upscaling an optimal shape parameterized platform with a larger turbine is a bespoke study recommended for research in the FOWT sector as it is anticipated to highly enhance the commercial competitiveness of the FOWT technology against the fixed-bottom technology.

Furthermore, future work should explore the use of surrogate models, as they can be a useful tool for modelling floating offshore wind platforms, allowing for more efficient and accurate design optimization with reduced computational time and resources. Surrogate models are simplified models that can be used to approximate the behaviour of a complex system, such as a floating offshore wind platform. These models can be trained using data from more complex and computationally intensive simulations, allowing for faster and more efficient optimization of design parameters.

Manufacturability of complex shapes is a potential limitation of the geometric shape design parameterization and optimization concept developed in this study. It

is recommended to explore the manufacturability of the optimal geometric shape variants using the new metal additive manufacturing technologies like Direct Energy Deposition family of additive manufacturing which consists of the Wire Arc Additive Manufacturing (WAAM). The WAAM process is conducted by depositing layers of metal on top of each other, until a desired 3D shape is produced. In addition to this, and as demonstrated with the Hywind Tampen Spar FOWTs (OceanNews, 2021), concrete slip-forming of platforms could be explored to ensure there is adequate capability in producing physical components of the bespoke FOWT designs.

In addition to the parametric curve comparison for modelling substructures of FOWT, conducted in this study, it is recommended to explore more free-form curves. Free-form curves like polygon curves, polyline, T-Spline, and alternative parametrization techniques like free-form deformation and CAD method can be explored for more effective approach to modelling FOWT substructures while taking their geometric characteristics into consideration.

Refining the weightage of NURBS curve for optimal geometry is an essential sensitivity study recommended to advance this research, as NURBS curves have been widely utilized in the field of data points approximation, their fitting accuracy can be improved by adjusting the values of their weights.

The selection process of the optimal platforms in this thesis is fundamentally reliant on a comprehensive hydrodynamic assessment, which provides a detailed hydrodynamic response and performance of the platform. To enhance the robustness of the selection criteria, it is recommended to integrate other criteria like manufacturability, environmental impact, aerodynamic performance and most importantly, a detailed structural assessment within the framework. This should include the evaluation of structural integrity of the platform, tower, and Rotor-Nacelle Assembly (RNA) under various structural and environmental loads. A

detailed structural assessment highlights the fatigue life, provides design life estimates which is a fundamental requirement for LCOE estimates.

References

- ABS 2014, Updated July 2020. Global Performance Analysis for Floating Offshore Wind Turbines.
- ABS 2015, Updated March 2018, 2020. Guide for Building and Classing Floating Offshore Wind Turbine Installations. American Bureau of Shipping.
- AGTE, J., DE WECK, O., SOBIESZCZANSKI-SOBIESKI, J., ARENDSSEN, P., MORRIS, A. & SPIECK, M. 2009. MDO: assessment and direction for advancement—an opinion of one international group. *Structural and Multidisciplinary Optimization*, 40, 17.
- ALDERSEY-WILLIAMS, J., BROADBENT, I. D. & STRACHAN, P. A. 2020. Analysis of United Kingdom offshore wind farm performance using public data: Improving the evidence base for policymaking. *Utilities Policy*, 62, 100985.
- ALDERSEY-WILLIAMS, J. & RUBERT, T. 2019. Levelised cost of energy – A theoretical justification and critical assessment. *Energy Policy*, 124, 169-179.
- ANAYA-LARA, O., TANDE, J. O., UHLEN, K. & MERZ, K. 2018. *Offshore Wind Energy Technology*, John Wiley & Sons.
- ASHURI, T., ZAAIJER, M. B., MARTINS, J. R., VAN BUSSEL, G. J. & VAN KUIK, G. A. J. R. E. 2014. Multidisciplinary design optimization of offshore wind turbines for minimum levelized cost of energy. *Renewable Energy*, 68, 893-905.
- AUBAULT, A., CERMELLI, C. & RODDIER, D. 2007. Parametric Optimization of a Semi-Submersible Platform With Heave Plates.
- BACHYNSKI, E. E. 2014. *Design and dynamic analysis of tension leg platform wind turbines*. NTNU.
- BACHYNSKI, E. E. & COLLU, M. 2019. Offshore support structure design. *Renewable Energy from the Oceans: From wave, tidal and gradient systems to offshore wind and solar*. Institution of Engineering and Technology.
- BACHYNSKI, E. E. & MOAN, T. 2012. Design considerations for tension leg platform wind turbines. *Marine Structures*, 29, 89-114.
- BAK, C., BITSCHKE, R., YDE, A., KIM, T., HANSEN, M., ZAHLE, F., GAUNAA, M., BLASQUES, J., DØSSING, M., HEINEN, J.-J. & BEHRENS, T. Light rotor: The 10-MW Reference Wind Turbine. European Wind Energy Conference & Exhibition, 2012.
- BASHETTY, S. & OZCELIK, S. 2021. Review on Dynamics of Offshore Floating Wind Turbine Platforms. *Energies*, 14.
- BIRAN, A. 2019. Chapter 7 - Cubic Splines. In: BIRAN, A. (ed.) *Geometry for Naval Architects*. Butterworth-Heinemann.

- BIRK, L. 2006. Parametric modeling and shape optimization of offshore structures. *International Journal of CAD/CAM*, 6, 29-40.
- BIRK, L. & CLAUSS, G. Parametric hull design and automated optimization of offshore structures. 10th Int. Congress of the Int. Maritime Association of the Mediterranean, Hellas, Greece, 2002.
- BIRK, L. & CLAUSS, G. N. F. Optimization of Offshore Structures Based on Linear Analysis of Wave-Body Interaction. ASME 2008 27th International Conference on Offshore Mechanics and Arctic Engineering, 2008. 275-289.
- BIRK, L., CLAUSS, G. N. F. & LEE, J. Y. Practical application of global optimization to the design of offshore structures. International Conference on Offshore Mechanics and Arctic Engineering, 2004. 567-579.
- BORG, M. & COLLU, M. 2015. A comparison between the dynamics of horizontal and vertical axis offshore floating wind turbines. *Philosophical Transactions of the Royal Society A: Mathematical, Physical and Engineering Sciences*, 373.
- BORTOLOTTI, P., TARRES, HELENA C, DYKES, KATHERINE L, MERZ, KARL, SETHURAMAN, LATHA, VERELST, DAVID, & ZAHLE, FREDERIK. 2019. IEA Wind TCP Task 37: Systems Engineering in Wind Energy - WP2.1 Reference Wind Turbines. United States.
- BOTTASSO, C. L., CROCE, A., RIBOLDI, C. & BIR, G. Spatial estimation of wind states from the aeroelastic response of a wind turbine. TORQUE 2010, The Science of Making Torque from Wind., 2010 Heraklion, Crete, Greece. 28-30.
- BUCKLEY, A. G. 1978. A combined conjugate-gradient quasi-Newton minimization algorithm. *Mathematical Programming*, 15, 200-210.
- CASTRO-SANTOS, L., MARTINS, E. & GUEDES SOARES, C. 2016. Cost assessment methodology for combined wind and wave floating offshore renewable energy systems. *Renewable Energy*, 97, 866-880.
- CAYLOR, J. P. & HANRATTY, T. P. 2020. Survey of multi criteria decision making methods for complex environments. CCDC Army Research Laboratory.
- CHEHOURI, A., YOUNES, R., ILINCA, A. & PERRON, J. 2016. Wind Turbine Designs : Multi-Objective Optimization. *Wind Turbine - Design, Control and Applications*. IntechOpen.
- CLAUSS, G. F. & BIRK, L. 1996. Hydrodynamic shape optimization of large offshore structures. *Applied Ocean Research*, 18, 157-171.
- COLLU, M. & BORG, M. 2016. Design of floating offshore wind turbines. *Offshore Wind Farms: Technologies, Design and Operation*. Elsevier Inc.
- COLLU, M., MAGGI, A., GUALENI, P., RIZZO, C. M. & BRENNAN, F. 2014. Stability requirements for floating offshore wind turbine (FOWT) during assembly and temporary phases: Overview and application. *Ocean Engineering*, 84, 164-175.

- COPPEDÉ, A., VERNENGO, G. & VILLA, D. 2018. A combined approach based on Subdivision Surface and Free Form Deformation for smart ship hull form design and variation. *Ships and Offshore Structures*, 13, 769-778.
- CORADDU, A., ONETO, L., KALIKATZARAKIS, M., ILARDI, D. & COLLU, M. Floating Spar-Type Offshore Wind Turbine Hydrodynamic Response Characterisation: a Computational Cost Aware Approach. Global Oceans 2020: Singapore – U.S. Gulf Coast, 5-30 Oct. 2020 2020. 1-8.
- CORDLE, A. & JONKMAN, J. M. State of the Art in Floating Wind Turbine Design Tools. 2011.
- CRAWFORD, C. & HAIMES, R. Synthesizing an MDO Architecture in CAD. 42nd AIAA Aerospace Sciences Meeting and Exhibit, 2004. American Institute of Aeronautics and Astronautics, 281.
- DIMAS, E. & BRIASSOULIS, D. 1999. 3D geometric modelling based on NURBS: a review. *Advances in Engineering Software*, 30, 741-751.
- DNV-GL 2020. Floating Wind: The Power to Commercialize.
- DNV-OS-C105 2008. Structural Design of TLPs (LRFD Method).
- DNV-OS-J101 2013. Design of Offshore Wind Turbine Structures.
- DNV. 2021. *Sesam Feature Description. Software suite for hydrodynamic and structural analysis of renewable, offshore and maritime structures* [Online]. DNV. Available: https://www.dnv.com/Images/Sesam-Feature-Description_tcm8-58834.pdf [Accessed 29/11/2021 2021].
- DNVGL-RP-0286 2019. Coupled Analysis of Floating Wind Turbines.
- DNVGL-SE-0422 2018. Certification of Floating Wind Turbines.
- DNVGL-ST-0119 2018. Floating Wind Turbine Structures.
- DNVGL HØVIK, N. 2019. SESAM User Manual, WADAM, Wave Analysis by Diffraction and Morison theory.
- DNVGL OSLO, N. 2018. Class Guideline DNVGL CG 0130: Wave Loads.
- DNVGLAS 2016. Loads and Site Conditions for Wind Turbines: Standard DNVGL-ST-0437,.
- DOU, S., PEGALAJAR-JURADO, A., WANG, S., BREDMOSE, H. & STOLPE, M. 2020. Optimization of floating wind turbine support structures using frequency-domain analysis and analytical gradients. *Journal of Physics: Conference Series*, 1618, 042028.
- DYKES, K., MEADOWS, R., FELKER, F., GRAF, P., HAND, M., LUNACEK, M., MICHALAKES, J., MORIARTY, P., MUSIAL, W. & VEERS, P. 2011. Applications of Systems Engineering to the Research, Design, and Development of Wind Energy Systems. National Renewable Energy Laboratory (NREL).
- FARIN, G. 1990. *Curves and Surfaces for Computer-Aided Geometric Design* New York, Academic Press.

- FARIN, G. 1993a. Chapter 4 - The Bernstein Form of a Bézier Curve. *Curves and Surfaces for Computer-Aided Geometric Design (Third Edition)*. Boston: Academic Press.
- FARIN, G. 1993b. Chapter 7 - Spline Curves in Bézier Form. *Curves and Surfaces for Computer-Aided Geometric Design (Third Edition)*. Boston: Academic Press.
- FERRI, G., MARINO, E. & BORRI, C. 2020. Optimal Dimensions of a Semisubmersible Floating Platform for a 10 MW Wind Turbine. *Energies*, 13, 1-20.
- FILGUEIRA-VIZOSO, A., CASTRO-SANTOS, L., IGLESIAS, D. C., PUIME-GUILLÉN, F., LAMAS-GALDO, I., GARCÍA-DIEZ, A. I., UZUNOGLU, E., DÍAZ, H. & SOARES, C. G. 2022a. The Technical and Economic Feasibility of the CENTEC Floating Offshore Wind Platform. *Journal of Marine Science and Engineering* [Online], 10.
- FILGUEIRA-VIZOSO, A., COSTOYA, X., CORDAL-IGLESIAS, D., PIEGARI, L., TRICOLI, P. & CASTRO-SANTOS, L. 2022b. Analysis of the economic feasibility of different floating offshore renewable energies in Canary Islands. *RENEWABLE ENERGY & POWER QUALITY JOURNAL*, 20, 525-529.
- FINDLER, N. V., LO, C. & LO, R. 1987. Pattern search for optimization. *Mathematics and Computers in Simulation*, 29, 41-50.
- FORREST, A. R. Computational Geometry in Practice. In: EARNSHAW, R. A., ed. *Fundamental Algorithms for Computer Graphics*, 1991// 1991 Berlin, Heidelberg. Springer Berlin Heidelberg, 707-724.
- FRANK LEMMER, K. M., WEI YU, & RICARDO FAERRON GUZMAN, M. K. 2016. Life50+ :- D4.3 Optimization framework and methodology for optimized floater design.
- FRIEDEMANN BORISADE, J. G., LINA HAGEMANN,, MATTHIAS KRETSCHMER, F. L., KOLJA MÜLLER, & DAVID SCHLIPF, N.-D. N., LUCA VITA 2016. Life50+ :- D 7.4 State-of-the-Art FOWT design practice and guidelines.
- FYLLING, I. & BERTHELSEN, P. A. WINDOPT: An Optimization Tool for Floating Support Structures for Deep Water Wind Turbines. Volume 5: Ocean Space Utilization; *Ocean Renewable Energy*, 2011. 767-776.
- GHIGO, A., COTTURA, L., CARADONNA, R., BRACCO, G., MATTIAZZO, G. & ENGINEERING 2020. Platform Optimization and Cost Analysis in a Floating Offshore Wind Farm. *Marine Science and Engineering*, 8, 835.
- GOLDMAN, R. 2003. A Dynamic Programming Approach to Curves and Surfaces for Geometric Modeling. In: GOLDMAN, R. (ed.) *Pyramid Algorithms*. San Francisco: Morgan Kaufmann.

- GRAY, J. S., HWANG, J. T., MARTINS, J. R. R. A., MOORE, K. T. & NAYLOR, B. A. 2019. OpenMDAO: An open-source framework for multidisciplinary design, analysis, and optimization. *Structural and Multidisciplinary Optimization*, 59, 1075-1104.
- GWEC 2022. Floating Offshore Wind - A Global Opportunity.
- HADKA, D. 2015. *Platypus Documentation* [Online]. Available: <https://platypus.readthedocs.io/en/latest/> [Accessed].
- HALL, M., BUCKHAM, B. & CRAWFORD, C. Evolving offshore wind: A genetic algorithm-based support structure optimization framework for floating wind turbines. OCEANS 2013 MTS/IEEE Bergen: The Challenges of the Northern Dimension, 2013. IEEE, 1-10.
- HARRIES, S. & NOWACKI, H. Form parameter approach to the design of fair hull shapes. 10th International Conference on Computer Applications (ICCAS), 1999 MIT, Cambridge, MA, USA.
- HE, J., HANNAPEL, S., SINGER, D. & VLAHOPOULOS, N. 2011. Multidisciplinary Design Optimisation of a Ship Hull Using Metamodels. *Ship Technology Research*, 58, 156-166.
- HEGSETH, J. M., BACHYNSKI, E. E. & MARTINS, J. R. 2020. Integrated design optimization of spar floating wind turbines. *Marine Structures*, 72, 102771.
- HENDERSON, A. R. & PATEL, M. H. Floating offshore wind energy. BWEA Conference, 1998.
- HERONEMUS, W. E. 1972. Pollution-free energy from the offshore winds. *8th Annual Conference and Exposition, Marine Technology Society*. Washington, D.C.
- HWANG, C.-L. & YOON, K. 1981. Methods for Multiple Attribute Decision Making. In: HWANG, C.-L. & YOON, K. (eds.) *Multiple Attribute Decision Making: Methods and Applications A State-of-the-Art Survey*. Berlin, Heidelberg: Springer Berlin Heidelberg.
- IEC61400-3-1 2019. Wind energy generation systems - Part 3-1: Design requirements for fixed offshore wind turbines.
- IEC-61400-1 2014. Wind Turbines—Part 1: Design Requirements
- IEC-61400-3-2 2019. Wind energy generation systems – Part 3-2: Design Requirements for Floating Offshore Wind Turbines. .
- IEC-61400-3 2009. Wind Turbines—Part 3: Design Requirements for Offshore Wind Turbines.
- IOANNOU, A., LIANG, Y., JALÓN, M. L. & BRENNAN, F. P. 2020. A preliminary parametric techno-economic study of offshore wind floater concepts. *Ocean Engineering*, 197, 106937.

- IRENA 2019a. Future of wind. deployment, investment, technology, grid integration and socio-economic aspects. *International Renewable Energy Agency*. Abu Dhabi.
- IRENA 2019b. Renewable power generation costs in 2018. *International Renewable Energy Agency*. Abu Dhabi.
- IZZO, D. B., F. 2015. *Welcome to PyGMO*. [Online]. Available: <https://esa.github.io/pygmo/index.html> [Accessed].
- JAMES, R. C. R., M. 2015. Floating Offshore Wind: Market and Technology Review.
- JAMSHID, A. A Survey of Shape Parameterization Techniques. NASA Conference Publication, 1999. Citeseer, 333-344.
- JANGA REDDY, M. & KUMAR, D. N. 2020. Evolutionary algorithms, swarm intelligence methods, and their applications in water resources engineering: a state-of-the-art review. *H2Open Journal* 3, 135-188.
- JIN, Y. 2011. Surrogate-assisted evolutionary computation: Recent advances and future challenges. *Swarm and Evolutionary Computation*, 1, 61-70.
- JONKMAN, J., BUTTERFIELD, S., MUSIAL, W. & SCOTT, G. 2009. Definition of a 5-MW reference wind turbine for offshore system development. National Renewable Energy Lab.(NREL), Golden, CO (United States).
- JONKMAN, J. M. 2007. *Dynamics modeling and loads analysis of an offshore floating wind turbine*, University of Colorado at Boulder.
- JONKMAN, J. M. Definition of the Floating System for Phase IV of OC3. 2010.
- JONKMAN, J. M. & MATHA, D. 2011. Dynamics of offshore floating wind turbines—analysis of three concepts. *Wind Energy*, 14, 557-569.
- JOURNÉE, J. M. J. & MASSIE, W. W. 2000. *Offshore Hydromechanics*, Delft University of Technology.
- KALDELLIS, J. K., APOSTOLOU, D., KAPSALI, M. & KONDILI, E. 2016. Environmental and social footprint of offshore wind energy. Comparison with onshore counterpart. *Renewable Energy*, 92, 543-556.
- KANG, E., JACKSON, E. & SCHULTE, W. An approach for effective design space exploration. In: CALINESCU, R. & JACKSON, E., eds. *Foundations of Computer Software. Modeling, Development, and Verification of Adaptive Systems*, 2011 Berlin, Heidelberg. Springer Berlin Heidelberg, 33-54.
- KARIMI, M. 2018. *Frequency domain modeling and multidisciplinary design optimization of floating offshore wind turbines*. Ph.D, University of Victoria.
- KARIMI, M., BUCKHAM, B. & CRAWFORD, C. 2019. A fully coupled frequency domain model for floating offshore wind turbines. *Journal of Ocean Engineering and Marine Energy*, 5, 135-158.

- KARIMI, M., HALL, M., BUCKHAM, B. & CRAWFORD, C. 2017. A multi-objective design optimization approach for floating offshore wind turbine support structures. *Journal of Ocean Engineering and Marine Energy*, 3, 69-87.
- KATSOUKIS, T., WANG, X. & KAKLIS, P. D. 2019. A T-splines-based parametric modeller for computer-aided ship design. *Ocean Engineering*, 191, 106433.
- KHAMLAJ, T. A. & RUMPFKEIL, M. P. 2018. Analysis and optimization of ducted wind turbines. *Energy*, 162, 1234-1252.
- KIKUCHI, Y. & ISHIHARA, T. 2019. Upscaling and levelized cost of energy for offshore wind turbines supported by semi-submersible floating platforms. *Journal of Physics: Conference Series*, 1356, 012033.
- KIM, H. & YANG, C. Design optimization of bulbous bow and stern end bulb for reduced drag. 2013 2013. OnePetro.
- KOCHENDERFER, M. J. & WHEELER, T. A. 2019. *Algorithms for optimization*, Mit Press.
- KOLIOS, A., BORG, M. & HANAK, D. 2015. Reliability analysis of complex limit states of floating wind turbines. *Journal of Energy Challenges and Mechanics*, 2, 6-9.
- KOLIOS, A. J., RODRIGUEZ-TSOUROUKDISSIAN, A. & SALONITIS, K. 2016. Multi-criteria decision analysis of offshore wind turbines support structures under stochastic inputs. *Ships and Offshore Structures*, 11, 38-49.
- KOLJA MÜLLER, D. M., MICHAEL KARCH, & SIMON TIEDEMANN, R. P. 2017. Life50+ :- D7.5 Guidance on platform and mooring line selection, installation and marine operations.
- KONSTANTINIDIS, E. & BOTSARIS, P. 2016. Wind turbines: current status, obstacles, trends and technologies. *IOP Conference Series: Materials Science and Engineering*, 161, 012079.
- KULFAN, B. & BUSSOLETTI, J. 2006. " Fundamental" Parameteric Geometry Representations for Aircraft Component Shapes. *11th AIAA/ISSMO Multidisciplinary Analysis and Optimization Conference*. American Institute of Aeronautics and Astronautics.
- KYOKAI, N. K. 2012. Guidelines for Offshore Floating Wind Turbines - Classification Survey.
- LAGUNA, M. & MARTÍ, R. C. 2003. *Scatter search: methodology and implementations in C*, Springer Science & Business Media.
- LE DIGABEL, S. 2011. Algorithm 909: NOMAD: Nonlinear Optimization with the MADS Algorithm. *ACM Transactions on Mathematical Software*, 37, 1-15.
- LEFEBVRE, S. & COLLU, M. 2012. Preliminary design of a floating support structure for a 5MW offshore wind turbine. *Ocean Engineering*, 40, 15-26.

- LEIMEISTER, M., BACHYNSKI, E. E., MUSKULUS, M. & THOMAS, P. Design optimization and upscaling of a semi-submersible floating platform. WindEurope summit, 2016a.
- LEIMEISTER, M., BACHYNSKI, E. E., MUSKULUS, M. & THOMAS, P. 2016b. Rational Upscaling of a Semi-submersible Floating Platform Supporting a Wind Turbine. *Energy Procedia*, 94, 434-442.
- LEIMEISTER, M. & KOLIOS, A. 2018. A review of reliability-based methods for risk analysis and their application in the offshore wind industry. *Renewable and Sustainable Energy Reviews*, 91, 1065-1076.
- LEIMEISTER, M., KOLIOS, A. & COLLU, M. Critical review of floating support structures for offshore wind farm deployment. *Journal of Physics: Conference Series*, 2018/10 2018. 1-11.
- LEIMEISTER, M., KOLIOS, A. & COLLU, M. 2020a. Development and Verification of an Aero-Hydro-Servo-Elastic Coupled Model of Dynamics for FOWT, Based on the MoWiT Library. 13, 1974.
- LEIMEISTER, M., KOLIOS, A. & COLLU, M. 2021. Development of a framework for wind turbine design and optimization. *Modelling*, 2, 105-128.
- LEIMEISTER, M., KOLIOS, A., COLLU, M. & THOMAS, P. 2020b. Design optimization of the OC3 phase IV floating spar-buoy, based on global limit states. *Ocean Engineering*, 202, 107186.
- LI, J. & LIU, C. 2022. Cubic Trigonometric Hermite Interpolation Curve: Construction, Properties, and Shape Optimization. *Journal of Function Spaces*, 2022.
- LI, L., LIU, Y., YUAN, Z. & GAO, Y. 2019. Dynamic and structural performances of offshore floating wind turbines in turbulent wind flow. *Ocean Engineering*, 179, 92-103.
- LOZANO-MINGUEZ, E., KOLIOS, A. J. & BRENNAN, F. P. 2011. Multi-criteria assessment of offshore wind turbine support structures. *Renewable Energy*, 36, 2831-2837.
- MAIENZA, C., AVOSSA, A. M., PICOZZI, V. & RICCIARDELLI, F. 2022. Feasibility analysis for floating offshore wind energy. *The International Journal of Life Cycle Assessment*, 27, 796-812.
- MAIENZA, C., AVOSSA, A. M., RICCIARDELLI, F., COIRO, D., TROISE, G. & GEORGAKIS, C. T. 2020. A life cycle cost model for floating offshore wind farms. *Applied Energy*, 266, 114716.
- MARKUS LERCH, J. A. N., PETTER ANDREAS BERTHELSEN 2019. Life50+ : D2.8 Expected LCOE for floating wind turbines 10MW+ for 50m+ water depth.

- MARTINEZ, A. & IGLESIAS, G. 2022. Mapping of the levelised cost of energy for floating offshore wind in the European Atlantic. *Renewable and Sustainable Energy Reviews*, 154, 111889.
- MARTINS, J. R. & LAMBE, A. B. 2013. Multidisciplinary design optimization: a survey of architectures. *AIAA*, 51, 2049-2075.
- MARTINS, J. R., MARRIAGE, C. & TEDFORD, N. 2009. pyMDO: an object-oriented framework for multidisciplinary design optimization. *ACM Transactions on Mathematical Software*, 36, 1-25.
- MATHWORKS. 2021. *MATLAB Global Optimization Toolbox - Pattern Search* [Online]. Available: <https://uk.mathworks.com/help/gads/patternsearch.html> [Accessed December 14 2021].
- MCCLARREN, R. G. 2018. Chapter 10 - Interpolation. In: MCCLARREN, R. G. (ed.) *Computational Nuclear Engineering and Radiological Science Using Python*. Academic Press.
- MORENO, C. A. S. 2021. Application of Cubic B-Spline Curves for Hull Meshing. *Ship Science and Technology*, 14, 53-62.
- MORENO, S. S. P. 2019. *A guideline for selecting MDAO workflows with an application in offshore wind energy*. Delft University of Technology.
- MUNIR, H., LEE, C. F. & ONG, M. C. 2021. Global analysis of floating offshore wind turbines with shared mooring system. *IOP Conference Series: Materials Science and Engineering*, 1201, 012024.
- MUSIAL, W., SPITSEN, P., DUFFY, P., BEITER, P., MARQUIS, M., HAMMOND, R. & SHIELDS, M. 2022. Offshore Wind Market Report. U.S Department of Energy, Office of Energy Efficiency and Renewable Energy.
- MUSKULUS, M., SCHAFHIRT, S. & ENERGY, W. 2014. Design optimization of wind turbine support structures-a review. *Journal of Ocean and Wind Energy*, 1, 12-22.
- MYHR, A., BJERKSETER, C., ÅGOTNES, A. & NYGAARD, T. A. 2014. Levelised cost of energy for offshore floating wind turbines in a life cycle perspective. *Renewable Energy*, 66, 714-728.
- NAM, J.-H. & BANG, N. S. 2017. A curve based hull form variation with geometric constraints of area and centroid. *Ocean Engineering*, 133, 1-8.
- NAM, J.-H. & PARSONS, M. G. 2000. A parametric approach for initial hull form modeling using NURBS representation. *Journal of ship production*, 16, 76-89.
- NEWMAN, J. N. 2018. *Marine hydrodynamics*, The MIT press.
- OCEANNEWS. 2021. *Next Step for Hywind Tampen* [Online]. Available: <https://www.oceannews.com/news/energy/next-step-for-hywind-tampen> [Accessed December 27 2023].

- OJO, A., COLLU, M. & CORADDU, A. 2022a. Multidisciplinary design analysis and optimization of floating offshore wind turbine substructures: A review. *Ocean Engineering*, 266, 112727.
- OJO, A., COLLU, M. & CORADDU, A. 2022b. Parametrisation Scheme for Multidisciplinary Design Analysis and Optimisation of a Floating Offshore Wind Turbine Substructure – OC3 5MW Case Study. *Journal of Physics: Conference Series*, 2265, 042009.
- OPENFAST. 2023. OpenFAST Documentation. Available: <https://openfast.readthedocs.io/en/main/>.
- OPENMDAO.ORG. 2016. Optimizer.
- PALACIO-MORALES, J., TOBÓN, A. & HERRERA, J. 2021. Optimization Based on Pattern Search Algorithm Applied to pH Non-Linear Control: Application to Alkalinization Process of Sugar Juice. *Processes* [Online], 9.
- PAPI, F. & BIANCHINI, A. 2022. Technical challenges in floating offshore wind turbine upscaling: A critical analysis based on the NREL 5 MW and IEA 15 MW Reference Turbines. *Renewable and Sustainable Energy Reviews*, 162, 112489.
- PATEL, M. H. 2013. *Dynamics of offshore structures*, Butterworth-Heinemann.
- PEREZ-MORENO, S. S., ZAAIJER, M. B., BOTTASSO, C. L., DYKES, K., MERZ, K. O., RÉTHORÉ, P. E. & ZAHLE, F. 2016. Roadmap to the multidisciplinary design analysis and optimisation of wind energy systems. *Journal of Physics: Conference Series*, 753, 062011.
- PÉREZ, F., CLEMENTE, J., SUAREZ SUAREZ, J. & GONZÁLEZ, J. 2008. Parametric Generation, Modeling, and Fairing of Simple Hull Lines With the Use of Nonuniform Rational B-Spline Surfaces. *Journal of Ship Research*, 52, 1–15.
- PÉREZ, F., SUÁREZ, J. A., CLEMENTE, J. A. & SOUTO, A. 2007. Geometric modelling of bulbous bows with the use of non-uniform rational B-spline surfaces. *Journal of marine science and technology*, 12, 83-94.
- QI, X., MIAO, A. & WAN, D. A NURBS-based Hull Surface Modification Method for Hydrodynamic Optimization. The Thirteenth ISOPE Pacific/Asia Offshore Mechanics Symposium., 2018 2018. OnePetro.
- RAHMDEL, S., WANG, B., HAN, C., KIM, K. & PARK, S. 2016. A parametric study of spar-type floating offshore wind turbines (FOWTs) by numerical and experimental investigations. *Ships and Offshore Structures*, 11, 818-832.
- RAMACHANDRAN, G., ROBERTSON, A., JONKMAN, J. & MASCIOLA, M. D. Investigation of response amplitude operators for floating offshore wind turbines. The Twenty-third International Offshore and Polar Engineering Conference, 2013. OnePetro.

- RASEKHI NEJAD, A., BACHYNSKI, E. E. & MOAN, T. 2017. On Tower Top Axial Acceleration and Drivetrain Responses in a Spar-Type Floating Wind Turbine.
- RIBUOT, J. 2019. *HEXAFLOAT Innovative Competitive Offshore Energy Production* [Online]. Available: <https://mcedd.com/wp-content/uploads/2019/04/MCEDD-2019-Presentation-SAIPEM-18-March.pdf> [Accessed 7th March 2021 2021].
- ROSZKOWSKA, E. 2011. Multi-criteria decision making models by applying the TOPSIS method to crisp and interval data. *Multiple Criteria Decision Making/University of Economics in Katowice*, 6, 200-230.
- SAAD, A., DONG, Z., BUCKHAM, B., CRAWFORD, C., YOUNIS, A. & KARIMI, M. 2019. A new Kriging–Bat Algorithm for solving computationally expensive black-box global optimization problems. *Engineering Optimization*, 51, 265-285.
- SAAD, A. H., DONG, Z. & KARIMI, M. 2017. A comparative study on recently-introduced nature-based global optimization methods in complex mechanical system design. *Algorithms*, 10, 120.
- SAENZ-AGUIRRE, A., ULAZIA, A., IBARRA-BERASTEGI, G. & SAENZ, J. 2022. Floating wind turbine energy and fatigue loads estimation according to climate period scaled wind and waves. *Energy Conversion and Management*, 271, 116303.
- SAMAREH, J. A. A survey of shape parameterization techniques. NASA Conference Publication, 1999. Citeseer, 333-344.
- SAMAREH, J. A. 2001. Survey of shape parameterization techniques for high-fidelity multidisciplinary shape optimization. *AIAA Journal*, 39, 877-884.
- SANDNER, F., WIE, F. Y., MATHA, D., GRELA, E., AZCONA, J., MUNDUATE, X., VOUTSINAS, S. & NATARAJAN, A. 2014. Deliverable D4. 33—Innovative Concepts for Floating Structures. *InnWind. EU*, 10, 11-31.
- SCLAVOUNOS, P., TRACY, C. & LEE, S. 2008. Floating offshore wind turbines: Responses in a seastate pareto optimal designs and economic assessment. *International Conference on Offshore Mechanics and Arctic Engineering*.
- SEDERBERG, T. W. & PARRY, S. R. 1986. Free-form deformation of solid geometric models. *ACM SIGGRAPH Computer Graphics*, 20, 151-160.
- SHI, M., LV, L., SUN, W. & SONG, X. 2020. A multi-fidelity surrogate model based on support vector regression. *Structural and Multidisciplinary Optimization*, 61, 2363-2375.
- SHIELDS, M., DUFFY, P., MUSIAL, W., LAURIENTI, M., HEIMILLER, D., SPENCER, R. & OPTIS, M. 2021. The Costs and Feasibility of Floating Offshore Wind Energy in the O'ahu Region. United States.
- SIARRY, P. 2016. *Metaheuristics*, Springer.

- SIEMENS 2009. Siemens wind turbine SWT-2.3-82 VS, Technical Brochure.
- SPEARMAN, D. K. & STRIVENS, S. 2020. Floating Wind Joint Industry Project - Phase II.
- STIESDAL. 2021. <https://www.stiesdal.com/offshore-windpower/> [Online]. Available: <https://www.stiesdal.com/offshore-windpower/> [Accessed 9th March 2021 2021].
- STRAATHOF, M. 2012. *Shape Parameterization in Aircraft Design: A Novel Method, Based on B-Splines*. Technische Universiteit Delft.
- TABOADA, J. V. Comparative analysis review on floating offshore wind foundations (FOWF). 2015 2015. 14-16.
- TONG, K. C. 1998. Technical and economic aspects of a floating offshore wind farm. *Journal of Wind Engineering and Industrial Aerodynamics*, 74-76, 399-410.
- TORCZON, V. & TROSSET, M. W. From evolutionary operation to parallel direct search: Pattern search algorithms for numerical optimization. *Computing Science and Statistics*, 1998. Citeseer, 396-401.
- TOWNSEND, J. C., SAMAREH, J. A., WESTON, R. P. & ZORUMSKI, W. E. 1998. Integration of a CAD System Into an MDO Framework. NASA Langley Technical Report Server.
- TRACY, C. H. 2007. *Parametric design of floating wind turbines*. Massachusetts Institute of Technology.
- VERITAS, B. 2010. Classification and Certification of Floating Offshore Wind Turbines.
- VERITAS, B. 2015, Updated 2019. Classification and Certification of Floating Offshore Wind Turbines.
- WAMIT-INC 2020. WAMIT user manual, version 7.4 (available for download from www.wamit.com).
- WANG, C. M., UTSUNOMIYA, T., WEE, S. C. & CHOO, Y. S. 2010. Research on floating wind turbines: a literature survey. *The IES Journal Part A: Civil & Structural Engineering*, 3, 267-277.
- WAYMAN, E. N. 2006. *Coupled dynamics and economic analysis of floating wind turbine systems*. Massachusetts Institute of Technology.
- WINDEUROPE 2019. Offshore Wind in Europe, Key trends and statistics 2019.
- WITHEE, J. E. 2004. Fully coupled dynamic analysis of a floating wind turbine system. Massachusetts Inst of Tech Cambridge.
- WOLPERT, D. H. & MACREADY, W. G. 1997. No free lunch theorems for optimization. *IEEE transactions on evolutionary computation*, 1, 67-82.
- WU, J. & KIM, M.-H. 2021. Generic Upscaling Methodology of a Floating Offshore Wind Turbine. 14, 8490.

- WU, X., HU, Y., LI, Y., YANG, J., DUAN, L., WANG, T., ADCOCK, T., JIANG, Z., GAO, Z., LIN, Z., BORTHWICK, A. & LIAO, S. 2019. Foundations of offshore wind turbines: A review. *Renewable and Sustainable Energy Reviews*, 104, 379-393.
- XIAN, X., SOON, S. H., FENG, T., LEWIS, J. P. & FONG, N. A powell optimization approach for example-based skinning in a production animation environment. *Computer Animation and Social Agents*, 2006. Citeseer, 2006.
- YANG, X.-S. 2019. 3 - Optimization algorithms. *In: YANG, X.-S. (ed.) Introduction to Algorithms for Data Mining and Machine Learning*. Academic Press.
- YOUNIS, A. & DONG, Z. 2010. Trends, features, and tests of common and recently introduced global optimization methods. *Engineering Optimization*, 42, 691-718.
- ZHANG, P., ZHU, D.-X. & LENG, W.-H. 2008. Parametric approach to design of hull forms. *Journal of Hydrodynamics, Ser. B*, 20, 804-810.
- ZHENG, X. Y. & LEI, Y. 2018. Stochastic Response Analysis for a Floating Offshore Wind Turbine Integrated with a Steel Fish Farming Cage. 8, 1229.
- ZHOU, H., FENG, B., LIU, Z., CHANG, H. & CHENG, X. 2022. NURBS-Based Parametric Design for Ship Hull Form. *Journal of Marine Science and Engineering*, 10, 686.
- ZHU, F. 2014. *Geometric parameterisation and aerodynamic shape optimisation*. University of Sheffield.